Digital Pulse Interval Modulation for Optical Communication Systems

Eraj Dulip Kaluarachchi

A thesis submitted in partial fulfilment of the requirements of Sheffield Hallam University for the degree of Doctor of Philosophy

Electronics Research Group
School of Engineering, Sheffield Hallam University
Sheffield, United Kingdom

October 1997

This thesis is dedicated to my parents

Acknowledgements

My deepest gratitude is due to the school of Engineering at Sheffield Hallam University for project funding throughout the whole duration of this work.

I would like to thank my director of studies Dr Z. Ghassemlooy for his invaluable advice, constant guidance, enthusiasm throughout this work and proof reading of this thesis.

Sincere thanks also goes to my supervisors Dr A.J. Simmonds, & Dr B. Wilson (of the UMIST) for their advice and fruitful discussions. Thanks is also due to Professor A K. Ray for his support.

I would also like to thank all my colleagues in the research group for making my stay in Sheffield enjoyable. They will all be missed. Also a word of thanks goes to the technical staff and secretaries who assisted me during this work at some point.

There are many friends and relatives in Sheffield and London who knowingly or unknowingly have helped me over the past few years. Their help and support will not be forgotten.

Finally, I would like to sincerely thank my mother and father for whom this thesis is dedicated to, without their guidance and support over the years would I ever have come this far.

Declaration

No portion of the work referred to in this thesis has been submitted in support of an application for another degree or qualification to this, or any other university, other institute of learning, or industrial organisation.

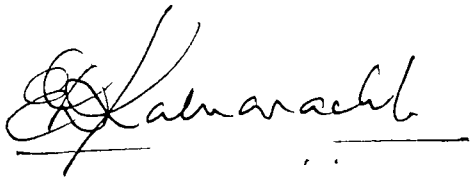

Eraj Dulip Kaluarachchi

October 1997

Abstract

Pulse time modulation (PTM) techniques have drawn considerable attention over the years as suitable schemes for transmission of information over optical fibres. PTM schemes are known to utilise the vast optical bandwidth to provide efficient transmission characteristics. Pulse code modulation is one such modulation scheme that has been used widely in various communication systems.

In this thesis digital pulse interval modulation (DPIM), a form of PTM, is proposed as a suitable modulation scheme for optical communication systems. In this scheme the information is represented by means of varying the anisochronous frame interval between two successive pulses. Each pulse fulfils the dual role of representing the frame boundaries and initiation of the next sampling event within the modulator or sample reconstruction in the demodulator. In this study DPIM frame structure is proposed and sampling criteria, information capacity, bandwidth requirements are discussed in depth.

The spectral behaviour of the scheme is investigated and a mathematical model is developed to represent the spectra. The model was numerically evaluated and verified with the practical measurements to prove its validity. Spectral predictions were made for random as well as periodic information signals showing the existence of the distinct slot frequency component, which is used for slot synchronisation. Frame synchronisation is not required as DPIM has self synchronised frame structure. For random signals, slot component is found to be about 15 dB and for periodic single tone sinusoidal signal this was at about 5 dB. Dependency of this component on the various system parameters such as bit resolution, pulse width, pulse shape are discussed.

A detailed account of the receiver performance is given. Receiver analysis was carried out for narrow band as well as for wide band channels. Possible error sources are presented and the system performance degradation with these error sources is discussed and a comparison is made with isochronous DPPM and PCM. For performance evaluation of analogue systems, signal-to-noise ratio was mathematically modelled and compared with PCM. This analysis showed that DPIM *SNR*s shows three important regions as compared to PCM. That is when the *SNR* is inferior, superior and identical to PCM performance. Threshold levels corresponding to the above regions vary depending on the system bit resolution.

A prototype DPIM system was designed and implemented to transmit low speed analogue signal (≈15 kHz) at bit resolutions of 4, 5 and 6 where the slot frequencies are at 510, 990 and 1950 kHz, respectively. Measurements were carried out in order to verify the predicted performance. This results showed close agreement with the predicted. Receiver sensitivity of the prototype at bit error rate of 10^{-9} was found to be about -45.5 dBm at all three cases with transmitted average power of -28.8 dBm allowing high optical power budget. The signal-to-noise ratio threshold level of the system was at -47 dBm. Finally, linearity measurements of the overall system were made at the above bit resolutions and the quantitative and qualitative results are presented.

Glossary of Abbreviations

ADC	Analogue to Digital Converter
AM	Amplitude modulation
AMI	Alternate mark inversion
APD	Avalanche photo diode
ASK	Amplitude shift keying
AWGN	Additive white Gaussian noise
BER	Bit error rate
CE-CC	Common emitter- common collector
DAC	Digital to Analogue Converter
DC	Zero frequency signal level
DPWM	Digital pulse width modulation
DPIM	Digital Pulse Interval Modulation
DPIWM	Digital pulse interval and width modulation
DPPM	Digital Pulse Position Modulation
FDM	Frequency division multiplexing
FM	Frequency modulation
FSK	Frequency shift keying
HDTV	High definition television
IC	Integrated circuit
ISI	Inter Symbol Interference
IR	Infra-red
LED	Light emitting diode
LP	Loop filter
LPF	Low pass filter
LD	Laser diode
NSPWM	Naturally sampled PWM
NRZ	Non return to zero
PAM	Pulse amplitude modulation
PCM	Pulse Code Modulation
PD	Phase detector
PLL	Phase lock loop
PM	Phase modulation
PSD	Power spectral density
PSK	Phase shift keying
PSM	Pulse slope modulation
PFM	Pulse frequency modulation
PTM	Pulse time modulation
PWM	Pulse width modulation
RB	Return to bias
RMS	Root mean square
ROM	Read only memory
RZ	Return to zero
SNR	Signal-to-noise ratio
SWFM	Square wave frequency modulation
USPWM	Uniformly sampled PWM
VCO	Voltage controlled oscillator

Glossary of symbols

Symbol	Definition
A	Receiver amplifier gain
A_c	PCM electrical pulse amplitude
A_i	Peak pulse amplitude at the pre-detection filter input
B	Source bit rate
B_L	PLL noise bandwidth
B_p	Required bandwidth for PPM transmission
B_n	Required bandwidth for naturally sampled PWM
B_U	Required bandwidth for uniformly sampled PWM
B_{min}	Minimum allowable receiver bandwidth
c	DPPM compression index
$c_{12\text{-}13}$	PLL timing capacitor
C_{DPIM}	DPIM information capacity
C_T	Receiver front-end total shunt capacitance
CNR	Carrier-to-noise ratio
CNR_{RC}	Carrier-to-noise ratio at the RC filter output
CNR_M	Carrier-to-noise ratio at the matched filter output
CNR_i	Carrier-to-noise ratio at the threshold detector of the DPIM receiver
CNR_c	Carrier-to-noise ratio at the threshold detector of the PCM receiver
E_i	Peak optical pulse energy at the DPIM photo detector
E_c	Peak optical pulse energy at the PCM photo detector
$E(\omega)$	Receiver equaliser transfer characteristics
E{ }	Ensemble average
L_s	Shortest DPIM frame
L_{avg}	Average DPIM code length
f_a	PIM average sampling frequency
f_b	PIWM average sampling frequency
f_c	Unmodulated sampling frequency of the analogue PTM schemes
f_d	DPPM slot frequency
f_f	Nyquist sampling frequency
f_g	Guard band requirements in PWM
f_m	Modulation signal frequency
f_s	DPIM slot frequency
f_v	Instantaneous sampling frequency variation
f_s	Slot rate
f_w	PWM slot rate
f_z	Frequencies of the troughs of the DPIM spectra
f_{DPIWM}	DPIWM slot rate
g_w	Guard band used in DPWM
G	Average detector internal gain
$G(f)$	Pulse shape transform
$h(t)$	Pulse shape at the detector
$h_{PD}(t)$	Pre-detection filter impulse response
HD_2	Second harmonic distortion level
HD_3	Third harmonic distortion level
$H_{PD}(\omega)$	Pre-detection filter frequency response
I_m	Number of time slots in DPIWM space
IF_{PWM}	*SNR* improvement factor in PWM

IF_{PPM}	*SNR* improvement factor in PPM
IF_{PIM}	*SNR* improvement factor in PIM
IF_{PIWM}	*SNR* improvement factor in PIWM
$J_k(\ )$	Bessel function of the first kind order k
$j!$	Factorial of j
K_D	Phase detector gain factor, V rad^{-1}
K_0	VCO gain factor, rad s^{-1} V^{-1}
L_n	Number of frames in the truncated window
L_{avg}	Average DPIM frame length
m_i	PIM modulation index
m_w	PWM modulation index
M	Bit resolution
M_c	Counter resolution
$n\{\ \}$	Number of elements in the vector
n_g	Guard interval
N_r	Number of real poles in the sub-optimum filter
N_c	Number of complex poles in the sub-optimum filter
P_C	Average power of PCM frame
P_D	Average power of DPIM frame
P_e	Probability of bit error of DPIM
P_f	Probability of False alarm error
P_e	Probability of Erasure error
P_P	Average power of DPPM frame
P_w	Probability of Wrong slot error
P_{symbol}	Probability of symbol error
$P_{\varepsilon 0}$	Probability of transmitted 0 being an error
$P_{\varepsilon 1}$	Probability of transmitted 1 being an error
P_{es}	Probability symbol error in DPPM
q	Electron charge
q_k	Quantisation noise
R_b	Optical detector bias resistance
R	Detector responsivity
R_F	Feedback resistance of the transimpedance amplifier
R_L	Receiver front-end total resistance
$R(k)$	Autocorrelation function
S	Vector of symbols
S_E	Two sided amplifier series noise source spectral height, $volt^2$/Hz
S_I	Two sided amplifier shunt noise source spectral height, $ampere^2$/Hz
S_m	m^{th} sample
$S_n(f)$	Double sided noise spectral density at the receiver
SNR_i	*SNR* of analogue PIM
SNR_p	*SNR* of analogue PPM
SNR_w	*SNR* of analogue PWM
SNR_{pw}	*SNR* of analogue PIWM
SNR_{out}	*SNR* at the receiver output
t_i	RMS full width of the received pulses
t_{pl}	DPIM sampling times
t_0	RMS full width of the pre-detection filter output
$t_{p\text{-}p}$	Peak-to-peak PIM pulse deviation
t_{RC}	Receiver time constant
t_w	Maximum pulse width deviation of PWM/PPM

t_{max}	Longest receiver time constant
T_a	Average PIM sampling time
T_d	DPPM time slot
T_k	Time delay to the k^{th} pulse in the DPIM pulse stream
T_s	DPIM slot period
T_b	Source bit time
T_c	Sampling time of the analogue PTM
T_f	Source frame period
T_{max}	Longest DPIM frame length
T_{DPIWM}	DPIWM slot time
t_{FWHM}	Full width half maximum pulse width
V_{DAC}	Conversion range of the DAC
V_{DC}	DC shift of the modulating signal
V_{DPIM}	Level shifted modulation signal
V_m	Modulation signal amplitude
V_{th}	Threshold level at the threshold detector
$v_{in}(t)$	Receiver pre-detection filter output
$v_{out}(t)$	Receiver threshold detector output
W	Receiver pre-detection filter bandwidth
W_m	Number of time slots in DPIWM mark
$x_p(t)$	Truncated DPIM signal
$x_B(t)$	Truncated DPIM signal
$X_p(f)$	Fourier transform of the truncated signal
$Z(\omega)$	Transfer characteristics of the receiver amplifier
α	Ratio of threshold level to peak pulse amplitude in DPIM
α_c	Ratio of threshold level to peak pulse amplitude in PCM
ε_d	Detection noise
φ	Maximum phase excursion in PPM
σ_c	RMS noise at the PCM receiver
σ_s^2	Clock timing variance
σ_τ^2	Threshold crossing timing variance
σ_{Fd}^2	Noise variance at the transimpedance amplifier
σ_{shot}^2	Dark current shot noise variance
$\sigma_{thermal}^2$	Thermal noise variance
ξ	PLL damping factor
γ	Pulse duty cycle within a time slot
τ_n	Random jitter
τ_p	PPM pulse width
τ_L	Time constant of the wide band receiver front end
θ_I	Phase of the input signal to the PLL
θ_0	Phase shift of the PLL output
ω_a	Angular frequency of the average PIM sampling process
ω_b	Angular frequency of the average PIWM sampling process
ω_c	Angular frequency of the unmodulated carrier signal
ω_m	Angular frequency of the modulation signal
ω_n	Natural angular frequency of the PLL
λ	Optical wavelength
λ_0	Dark current electrons per second

List of Figures

List of Tables

Contents

Chapter One

Introduction

Optical fibre transmission technology has made a significant progress in the past decade owing to the remarkable reduction of loss in the fibre and advancement of optical devices. In the early stage of development, when the silica glass fibres were first introduced, systems using short wavelength (0.8-0.9 μm region) and with multimode fibre were dominant. However, after lower attenuation was attained at longer wave lengths (around 1.1-1.5 μm), major efforts were concentrated on the development of systems in this region using single mode fibres [*Nakagami*]. Within the first decade of the deployment of optical fibre 60 % of the worlds' telecommunication traffic were carried by optical fibre and this is predicted to be 95 % by the turn of the century [*Cochrane*].

The major driving forces behind migration from copper based systems to fibre have been mainly economic and advancement of fibre technologies. Fibre cables are inherently less costly than copper cables due to their low material/refining costs

Technologically, they tend to have low loss (< 0.4 dB/km), negligible crosstalk, high immunity to interference, complete electrical isolation and are reported to offer virtually infinite bandwidth (≈ 50,000 GHz) [*Heatley91*] giving the perfect solution for bandwidth hungry applications likely by the end of the century. Thus, take up of optical fibre has reduced the per-channel installation and running costs owing to the greater available transmission capacity. Furthermore, repeater spacing has increased with different phases of development. Many optical fibre links today are repeaterless and those which require repeaters are migrating towards the optical amplifiers, thereby significantly reducing the component count along the route, increasing the link reliability.

The long term traffic growth on both national and international trunk telecommunication routes demand high speed transmission links. The first generation transoceanic optical-fibre (TAT 8) connected United States to the United Kingdom and France. It handles data rates upto 280 Mb/s and has been operational since 1988. This system uses 1.3μm zero dispersion fibre and a repeater spacing of 70 km across the Atlantic ocean, spanning a distance of 6000 km. The second generation system TAT 9/10/11 connects United States to the United Kingdom, France and Spain and has operated at 560 Mb/s. Advancement of technology enabled the TAT 9 series to operate at a wavelength of 1.5 μm in low loss fibre (less than 0.2 dB/km) [*Runge*]. Migration from 1.3 to 1.55 μm wavelength along with APDs (avalanche photo diodes) instead of PIN diodes gave improved repeater spacing of 150 km. Currently third generation optical fibre link has been laid between United Kingdom and Japan (FLAG-Fibre Optic Link Around the Globe). This is expected to handle data rates upto 5.3 Gb/s and when it is completed at the end of 1997 it will be capable of handling 600,000 simultaneous telephone conversations at the same rate as in TAT 8 [*Denniston*], [*Harrison*].

Fibre optic systems have already replaced coaxial-cable systems in high capacity applications as explained in the few examples above. With the advent of the information society, today optical fibre networks are being widely used to provide broadband telecommunication services through telecommunication networks. As the demand for telecommunication services has increased tremendously over the past few years the need to develop high speed networks/links was identified by the various types of information services providers. Emphasis is given on the Telco interoffice trunks, CATV trunks, mainframe interconnections and fibre to the curb for the natural end users of photonic communication technology.

Optical communication can play an important role in unguided applications too, such as in intersatellite and deep-space communication links and in diffused-radiation optical links in office environments. A few reasons for the consideration of optical systems for such applications are that they do not use scarce and expensive RF spectrum and provide an alternative to traditional RF systems. Optical wireless systems operate in the infrared region and are intrinsically broadband [*Wisely*]. Radiated signals are completely contained within the room in which the system is operating, thus security is better than either radio or microwave wireless systems and also can afford the required mobility within buildings. Currently optical wireless free space transmission systems are been proposed for simple remote controller through to local-area networks [*Gfeller*], [*Nicholls*] & [*Baister*].

Since the evolution of optical fibre technology, most of the research carried out has been to improve the physical properties of the fibre and the associated optical devices to improve the transmission throughput. Recently, the emphasis has been to develop efficient modulation techniques to achieve higher signal quality at the expense of vastly

available optical-fibre bandwidth. In this context pulse transmission techniques have drawn a considerable attention among many researchers world-wide. Pulse transmission techniques, such as pulse time modulation (PTM) are well known. In PTM a time parameter of each pulse in a train of pulses is modulated by the sample values of the message signal e.g. pulse width, position, interval. This technique can be used to trade bandwidth with higher receiver sensitivity. But bandwidth is not an issue anymore, only a fraction of the virtually infinite bandwidth offered by a single mode fibre has been used by current communication systems. The pulsing allows average laser power to be converted to narrow, highly peaked optical pulses to aid detection under noisy environment at higher data rate [*Prati*]. In many communication systems semiconductor lasers are modulated with either 50 % duty-cycle pulses or with analogue waveforms, but several applications demand more elaborate modulation formats in particular low duty cycle pulse operation. For example, pulse schemes are the preferred modulation scheme for direct-detection free space optical communication systems that are either adversely affected by high levels of background radiation (line-of-sight terrestrial links, airplane-to-airplane links), or in very low background environments, where the quantum aspects of light can be used to obtain high energy efficient transmission [*Katz*].

Analogue PTM techniques have been used in many applications such as audio, video and instrumentation signal transmissions. These schemes can deliver required signal-to-noise ratio (*SNR*) in many applications, but have been shown to suffer from non linearity problems due to the nature of the signal generation[*Wilson*95/2]. In contrast in digital PTM schemes this problem does not arise due to the use of advanced digital technology[*Ghassemlooy*93/3]. Pulse code modulation (PCM) has been the dominant digital PTM scheme that has been used since its introduction. Much of the current telecom infrastructure equipment is based on PCM schemes. This does not mean that

this is the only digital PTM scheme that can support high quality signal transmission. There are other digital PTM schemes available capable of delivering high quality signals with less circuit complexity compared to PCM. Out of many such schemes digital pulse position modulation (DPPM) has been studied by many researchers over the past decade and it has been shown to outperform PCM on similar platforms. Little or no attention has been paid to other digital PTM schemes such as the digital version of pulse interval modulation (PIM), pulse interval and width modulation (PIWM) and pulse width modulation (PWM). Analogue PIM had been used under experimental conditions for transmission of telephone and video signals and shown to give good receiver sensitivity in optical systems but shown to suffer from non-linearity introduced by the analogue circuitry at transmitter and the receiver [*Sato*78. This scheme has not been reported to be used since. A possible reason been the advancement of other digital schemes that can offer higher system performance such as PCM. Thus the potential of PIM has not been fully explored. In this work PIM is proposed in digital means, i.e. digital pulse interval modulation. This will not only avoid non-linearity introduced at the transmitter and the receiver but also enable to support discrete information. During this work the major emphasis is placed on the DPIM scheme as a discrete PTM scheme for information transmission at low-to-moderate speed.

1.1 Aims and Organisation of the Thesis

The aim of the work has been to investigate the transmission characteristics of DPIM over optical fibre link. This scheme is considered to be suitable for transmission of analogue as well as digital information.

The thesis is divided into 10 chapters. Following the introduction, chapter two gives a brief account of pulse time modulation techniques. The isochronous analogue and digital modulation schemes are further investigated.

Chapter three describes analogue and digital anisochronous pulse time modulation schemes. It also compares *SNR* performance of analogue schemes and information capacity of digital schemes.

Chapter four gives an introduction to DPIM. Code properties such as deriving fundamental slot frequency to support a particular source of information are presented. This is followed by a detailed account of spectral profile. Two approaches are considered in representing the spectrum. Both spectral models are simulated and compared with the results obtained from the prototype. The spectral variation is investigated in the presence of random and periodic signal inputs. The effects of pulse width, dispersive channel nature and the bit resolution on the slot spectra is also presented.

Chapter five, gives a detailed account of a DPIM point-to-point link at a functional point of individual sub systems. The chapter starts by describing the functionality of the modulator and demodulator for analogue and digital signals, then goes on to investigate the variation of the slot rate with bit resolution. The average power of DPIM frame is compared with DPPM and a means of reducing it is suggested. Receiver architectures for the scheme are presented which include pre-detection filter strategies, different threshold detectors and synchronisation. Finally the maximum slot rate that the link can operate is estimated.

Chapter six presents a detailed mathematical analysis of the receiver operation and system performance. Analysis is performed for a wide-band as well as for a narrow

band channel. Signal detection at the receiver employing a matched filter and a simple RC filter is discussed. Error sources that degrades DPIM system performance are presented and a detailed analysis of their effect under various receiver and channel conditions, such as threshold level, received pulse width, bit resolution, receiver bandwidth, are presented. Expressions for the system probability of error are developed in terms of carrier-to-noise (*CNR*) ratio and the simulated results are compared with that of DPPM and PCM. For analogue systems the output signal-to-noise ratio (*SNR*) is mathematically modeled against *CNR* and simulated results are compared with that of PCM.

Chapter seven discusses the detailed implementation of the point-to-point DPIM prototype link. Modulator and demodulator operation together with relavent waveforms are presented.

System resullts are presented in chapter eight and are compared with predicted performance. The chapter starts by presenting the spectral power variation of the slot component with the modulation index and continues on to cover *SNR*, system linearity. Finally the results are presented for the system probability of error for varying threshold level and bit resolutions.

Chapter nine is devoted to conclusions and the major contributions of this thesis.

Chapter ten describes further work.

Chapter Two

Pulse Time Modulation Schemes

There are a number of modulation techniques available to suit various types of communication applications. In this chapter a brief account of currently available modulation schemes are presented and an introduction to pulse time modulation (PTM) is given. A special emphasis is placed on isochronous PTM schemes.

2.1 Introduction

The dawn of today's communication era was laid by Samuel *Morse* with his first telegraph message in 1838. Today, communication systems are deployed wherever information is to be transmitted from one point to another. These systems fall into many categories: systems that deliver global news coverage to homes such as terrestrial/satellite/cable television; radio; long distance telephone links; computer networks that span the entire globe; radar telemetry systems that play a vital role in navigation; defence; undersea research; and even inter planetary systems that are searching for extra terrestrial intelligence.

A communication system is a totality of mechanisms that provides the information link between source and destination, see Fig. 2.1. The transmission channel may be copper, optical fibre, liquid media, or free space.

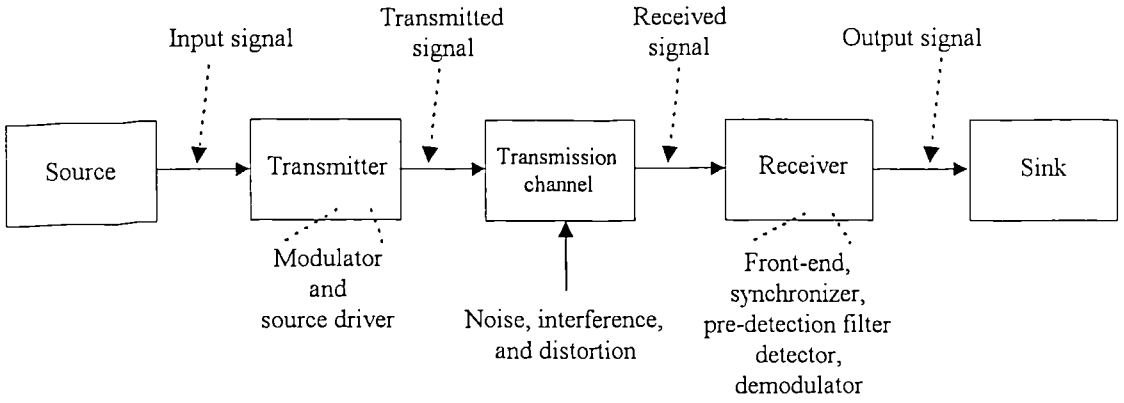

Fig. 2.1 General elements of a communication system

The aims of the designers of all the communication systems are to represent the information in such a way that it will be delivered to its destination efficiently, with minimum errors and at low cost. To a large extent, the efficiency of a communication system in a given mission depends on how the information is represented or on the modulation scheme, so much so that the type of modulation is a pivotal decision in a system design. Since *Morse* introduced telegraphy, different modulation techniques have evolved to enhance various aspects of system performance. As new requirements came into being, new techniques were introduced.

The classification of currently available modulation schemes may be given as in Fig. 2.2, modifying the PTM tree presented by [*Wilson*91/92/93]. Modulation techniques can be mainly divided into three categories, namely analogue, pulse and digital. AM, FM and PM are analogue modulation schemes, where the amplitude, frequency and phase of an analogue carrier is varied continuously depending on the instantaneous signal

amplitude. On the other hand ASK, FSK and PSK are digital modulation schemes where amplitude, frequency and phase of an analogue carrier is varied discretely with the incoming data.

Pulse modulation schemes fall into two main categories, i.e. analogue (continuous) and digital (discrete). In analogue schemes, some time property of a stream of pulses is varied continuously in sympathy with the modulation signal. On the other hand, in digital schemes each discretised amplitude of the modulating signal is presented by means of varying a pulse property in discrete time. Time taken by a sample may vary depending on the modulation scheme, i.e. isochronous schemes represents a sample by a fixed time period (fixed frame) whereas anisochronous schemes take variable time period (variable length frame). Furthermore, discrete time correspond to samples can be reorganised in such a way that it will improve the transmission characteristics. This is called encoding and is only possible with digital PTM schemes.

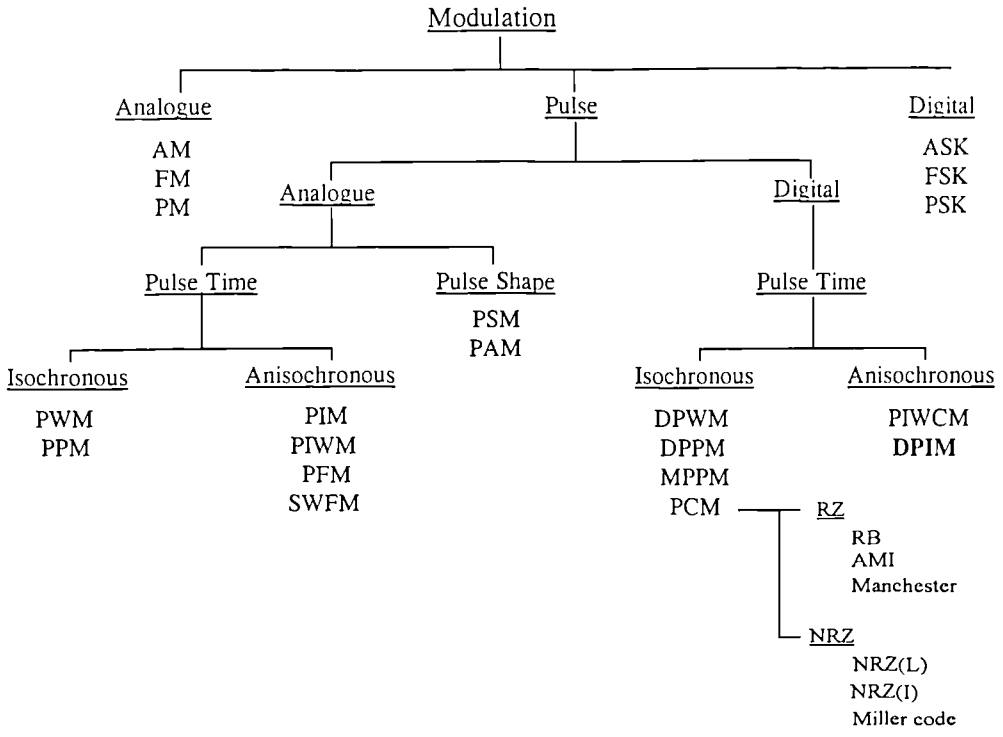

Fig. 2.2 Modulation tree.

Analogue pulse modulation can be further divided into pulse time and pulse shape. Pulse slope modulation (PSM) and Pulse Amplitude Modulation (PAM) are examples of pulse shape modulation. In PSM, the positive slope of the pulse carrier is modulated by the information [*Issa*], whereas in PAM the pulse amplitude is modulated. In these two schemes the physical appearance of the pulses are modulated, therefore, the system performance depends on the linearity of the light sources. Thus, their application in fibre based systems are limited.

In Pulse time modulation schemes, one of many time properties of a pulse carrier is modulated by the information, see Table 2.1 [*Wilson*93]. PTM techniques have been shown to offer carrier-to-noise ratio (*CNR*) inversely proportional to system bandwidth [*Jelonek*]. Thus, in the optical fibre domain, the enormous available bandwidth can be utilised to deliver the required *CNR*. Adoption of PTM techniques has certain beneficial consequences from the standpoint of opto-electronic sub-system specification. Since PTM techniques deals exclusively with a pulse format, there are no concerns over LED or laser diode linearity, as would be the case with analogue intensity modulation schemes over optical fibre. In addition, for narrow pulse formats, the peak optical output power may be maintained at a high level to ensure good noise performance at the receiver without compromising the device lifetime. PTM scheme may be chosen primarily for their maximum peak power level, with little regard to device linearity, in order to maximise receiver noise performance [*Grieg*].

PTM scheme	Variable
PPM/DPPM/MPPM	Position
PWM/DPWM	Width (duration)
PIM/DPIM	Interval
PFM	Frequency
PIWM/DPIWM	Interval and width
SWFM	Frequency

Table. 2.1 PTM family.

All the above PTM schemes fall into two categories depending on the sampling form, namely anisochronous and isochronous. In the former category, the sampling frequency component of the pulse train varies with the instantaneous amplitude of the modulating signal and there is no fixed frame structure. In pulse frequency modulation (PFM), the instantaneous frequency of a train of narrow pulses is determined by the modulating signal amplitude, Fig. 2.3a. Pulse density variation is analogous to frequency variation in analogue FM. PFM has been used extensively for the optical fibre transmission of video and broadcast quality TV signals [*Heatley*83], [*Wilson*93] & [*Wu*]. Square wave frequency modulation (SWFM) is closely related to PFM, where the pulse stream consist of square wave edge transitions occurring at the zero crossing points, Fig. 2.3b. This scheme is employed for the transmission of HDTV and other wide-band instrumentation signals over fibre links [*Wilson*93,95], [*Ghassemlooy*93/1]. SWFM can be derived from PFM by simply sending the PFM pulse stream through a bistable; conversely, PFM may be obtained from SWFM by means of differentiating the pulse edges.

In pulse interval modulation (PIM), variable intervals between adjacent narrow pulses are determined by the instantaneous amplitude of the modulating signal, Fig. 2.3c. Pulse interval and width modulation (PIWM) is derived directly from PIM, by means of

sending it through a bistable, Fig. 2.3d. Information is imbedded in both the mark and space periods. Discrete version of both PIM and PIWM have been introduced by *Ghassemlooy et al* namely DPIM [*Ghassemlooy*95/1], [*Kaluarachchi*96/2] (Fig. 2.3e) and DPIWM [*Ghassemlooy*95/2] (Fig. 2.3f) respectively. In these digital schemes information is encoded in terms of discrete time slots. The anisochronous nature suggests that each successive frame commences immediately after the previous pulse, unlike isochronous schemes.

In isochronous schemes a time property, such as the position or width of a pulse, is modulated in sympathy with the instantaneous modulation signal, but a constant sampling frequency is maintained. In pulse width modulation (PWM), the width of the pulses within a predetermined time frame is modulated according to the sampled value of the modulating signal, see Fig. 2.4a. Pulse position modulation (PPM), may be considered as differentiated PWM, and carries information by virtue of the continuously variable position of a narrow pulse within a fixed frame, see Fig. 2.4b. In the digital domain, PTM schemes encode source data, rather than modulate a pulse carrier.

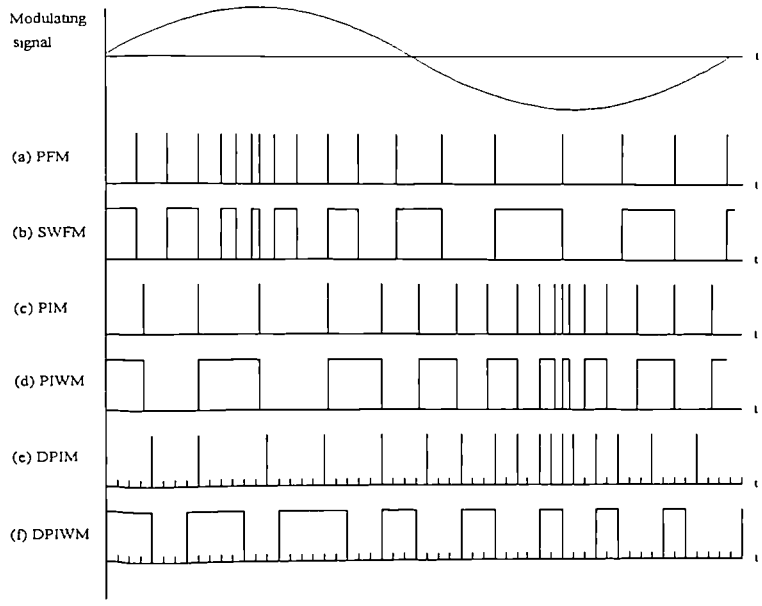

Fig. 2.3 Anisochronous PTM techniques.

Digital versions of PWM and PPM are namely DPWM (Fig. 2.4c) and DPPM (Fig. 2.4e) respectively, which employ discrete time slots to represent discritised samples within an isochronous frame. Pulse code modulation (PCM) (Fig. 2.4d) is a digital isochronous PTM scheme. It has become the dominant pulse modulation format in optical fibre communication systems largely due to its high *SNR* ratio and low distortion performance, coupled with the ease with which waveforms may be regenerated in both long-haul links and multi-point networks.

Other PTM techniques have not been as popular, due to high bandwidth requirements, even though they tend to give high *SNR* ratios and have less complex circuitry [*Biase*], [*Grieg*]. However, bandwidth is not a major issue at the moment since optical fibre offers virtually infinite at low cost. Thus, investigation of other alternative PTM schemes is worthwhile for efficient information transmission in various applications.

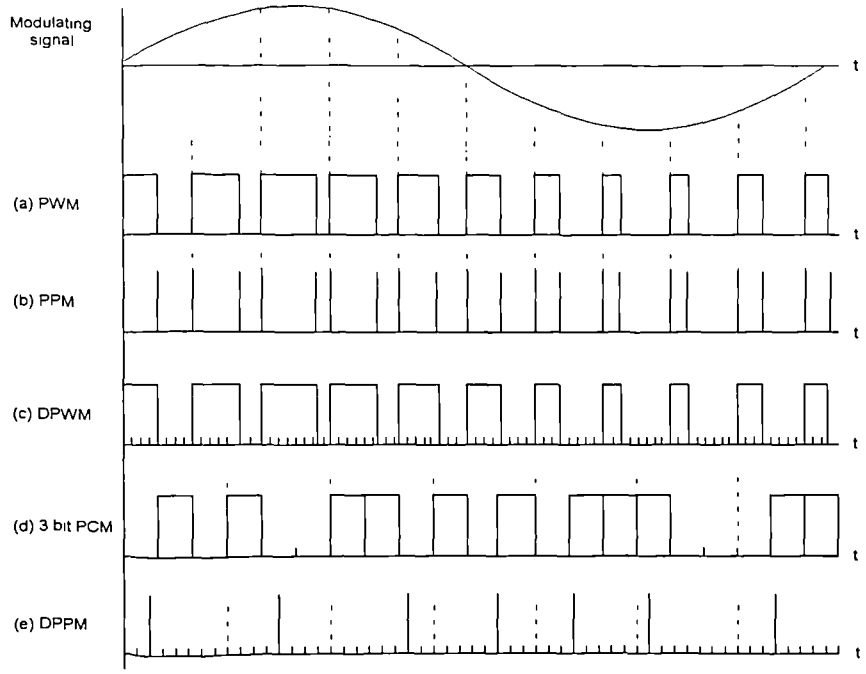

Fig. 2.4 Isochronous PTM techniques.

2.2 PTM Spectra

A closer look at PTM spectra reveals that both analogue and digital PTM schemes show unique profiles. Analogue PTM spectra is derived from a continuously varying pulse stream in continuous time, similar to spectra of analogue modulation schemes, and consists of a diminishing set of side tones centred around the carrier (sampling) frequency and its harmonics. Side tones are separated in frequency by an amount equal to the modulating frequency. The number and the strength of the side tones is a characteristic unique to each PTM technique. In addition, a baseband component is also present in some PTM methods along with harmonics depending upon the form of sampling employed in the modulator [*Wilson*93]. Whereas, digital PTM spectra are derived from rectangular pulses and discritised time, which is a function of rectangular pulse shape transform.

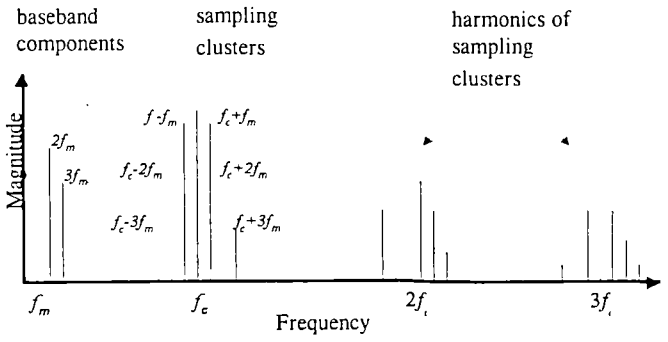

(a)

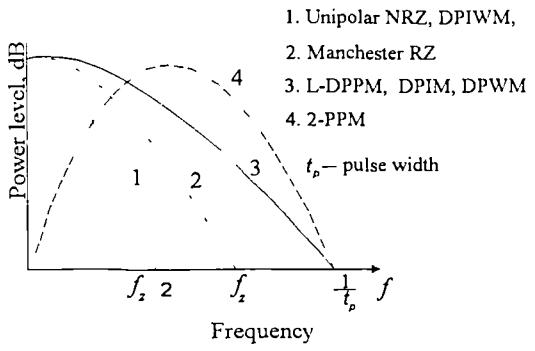

(b)

Fig. 2.5 PTM spectral profile, (a) analogue PTM, (b) digital PTM.

Figure 2.5(a) and (b) shows the general spectral profile for analogue and digital PTM schemes, respectively, where f_m is the baseband, f_c is the sampling frequency for analogue schemes, f_z is the clock frequency of PCM schemes and t_p is the pulse width in 2-PPM, L-DPPM and DPWM schemes.

In analogue PTM spectra, the side tone profile is unique to each scheme. In addition the base band component and its harmonics are also present in some schemes, depending on the form of sampling employed in the modulator, i.e. uniformly sampled or naturally sampled. Naturally sampled modulators operate directly on the input signal, and the precise sampling instants are variable and determined by the location of the pulse edges. For uniform sampling, the input signal is routed via a sample and hold circuit which produces flat-topped amplitude modulated pulses, so that the PTM modulator is operating on uniformly spaced and stored input samples. It is not necessary that modulation imposed on the pulse stream should be the same type as at the final demodulation stage. Certain properties of different schemes can be used to enhance the link performance. It is sufficient if, in the sequence of pulse transformations in the modulator and demodulator, some characteristic of the pulse shape or position is linearly preserved. Hence, for the final demodulation stage a type of pulse modulation can be chosen which gives low distortion even at low recurrence frequencies or reinstates the baseband component. For example, SWFM does not contain the baseband component in the spectra, but can be converted to PFM by simply differentiating it to reinstate the baseband components. Thus, different stages of modulation can be used within a transmission link to improve system performance in terms of complexity or cost. In contrast, digital PTM spectra is based on the pulse shape transform. For rectangular pulses this can be given as in Fig. 2.5(b): troughs in the spectrum for unipolar pulses are determined by the clock frequency and the pulse width. For

example, in non-returned-to-zero (NRZ) or full slot PCM pulses, troughs are placed at harmonics of half the slot frequency ($nf_z/2$, $n \in 1,2,3...$). In the other schemes shown, the pulse width is shorter than a full slot, thus the trough positions vary accordingly. DPIM, PIWM, *L*-DPPM, PWM and PCM-RZ spectral profiles can also be explained using the above phenomenon. Spectra corresponding to certain digital PTM schemes consist of distinct slot or frame rate components, which is used for clock phase extraction at the receiver. Chapter four gives a full detail analysis of the DPIM spectral characterisation.

Analogue PTM schemes have been employed in many applications, but a very little work has been done on their digital counterparts. PCM is the only modulation scheme that has been reported and widely been used. Recently, with the development of semiconductor technology and applications in different areas of communication, DPPM has drawn a considerable attention as a suitable alternative modulation scheme, specially in the areas of optical fibre long haul as well as deep space probes and wireless applications [*Sun*90/2], [*Cryan*93/1] & [*Kahn*]. However, the potentials of DPIM, DPWM, DPIWM have not been widely explored. In this work, DPIM is investigated for its suitability in optical fibre communication systems. In the remainder of this chapter, digital and analogue isochronous PTM schemes are briefly explained, mainly to aid comparisons made in a later chapter of the thesis.

2.3 Isochronous Modulation Schemes

Analogue or digital information is transmitted in fixed blocks, or, in other words, fixed frames. Modulation is imposed on the pulse stream, consisting of fixed carrier frequency or frame frequency. The frame frequency is determined solely by the choice of modulating signal maximum frequency. Analogue PTM schemes, such as PWM,

PPM, as well as digital schemes such as PCM, DPPM and DPWM, fall into this category. In the following sections each of these schemes are briefly explained.

2.3.1 Analogue pulse width modulation (PWM)

In PWM the width of a constant amplitude pulse carrier within an isochronous frame is modulated in sympathy with the modulating signal. Leading, trailing or double edge modulated PWM may be generated by comparison of the input signal with a linear ramp waveform, triangular in the case of double-edge-modulation. Leading or trailing edge modulated PWM may be generated by comparison of the modulating signal with a constant amplitude linear ramp waveform, see Fig. 2.6. The frequency of the ramp signal is constant and must be equal to or greater than twice the modulating signal frequency [*Suh*]. PWM may again be divided into two categories depending on the sampling form: naturally sampled PWM (NSPWM) or uniformly sampled PWM (USPWM). In the former case, comparison is directly carried out at the comparator, whereas in the latter case the level shifted modulating signal is routed first through a sample and hold circuit where samples are equally spaced in time irrespective of the input signal amplitude, see Fig. 2.6. The comparator gives a logic high output as long as the ramp waveform stays below the level shifted modulating signal.

The trailing edge modulated naturally sampled PWM pulse train may be expressed as [*Wilson*93],

$$u(t) = \frac{1}{2} + \frac{m_w}{2}\sin\omega_m t + \sum_{n=1}^{\infty}\frac{\sin\left(n\omega_c t\right)}{n\pi} - \sum_{n=1}^{\infty}\frac{J_k\left(n\pi m_w\right)}{n\pi}\sin\left(n\omega_c t - n\pi\right) - \sum_{n\ 1}^{\infty}\sum_{k=\pm 1}^{\pm\infty}\frac{J_k\left(n\pi m_w\right)}{n\pi}\sin\left[\left(n\omega_c + k\omega_m\right)t - n\pi\right] \tag{2.1}$$

where m_w is the PWM modulation index ($0 < m_w < 1$), ω_m and ω_c are the modulating signal and carrier angular frequencies, respectively. $J_k(x)$ is the Bessel function of the first kind, order k.

The second term of Eqn. 2.1 shows the base band component, whereas the combination of the third and fourth components produces the carrier frequency and its harmonics. The double summation represents the characteristic PTM series of diminishing side tones set around the carrier frequency and all its harmonics, see Fig. 2.7.

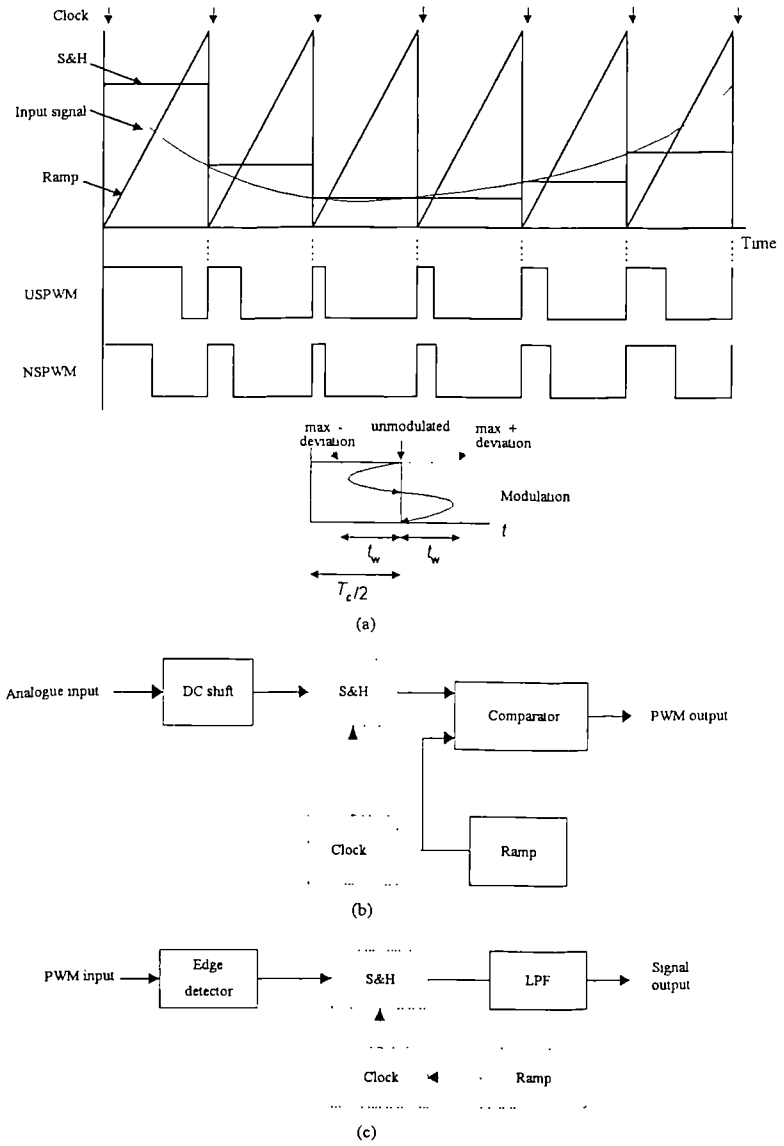

Fig. 2.6 PWM signal generation: (a) PWM waveforms, (b) modulator and (c) demodulator.

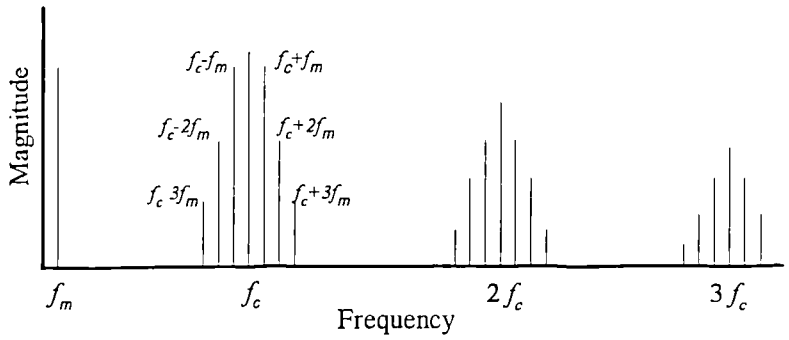

Fig. 2.7 Naturally sampled PWM spectrum.

In comparison, USPWM spectrum contains harmonics of the signal frequency in the baseband region [*Wilson*88,91]. Thus, at the receiver, conversion to PAM waveform is required before the filtering process, whereas demodulation of NSPWM is accomplished by threshold detection and simple low pass filtering. From the hardware point of view, NSPWM is preferred because of its simplicity. However, if the pulse duration is small compared to sampling period, then the difference between these two schemes is insignificant [*Carlson*]. The main advantage of USPWM is that it produces lower distortion and higher signal to noise ratios by virtue of the greater modulation index that may be used [*Ghassemlooy*94].

In both PWM schemes, the amplitudes of the side tones increases with the sampling ratio and the modulation index. The modulation index is defined as the maximum pulse width deviation to the unmodulated pulse width, when the unmodulated pulse width is half the sampling time, see Fig. 2.6, The modulation index, m_w can be expressed as,

$$m_w = 2\frac{t_w}{T_c} \tag{2.2}$$

where t_w is the maximum pulse width variation, see Fig. 2.6. The unmodulated pulse width is assumed to be $T_c/2$, where $T_c = 1/f_c$. The optical bandwidth requirements for USPWM is [*Ghassemlooy*91/1],

USPWM $B_u = f_m(3 + \pi m_w) + 2f_g$ (2.3)

and for NSPWM is,

$$B_n = f_m \tag{2.4}$$

where f_m is the baseband frequency and f_g is the guard band.

The *SNR* of the regenerated signal at the NSPWM optical receiver output is given by,

$$SNR_n = \left(\frac{m_w}{2}\right)^2 CNR \tag{2.5}$$

and for the USPWM system,

$$SNR_u = \frac{1}{2}\left(\frac{m_w \pi B_u}{2f_c}\right)^2 CNR \tag{2.6}$$

From Eqns. 2.5 and 2.6 it is evident that the performances of both the PWM schemes are modulation index dependant. Furthermore, from Eqns. 2.3 to 2.6, USPWM performance is also bandwidth as well as sampling ratio dependant. The main factor that determines the maximum modulation index is the linearity of the analogue ramp. For the transmission to be linear, the ramp waveforms employed at the transmitter and the receiver should be identical, since any nonlinearity here will cause harmonic distortions in the recovered signal [*Berry*]. This is not always achievable due to component tolerances and operating conditions. *Ghassemlooy et al* reported that for good linearity system should be operated below modulation index of 50 % when it gives 2nd harmonic distortion of -35 dB, for higher indices the harmonic distortion further increases accordingly [*Ghassemlooy*94]. However, this short coming can be avoided by adopting digital techniques for implementing PWM, thus the name digital pulse width modulation (DPWM) [*Ghassemlooy*93/3]. Here the pulse widths are defined in terms of

discrete time slots which are proportional to the instantaneous amplitude of the modulating signal. Figure 2.8 shows the system block diagram.

The modulator contains a M bit counter which counts from 0 to 2^M-1 within the sampling period. Thus the counter clock frequency f_w is determined by,

$$f_w = f_c\left(2^M + g_w\right) \tag{2.7}$$

Where f_c is the sampling frequency as in analogue PWM. A few additional time slots (g_w) are included in each PWM frame to avoid pulse overlapping.

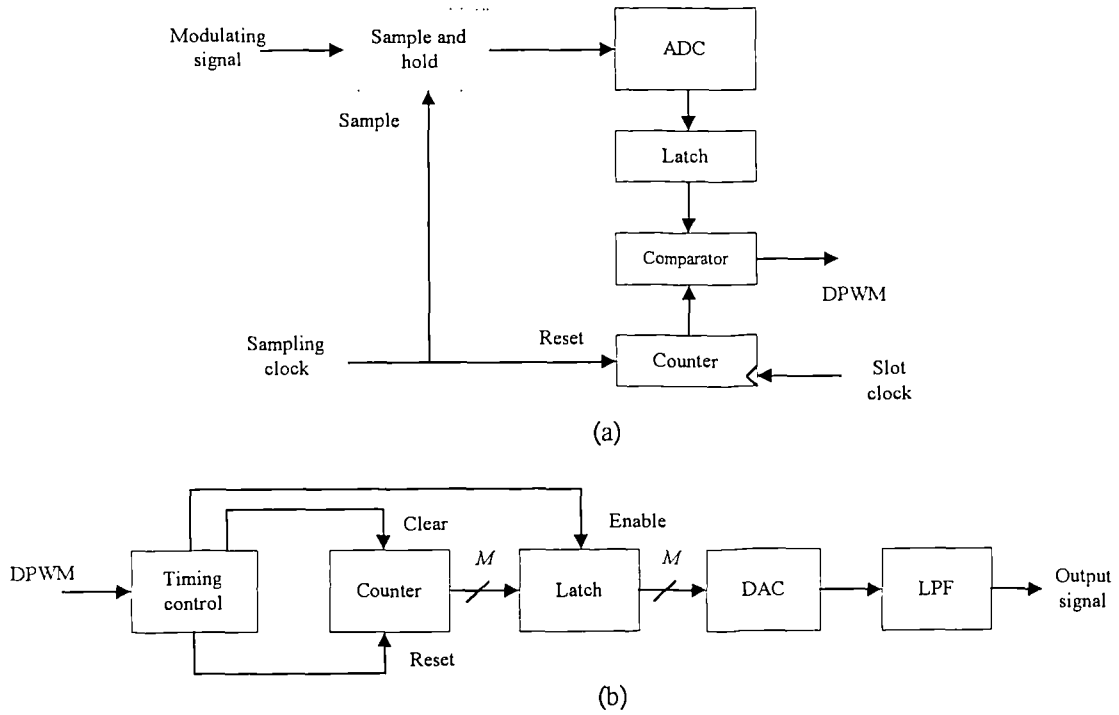

Fig. 2.8 DPWM system block diagram (a) modulator and (b) demodulator.

The counter is reset to zero at every sampling instant. The counter output is compared with the latched symbol corresponding to the present signal sample, i.e. the output from the ADC. When they are equal, the comparator output goes low generating the desired DPWM signal. At the demodulator a counter is employed which simply counts the number of clock cycles for which the DPWM input signal is active. The DAC generates a PAM signal from the recovered symbols, which is then sent through a low pass filter

to extract the transmitted signal. This scheme has been shown an exceptional linearity compared to analogue PWM and does not suffer from harmonic distortion at higher modulation indices. However, it suffers from quantisation error. Quantisation error can be minimised by choosing higher resolution ADC/DAC. Results presented by *Ghassemlooy* shows that digital PWM outperforms analogue PWM by up to 6-10 dB when operated at 50 % modulation index [*Ghassemlloy*93/3].

2.3.2 Analogue pulse position modulation (PPM)

In PWM, information is represented by the stretched pulse edges in each frame. One of the main disadvantages of PWM is its power requirement compared to short duration PTM schemes. At low modulation indices the power penalty is not as severe as in high modulation indices, where the power fluctuation is at its greatest. For an optical system this is not desirable. Therefore, an alternate scheme which avoids this problem and provides high peak power and low average power is preferable. One way of achieving this is by simply generating a short pulse corresponding to the modulated edge of the PWM. This scheme is better known as pulse position modulation or also named as differentiated PWM which carries information by virtue of the continuously variable position of a narrow pulse within a fixed time frame. In applications which demand low harmonic distortion, uniformly sampled PPM is used, whereas when harmonic distortion is not critical, naturally sampled PPM is more attractive because of its simplicity and low cost [*Muoi*78], see Fig. 2.9. The PPM frequency spectrum is very similar to that of the PWM except that there is no base band component. However, *Ghassemlooy* has shown that in real systems the spectrum does contain a baseband component, which disappears when the pulse width tends to zero [*Ghassemlooy*93/4].

The spectra is a function of the modulating signal frequency, pulse duration, modulation index and carrier pulse amplitude.

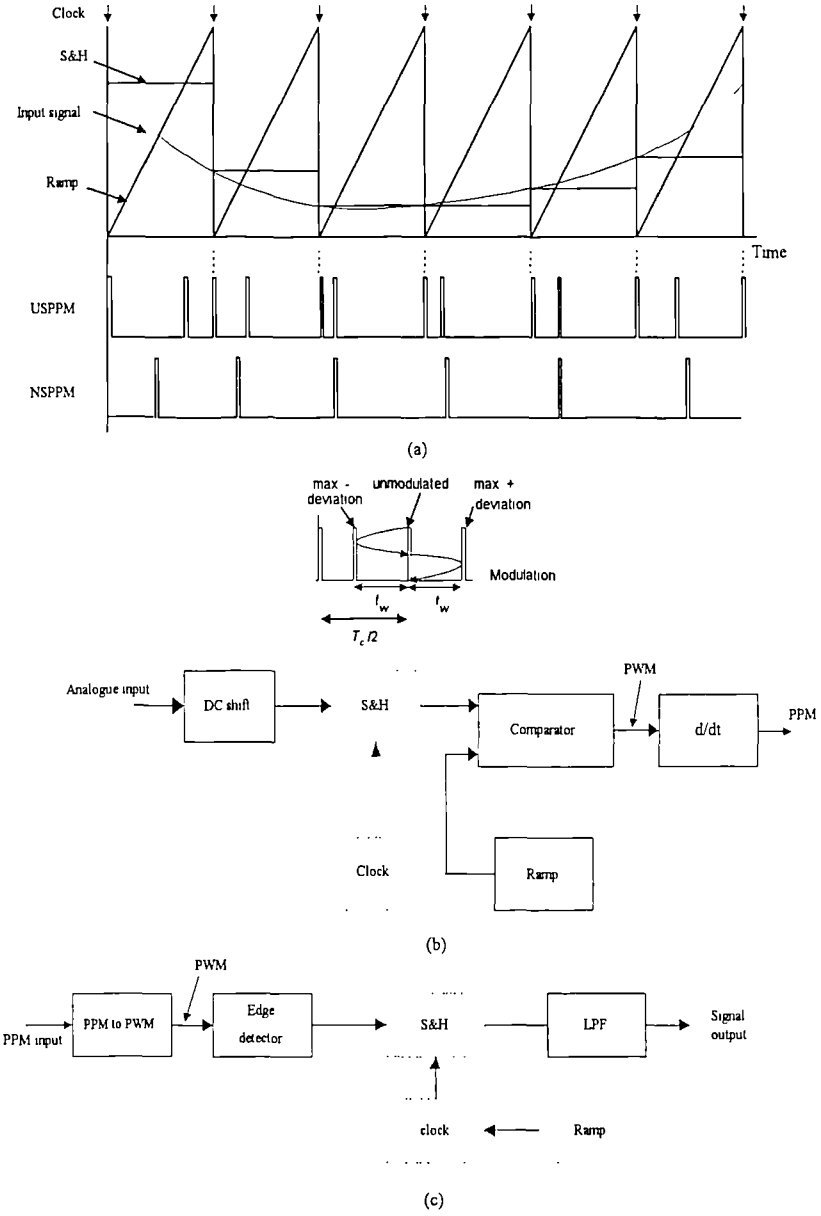

Fig. 2.9 PPM system: (a) PPM waveform, (b) modulator and (c) demodulator.

The spectrum was presented for fixed finite width pulses [*Ghassemlooy*92] as,

$$f(t)=\frac{V_o}{\pi}\Big[\omega_c\tau_p+\varphi\sin\omega_m\tau_p\cos\omega_m t+ 2\sum_{n=-\infty}^{\infty}\sum_{k=1}^{\infty}J_n(k\varphi)\sin\left(\frac{\sin(k\omega_c+n\omega_m)\tau_p}{k}\right)\cos(k\omega_c+n\omega_m)t\Big] \tag{2.8}$$

where V_o is the pulse amplitude, ϕ is the maximum phase excursion corresponding to peak pulse deviation, ω_c is the sampling frequency, ω_m is the input frequency, τ_p is the pulse width and $J_k(x)$ is the Bessel function of the first kind of order k. In the Eqn. 2.8, the first term is the dc component of the unmodulated pulse carrier wave, the second term is the baseband component in differentiated form while the last term shows the phase-modulated carrier signal producing spectral components at the carrier frequency ω_c and its harmonic frequencies along with the cluster of side-tones separated by an amount equal to the modulating signal ω_m, see Fig. 2.10. In PPM, demodulation is normally carried out by converting it into PWM (equivalent to integrating) and then low pass filtering, see Fig. 2.9.

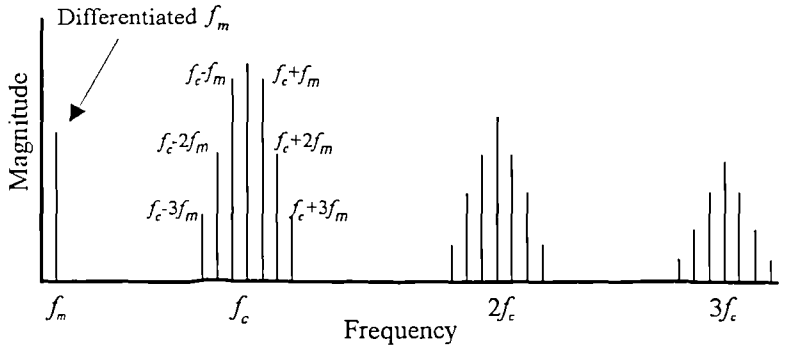

Fig. 2.10 PPM spectra.

PPM systems have been reported by many authors. *Holden* used PPM to transmit an audio signal of frequency band limited to 3.4 kHz [*Holden*]. Here, the PPM clock or the carrier frequency was extracted directly from the incoming data stream at the receiver by means of employing a PLL. *Van Den Broeke* multiplexed PPM in transmission of video surveillance information in subway stations and distribution of video data at airports. In this work, PPM was favoured over amplitude and frequency modulation schemes as PPM does not suffer from non linearity which could cause crosstalk between the video signals [*Van Den Broeke*93,95]. PPM shows a threshold effect, a

level below which the output is severely affected by false pulses due to noise crossing the threshold level [*Blachman*], [*Hubbard*]. In this work, it was shown that the signal-to-noise ratio becomes negligibly small within 1 dB below the threshold. *Ghassemlooy* derived a general *SNR* expression for NSPPM, when the modulation index is given by Eqn. 2.2 [*Ghassemlooy*91/1], but in this case t_w is defined as the maximum pulse deviation.

$$SNR_p = \left(\frac{m_w \pi B_p}{2 f_c}\right)^2 CNR \tag{2.9}$$

where B_p is the bandwidth requirements for PPM transmission, and is given by,

$$B_p = \frac{1}{\tau_p} \tag{2.10}$$

where τ_p is PPM pulse width.

Equation 2.9 shows that the PPM *SNR* is dependant on the modulation index and the bandwidth expansion. The modulation index is limited by the pulse width. System linearity depends on the linearity of the ramp signals employed at the transmitter and the receiver. Linearity dependence performance is minimized by incorporating digital techniques as in DPWM. The next section looks at the digitally generated PPM or DPPM.

2.4 Digital Pulse Position Modulation (DPPM)

DPPM can be used to transmit an analogue signal or a block of symbols. In the former case, input to the DPPM modulator is M bit symbols generated by an ADC. The DPPM frame time is made equivalent to the sampling time of the analogue signal. In the later case, the frame time is equivalent to the M bit symbol time. Figure 2.11 shows the

parameters used to describe a DPPM frame. An M bit symbol is encoded as a single pulse of one time slot duration placed in a frame of L time slots (T_d), where $L = 2^M$ accommodating all the M bit symbol permutations. A guard space is introduced in each frame to avoid inter frame interference due to dispersion in narrow band channels. Thus, an actual frame is a combination of a guard space and an effective frame. The ratio of effective frame to actual frame is given in terms of compression index (c), which is also known as modulation index in most of the literature on DPPM. The number of time slots in the guard band is given by $(1-c)\log_2 L/c$. The compression index determines the effective frame, hence the slot width. The higher the compression index the longer the effective frame and vice versa.

A DPPM time slot T_d can be represented by,

$$T_d = \frac{c\log_2 L}{L} T_b \tag{2.11}$$

where T_b is the source bit period.

The slot frequency (f_d) can be determined by,

$$f_d = \frac{LB}{c\log_2 L} \tag{2.12}$$

where B is the source bit rate.

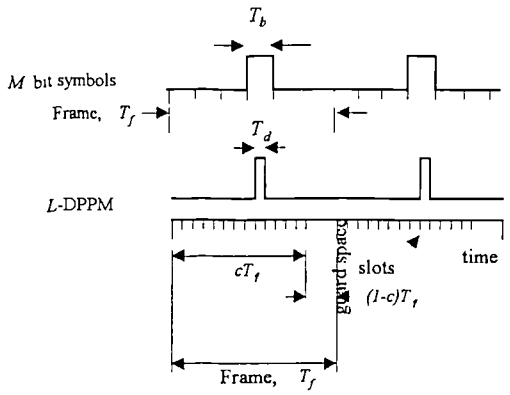

Fig. 2.11 A typical DPPM frame.

The pulse stream shown in Fig. 2.11 can be represented by,

$$x(t) = \sum_{k=-\infty}^{\infty} g\left(t - kT_f - S_k T_d\right) \tag{2.13}$$

where S_k represents the random symbol sequence coded into DPIM process.

This scheme was initially proposed in the late 1960s as a suitable modulation scheme for deep space communications [*Karp*]. It was shown that information capacity can be increased by selecting a higher symbol level. But the drawback is as the symbol level increases the slot width or the pulse width reduces, demanding higher transmission bandwidth. *Garrett* proposed DPPM for optical fibre communications, where bandwidth is not a bottleneck. In this work he showed that receiver sensitivity is optimum for coding level of M = 5 and a matched filter followed by a proportional-derivative and delay network can be used to improve the detection process [*Garrett*83/1,2]. *Calvert* reported receiver sensitivity improvement upto 4.2 dB [*Calvert*], whereas *Garrett* reported a further 3.5 dB more compared to equivalent PCM [*Garrett*89]. Further improvement is possible when using APDs over long haul communication links [*Pires*]. *Matin* investigated DPPM over local area networks and concluded that it is feasible to deploy DPPM which provide pulses with higher peak power than that of PCM [*Matin*89,92]. This is ideal for applications where laser or LED is used as an optical source. Furthermore, high peak narrow optical pulses aid detection under noisy environment [*Prati*].

Figure 2.12 shows block diagram representation of the modulator and demodulator for transmission of an analogue signal or a block of symbols. System modulator and demodulator are shown in Fig. 2.12 and can be simply described as follows. The input to the modulator is either a serial bit stream of B bps or M bit symbols from an ADC at

symbol rate of $f_f = 1/T_f$. In the former case, serial to parallel conversion has taken place while in the latter the ADC converts the modulating signal to M bit symbols. In both cases, symbols are stored into the data latch in a controlled manner defined by an enable signal. This signal allows a sufficient time for the comparator to identify the symbols in the latch before comparison takes place. The counter is clocked at the slot rate and is reset by the source symbol rate. The slot frequency is chosen to be an integer multiple of the symbol frequency and the two signals are in phase with each other.

From Eqn. 2.12,

$$\frac{f_d}{f_f} = \frac{L}{c} \tag{2.13}$$

To include a guard space in an each frame, the counter resolution (M_c) should be selected to be higher than the symbol resolution. When the counter output is equivalent to the source symbols the comparator gives a pulse of one slot duration. This is in fact the DPPM signal.

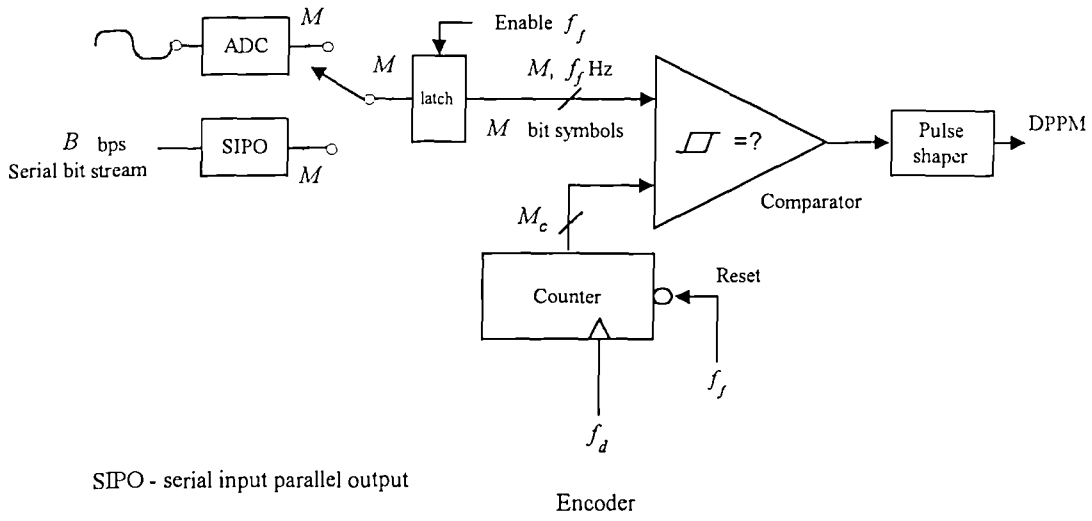

(a)

Fig. 2.12 (a) DPPM block diagram: Modulator for an analogue or a digital link

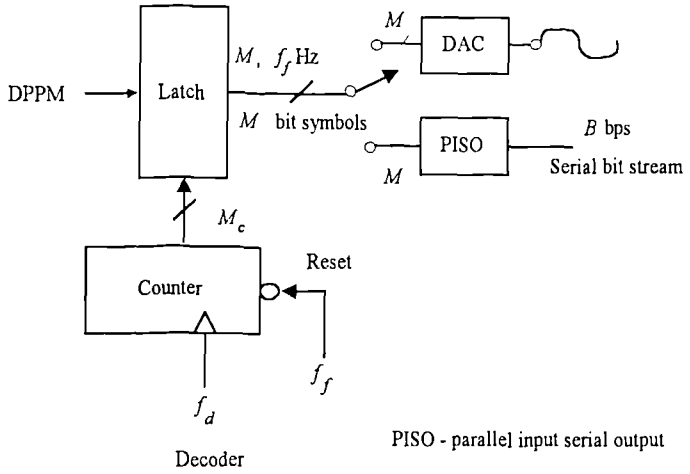

(b)

Fig. 2.12 (b) DPPM block diagram: Demodulator for an analogue or a digital link.

A pulse transform circuit is applied at the comparator output if a different form of pulse is required. The guard band is chosen by selecting c according to Eqn. 2.12 and the counter is selected with resolution of M_c such that $M_c > L/c$.

At the receiver the incoming DPPM signal is used to extract slot frequency and frame phase [*Elmirghani*94/1,3], [*Davidson*89], [*Sun*90]. The recovered slot clock is used as the clock for the counter and the frame clock resets the counter at regular frame intervals. The counter output is latched on occurrence of a pulse in the incoming signal. In the case of analogue signal transmission the latched symbols are sent through a DAC and the original signal is reconstructed, whereas for discrete information source the latched symbols are sent through a parallel to serial converter. DPPM spectral profile has been presented by *Elmirghani* for pulse shape of $g(t)$ as [*Elmirghan*94/1,95],

$$S(f) = \frac{1}{L_n T_d \left(\frac{L}{c}\right)} \left\{ \left| G(f) \sum_{k=0}^{L_n} e^{-j\pi f T_d \left(k\frac{L}{c} + \frac{S_k}{T_d}\right)} \right|^2 \right\} \qquad (2.14)$$

where L_n is the number of DPPM frames used in the spectral realisation and $G(f)$ is the pulse shape transform $G(f) \triangleq \Im\{g(t)\}$. Figure 2.13 shows the spectra corresponding to rectangular half slot width pulses. Spectra have been shown to exhibit a distinct component at odd harmonics of the slot frequency. The power of the slot frequency component is sensitive to the pulse width. It is optimum for pulse width of half a time slot. For dispersed pulses i.e. Gaussian shaped pulses, the spectra become flattened and the slot component remains distinct along with its harmonics. The slot frequency and the correct phase can be extracted by simply using a phase lock loop (PLL) .

At high speed and high coding levels slot and frame synchronisation becomes a complex and tedious task. To ease this, line coding [*Yichao*]; transition sequence detection [*Elmirghani*93], block synchronisation [*Sugiyama*93] or sequence detection [*Gagliadi*87] have been suggested.

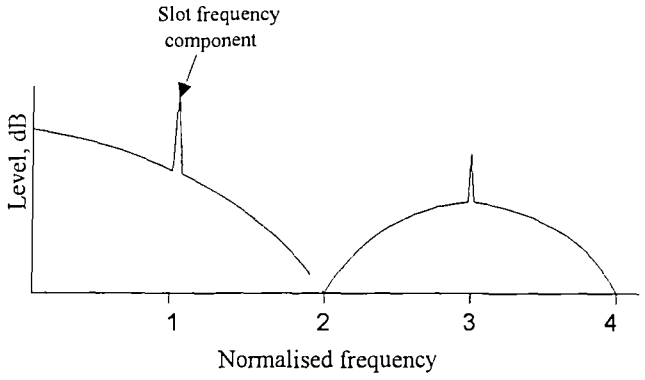

Fig. 2.13 DPPM spectral profile for half slot width pulses.

Receiver sensitivity performance is said to be limited by the effect of three error sources in noisy conditions, namely: erasure, false alarm and wrong slot errors. Erasure is when the pulse goes undetected due to noise forcing the actual pulse below the receiver threshold. The reverse effect causes the false alarm error. That is, noise crossing the threshold and falsely indicating a presence of a pulse. A wrong slot error occurs when

adjacent slots, corresponding to a correct pulse are wrongly detected. This is due to noise corrupting the pulse edges. Receiver sensitivity of the system is determined by the above three error sources.

2.5 Multiple Pulse Position Modulation (MPPM)

With the increase of coding level, DPPM slot width decreases, increasing the required transmission bandwidth exponentially. Although optical fibre offers virtually infinite bandwidth, there is a practical limitation on the electrical part of the system. To over come this limitation, multiple pulse position modulation has been introduced recently as a way of improving the band-utilisation efficiency in optical DPPM [*Sugiyama*89]. This scheme reduces the band width to about half that of conventional DPPM at the same transmission efficiency [*Sato*94].

In MPPM, multiple optical pulses (k) are transmitted in one single frame, see Fig. 2.14. If the frame contains l slots and k pulses, MPPM can give ${}_lC_k$ $(=l!/(k!(l-k)!))$ frame patterns. In other words single frame can transmit $\log_2 {}_lC_k$ bits of information [*Shalaby*95/2] while for DPPM this rate is $\log_2 l$ bits.

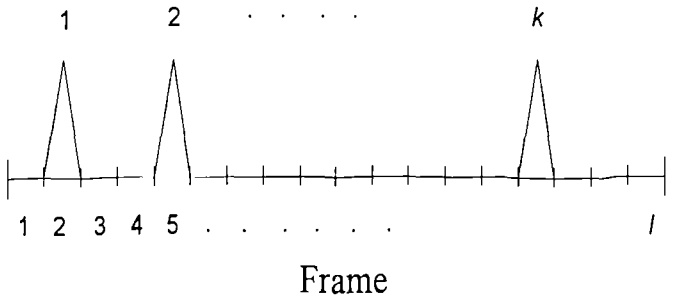

Fig. 2.14 MPPM frame.

For k = 2, there are only two pulses per frame. Figure 2.15 shows the variation of MPPM information capacity with respect to DPPM as the number of slots in a frame

vary. This figure shows that MPPM information capacity is twice as compared to DPPM. Consider a (12,2) MPPM scheme. In this case each frame consist of 12 slots and 2 pulses. Information capacity (symbol capacity) per frame is $\log_2(66) \cong 6$ for simplicity. In other words, 6 source symbols are transmitted by the 12 slot frames, having 64 different frame patterns.

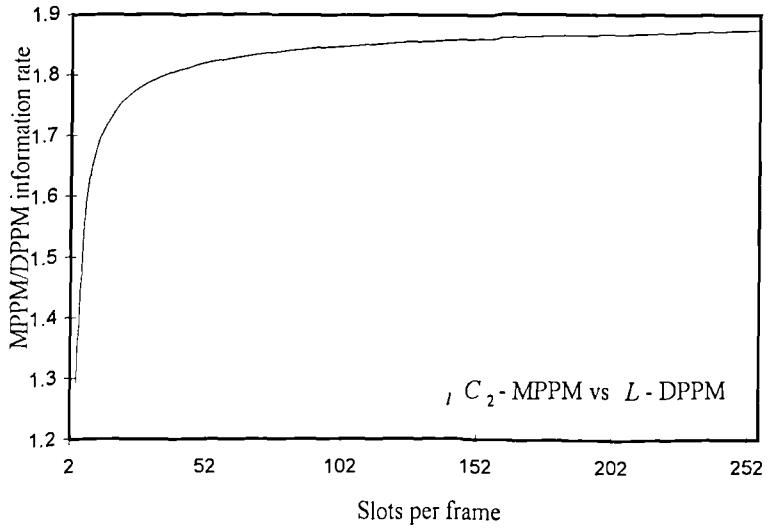

Fig. 2.15 MPPM information capacity with respect to DPPM.

Thus the encoder maps the different symbol pattern (6 bits in this case) into 12 bit frames, see Fig. 2.16.

Symbol	Bit pattern	Representation	MPPM frame
0	000000	[4 , 7]	000100100000
1	000001	[2 , 8]	010000010000
2	000010	[1 , 5]	100010000000
3	000011	[9 , 12]	000000001001
..	.....	.....	.....
63	111111	[1 , 12]	100000000001

Fig. 2.16, MPPM frames for 6 bit symbols.

In Fig. 2.16, the first column shows the source symbol, the second column the source symbol frame, the third column the MPPM representation (e.g. [4,7] means in the MPPM frame, the 4^{th} and 7^{th} bits contain pulses) and the last column shows the MPPM 12 slot frame. In other words detection of pulses at the 4^{th} and 7^{th} time slots in MPPM frame corresponds to transmission of the symbol 0. Thus, at the receiver, by means of a look up table or mapping scheme, received source symbols are restored from the MPPM frames. If only one pulse is detected, i.e. an erasure error has occurred, the mean value of received photons in each slot is measured and the highest is taken as the possible pulse location. This requires a sophisticated receiver, such as a photon counting receiver.

The amount of information MPPM can carry is increased with the number of pulses within a fixed length frame. The drawback is that if one or more of these pulses are erroneous, the frame is demodulated incorrectly, so many source bits are affected. Although MPPM is inferior to DPPM in terms of error performance, it offers an information capacity twice that of DPPM. In MPPM approximately half of the slot rate may be chosen to transmit the same information thus reducing the bandwidth requirements [*Budinger*] . Frame and slot synchronisation is similar to that of DPPM. Due to the receiver complexity, this scheme is better suited for high capacity long haul data links.

2.6 Pulse Code Modulation (PCM)

In PCM a symbol is represented by a group of discrete amplitude pulses. If the symbol is a combination of a group of M pulses that are either on or off, they can represent $L = 2^M$ unique combinations. Thus an analogue signal can be divided (i.e. quantised) into L levels and each of these is represented by a unique symbol. This is the definition of

PCM. In the quantisation process some of the original information is discarded and it thus impossible to exactly regenerate the original signal at the receiver. However, as the value of M is increased the error is decreased.

In terms of circuitry, there are three popular techniques to implement the analogue to digital encoding operation. These are the counting (or ramp), serial (or successive approximation), and parallel (or flash encoders) [*Couch*]. The first method of generation is presented for comparison with the other PTM techniques, see Fig. 2.17.

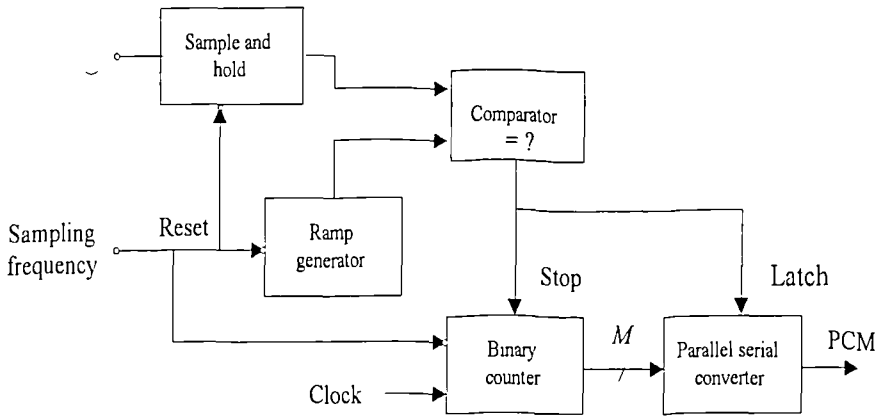

Fig. 2.17 PCM modulator block diagram.

The sampling frequency is chosen at least twice that of the modulating signal. The counter clock is chosen such that the time taken for the M bit counter to count from 0 to 2^{M-1} is at least equivalent to the sampling time. At the same time that a sample is taken the ramp generator is energised and the binary counter is started. The output of the ramp generator is continuously compared to the sample value. When the value of the ramp becomes equal to the sample the counter value is read and this is the desired PCM word. The parallel to serial converter converts the M bit symbol ready for transmission. The chief limitation of this technique is the linearity of the ramp and the

speed of the counter. Figure 2.18 shows a simple PCM demodulator for analogue signal transmission.

There are several levels of synchronisation necessary in PCM systems for example a bit clock is required for pulse detection from the incoming signal and a symbol clock for establishing the start of the each symbol and the operation of the sample and hold.

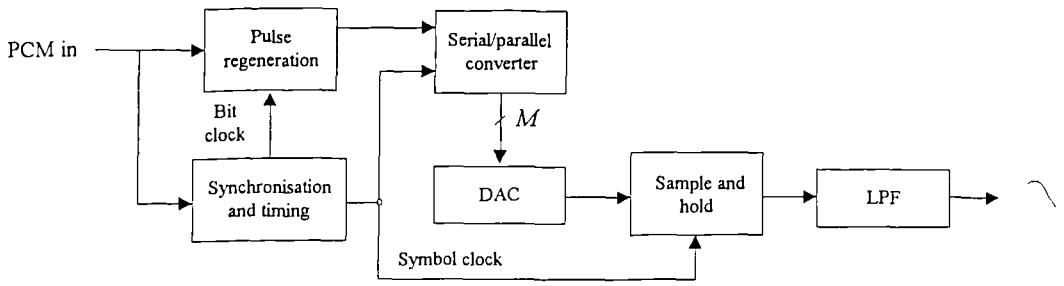

Fig. 2.18 PCM demodulator block diagram.

PCM symbols are often encoded into different forms to enhance the link performance, i.e. to provide enough transitions that receiver regeneration circuitry can phase or frequency lock onto the signal timing for low bandwidth occupancy etc. Furthermore, optical receivers are capacitively coupled and cannot respond to variations in the average DC signal level, thus causing signal baseline drifts. Certain encoding schemes may be adopted to minimise base line wander at the receiver amplifier. As shown in Fig. 2.1, PCM encoding schemes are divided into two categories: return-to-zero (RZ) and non-return-to-zero (NRZ). Return-to-bias (RB), alternate mark inversion (AMI) and Manchester encoding schemes fall into RZ, whereas non return to zero constant level NRZ(L), non return to zero level change NRZ (I), and Miller code fall into NRZ category. Spectral occupancy of these schemes are shown in Fig. 2.5 for a bit rate of f_z. Most of the texts on communication theory give a detailed description of the above encoding schemes [*Stremler*], [*Couch*].

The advantages of PCM have been well defined. The most important are that it has good *SNR* performance and good system linearity, both of which are to a great extent, independent of the channel quality. The noise at the output of the PCM demodulator is mainly determined by the quantisation noise at the modulator. For M bit PCM the *SNR* at the receiver output (SNR_{out}) is given by [*Downing*],

$$SNR_{out} = \frac{3.L^2}{1+4P_e\left(L^2-1\right)} \tag{2.15}$$

where P_e is the bit error probability in the recovered binary signal, $L = 2^M$ and P_e is given in section 6.6. By increasing the coding level or the number of bits M, the quantisation noise can be minimised and hence the *SNR* and system distortion are reduced.

2.7 Summary

In this chapter present modulation techniques are categorised into analogue, pulse and digital. Pulse modulation techniques are further categorised into isochronous and anisochronous.

Unlike PWM, the PPM spectrum does not contain a base band component. Therefore, at the receiver conversion back into PWM is required in order to recover the information. Both PWM and PPM schemes suffer from non-linear distortions introduced at the transmitter and receiver due to mismatch in ramp waveforms. This can be avoided by generating ramp waveform digitally, but the penalty paid is an increase in bandwidth. In DPPM transmission capacity may be improved by means of MPPM, where more than one pulse is placed within the isochronous frame. On the other hand PCM has been used widely due to its improved error performance and power efficiency.

Chapter Three

Anisochronous PTM Schemes

In the previous chapter an overview of currently available modulation techniques has been presented and each isochronous scheme is briefly discussed. In this chapter anisochronous schemes are investigated and a comparison of these schemes along with the ones in the previous chapter is made on the basis of *SNR* performance for analogue signals and bandwidth occupancy for digital schemes.

3.1 Introduction

Isochronous schemes are described as having a fixed sampling frequency or fixed frame structure. In contrast, anisochronous schemes are based around feedback structures, hence they do not have a fixed sampling process. The sampling frequency in the spectra is seen either to vanish for certain values of modulation indices or their level changes in both amplitude and frequency. The effective sampling frequency utilised within the respective modulator is modified dramatically by the presence of the source modulating signal showing unequal sampling periods under modulation conditions [*Wilson*93]. With reference to Fig. 2.1 there are a few schemes which fall into this category. In the

remainder of this chapter, analogue and digital pulse interval, pulse interval and width modulation schemes are briefly described.

3.2 Analogue Pulse Interval Modulation (PIM)

In PIM, the modulating signal is represented by a stream of pulses where the information is encoded in the time between two successive pulses. Unlike PPM no synchronisation of reference frame positions between modulator and demodulator is required. Demodulation is simply carried out by generating a sawtooth waveform, triggered by the received PIM signal, followed by a low pass filter to recover the original signal. Therefore, PIM offers the attractive features of PPM together with a less complex circuitry. Figure 3.1 shows PIM modulator and demodulator block diagrams and waveforms.

Ueno et al introduced PIM as modified PPM for transmission of a colour TV signal or 600 telephone channels [*Ueno*78]. He showed that low repetition rate of the modulating signal is also immune from the pattern effect due to the turn on delay of the laser in optical systems.

In Fig. 3.1, the modulating signal is compared with a linear ramp signal. The comparator generates an output signal (a pulse) every time the ramp signal exceeds the modulating signal. The pulse density of the PIM signal is high when the modulating signal amplitude level is low and vice versa. The PIM characteristic is exactly opposite to that of PFM. *Okazaki* investigated PIM for narrow-band transmission in industrial television systems [*Okazaki*78]. He showed that PIM is highly suitable for this type of application due to the reduction of the transmission time, low cost and reduced circuit complexity [*Okazaki*79].

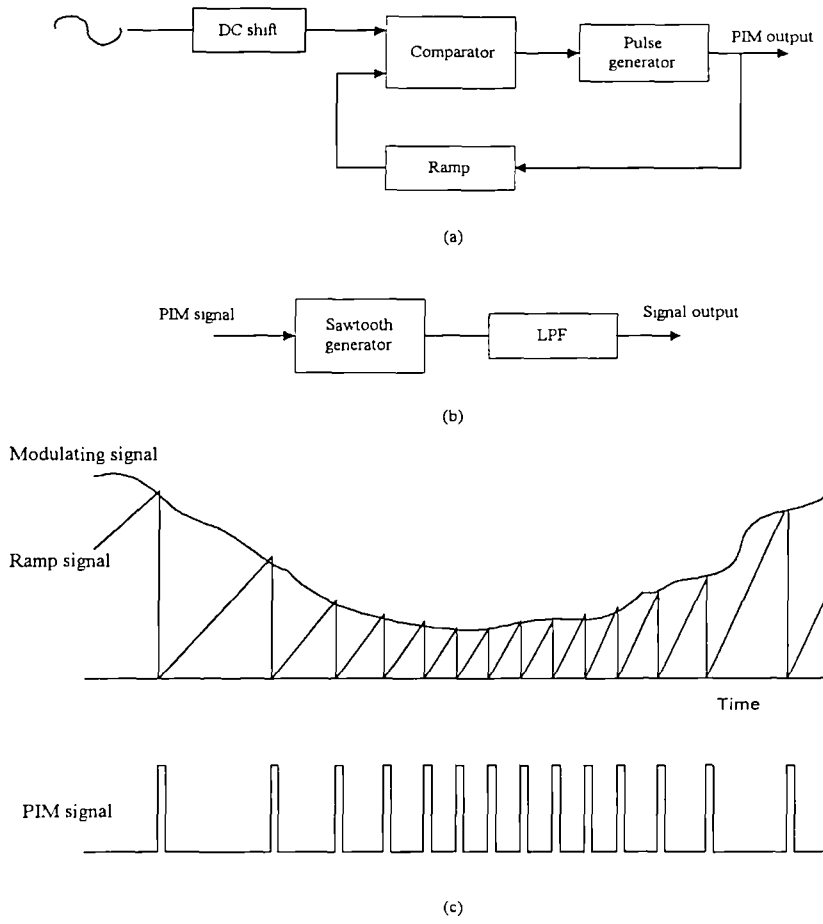

Fig. 3.1 PIM system block diagram: (a) modulator, (b) demodulator and (c) waveforms.

Nishida et al showed that PIM noise characteristics are similar to that of analogue FM and it can be further improved by employing pre-emphasis techniques [*Nishida*]. *Fyath et al* analysed the PIM spectral profile and showed that just like PWM and PFM it too contains a baseband component. The spectral profile is expressed as [*Fyath*].

$$x_\delta(t) = V_o f_a \left[1 + \sum_{k\ 1}^{\infty} 2b^k \cos k\omega_m t \right] \times \left[1 + 2 \sum_{n-1}^{\infty} \prod_{k=1}^{\infty} \sum_{L_k=-\infty}^{\infty} J_{L_k}(n\beta_k) \cos\left(n\omega_a t + L_k k\omega_m t\right) \right] \qquad (3\ 1)$$

where

$$f_a = f_c \frac{1+b^2}{1-b^2}, \qquad b = \frac{1-\left(1-\gamma^2\right)^{1/2}}{\gamma}, \qquad \beta_k = \frac{2b^k f_a}{k f_m}, \qquad \gamma \quad m_i A, \qquad m_i = t_{F\ F} \ 2 f_a$$

f_a - Average PIM sampling frequency,

f_c - PIM unmodulated sampling frequency

m_i - PIM modulation index

$t_{p\text{-}p}$ - Peak-to-peak pulse deviation

T_a - Average sampling time

A - Modulating signal peak amplitude.

V_o - PIM pulse amplitude,

f_m - Modulating signal frequency

In Eqn. 3.1, the first square bracket contains the modulating signal and its harmonics, whereas the second square bracket shows the sampling frequency, its harmonics and a set of side tones displaced by the modulating signal frequency around them, see Fig. 3.2.

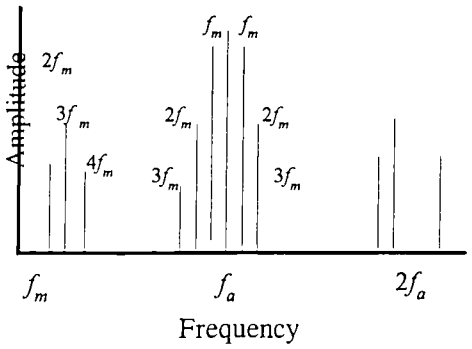

Fig. 3.2 PIM spectra.

Spectral results were confirmed by *Tripathi* [*Tripathi*80]. From Eqn. 3.1, the baseband component and its harmonics can be given by,

$$x_m(k) = 2V_0 f_a \left(\frac{1-\left(1-\gamma^2\right)}{\gamma} \right)^k \tag{3.2}$$

where $x_m(k)$ represents the k^{th} harmonic component.

From Eqn. 3.2, the harmonics of the modulating signal frequency are modulation index dependant and the results for second and the third harmonic distortion are presented in Fig. 3.3.

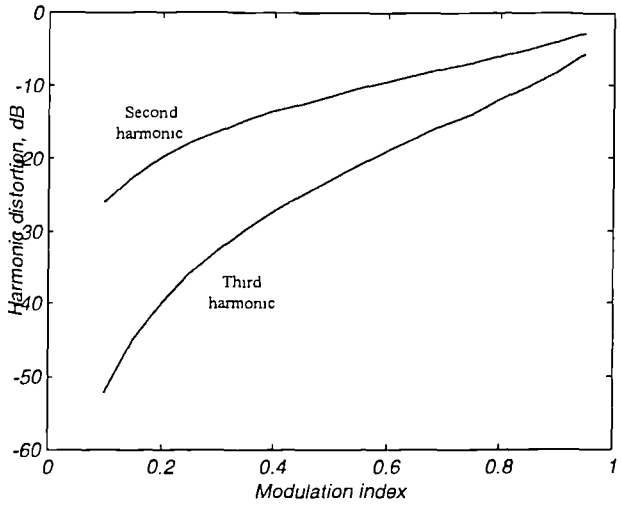

Fig. 3.3 PIM harmonic distortion.

From Fig. 3.3, it can be seen that second and the third harmonic level increases with the modulation index. At low modulation indices (<20 %), where harmonic distortion levels are small, a low order low pass filter may be used to recover the information signal. At higher modulation indices, spectral overlap may take place in the base band region, and a higher order low pass filter is required.

The required bandwidth (B) for PIM depends on the pulse width τ such that,

$$B \geq \frac{1}{\tau} \tag{3.3}$$

Both the channel and the receiver must provide adequate bandwidth in order to propagate and regenerate the PIM pulse train. The sampling interval must also be large enough so that the minimum interval between two pulses is large enough in order to avoid inter pulse interference. *Ueno et al* investigated PIM for frequency division multiplexed (FDM) telephone signals transmission over optical fibre [*Ueno*78]. The *SNR* expression developed for FDM signals can be modified for a single base band signal by assuming that the system transmission bandwidth is B, sampling ratio is 2,

average sampling frequency is twice the unmodulated PIM frequency and pulse rise time $\tau_r = 2/\pi B$ [*Black*]. This is given by,

$$SNR_i = \frac{\pi^2}{2}\left(\frac{m_i B}{f_a}\right)^2 CNR \tag{3.4}$$

Tripahy has reported that PIM demonstrate a threshold effect at *CNR* of about 18 dB at corresponding to the output *SNR* of 17 dB and it gives *SNR/CNR* gradient of 1 dB for any further increase in *CNR* [*Tripathy*83]. *Ueno* also showed that when applied in optical transmission of colour TV signal, PIM can achieve an output *SNR* of 52 dB for -20 dB of peak optical power [*Ueno*75].

The predominant source of non-linear distortion of the demodulated signal in the PIM signal is the non-linearity of the ramp waveforms. This can be reduced by proper circuit design as it does not require absolute linearity of the ramp signal but there must be identical slopes at the modulator and demodulator. It has also been reported that there exists self-imposed non-linear distortion as the PIM signal also has a component of pulse density modulation because of the modulation principal [*Ueno*78]. The source of this distortion is inherent in the ramp signal and the reset operation to the reference level after each sample of the input signal. The deviation in reset time translates itself into density modulation. At the demodulator, by converting PIM pulse train into a ramp waveform this effect can be reduced. *Ghassemlooy* has shown that, this distortion can be kept to a minimum provided the ramp waveform is reset within a PIM pulse duration, no matter what the amplitude of the modulating signal is. Therefore, PIM pulse become less dependant on the reset time [*Ghassemlooy*97].

Ghassemlooy et al proposed digital means of generating PIM, namely digital pulse interval modulation (DPIM) to over come the non-linearity problems caused by the mismatches of the ramp waveforms [*Ghassemlooy*95/1].

3.3 Analogue Pulse Interval and Width Modulation (PIWM)

PIWM is derived directly from its anisochronous counterpart, PIM, by passing them through a bistable to produce a waveform in which both mark and space convey information [*Sato*78]. A PIWM modulator is attained by simply adding a bistable at the output of PIM modulator, see Fig. 3.1(b) and Fig. 3.4. PIWM is characterised by comparison with PIM as having:- reduced pulse repetition frequency (by half), 50 % duty cycle, higher average power (which may be used to improve *CNR*), and low transmission bandwidth.

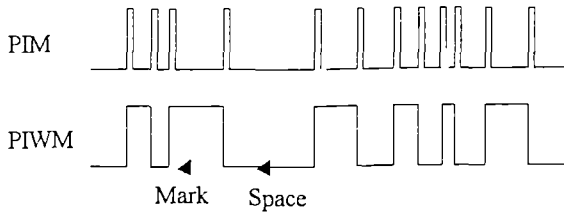

Fig. 3.4 PIM and PIWM pulse streams.

The anisochronous nature of both PIM and PIWM arise because the modulator ramp is reset at a point determined by the instantaneous value of the input signal and not by a pre-determined interval controlled by the choice of carrier (sampling) frequency. *Wilson et al* investigated PIWM spectral properties and showed that it can be represented by [*Wilson*91/2, 92/2],

$$v(t) = V_o\left\{\frac{1}{2} + \sum_{k=1}^{\infty}\sum_{n1=-\infty}^{\infty}\sum_{n2=-\infty}^{\infty}\frac{\sin(k\pi\ 2)}{k\pi\ 2} \times J_{n1}(kB_1)J_{n2}(kB_2) \times \right.$$
$$\left. \cos\left[k\omega_b + (n_1 + 2n_2)\omega_m\right]t\right\} \tag{3.5}$$

where V_o and ω_c are the amplitude and the unmodulated free running frequency of the PIWM pulse stream, respectively. ω_m is the modulating signal angular frequency and $\omega_b = A_0\omega_c$ represents the average modulated sampling frequency.

where

$$A_0 = \sum_{r-0}^{\infty}\left(\frac{m_i}{2}\right)^{2r}\binom{2r}{r} \tag{3.5a}$$

and m_i is the modulation index similar to PIM modulation index.

For $m_i < 1$ and $2 > A_0 > 1$,

$$B_p = \frac{2\omega_c}{p\omega_m}\left(\frac{m_i}{2}\right)^{p}\sum_{r=0}^{\infty}\left(\frac{m_i}{2}\right)^{2r}\binom{p+2r}{r} \tag{3.5b}$$

where p = 1,2 and $J(kx)$ as defined before. The PIWM spectrum contain a diminishing set of side tones set around the average modulated sampling frequency and all its odd harmonics, see Fig. 3.5. Unlike PIM it does not have baseband components, therefore, at the receiver it is necessary to convert back into a PIM pulse train before recovering the modulating signal by simple low pass filtering. Conversion can be performed by differentiating the incoming PIWM pulse stream.

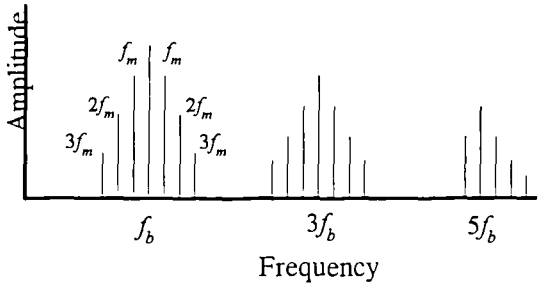

Fig. 3.5 PIWM spectral profile.

The PIWM spectrum was shown to have a slightly asymmetric side tone structure which closely resembles a SWFM spectra [*Wilson*92/2]. PIWM baseband harmonic components are modulation index dependant as with PIM. *Reyher* has modified the PIWM *SNR* ratio expression given by *Ueno et al* [*Ueno*78] and is given as [*Reyher*],

$$SNR_{iw} = \pi^2 \left(\frac{m_i B}{f_c} \right)^2 CNR \tag{3.6}$$

Marougi et al investigated the *SNR* performance of PIWM showing linear characteristics with a distinct PTM threshold effect around *CNR* of ≈15 dB when the *SNR* is 18 dB [*Marougi*]. Similar performance were also reported by *Tripathi* for PIM [*Tripathy*83]. System harmonic distortion (2^{nd} and 3^{rd}) is also sensitive to the modulation index, i.e. it increases with the modulation index. *Wilson et al* reported that it is possible to achieve 2^{nd} and 3^{rd} harmonic distortion levels about -45 dB and -70 dB, for modulation indices less than 50 %, respectively [*Wilson*92/2].

PIWM also suffers from the same nonlinearity phenomenon, i.e. non-linearity problems associated with PIM, see section 3.2. *Sato et al* proposed digitally generated PIWM or in other words digital pulse interval modulation (DPIWM) to over come these problems [*Sato*79].

3.4 Digital Pulse Interval and Width Modulation (DPIWM)

In DPIWM, both mark and space carry information as with analogue PIWM, but the signal is generated by digital means. Unlike analogue PIWM, DPIWM requires a discritised signal at the input of the modulator in order to generate frames consisting of a mark and space of a given number of time slots. The number of time slots associated with mark and space are proportional to the decimal value of the symbols. This

therefore results in an effective code pattern where low signal levels are associated with shorter code lengths. Each frame starts with a mark followed by a space, thus showing the synchronised frame structure.

Sato et al proposed a novel method of generating DPIWM. At the modulator, input symbols are divided into two sets, one set to generate a mark and the other to generate a space. Parallel M bit symbols are divided into two equal sets of k bits each. The least significant k bits and the most significant k bits of the M bit symbol are taken to generate a space and mark, respectively [*Sato*79]. Mark (W_m time slots) and space (I_m time slots) are therefore derived by the weight of each k bits. One additional time slot is added to both mark and space to avoid inter-frame interference. Figure 3.6 shows a block diagram of a DPIWM modulator, demodulator and waveforms. Waveforms presented are correspond to 2 frames of 4 bit PCM.

The modulator consist of counters, a clock, comparator and a combiner. The latter usually based on a flip-flop circuit. The DPIWM output is set high while counter 1 counts up to W_m, and it is set low while counter 2 counts up to I_m. The demodulator consists of counters, a slot clock and a combiner usually a data latch. During the mark interval of the received DPIWM signal counter 1 counts up from 0 while counter 2 is held at 0. At the negative transition counter 1 data are latched. Similarly, during the space interval counter 2 counts from 0 while counter 1 is held at 0. At the positive transition this data is latched. The high and low significant k bits corresponding to mark and space, respectively are combined to regenerate the M bit symbol.

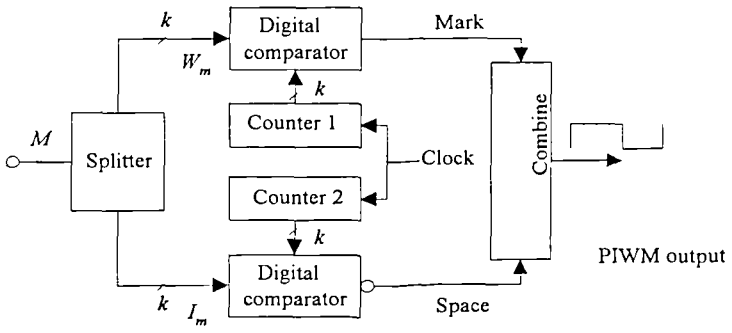

(a)

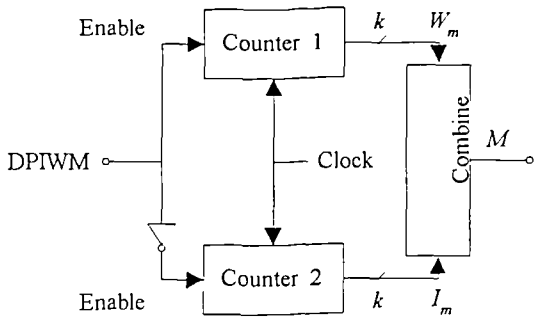

(b)

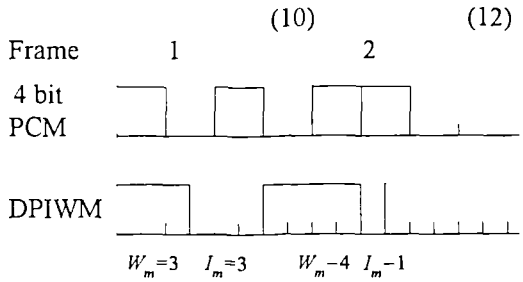

(c)

Fig. 3.6 DPIWM (a) modulator, (b) demodulator and (c) waveforms.

The range of mark, space and frame length (l_m) variation can be given in terms of time slots as:

$$W_m \in 1..2^{\frac{M}{2}}, \qquad I_m \in 1..2^{\frac{M}{2}}, \qquad l_m \in 2..2^{\frac{M}{2}+1} \tag{3.7}$$

If the M bit symbol rate is given by f_f then the DPIWM slot rate (f_{dpiwm}) can be written as:

$$f_{dpiwm} = 2^{\frac{M}{2}+1} f_f \tag{3.8}$$

Thus, the system slot rate increases exponentially with the bit resolution, M.

Ghassemlooy et al investigated the spectral properties of DPIWM expressed as [*Ghassemlooy*95/3],

$$S(f) = \frac{1}{\sum_{k=0}^{L}(W_k + I_k)\, T_{dpiwm}} \left\{ \left| \sum_{k=0}^{L} G_W(f).e^{-j2\pi f T_{dpiwm}\left(\sum_{m=0}^{k-1}(W_m + I_m)\right)} \right|^2 \right\} \tag{3.9}$$

where $G_W(f)$ is the pulse shape transform and W_m and I_m are the symbols used in mark and space generation, respectively. This spectral expression is numerically evaluated and the result is shown in Fig. 3.7.

From Fig. 3.7 it can be seen that the spectra shows singularities at the slot frequency and its harmonics. Unlike DPPM, it does not show a distinct slot component which may be used for synchronisation.

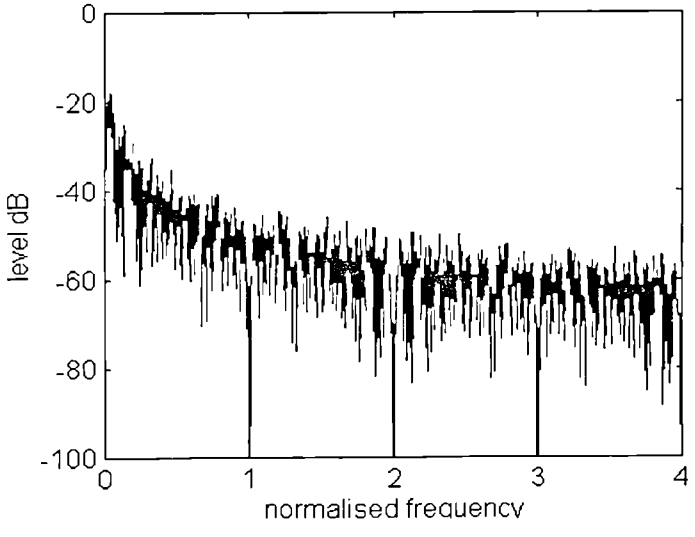

Fig. 3.7 DPIWM spectral profile normalised to slot frequency.

Non-linear processing such as differentiation of the incoming pulse stream may be performed in order to generate the slot component. DPIWM has twice as much information capacity compared to PCM along with a self-synchronised frame structure [*Ghassemlooy*95/2, 96].

3.5 Comparison of Modulation Schemes

In this section analogue as well as digital PTM schemes are compared and their suitability for optical fibre communication systems are investigated. PFM and SWFM schemes have not been described in detail as they have no digital counterparts.

A comparison of modulation techniques is based on various parameters such as bandwidth occupancy, harmonic distortion, *SNR*, suitability for the transmission channel, probability of error etc. No one scheme will have an optimum performance and they all have the ability to trade-off one requirement against another.

Analogue schemes have been widely been used over the years due to their simplicity and bandwidth efficiency. But these schemes cannot deliver the required *SNR* in most applications. On the other hand, digital schemes are based on analogue signalling, and their usage is limited to discrete level signal transmission. In contrast, applications for pulse modulation schemes are wide range. These applications fall into two categories, continuous or discrete signal transmission. Analogue PTM schemes are best suited for analogue signal transmission, while the other can support both.

The spectra of different analogue PTM techniques share common features as shown in the previous sections. Naturally sampled PWM and PIM have been shown to contain a baseband component that can be recovered by simply filtering at the receiver, requiring a lower component count. But the drawback is that the harmonic level of the baseband

component increases with the modulation index, giving rise to an increase in harmonic distortion. One way of reducing the harmonic distortion is to increase the sampling ratio. To achieve -40 dB distortion level, a sampling ratio of 4 has been specified at an optimum modulation index of 70 % [*Wilson*95/2]. On the other hand, PPM and PIWM do not have a base band component, thus conversion back to PWM and PIM, respectively, is essential for signal recovery.

In terms of bandwidth occupancy, both PPM and PIM require wide transmission bandwidth due to their very low pulse duty cycle. However, PWM and PIWM average pulse duration are considerably higher than the above two case, therefore, demanding comparably lower bandwidth. For optical transmission, PPM and PIM are the most preferred schemes due to their high peak power and low average power characteristics.

The output *SNR* versus *CNR* for different techniques have been presented in the previous sections. For PWM, PPM, PIM and PIWM, the *SNR* above threshold levels is best given as an improvement factor *IF*, which is derived as *SNR* minus *CNR*. From Eqns. 2.6, 2.9, 3.4 and 3.6, the *IF* are given as [*Wilson*93]:

$$IF_{PWM} = \frac{\pi^2}{8}\left(\frac{m_w B}{f_c}\right)^2 \tag{3.10}$$

$$IF_{PPM} = \frac{\pi^2}{4}\left(\frac{m_w B}{f_c}\right)^2 \tag{3.11}$$

$$IF_{PIM} = \frac{\pi^2}{2}\left(\frac{m_i B}{f_c}\right)^2 \tag{3.12}$$

$$IF_{PIWM} = \pi^2 \left(\frac{m_i B}{f_c} \right)^2 \tag{3.13}$$

where B is the transmission bandwidth (note in PIM $f_c \equiv f_a$).

Using Eqns. 3.10, 11, 12, 13 and 2.15, *SNRs* Vs *CNR* for all the schemes are plotted in Fig. 3.8, along with 8 bit PCM for comparison, when $P_e < 10^{-9}$. This method of comparison directly takes into account different sampling ratio behaviour and modulation indices of each scheme. The *CNR* is defined as the ratio of the peak received carrier signal power to the equivalent noise power falling into the signal band.

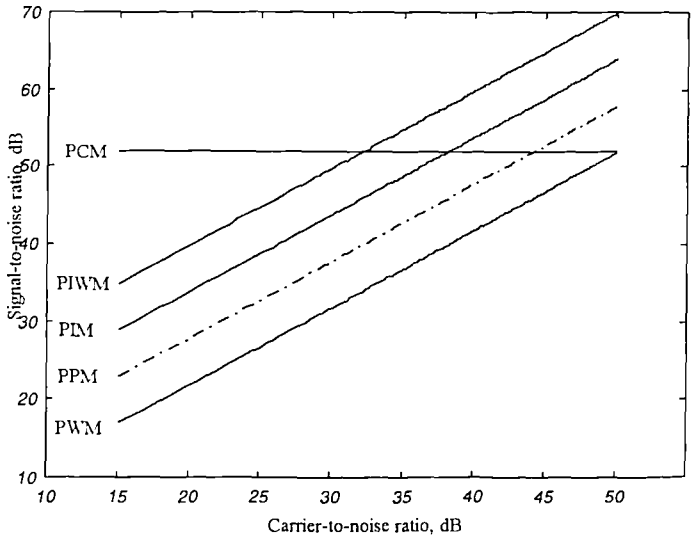

Fig. 3.8 *SNR* Vs *CNR* for PWM, PPM, PIM and PCM.

At a modulation index of 0.5 and $B/f_c = 2$, PWM can achieve an improvement factor of 2 dB. Similarly, for a modulation index of 20 % and $B/f_c = 5$ PPM can achieve an improvement factor of 7.8 dB. In the same manner PIM and PIWM also can achieve *SNR* improvements as shown in Fig. 3.8 for different transmission parameters.

Out of all the above three schemes PIWM uses the lowest sampling ratio in order to achieve a higher improvement factor. PPM and PIM on the other hand require higher bandwidth (higher than PIWM) and deliver higher *SNR* performance compared to

PWM. The disadvantage of PPM is the need for the frame synchronisation thus requiring additional circuitry compared to the other three schemes.

PCM offers the best *SNR* performance compared to the other reported PTM schemes. This is achieved at the expense of the circuit complexity and higher bandwidth overhead. However, other PTM schemes, such as DPPM, MPPM and DPIWM, may outperform PCM provided the required transmission bandwidth is available.

The fundamental difference between analogue and digital PTM pulse stream is in the way the information is represented. In the latter case this is achieved by representing pulse train in discrete format composed of time slots. Its performance depends on the bit resolution (or the coding level). In the absence of receiver noise, quantisation noise is the dominant source. Digital PTM transmission bandwidth is a function of the pulse width which in turn is dependant on the time slots. Figure 3.9 shows the required transmission bandwidth versus bit resolution performance for various PTM schemes for the same information capacity.

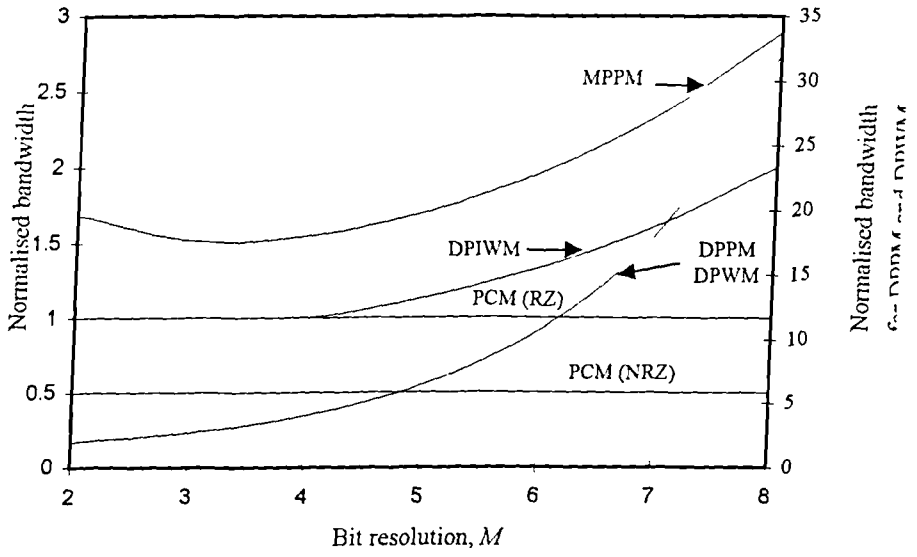

Fig. 3.9 Transmission bandwidth normalised to source bit rate, for PCM, DPPM, MPPM, DPIWM and DPWM.

In Fig. 3.9, primary y-axis (left hand y-axis) shows the required transmission bandwidth normalised to the source bit rate, for MPPM, DPIWM and PCM (RZ, NRZ). Whereas, the secondary y-axis (right hand y-axis) shows the bandwidth for DPPM and DPWM. NRZ PCM shows the lowest transmission bandwidth requirement at all symbol levels, whereas DPPM and DPWM show the highest bandwidth requirement. At a source symbol level of 8, transmission bandwidth requirements of NRZ and RZ are equivalent to half the source bit rate and the bit rate, respectively. In case of DPIWM, MPPM, and DPPM/DPWM this requirement increases to 2, 3 and 32 times the bit rate, respectively. Digital PTM schemes require slot and frame synchronisation between the transmitter and the receiver. In DPPM and RZ-PCM this is achieved by the presence of slot frequency component within the spectrum. On the other hand, in MPPM, DPWM and DPIWM, where full slot pulses are transmitted, non-linear processing such as differentiation, is required to achieve a distinct slot component for clock extraction. In MPPM and DPPM time synchronisation is vital in order to avoid any pulse position mismatches, which could have an adverse effects on the system performance. This is even more critical at high speed long-haul transmission systems.

DPPM has the ability to trade-off bandwidth for receiver sensitivity performance. *Cryan* showed that, in optical communication systems DPPM can achieve 5-7 dB receiver sensitivity improvement over equivalent PCM [*Cryan*92/1]. MPPM outperforms DPPM in information capacity and bandwidth efficiency at the expense of higher circuit complexity [*Sugiyama*89]. DPIWM has information capacity twice that of DPPM along with self synchronised frame structure [*Ghassemlooy*95/3]. Each of the digital PTM schemes contain unique advantages and disadvantages and their selection really depends on the application.

3.6 Summary

PIM and PIWM are PTM schemes which are suitable for transmission of low to moderate speed signals over optical fibre links. Unlike PIWM, PIM spectra contain a baseband component which makes demodulation rather simple. In case of PIWM conversion into PIM is required for signal recovery at the receiver.

System linearity dependants on the linearity of the ramp signals employed both in the transmitter and the receiver. In DPIWM this problem does not exists since mark and space are generated in terms of a fixed clock which can be replicated at the receiver. This scheme has an information capacity twice that of PCM and DPPM and lower transmission bandwidth compared to DPPM. The self synchronised frame structure simplifies the circuitry, but non-linear processing such as differentiation of the pulse stream may be required to aid clock extraction since the spectra shows singularities at the slot frequency and its harmonics. Different PTM techniques have unique features that may be used to enhance information transmission and the choice of a particular scheme will depend on the application, cost, complexity, performance etc.

Chapter Four

DPIM Code Properties

In the previous chapter anisochronous PTM techniques are briefly discussed and transmission capacity of digital PTM schemes are compared. This chapter describes the DPIM code properties and spectral profile in detail. A mathematical model is developed to represent the spectral profile. This model is numerically evaluated and verified with the measured spectra.

4.1 Introduction

The digital pulse interval modulation scheme is the discrete version of continuous pulse interval modulation. In DPIM, each frame starts with a pulse of short duration followed by number of empty time slots that are determined by the information content of the sampled data. In other words, a symbol is represented by a discrete time interval between two successive pulses belonging to two consecutive frames. Unlike isochronous schemes, e.g. DPPM where the frame length is fixed, the frame length in DPIM is variable depending on sample values, as shown in Fig. 4.1.

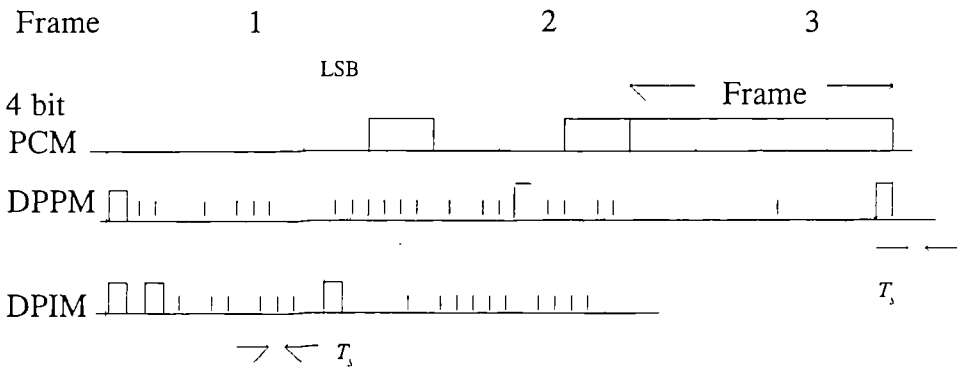

Fig. 4.1 PCM/DPPM/DPIM frame structure.

In DPPM, an M bit symbol of duration T_f (where $T_f = MT_b$, T_b is the equivalent binary bit period) is represented by a single pulse located in one of L (= 2^M) time slots. In DPIM, an M bit symbol is represented by a single pulse followed by a discrete number of time slots. DPIM waveforms are however similar to DPPM, except for the variable frame length and a pulse being located at the start of a frame. To avoid zero length frames, an additional time slot is added to each frame immediately after the pulse. Thus frame lengths may vary as given by n time slots, where $2 \le n \le L+1$. A guard interval n_g time slots may also be included at the end of each frame to prevent inter-frame interference for dispersive channels, see Fig. 4.2.

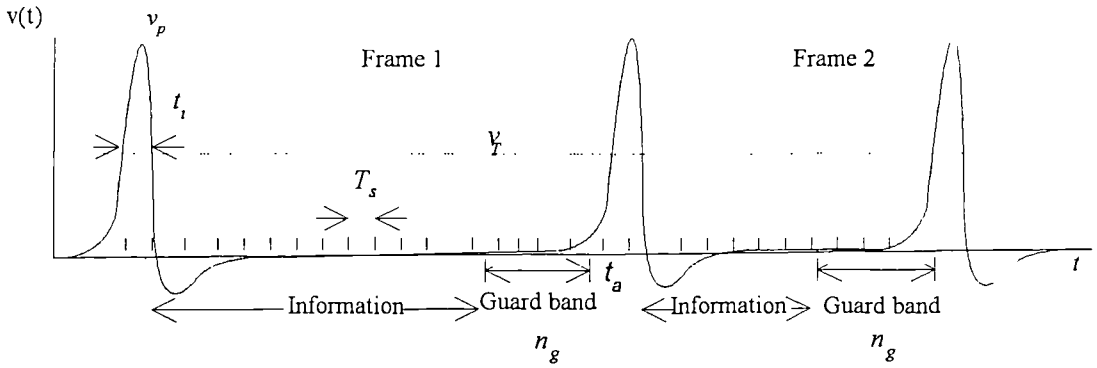

Fig. 4.2 DPIM pulse train with guard interval of n_g.

The guard interval n_g is given as $n_g = b(L+1)$, $b < 1$ is chosen such that n_g gives an integer value, this is mainly for implementation purposes. With a guard band of n_g time slots the longest DPIM frame may be expressed as:

$$T_{\max} = L + 1 + n_g \tag{4.1}$$

and the slot duration is defined as,

$$T_s = \frac{T_f}{L+1+n_g} \tag{4.2}$$

where T_f is the M bit PCM symbol time. The PCM bit period is given by: $T_b \quad T_f \quad \log_2 L$

For a given PCM bit resolution (M), the DPIM slot frequency can be evaluated by,

$$f_s = \frac{2^M + 1 + n_g}{M} B \tag{4.3}$$

where B is the PCM bit rate.

Figure 4.3 illustrates the DPIM and DPPM slot rates normalised to the PCM bit rate, against bit resolution. Guard intervals are 0 and $2^{M-1}/4$ time slots.

From Fig. 4.3, the DPIM and DPPM slot rates increase exponentially compared to PCM bit rate with increase in bit resolution. This increment becomes higher when both systems are included with a guard band. The increase in slot frequency, increases bandwidth requirements e.g. 4 bit resolution DPIM and DPPM require a 4 fold increase of bandwidth compared to the equivalent PCM value as shown in Fig. 4.4.

The DPIM information capacity normalised to M bit PCM frame rate is given by: [*Ghassemlooy*95/2],

$$C_{DPIM} = \frac{2(L+1)\log_2 L}{L+3} \tag{4.4}$$

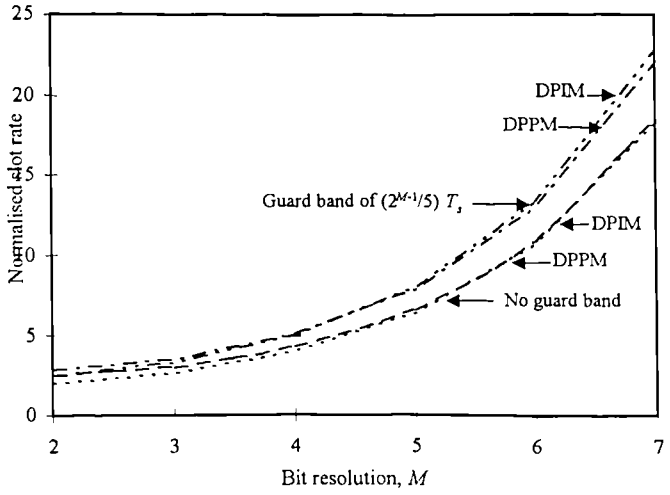

Fig. 4.3 Normalised slot frequency variation with bit resolution.

Fig. 4.4 illustrates DPIM, DPPM, DPWM and DPIWM transmission capacity, normalised to an M bit PCM frame rate.

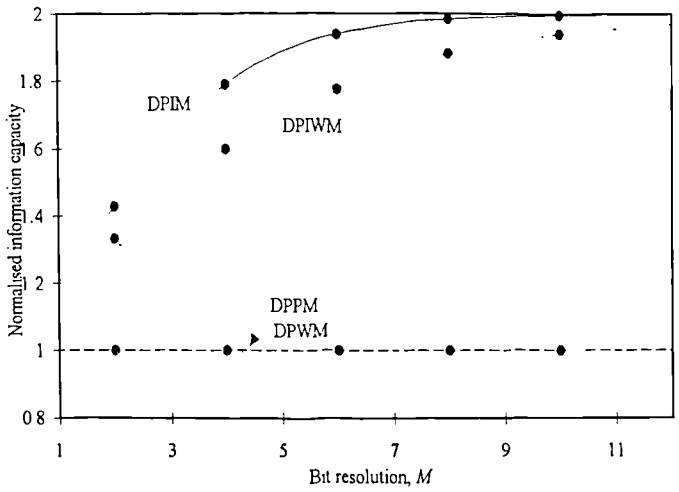

Fig. 4.4 Transmission capacity normalised to M bit PCM frame rate.

In Fig. 4.4, DPIM, DPIWM, DPWM and DPPM information capacity normalised to M bit PCM frame rate is drawn against bit resolution. Isochronous DPPM and DPWM shows similar information capacity compared to equivalent PCM, whereas anisochronous DPIM and DPIWM give higher capacity as the bit resolution increases reaching twice that of PCM for bit resolutions of 8 and above. Furthermore, DPIM shows higher information capacity with respect to DPIWM.

4.2 Spectral Properties

The use of coding in digital communication is mainly to utilise the available channel with highest efficiency. In order to analyse the code effectively it is useful to evaluate the power spectral density of a truncated realisation from which the variation of power at different frequencies, the optimum bandwidth requirements can be determined. A mathematically infinite length DPIM pulse stream can be represented by,

$$x(t) = \sum_{k\ -\infty}^{\infty} a_k g\left[t - T_s\left(2k + \sum_{m\ -\infty}^{k\ 1} S_m \right) \right] \tag{4.5}$$

where $g(t)$ represents the pulse shape of duration γT_s ($1>\gamma>0$) and an amplitude of a_k, T_s is the slot width, and S ($S_m \in S$) is the stochastic random data sequence that represents the data coded into DPIM. The temporal representation of a DPIM pulse stream takes into account the history of data samples. The k^{th} sample in the sequence is such that,

$$0 \le S_k \le 2^M - 1 \tag{4.6}$$

The numerical spectral model for DPIM is obtained as the sum of contributions from a set of delayed pulses, similar to the approach outlined deriving spectral model of DPPM [*Elmirghani*94/1, 95/1]. The delayed pulses are random in nature, following a rule

dictated by the probability distribution of the input data, and are represented by the vector of symbols S, as given in Eqn. 4.6. The infinite length DPIM pulse stream is truncated in order to estimate the power spectral density (PSD) of the DPIM process. With $x(t)$ as a power signal, the truncated version of the infinite data stream is given by:

$$x_P(t) = \begin{cases} x(t) & if\ 0 \le t \le T \\ 0 & \text{otherwise} \end{cases} \tag{4.7}$$

where T is the truncated window such that,

$$x(t) = \lim_{T \to \infty} x_p(t) \tag{4.8}$$

The truncated function $x_p(t)$ has finite energy and its Fourier transform can be given by,

$$X_p(f) = \int_{-\infty}^{\infty} x_p(t).e^{\ j2\pi ft} dt \tag{4.9}$$

For an energy-type signal, the energy spectral density of a truncated signal is $|X_p(f)|^2$ [*Proakis*] and power in $x(t)$ in the period $(0,T)$ is:

$$P = \int_{\infty}^{\infty} \frac{1}{T} |X_p(f)|^2 df \tag{4.10}$$

The function under the integral in Eqn. 4.10 describes the required power spectrum of the truncated realisation of $x(t)$. The power spectral density of the realisation is obtained by averaging over a large time interval T as given by:

$$S_p(f) = \lim_{T \to \infty} \frac{1}{T} |X_p(f)|^2 \tag{4.11}$$

Eqn. 4.11 describes the PSD of the individual realisation of the DPIM process. However, to characterise the whole process, first averaging over the realisation and then performing the limiting operation is essential [*Proakis*].

$$S(f) = \lim_{T \to \infty} \frac{1}{T} E\left\{ \left| X_p(f) \right|^2 \right\} \tag{4.12}$$

In this work both the approaches given in Eqns. 4.11 and 12 are used to obtain the spectral characterisation of DPIM process.

The results of Eqn. 4.11 can be used to represent the spectral characterisation provided the following assumptions are made

(1) The limit as $T \to \infty$ will be taken as $T >> T_f$. This lends itself to numerical implementation.

(2) Numerical results of power spectral characterisation of Eqn. 4.11 will be compared with the measured data without employing averaging or carrying out expectations. The correlation of the measured and evaluated spectral results enable the validation of the spectral model.

Initially the PSD of the truncated realisation is obtained as given in Eqn. 4.11, assuming that the observation interval T is much greater than T_f (T>> T_f). The number of DPIM frames in the truncated time are given by $n\{S\} = L_n$, where S is the vector containing samples of the truncated sequence.

Taking DPIM samples S, then from Eqn. 4.5 the time delays to the k^{th} pulse in the truncated window can be represented by,

$$T_k = \left(2k + \sum_{m=0}^{k-1} S_m \right) T_s \tag{4.13}$$

From Eqn. 4.9, 11 and 13, the PSD is given by,

$$S_p(f) = \frac{1}{T_s\left(S_0 + S_1 + \ldots\ldots S_L + 2L_n\right)} \left| \Im\left\{ g(t) + + g\left(t - T_s\left(2 + S_0\right)\right) + \right.\right.$$
$$\left.\left. g\left(t - T_s\left(4 + S_0 + S_1\right)\right) + \ldots\ldots\ldots + g\left(t - Ts\left(2L_n + \sum_{m=0}^{L_n - 1} S_m \right)\right)\right\}\right|^2 \quad (4.14)$$

In Eqn. 4.14 the Fourier transform of the initial pulse and its delayed versions are represented by the first and subsequent terms, respectively. Equation 4.14 is best represented as,

$$S_p(f) = \frac{\left|G(f)\right|^2}{T_s\left(2L + \sum_{m\ 0}^{L_n} S_m \right)} \left| 1 + e^{-j2\pi f T_S (2 + S_0)} + e^{-j2\pi f T_S (4 + S_0 + S_1)} + \right. \quad (4.15)$$
$$\left. \ldots\ldots + e^{-j2\pi f T_S \left(2k + S_0 + S_1 + \ldots.. S_{L_n\ 1}\right)} \right|^2$$

where $G(f)$ is the DPIM pulse shape transform i.e. $G(f) = \Im\{g(t)\}$.

Finally, from Eqn. 4.15 the approximated DPIM PSD model can be given as,

$$S_p(f) = \frac{1}{T_s\left(2L_n + \sum_{m=0}^{L_n} S_m \right)} \left\{ \left| G(f) \sum_{k-0}^{L_n} e^{-j2\pi f T_s \left(2k + \sum_{m\ 0}^{k-1} S_m \right)} \right|^2 \right\} \quad (4.16)$$

The spectral model approximated by Eqn. 4.16 shows the direct evaluation of PSD from Eqn. 4.11, but does not explain the DPIM spectrum without numerically evaluating it. The PSD can also be evaluated indirectly from Eqn. 4.12 by representing the DPIM pulse stream at the slot level. This approach is similar to that adopted in the

evaluation of the PSD of a polar baseband signal with random binary data stream [*Couch*].

A DPIM pulse train can alternatively be modelled as,

$$x_B(t) = \sum_{n=-\infty}^{\infty} a_n g\left(t - nT_s - \tau_n\right) \tag{4.17}$$

where $g(t)$ is the signalling pulse shape, T_s is the slot duration, and τ_n is the random jitter within a time slot at threshold crossing at the receiver. The digital message may be regarded as a random time series of discrete numbers. A typical ensemble corresponds with a discrete message that can have an infinite discrete time sequence, ...a_{-2}, a_{-1}, a_0, a_1, a_2, ... Thus $\{a_n\}$ is a random variable that represents the presence or absence of a pulse in the n^{th} time slot. Knowing that the data coded into DPIM is of random nature, where the presence of a pulse is represented by $a_n = 1$ and absence by $a_n = 0$, their probabilities may be approximated by taking the average DPIM frame length (L_{avg}) into account,

$$P(a_n = 1) = \frac{1}{L_{avg}}, \qquad P(a_n = 0) = \frac{L_{avg} - 1}{L_{avg}} \tag{4.18}$$

The PSD is obtained by initially using the definition given in Eqn. 4.12 and taking into account the autocorrelation of data coded into DPIM along with the random jitter. Using Eqn. 4.12 on the truncated $x_B(t)$ given in Eqn. 4.17, when $x_p(t) = x_B(t)$, the PSD can by given by,

$$S(f) = \lim_{T\to\infty} \frac{1}{T} E\left\{ \left| G(f) \sum_{n=-N}^{N} a_n e^{-j2\pi f T_s} e^{-j2\pi f \tau_n} \right|^2 \right\} \tag{4.19}$$

where the observation interval $T = (2N+1)T_s$ and $2N+1$ is the total number of time slots. Then Eqn. 4.19 becomes,

$$S(f) = |G(f)|^2 \lim_{T\to\infty} \frac{1}{T}\left(\sum_{n=-N}^{N} \sum_{m}^{N} E\{a_n a_m\} E\left\{ e^{-j2\pi f(\tau_m - \tau_n)} \right\} e^{j2\pi f(m-n)T_s} \right) \tag{4.20}$$

To obtain Eqn. 4.20 in terms of the autocorrelation of discrete slots, the following definitions can be made,

$$R(k) = E\{a_n a_{n+k}\},\ M(f) = E\left\{ e^{-j2\pi f(\tau_m - \tau_n)} \right\}$$

letting $m = n+k$, substituting for T, and taking $(\tau_m - \tau_n) = \tau_k$, since τ is an independent identically distributed set of random variables, Eqn. 4.20 is simplified to,

$$S(f) = |G(f)|^2 \lim_{N\to\infty} \frac{1}{(2N+1)T_s} \left((2N+1) \sum_{k=-n-N}^{-n+N} R(k) |M(f)|^2 e^{j2\pi f k T_s} \right) \tag{4.21}$$

Since $\sum_{n=-N}^{N} = 2N+1$ and $N\to\infty$, $-n-N \to -\infty$ Eqn. 4.21 can be given as,

$$S(f) = \frac{|G(f)|^2}{T_S} \left(\sum_{k}^{\infty} R(k) |M(f)|^2 e^{j2\pi f k T_s} \right) \tag{4.22}$$

Separating $k = 0$ from other terms results in,

$$S(f) = \frac{|G(f)|^2}{T_S} \left(R(0)|M(f)|^2 + \sum_{k=-\infty}^{1} R(k) |M(f)|^2 e^{j2\pi f k T_s} + \sum_{k=1}^{\infty} R(k) |M(f)|^2 e^{j2\pi f k T_s} \right) \tag{4.23}$$

Changing the limits on the first summation yields,

$$S(f) = \frac{|G(f)|^2}{T_S} \left(R(0)|M(f)|^2 + \sum_{k=1}^{\infty} R(-k) |M(f)|^2 e^{-j2\pi f k T_s} + \sum_{k=1}^{\infty} R(k) |M(f)|^2 e^{j2\pi f k T_s} \right) \tag{4.24}$$

From the properties of autocorrelation $R(-k) = R(k)$ and, when $k = 0$, Eqn. 4.24 simplifies to,

$$S(f) = \frac{|G(f)|^2}{T_S}\left(R(0)|M(f)|^2 + 2\sum_{k-1}^{\infty} R(k)|M(f)|^2 \cos(2\pi f k T_s)\right) \tag{4.25}$$

Thus, collecting terms in Eqn. 4.25, the PSD representation becomes,

$$S(f) = \frac{|G(f)|^2}{T_S}\left(\sum_{k\ \infty}^{\infty} R(k)|M(f)|^2 e^{-j2\pi f k T_s}\right) \tag{4.26}$$

$R(k)$ can be given for the pulse stream as follows[*Couch*],

$$R(k) = \sum_{i-1}^{I} (a_n a_{n+k})_i P_i \tag{4.27}$$

where P_i is the probability of obtaining the product $(a_n a_{n+k})_i$ and has I possible combinations. From Eqn. 4.26, it can be seen that the PSD of the DPIM pulse stream is influenced by the spectrum of the pulse shape and discrete data, as well as the jitter effect. Assuming that data symbols are uncorrelated and the mean value of the discrete pulses is non zero, from [*Couch*], [*Sklar*],

$$\begin{aligned} &\text{for } k = 0,\ R(0) = \overline{a_n^2} = \sigma_a^2 + m_a^2 \\ &\text{for } k \neq 0,\ R(k) = \overline{a_n a_{n+k}} = m_a^2 \end{aligned} \tag{4.28}$$

where the mean and variance are $m_a = \overline{a_n}$ and $\sigma_a^2 = \overline{a_n^2} - m_a^2$, respectively. Substituting in Eqn. 4.26,

$$S(f) = \frac{|G(f)|^2|M(f)|^2}{T_S}\sigma_a^2 + \frac{|G(f)|^2}{T_S} m_a^2 \sum_{k=-\infty}^{\infty} |M(f)|^2 e^{-j2\pi f k T_s} \tag{4.29}$$

where m_a^2 and σ_a^2 are found to be,

$$m_a^2 = \frac{1}{L_{avg}^2}$$

$$\sigma_a^2 = \frac{L_{avg} - 1}{L_{avg}^2} \tag{4.30}$$

From the Poisson sum formula,

$$\sum_{k=-\infty}^{\infty} e^{j2\pi fkT_s} = \frac{1}{T_s} \sum_{k=-\infty}^{\infty} \delta(f - nf_s)$$

Simplifying Eqn. 4.29,

$$S(f) = \frac{|G(f)|^2 |M(f)|^2}{T_S} \sigma_a^2 + \frac{|G(f)|^2}{T_s^2} m_a^2 \sum_{n=-\infty}^{\infty} |M(nf_s)|^2 \delta(f - nf_s) \tag{4.31}$$

The first term gives the continuous part of the spectrum, whereas the second term gives the discrete part representing the slot frequency harmonics. From Eqn. 4.31, it can be assumed that the first term represents the noise floor around the discrete frequency components. A phase lock loop (PLL) can be used to extract the slot timing. However, the extracted slot component will experience jitter due to the noise seen by the PLL (the continuous part).

Therefore, the noise power spectrum may be written as,

$$N_f = \frac{|G(f)|^2 |M(f)|^2 \sigma_a^2}{T_S} \tag{4.32}$$

and the total power at the slot fundamental frequency is given by,

$$P_s = \frac{|G(f_s)|^2}{T_s^2} |M(nf_s)|^2 m_a^2 \tag{4.33}$$

If the random jitter due to noise, represented by τ_n, is considered as zero mean Gaussian random variables, then

$$M(f) = e^{-2\pi^2\sigma_\tau^2 f^2} \tag{4.34}$$

where σ_τ^2 represents the threshold crossing timing variance. To evaluate $M(f)$, a knowledge of the receiver noise is essential. It has been shown that bit transition jitter, due to the additive channel noise has little effect on the bit timing jitter, whereas the noise, due to the randomness in the received bit pattern is the primary cause of the clock timing jitter [*Gangopadhyay*]. The jittered extracted slot timing can cause the ideal pulse to fall into the adjacent slots in the extreme case. With a linearised PLL model the slot clock timing variance can be expressed in rad^2 as [*Gardner*79],

$$\sigma_s^2 = \frac{B_L N_f}{P_s} \tag{4.35}$$

where B_L is the PLL bandwidth.

The error due to jitter effect is denoted by,

$$P_{ss} = erfc\left(\frac{\pi}{\sigma_s}\right) = erfc\left(\frac{\pi m_a}{\sqrt{B_L T s \sigma_a}}\right) \tag{4.36}$$

The probability of a pulse being detected in an adjacent slot, corresponding to a proper slot due to the jitter effect is evaluated in a later section. In this section the DPIM model given in Eqn. 4.16 and 4.31 are further investigated. Since the spectrum is mainly dependent on the pulse shape, the PSD is obtained for rectangular as well as for Guassian shape pulses.

4.2.1 Rectangular shape pulses

In wide band systems, rectangular shaped pulses are little effected by the dispersive nature of the channel. Thus the pulse shape transform can be approximated by a *sinc* function whose poles and zeros may be varied by varying the duty cycle (γ) of a pulse. The pulse transform is given by,

$$G(f) = \frac{1}{\pi f}\sin(\pi f T_s \gamma) \tag{4.37}$$

Equation 4.16 can be explained in two parts, i.e. the pulse shape transform $G(f)$ and the frequency domain representation of the delayed pulses corresponding to different frame $T(f)$, where,

$$T(f) = \sum_{k=0}^{L} e^{\,j2\pi f T_s \left(2k + \sum_{m=0}^{k-1} S_m\right)} \tag{4.38}$$

The spectral behaviour can be explained in two steps: (1) frequencies at poles and troughs and (2) all other frequencies.

A rectangular pulse of width γT_s gives troughs in the frequency domain at the frequencies corresponding to slot frequency harmonics given by,

$$f_z = \left(\frac{z+1}{\gamma}\right)\frac{1}{T_s} \tag{4.39}$$

where $z = 0, 1, 2...N$, e.g. for γ=0.5 zeros at $2/T_s$, $4/T_s$, $6/T_s$ .....etc

From Eqn. 4.38 let,

$$Q_k = 2k + \sum_{m=0}^{k-1} S_m \tag{4.40}$$

where Q_k is the time delay to the k^{th} pulse, which is always an integer.

Equation 4.38 can be rewritten using Q_k as,

$$T(f) = \sum_{k=0}^{L} \cos 2\pi Q_k T_s f - j \sin 2\pi k Q_k T_s f \tag{4.41}$$

From Eqn. 4.41, when fT_s is an integer i.e. at slot frequency harmonics, $T(f)$ gives a summation in phase with $G(f)$ irrespective of the pulse duty cycle, see Fig. 4.5. The combination of $T(f)$ and $G(f)$ gives the resultant spectra.

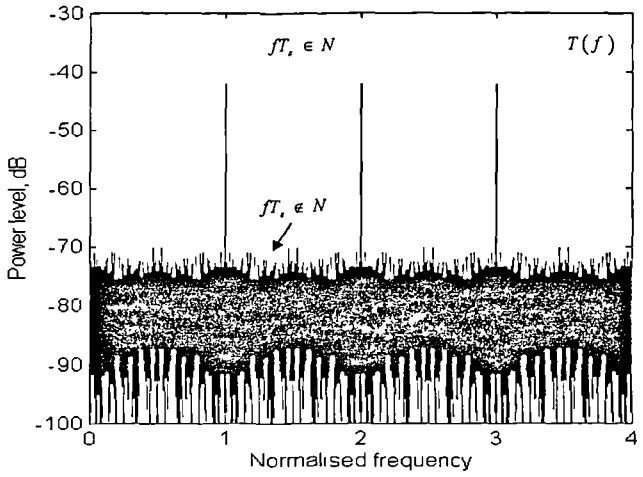

Fig. 4.5 Exponential term for a given random data sequence.

Slot frequency harmonics that overlap with the zeros of the pulse transform result in low power spectral components, whereas non overlapping harmonics result in distinct spectral components. For frequencies not harmonically related to slot frequency, the summation $T(f)$ can be described as non-zero amplitudes with magnitudes always smaller than those which are at slot frequency harmonics, see Fig. 4.5. Thus the spectrum consist of distinct frequency components at the slot frequency and its harmonics, other than those at which the pulse transform give zeros as given by Eqn. 4.39. This suggests that presence of the slot rate component is affected by the pulse shape transform.

Equation 4.16 was numerically evaluated in order to verify the predicted spectral properties. A random data generator was used to obtain a number of random frames within a specific period at specified bit resolution. A bit resolution of 4 was initially chosen to give 16 (= 2^4) different DPIM frames with shortest and longest frame lengths of $2T_s$ and $17T_s$ respectively. The probability of an occurrence of a particular symbol was held at 1/16. The selected DPIM pulse stream contains 4000 random frames, the probability of frame variation is shown in Fig. 4.6. This figure shows that the frames are approximately equally distributed.

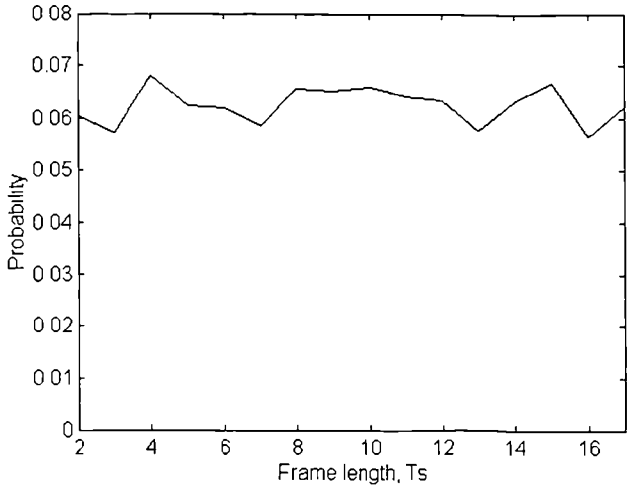

Fig. 4.6 Probability distribution of the random frames.

The spectral behaviour of the above samples was numerically evaluated using Eqn. 4.16 and the results obtained are shown in Fig. 4.7(a)-(d) for pulse duty cycle γ = 0.25, 0.5, 0.75 and 1 respectively.

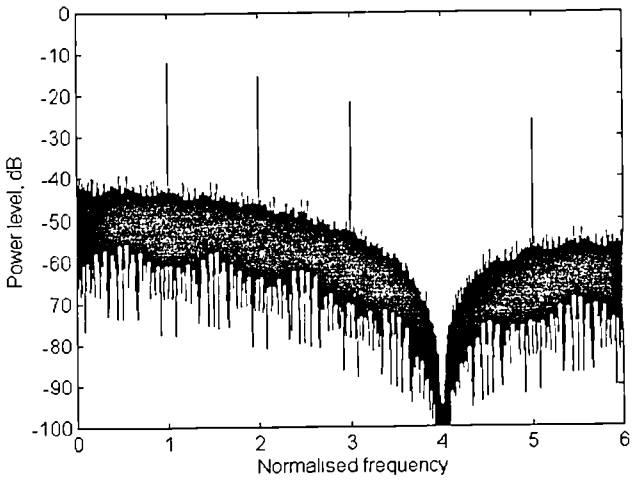
Power level, dB
Normalised frequency

(a)

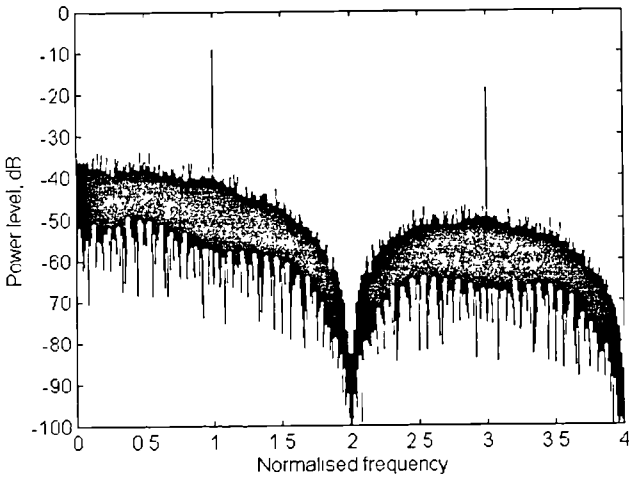
Power level, dB
Normalised frequency

(b)

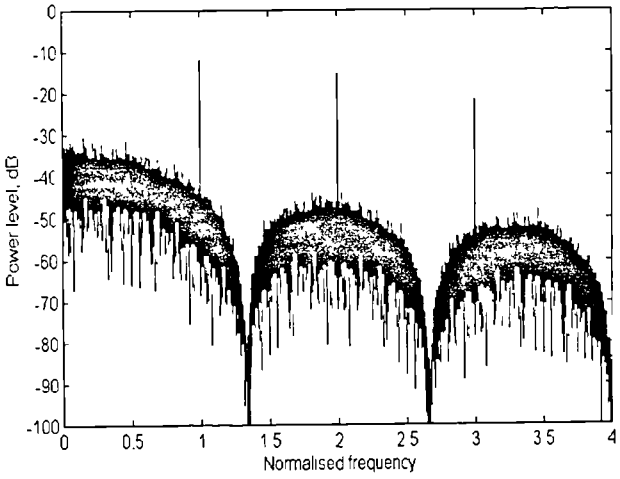
Power level, dB
Normalised frequency

(c)

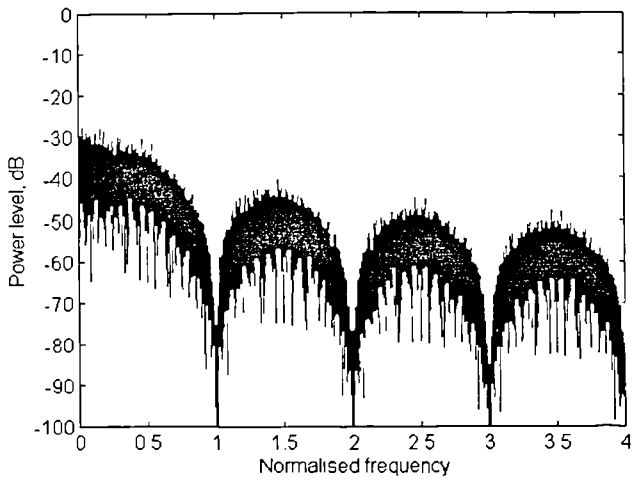

(d)

Fig. 4.7 DPIM PSD for 4 bit and pulse duty cycle γ of :
(a) 0.25, (b) 0.5, (c) 0.75 and (d) 1.

Zero or low power slot frequency harmonics can be observed in each case, as predicted from Eqn. 4.39, i.e. at $4f_s$, $8f_s$ .... corresponding to $\gamma = 0.25$; at $2f_s$, $4f_s$ .... corresponding to $\gamma = 0.5$; at $4f_s/3$, $8f_s/3$ .... corresponds to $\gamma = 0.75$; and at f_s, $2f_s$ ..... corresponding to $\gamma = 1$. The position and amplitude of the distinct slot frequency component changes as the pulse duty cycle is varied. When the pulse for $\gamma = 1$ (i.e. pulse of full slot duration), zero crossing frequency components coincides with the slot frequency components, and the spectral profile resembles a general *sinc* envelope shape, cancelling out the distinct slot component, see Fig. 4.7(d). To regain the slot component non-linear processing is required at the receiver. The presence of the slot rate component is therefore affected by the pulse shape only.

4.2.2 Gaussian shape pulses

The transfer characteristics of a guided path or the transmission media may vary sufficiently over a wide band of frequencies (wavelengths in the case of optical fibre). If the dispersion is significant then the received pulse can be approximated to be a Gaussian shape, see Fig. 6.2. The pulse shape can be expressed as,

$$g(t) = \frac{1}{\sqrt{2\pi}\sigma} e^{-\frac{t^2}{2\sigma^2}} \tag{4.42}$$

where σ is the RMS pulse width.

The pulse transform can be given by,

$$G(\omega) = e^{\frac{\omega^2\sigma^2}{2}} \tag{4.43}$$

Depending on the amount of pulse spreading, the received RMS pulse width may vary. The enhancement of the slot rate component with dispersed pulses is limited by the availability of the channel bandwidth. Spectral components at the nulls of the spectrum observed with rectangular pulses are increased, giving rise to a flat PSD. Unlike rectangular pulses, the pulse transform does not show singularities at the slot frequency, thus ensuring a distinct slot frequency component. The spectra were obtained for a Gaussian shaped pulse with $t_{FWHM} = 0.2T_s$, using the same data sequence used with rectangular pulses, see Fig. 4.8.

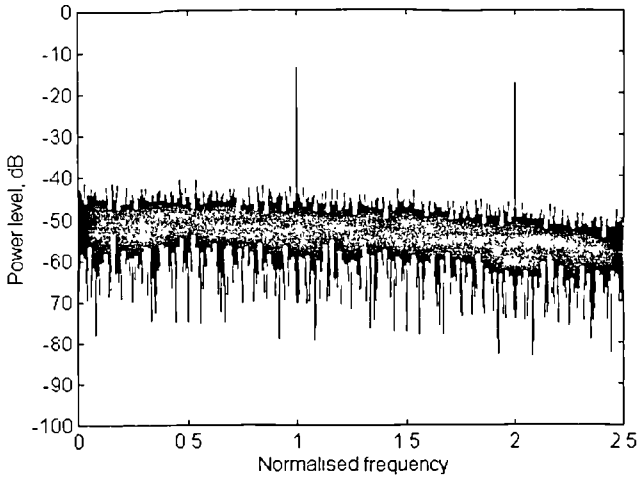

Fig. 4.8 Spectral synthesis for Gaussian received pulses for t_{FWHM} of 0.2 T_s.

From Fig. 4.8 distinct slot components exist at the slot frequency and its harmonics. There are no singularities in the Gaussian pulse shape at the slot component. Therefore dispersed received Gaussian pulses always guarantee the presence of a distinct slot component.

4.3 Spectral Prediction

For different pulse shapes, Eqn. 4.24 can also be used to predict DPIM spectral shape. Fig. 4.9(a)-(d) gives predicted spectra for rectangular pulses of slot duty cycle (γ) 0.25, 0.5, 0.75 and 1 T_s respectively.

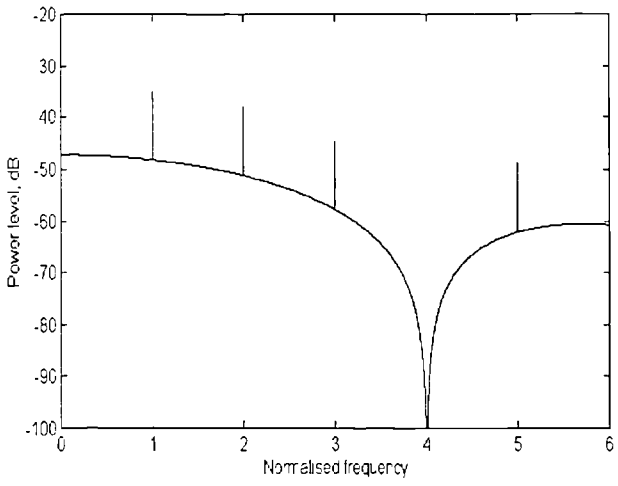

(a)

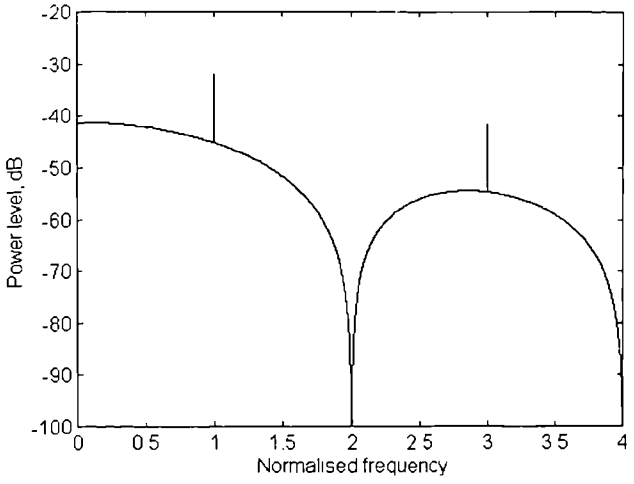

(b)

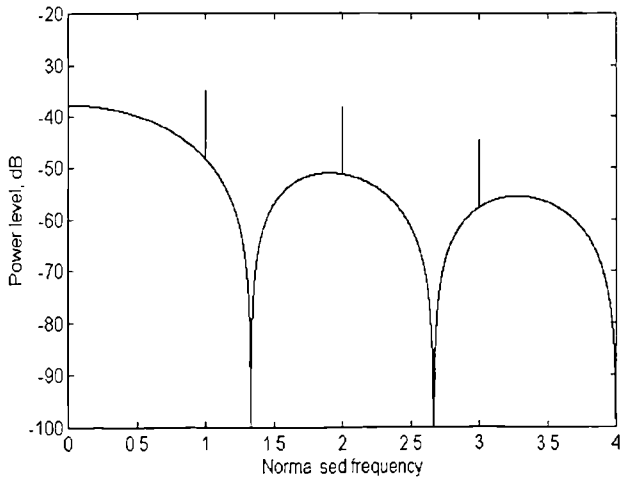

(c)

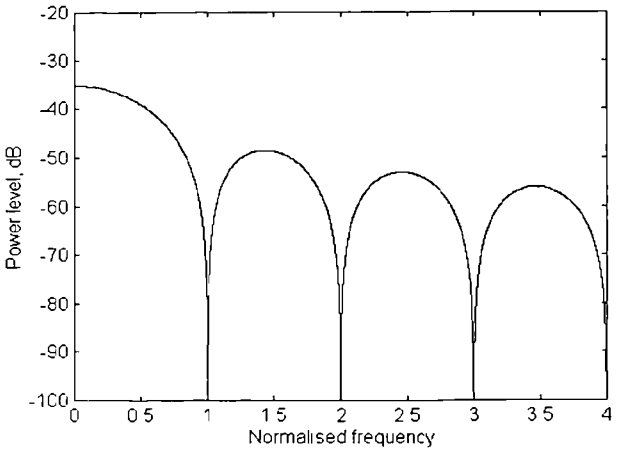

(d)

Fig. 4.9 Predicted DPIM PSD for 4 bit and pulse duty cycles γ of :

(a) 0.25, (b) 0.5, (c) 0.75 and (d) 1.

Comparing Fig. 4.7(a)-(d) with 4.9(a)-(d) it can be seen that spectral predictions by Eqn. 4.31 closely match with the respective spectral synthesis by Eqn. 4.16.

4.4 Spectral Verification

A 4-bit DPIM prototype system given in section (7.1), operating at slot frequency of 1MHz, has been used to verify the spectral results. Initially, a random data sequence is used with pulse duty cycle (γ) of 0.25, 0.5, 0.75 and 1 T_s and the results are shown in Fig. 4.10(a)-(d) respectively.

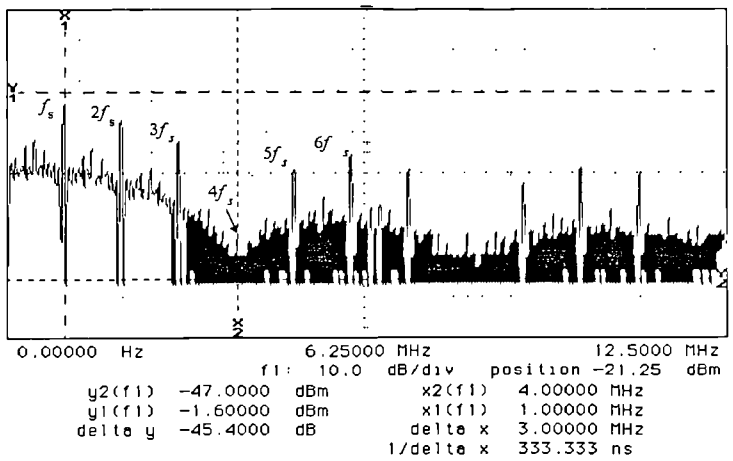
f_s
$2f_s$
$3f_s$
$4f_s$
$5f_s$
$6f_s$
0.00000 Hz
6.25000 MHz
12.5000 MHz
f1: 10.0 dB/div position -21.25 dBm
y2(f1) -47.0000 dBm
y1(f1) -1.60000 dBm
delta y -45.4000 dB
x2(f1) 4.00000 MHz
x1(f1) 1.00000 MHz
delta x 3.00000 MHz
1/delta x 333.333 ns

(a)

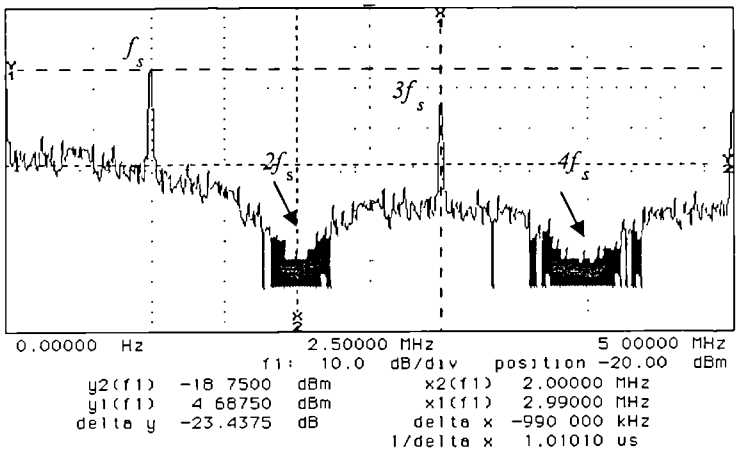
f_s
$2f_s$
$3f_s$
$4f_s$
0.00000 Hz
2.50000 MHz
5.00000 MHz
f1: 10.0 dB/div position -20.00 dBm
y2(f1) -18.7500 dBm
y1(f1) 4.68750 dBm
delta y -23.4375 dB
x2(f1) 2.00000 MHz
x1(f1) 2.99000 MHz
delta x -990.000 kHz
1/delta x 1.01010 us

(b)

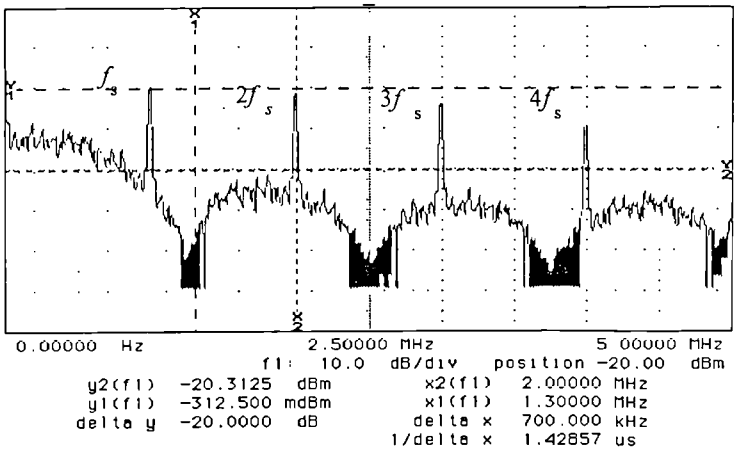
f_s
$2f_s$
$3f_s$
$4f_s$
0.00000 Hz
2.50000 MHz
5.00000 MHz
f1: 10.0 dB/div position -20.00 dBm
y2(f1) -20.3125 dBm
y1(f1) -312.500 mdBm
delta y -20.0000 dB
x2(f1) 2.00000 MHz
x1(f1) 1.30000 MHz
delta x 700.000 kHz
1/delta x 1.42857 us

(c)

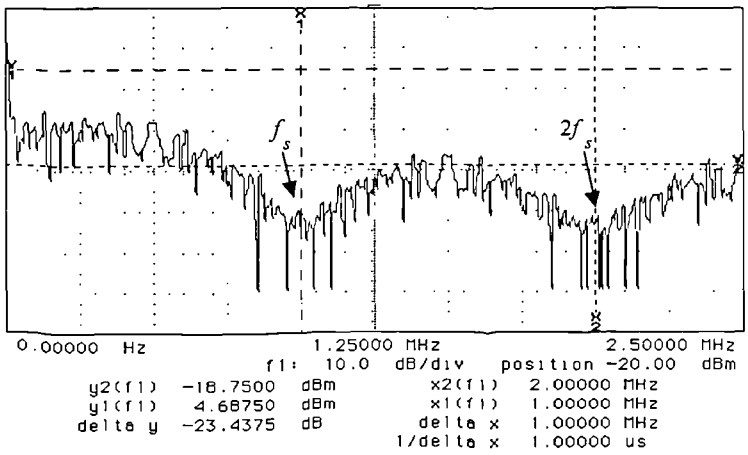

(d)

Fig. 4.10 Measured DPIM PSD for 4 bit system with γ of :

(a) 0.25, (b) 0.5, (c) 0.75 and (d) 1.

The spectral results show the presence of distinct slot components, the pulse shaping effect and a continuum due to the random data, closely agreeing with the predicted spectra obtained using Eqn. 4.16 and 4.31 (see Fig. 4.7(a)-(d) and 4.9(a)-(d)). This close agreement leads strong support to the validity of the mathematical models developed.

In the case of a dispersive channel, the received pulse shape is expected to be a Gaussian shaped, as given by Eqn. 4.42. The predicted spectrum of a DPIM pulse train obtained by Eqn. 4.16 for a pulse transform given by Eqn. 4.43, is shown in Fig. 4.8. Pulses have a full-width half-maximum $t_{FWHM} = 0.2\ T_s$, with the frequency and signal level being normalised as in the previous figures. Figure 4.11 illustrates the measured spectra obtained at a receiver placed at the end of a 550 meter spool of multimode graded index fibre with attenuation of 30 dB/km. The received pulses are dispersed, near Gaussian shaped, and the spectra closely agrees with the predicted results (see Fig. 4.8). In both plots, the spectrum contains a distinct slot component and harmonics. Both the plots show that the slot component is about 22 dB above the noise floor.

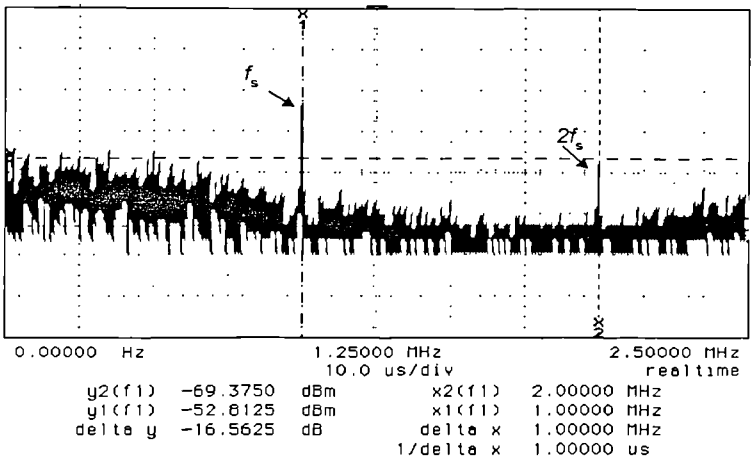

Fig. 4.11 Measured spectra for Gaussian received pulses.

The spectra do not posses singularities at the harmonics given by Eqn. 4.39 due to the pulse transform. This proves the validity of spectral model for different pulse shapes. Furthermore, the presence of a distinct slot component in the pulse stream for dispersed pulses as well as rectangular pulses indicates the possibility of employing a PLL for clock extraction in wide band as well as band limited channels.

4.5 PSD for Periodic Frame Structure

The PSD obtained in section 4.3 was for random frame sequences. Here the spectra are investigated for a data sequence with built in frame periodicity. Spectral variation in the presence of a strong periodic component in the modulating signal can be investigated by using a single tone periodic signal.

Assume that input to the DPIM modulator is given by,

$$V(t) = V_m \sin 2\pi f_m t \tag{4.44}$$

where V_m is the signal amplitude and f_m is the frequency.

A DC level (V_{DC}, where $V_{DC} \geq V_m$) is added to the modulating signal to avoid negative signal swing. Thus the input to the DPIM modulator can be given by,

$$V_{DPIM}(t) = V_{DC}\left(1 + m\sin\left(2\pi f_m t\right)\right) \tag{4.45}$$

where m is the modulation index (defined as the ratio of peak modulating signal amplitude to the DC voltage). The conversion range of the DAC in this case is V_{DAC}, where $V_{DAC} \geq 2V_m$.

At the modulator, the level shifted modulating signal is sampled by the sampler given by,

$$x_\delta(t) \triangleq \sum_{p1=-\infty}^{\infty} \delta\left(t - t_{p1}\right) \tag{4.46}$$

where the sampling times t_{p1} depends on the modulating signal and can be given by,

$$t_{p1} = T_S\left\{\sum_{m1}^{p} \left(2 + \frac{2^M}{V_m} V_{DC}\left(1 + m\sin 2\pi f_m t_{m1}\right)\right)\right\} \tag{4.47}$$

From Eqn. 4.47, t_{p1} approximates the frames associated with the modulating signal given by Eqn. 4.45. Using a periodic modulating signal as the baseband signal, pulse displacement can be taken as periodic. DPIM spectral performance in the presence of periodicity in the modulating signal can be observed by substituting for f_m and f_s in Eqn. 4.16, at slot frequency and modulating frequency harmonics.

$$S(f_{pf_s+qf_m}) = \frac{1}{T_s\left(2L_n + \sum_{m=0}^{L} S_m\right)}\left\{\left|G(f)\sum_{k=0}^{L_n} e^{-2j\pi(pf_s \pm qf_m)T_s Q_k}\right|^2\right\} \tag{4.48}$$

where pf_s and qf_m gives the slot frequency and modulating signal harmonics for p – 0,1,2,.... and q = 0,1,2,3.. respectively. At slot frequency harmonics q = 0, the exponential term gives a summation that is in phase with the pulse shape transform as described in section 4.3.

$$S(f_{f_s+qf_m}) = \frac{1}{T_s\left(2L_n + \sum_{m=0}^{L_n} S_m\right)} \left\{ \left| G(f) \sum_{k-0}^{L_n} e^{-j2\pi p f_s Q_k} e^{\ 2\pi q f_m T_s Q_k} \right|^2 \right\} \tag{4.49}$$

As $\left| e^{\ j2\pi pQ_k} \right| = 1$ Eqn. 4.55 equation simplifies to,

$$S(f_{pf_s+qf_m}) = \frac{1}{T_s\left(2L_n + \sum_{m=0}^{L_n} S_m\right)} \left\{ \left| G(f) \sum_{k=0}^{L_n} e^{-jq\frac{Q_k}{2^M+1}} \right|^2 \right\} \tag{4.50}$$

For $Q_k = r(2^M+1)$, where r is an integer Eqn. 4.50 gives components which are inphase with the pulse transform. Distinct frequency components at harmonics of the modulating signal are thus dependant on the data S. Periodicity in the data does not guarantee that Q_k is an integer multiple of 2^M+1. For frequencies other than harmonics of the modulating signal, frequency summation gives a non zero resultant with a phase which is not as strong as that obtained for frequencies corresponding to harmonics of the modulating signal frequency. Figure 4.12 shows the numerically evaluated exponential term for a periodic single tone sinusoidal signal.

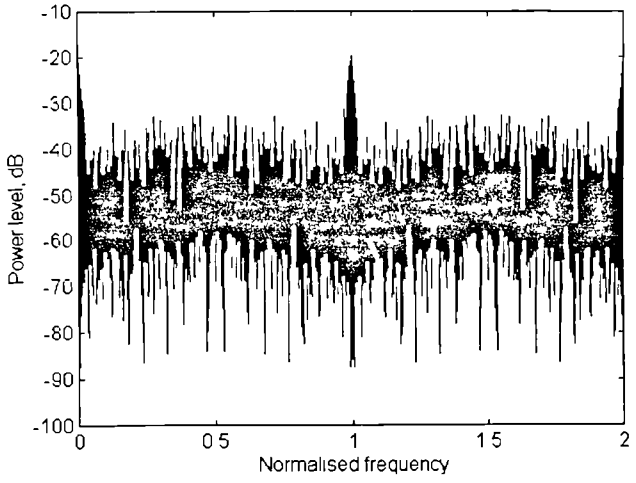

Fig. 4.12 Spectral behaviour of the exponential term for a periodic data sequence.

This is combined with the pulse transform and the resultant spectrum is shown in Fig. 4.13.

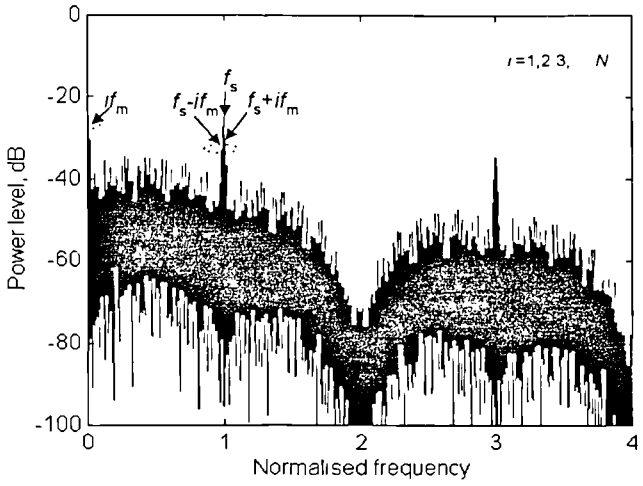

Fig. 4.13 Spectral synthesis corresponds to single tone periodic baseband.

Closer examination of Fig. 4.13 reveals that there are clusters of frequency components, spaced by the modulating signal frequency and its harmonics, around the slot component. This was confirmed by PSD measurements, obtained from a single tone sinusoidal signal at 20 kHz as the input to the modulator, see Fig. 4.14.

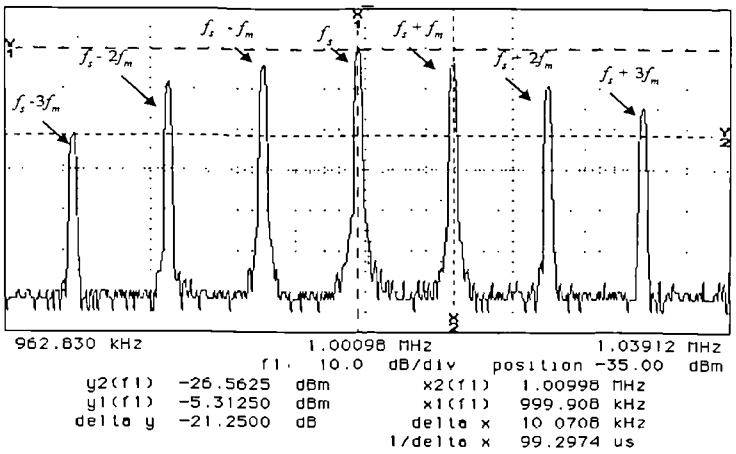

Fig. 4.14 Spectral components around the slot component.

Compared to the spectrum obtained for the random data case (see Fig. 4.7(a)-(d)), the slot frequency component is less distinct, therefore fine tuning of the PLL is essential in

order to establish slot synchronisation. Also the presence of baseband component and its harmonics is confirmed as predicted in Fig. 4.13. Measured results are shown in Fig. 4.15.

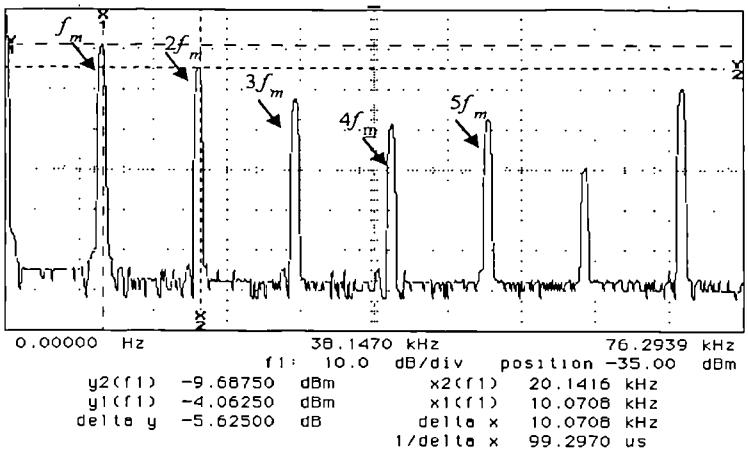

Fig. 4.15 Spectral components at the baseband region.

Similar measurements were carried out for a periodic rectangular modulation signal. With such signals spectra around the slot component found to be crowded and less distinct slot component requiring further constraints on the PLL. The amplitudes of the base band components strongly depend on the bit resolution. Figure 4.16 illustrates the 2^{nd} and 3^{rd} harmonic distortion as the bit resolution vary. For 4 bit and higher resolution, 2^{nd} and 3^{rd} harmonic distortion closely agree with the measured values, as shown in Figs. 4.15 and 4.16. Since harmonic distortion is relatively high in the baseband region, in contrast to continuous PIM, simple low-pass filtering of the baseband component will result in a highly distorted signal, unless an ideal brick wall filter response is achieved. Therefore, to avoid higher level of harmonic distortion, a regeneration scheme is recommended for signal recovery.

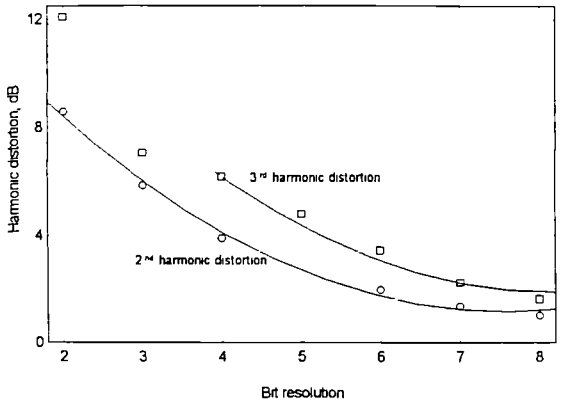

Fig. 4.16 2nd and 3rd harmonic difference variation with the bit resolution.

4.6 Slot Power Variation with Pulse Width

For varying pulse widths *Gardner* has noted variation of power in the slot component in pulse modulation techniques [*Gardner*79]. For DPIM the slot power level was evaluated using Eqn. 4.23 and the result is plotted against pulse width is shown in Fig. 4.16.

Slot power level is evaluated above the continuum of the spectrum at the slot component. Figure 4.17 shows that, as the slot width increases from the low level power associated with the slot component, a maximum occurs for a duty cycle of 50 %. Further increase results in a symmetrical decrease.

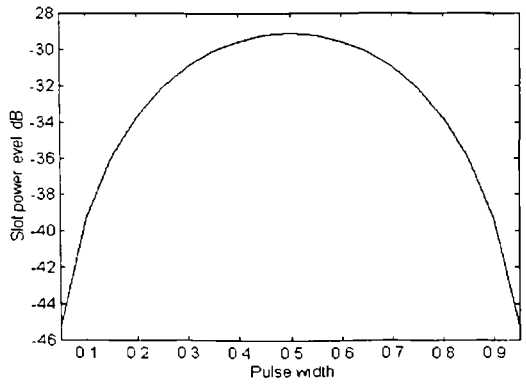

Fig. 4.17 Slot power as a function of the DPIM pulse width.

4.7 Slot Power Variation with Bit Resolution

From Eqn. 4.16, the DPIM spectrum is affected by pulse shape. As the bit resolution increases the time slots become smaller. Thus, slot power also varies with the bit resolution. Figure 4.18 shows the normalised power level of the slot component against the bit resolution. This shows that the power associated with the slot component drops at a rate of 2.6 dB per 1 bit increase of the resolution. At high bit resolution the slot component level drops significantly into the noise floor, thus making recovery quite complex.

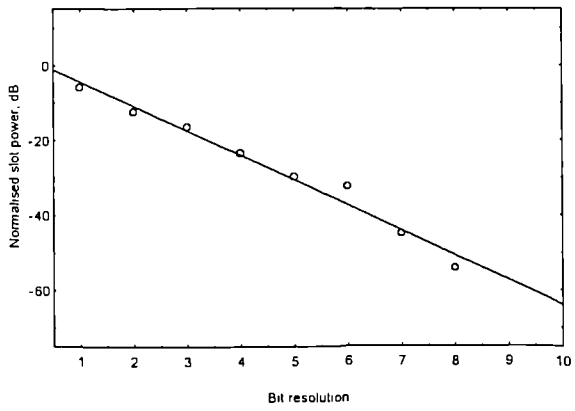

Fig. 4.18 Slot power variation with bit resolution.

4.8 Summary

In this chapter some properties of the DPIM code are presented. DPIM transmission capacity through to a detailed spectral profile have been investigated. DPIM is shown to have higher information capacity compared to anisochronous DPIWM and isochronous PCM/DPPM. Its capacity approaches twice that of PPM/DPPM for a bit resolution of 8 and over. Its spectrum contains distinct slot components for rectangular as well as for Gaussian shaped pulses, enabling PLL for clock extraction in both wide-

band and band-limited channels. The power level of the distinct component is found to be dependant on the pulse width and bit resolution: symmetrical variation around pulse width of 50 % duty cycle and dropping at 2.6 dB per 1 bit increase, respectively. The modulation spectrum contains base band components with high level of harmonic distortion, suggesting that regeneration rather than simple low-pass filtering is necessary to avoid higher levels of harmonic distortion in the recovered signal.

Chapter Five

DPIM System Overview

In the previous chapter spectral behaviour of DPIM was investigated and mathematical expressions were presented. This chapter looks at the building blocks of point-to-point optical fibre DPIM system. Initially, DPIM modulator and demodulator structures are presented for analogue and digital information transmission. The overall system which has been illustrated is that to support analogue signal transmission.

5.1 Introduction

The block diagram representation of a typical optical fibre DPIM system is shown in Fig. 5.1. Transmitter consist of DPIM modulator and an optical source driver. Input to the transmitter can be either a continuous (analogue) or discrete (digital) signal. In both cases the information is represented as an M bit parallel data into the modulator. Optical source driver converts the DPIM electrical pulse stream to suit the transmission channel, in this case optical fibre.

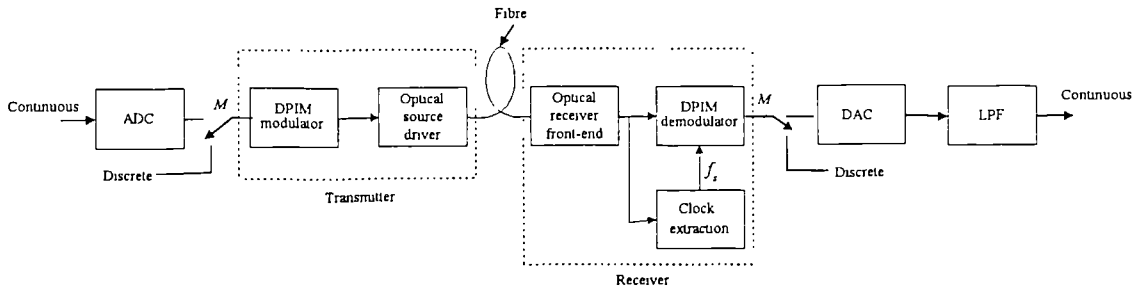

Fig. 5.1 Optical fibre DPIM communication system.

The receiver consists of optical signal detection and amplification (front-end), clock extraction and the decoding subsystems. The following sections describe the function of each module.

5.2 Modulator Structures

To minimise ISI in dispersive channels, a guard band can be included in each frame as described in section 4.2. However, at low data rate transmission over fibre, guard band may be ignored due to the negligible pulse spreading. As block diagram of a typical modulator is illustrated in Fig. 5.2. DPIM modulator and demodulator can take two different forms depending on the type of information being transmitted, analogue or digital.

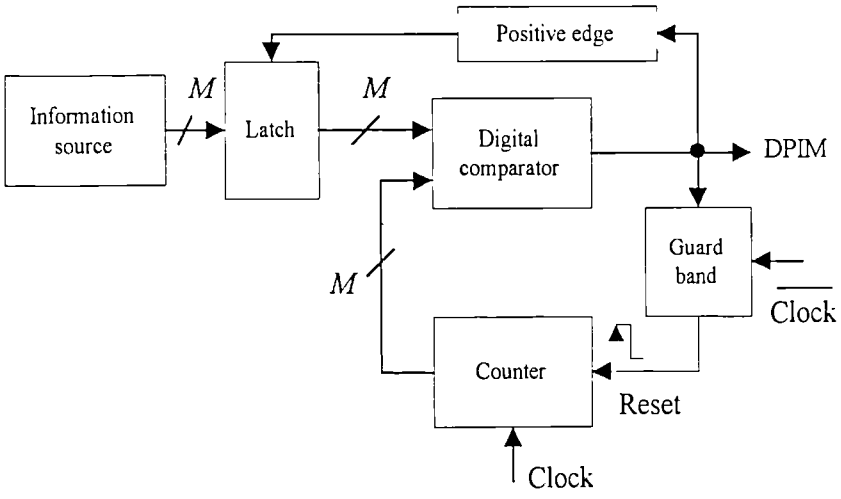

Fig. 5.2 Typical DPIM modulator structure.

The counter is clocked at the rate of slot frequency. M bit symbols from the latch and counter are input to the comparator, the output of which stays high when the two input symbols are equal. The counter then is forced to stay low for a period of one time slot (delay). A symbol is latched for the next DPIM frame at the positive edge of the comparator output. For analogue signal transmission, the information source is effectively an ADC which converts the analogue signal into a set of symbols. At the positive edge of the pulses the symbols are latched.

The anisochronous nature of the scheme suggests that DPIM sampling points vary depending on the symbol or the signal amplitude level. For an analogue signal the slot frequency is determined such that the lowest possible sampling frequency variation is equal to the Nyquist rate. Lowest sampling frequency, or the longest frame length, corresponds to the maximum signal level that can be accommodated by the ADC. For modulation signal frequency of f_m the slot frequency can be worked out as:

$$f_s = 2f_m(L+1) \tag{5.1}$$

where $L = 2^M$.

The DPIM modulator for an analogue signal transmission can be simplified by considering the successive approximation ADC operation (see Fig. 5.3). A level shifted analogue signal is input to the comparator. Level shifting is performed in order to avoid a negative signal swing. The parallel M bit counter output is the input to the digital-to-analogue converter (DAC). The output of the DAC is a ramp waveform which is then input to the comparator. The output stays high when both the inputs at the comparator are equal, see Fig. 7.2 in chapter seven. The delay block holds the counter at 0 for a given number of time slots.

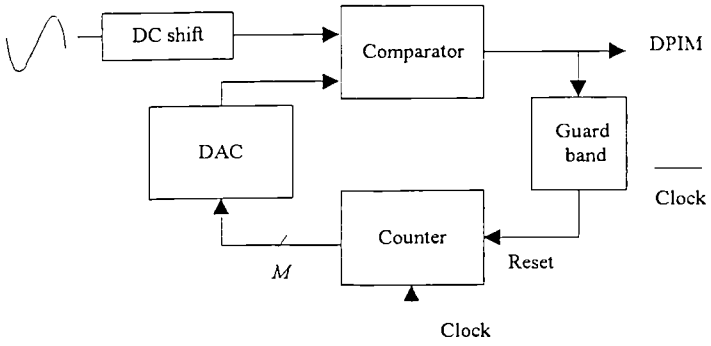

Fig. 5.3 DPIM modulator for analogue signal transmission.

5.3 Demodulator Structure

In the DPIM modulation process a pulse located at the start of each frame has dual role of frame initiation and time reference for the proceeding and succeeding frames. Therefore, at the receiver the demodulation process becomes far easier compared with DPPM, and is simply performed by counting time slots between two successive pulses. Figure 5.4 illustrates a block diagram of a DPIM demodulator.

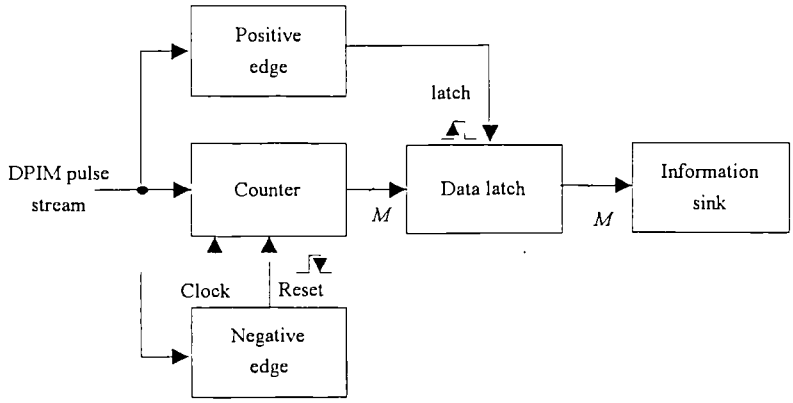

Fig. 5.4 DPIM demodulator block diagram.

The positive edges of the received DPIM pulse train is used to latch M bit symbol into the data latch, while the negative edge resets the counter. The counter is then held for the duration of guard band. This is equivalent to subtracting a number of time slots

from each frame. For analogue signal transmission, the data at the output of the latch is then dumped into a DAC.

5.4 Optical Source Driver

The function of the optical source is to convert electrical energy, in the form of current, into an optical energy and to launch it into an optical fibre. Mainly two types of sources can be employed in pulse transmission systems:- LED (light emitting diode) or laser diode (LD). The optical source should ideally be linear, directional, efficient and emit wavelengths corresponding with low fibre losses and dispersion. Selection criteria mainly depends on the data rate being used. Figure 5.5 shows LED and LD limits along with the slot frequency variation with source data rate. Choice of word size or the bit resolution is also dependant on the device peak-to-average power ratio. With average power limited sources, data rate may be maximised by maximising the coding efficiency, whereas in peak power limited sources the data rate dependency is proportional to the inverse of the bandwidth expansion [*Mecherle*85].

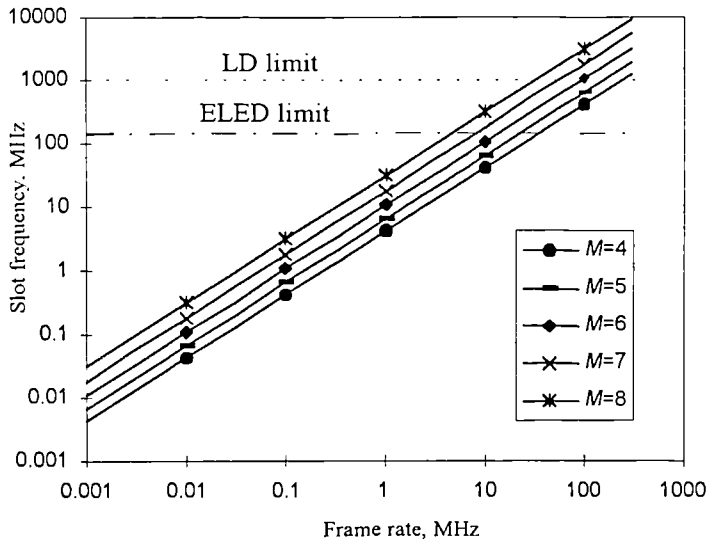

Fig. 5.5 Slot frequency Vs. frame rate for different bit resolutions.

Figure 5.5 shows that at frame rate of 10 MHz ELED can be used in 4, 5 and 6 bit DPIM systems, whereas 7 and 8 bit systems require LD optical sources. The average power variation of DPIM with respect to PCM can be given by,

$$\frac{P_D}{P_C} = \frac{2}{L_x}\frac{\sqrt{(L+1)\gamma}}{\sqrt{\log_2 L}} \tag{5.2}$$

where γ is the slot duty cycle, L_x represents varying DPIM frame length in time slots, and P_D and P_C are the DPIM and PCM average power, respectively. From Eqn. 5.2 average power level depends on the source symbols which in turn determines the frame length.

Average power variation of DPPM, P_P, with respect to PCM can be given by,

$$\frac{P_P}{P_C} = \frac{2\sqrt{c\gamma}}{\sqrt{L\log_2 L}} \tag{5.3}$$

where c is the DPPM compression index.

DPPM average power is constant compared to PCM where power is dependant on the symbol. From Eqns. 5.2 and 5.3 the DPIM average power with respect to DPPM can be given by,

$$\frac{P_D}{P_P} = \frac{1}{L_x}\sqrt{\frac{L(L+1)}{c}} \tag{5.4}$$

Figure 5.6 shows DPIM and DPPM average normalised to PCM average power for different symbols.

Number of time slots within a DPPM/DPIM is bit resolution dependant. From Fig. 5.6, the dotted line shows the DPPM average power for a particular bit resolution and the solid line shows the DPIM average power for different frame patterns.

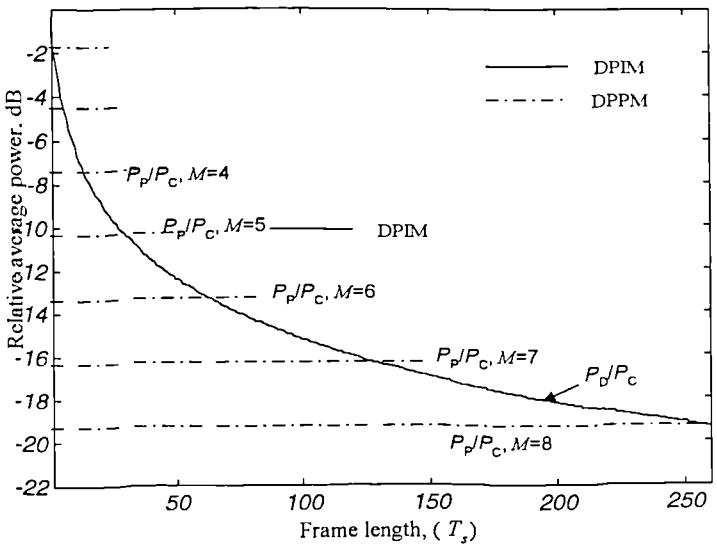

Fig. 5.6 DPIM and DPPM average power normalised to PCM vs. frame length.

For a particular bit resolution DPPM display a constant average power per frame, whereas for DPIM, due to variable frame structure, the average power is frame dependent. DPIM systems display higher average power than DPPM except at the longest frame length where both schemes have the same power.

5.4.1 Coding to reduce average power

As discussed in section 5.4, DPIM average power is considerably higher compared with DPPM. Therefore, operating it at the same power level as DPPM may result in saturation of the receiver. However, this effect can be reduced by reorganising the frame structure by means of a lookup table before converting into DPIM. For an example, an arbitrarily assigned lookup table for 4 bit DPIM can be given by table 5.1 as,

Symbol	0	1	2	3	4	5	6	7	8	9	10	11	12	13	14	15
Encoded to	0	14	2	12	4	10	6	8	7	9	5	11	3	13	1	15

Table 5.1 DPIM transmitter lookup table.

The reorganising of frames can be optimised for best average power performance. Furthermore, the encoding process breaks the periodicity of the input signal occurring in the pulse stream which will aid phase locking due to the absence of sidebands around the slot frequency. The lookup table can be implemented in terms of a read only memory (ROM) and placed between the latch and the digital comparator in the modulator that was shown in Fig. 5.2, and the reversed lookup table (converts the encoded symbols to original) is placed between the latch and the information sink in the demodulator that shown in Fig. 5.4. However, the above lookup table is for a random symbol source. Probability of occurances of different frames depends on the application. Thus, for optimum performance a knowledge of the information source is a must.

5.5 DPIM Receiver Front-End

A transmitter optical driver couples the DPIM pulse stream into the optical fibre. Optical pulses are dispersed and attenuated during transmission, due to the nature of the fibre media. The task of the optical receiver is to convert the incoming light pulses into an electrical signal and to process it further in order to extract the imbedded information. Receiver performance is given in terms of receiver sensitivity, which indicates the minimum optical power required at the photo detector in order to achieve a specific bit error rate in digital systems or *SNR* in analogue systems. Receiver sensitivity, on the other hand, is *CNR* dependant at the input to the decision circuitry. Since noise is dominated by thermal noise sources in the pre amplifier, the sensitivity can be improved either by applying gain within the detector, as in APD, or by reducing the noise in the pre amplifier.

APDs are more sensitive compared to PIN diodes due to their internal gain. Experimental results indicate that PIN can tolerate up to 1 mW of power before

measurable distortion occurs [*Mogensen*] whereas APDs can tolerate optical power as low as 0.1 mW before measurable distortion occurs, but at the expense of high bias voltage, 100 V [*Nakagami*].

Preamplifier is the dominant noise source at the receiver front end and its selection criterion is based on the detector chosen, bandwidth, dynamic range required and practical limitations such as cost. It can be designed using either bipolar or field effect transistors. The former is adequate for frequencies up to 50 MHz, but for higher frequencies, the latter approach is the best choice for low noise operation. The choice of design does also depend on the photo detector being used. If an APD is chosen then the important criteria are low noise, wide dynamic range and low cost rather than high gain. On the other hand, if a PIN photo diode is chosen then high gain as well as low noise are both essential.

5.5.1 Preamplifier topologies

The photo current generated by the detector must be converted to a usable signal for further processing with the minimum amount of noise added. The preamplifier is the first stage of amplification and it normally is the dominant source of noise added to the signal and hence its design will be the principal factor that determines the receiver sensitivity [*Brain*]. There are two main factors involved in designing preamplifier: thermal noise and bandwidth. Depending on the amplifier type used receiver is categorised as high bandwidth, low noise or wider dynamic range. There are three main preamplifier types i.e. low impedance, high impedance and transimpedance. Maximum DPIM bit rate is limited by the receiver front end time constant, due to the total capacitance and resistance. At different slot frequency, front end resistor variation is drawn for time constant of half the slot period at three different front end capacitance.

e.g. 5, 10 and 30 pF, see Fig. 5.7. Incoming source signal bit rate is set at 1 MHz and DPIM bit resolution is varied giving varying slot frequency. For low bit rate receiver front end requires higher resistance for fixed capacitance and vice versa. One the other hand, pulse repetition rate is high for low end of the symbols. Thus, receiver time constant in DPIM limits the maximum operating frequency. For higher time constant pulse spreading into the adjacent time slots give rise to inter slot interference. Therefore, the choice of receiver amplifier is an important factor in designing DPIM system.

5.5.1.1 Low impedance design

Low impedance amplifier can be regarded as a two stage circuit, where the first stage consist of low resistive load converting the photo current generated by the photo diode into a voltage, and the second stage is an amplifier which boosts this voltage. The detector bias resistance, is made low typically 50, 75 Ω. This give rise to higher level of thermal noise, in turn reducing the sensitivity.

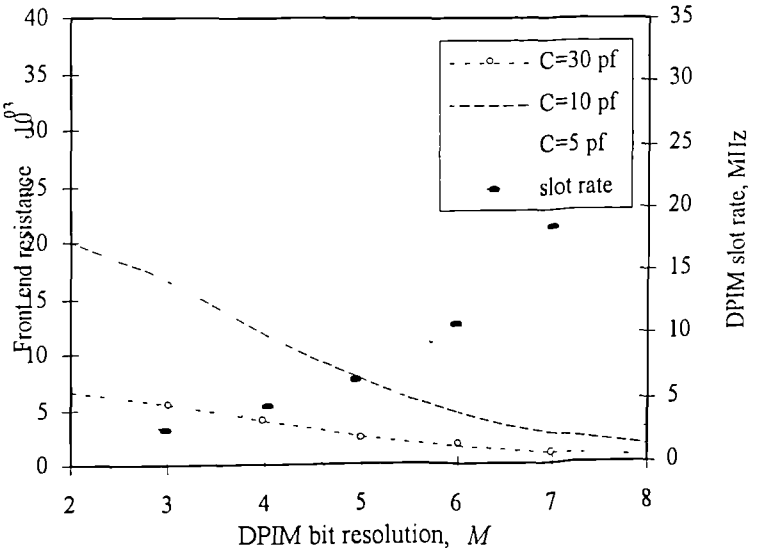

Fig. 5.7 Receiver front end resistance variation vs. DPIM bit resolution.

Receiver bandwidth is determined by the effective resistance and total front end capacitance (combination of detector capacitance, amplifier input capacitance and stray capacitance). Thus bandwidth increases due to low effective resistance. Low impedance design has been reported to have lowest sensitivity but widest dynamic range [*Kashima*], trades off with high thermal noise.

5.5.1.2 High impedance amplifier

High impedance amplifier is characterised as having high input impedance together with a large detector bias resistance. The advantage of high impedance design is high sensitivity due to low level of thermal noise. The disadvantage is that as the resistance increases so does the receiver time constant, in turn reducing the bandwidth. Beyond certain time constant the receiver becomes an integrator. This effect has led to high impedance design being termed as an integrating front-end. The integrating effect can result in baseline wander and can distort the signal if the front end impedance is not carefully selected. This effect may be rectified by differentiation with the use of an equaliser.

High impedance design gives significant improvement on noise but it creates heavy demand on equalisation. The amplifier may saturate for low frequency high level signals. Thus when the amplifier saturates before equalisation has taken place the signal is heavily distorted. Therefore, the dynamic range is limited by the amount of integration and subsequent equalisation employed.

5.5.1.3 Transimpedance amplifier

A transimpedance amplifier is a low noise, high impedance amplifier with a negative feedback [*Hullett*75/1]. Negative feedback reduces noise and the effective impedance,

thus increasing the bandwidth which is high compared with high impedance, but is low compared with low impedance.

Frequency response of the transimpedance amplifier with feedback resistance, capacitance and gain of R_F and C_F and A, respectively is given by:

$$Z(f) = \frac{R_F}{1 + j2\pi f R_F (C_F + C_T / A)} \tag{5.5}$$

where C_T is the total shunt capacitance of the front end.

Cut off frequency can be approximated to:

$$f_c = \frac{A}{2\pi R_F C_T} \tag{5.6}$$

From Eqn. 5.6, for high gain, cut off frequency depends on the feedback resistance and the total capacitance. As far as the noise is concerned, thermal noise can be made as low as that with non feedback high impedance case by carefully making the feedback resistance equal to the effective resistance in the non feedback design. On the other hand, when feedback resistance is much smaller than the total front end resistance the major noise contribution is from thermal noise generated in the feedback resistance. However, good *SNR* can still be obtained with far less demand on the equaliser [*Hullet*76].

In Appendix A, noise analysis of the receiver front end for DPIM pulse stream is presented based on the approach adopted by *Personick* for PCM receiver [*Personick*73/1]. The variance of the noise can be given for transimpedance amplifier based receiver from Eqn. A.34,

$$\sigma_{Fd}^2 = \left(\frac{h\Omega}{\eta}\right)^2 \left\{ \frac{\eta}{h\Omega} G^2 (I_1 + \Sigma_1 - I_x) + \frac{T_s}{q^2} \left(\left(\lambda_0 q^2 G^2 + \frac{2k\theta}{R_b^1} + S_I + \frac{S_E}{R_x^2} \right) I_2 + \frac{S_E}{T_s} (2\pi C_T)^2 I_3 \right) \right\} \tag{5.7}$$

where $R_b^1 = \frac{R_b R_F}{R_b + R_F}$ and $R_x = \frac{R_F R_T}{R_F + R_T}$

R_F is the feedback resistor, R_b is the bias resistor, R_a is the amplifier resistance, and $R_T = R_a \,||\, R_b$. For the remaining abbreviations of Eqn. 5.7. see appendix A.

In Eqn. 5.7, signal dependant and independent (dark current) shot noise is,

$$\sigma_{shot}^2 \triangleq \left\{ \frac{\eta}{h\Omega} G^2 (I_1 + \Sigma_1 - I_x) + T_s (\lambda_0 G^2) I_2 \right\} \tag{5.8}$$

and signal independent thermal noise contribution due to bias resistor, shunt current source (S_I) and amplifier series voltage source (S_E) is,

$$\sigma_{thermal}^2 \triangleq \frac{T_s}{q^2} \left(\left(\frac{2k\theta}{R_b^1} + S_I + \frac{S_E}{R_x^2} \right) I_2 + \frac{S_E}{T_s} (2\pi C_T)^2 I_3 \right) \tag{5.9}$$

where I_1, I_2 I_3 I_x and Σ_1 are definite integrals which are dimentionless and only depend on the received pulse shapes. It can be seen from Eqns. 5.7-9 that for a fixed receiver, thermal noise decreases as the bit duration T_s reduces until the noise term involving I_3 dominates. Furthermore, shot noise due to dark current in Eqn. 5.8 also drops while the shot noise due to the signal are independent. DPIM time slots are much narrower compared to PCM. Thus, DPIM is less affected by signal independent noise sources. Thermal noise contribution can be reduced by means of increasing the resistance R_b ,R_F , R_T, and reducing the amplifier and other capacitive elements. But this is at the reduced bandwidth as shown in Eqn. 5.6.

5.5.2 Pre-detection filter

DPIM is a digital pulse transmission scheme. The figure of merit is the probability of error. Role of the pre-detection filter is twofold. It limits the noise added to the signal

during the amplification process and entering into the detection device and it shapes the received pulses in order to minimise the effects of pulses spreading into the adjacent slots (i.e. inter slot interference). The slope of the input signal determines the amount of timing jitter due to additive noise of the amplification process. The slower the pulse rise time, the greater is the output jitter [*Collins*]. For band limited channels pulse shaping is important in order to avoid inter frame interference. This may be a critical factor in DPIM systems since the shortest frame length is just two time slots. There are many different types of pre-detection filters: integrate and dump, matched and sub-optimum filter.

Let the equalised pulse at the input of the filter be $p(t)$, the pre detection filter impulse response $h(t)$, and the pulse duration within a time slot be $t_m = \gamma T_s$ where $1 > \gamma > 0$.

Filter output is then,

$$p_0(t) = \frac{1}{2\pi}\int_{-\infty}^{\infty} P(\omega)H(\omega)e^{j\omega t}d\omega \tag{5.10}$$

where $P(\omega) = \Im\{p(t)\}$, $H(\omega) = \Im\{h(t)\}$

For receiver noise spectral density of $S(\omega)$ $V^2/\sqrt{Hz}$ mean square noise power at the pre-detection filter output is given by:

$$\sigma_n^2 = \overline{n_0^2(t)} = \frac{1}{2\pi}\int_{-\infty}^{\infty} S_n(\omega)\left|H(\omega)\right|^2 d\omega \tag{5.11}$$

SNR at the output of the filter is:

$$\rho^2 = \frac{1\ 2\pi\left[\int_{-\infty}^{\infty} P(\omega)H(\omega)e^{j\omega t_m}d\omega\right]^2}{\int_{-\infty}^{\infty} S_n(\omega)\left|H(\omega)\right|^2 d\omega} \tag{5.12}$$

In Eqn. 5.12, t_m is the time at the peak signal at the filter output. The task of the pre-detection filter is to maximise the ratio given in Eqn. 5.12.

5.5.2.1 Integrate and dump filter

The integrate and dump filter has been presented as the optimal filter for detection of rectangular polar signals in Additive White Gaussian Noise (AWGN) environment [*Boerner*], [*Carlson*]. It integrates the incoming rectangular pulses and dumps the energy gathered at the falling edge. Ideally the filter output rises linearly over the pulse duration until the falling edge where the energy in the filter is maximum. At the end of pulse duration a decision is made whether a pulse is present or not. This type of filter can be employed in receivers where there are no constraints on the channel bandwidth thus, the received pulses are not dispersed. When the pulse shape shifts from rectangular, filter output tends to spread severely into the adjacent time slots [*Carlock*]. Integrating and dumping energy under this condition become increasingly difficult. Therefore, other forms of pre-detection filter must be considered for non-rectangular shape pulses.

5.5.2.2 Matched filter

The matched filter has been identified as the optimum pre-detection filter in a white noise dominated receivers for low probability of error. In a coloured noise dominant receiver, a pre-whitening filter is used before the matched filter [*Muoi*78], [*Cryan*93/1]. If shape of the input waveform to the filter is given by $p(t)$, then matched filter impulse response is given by,

$$H(\omega) = k\frac{P(-\omega)e^{-j\omega t_m}}{S_n(\omega)} \tag{5.13}$$

where k is an arbitrary constant and $S_n(\omega)$ is the noise power spectral density.

$$h(t) = \Im^{-1}\left\{k^1 P(-\omega)e^{-j\omega t_m}\right\} \tag{5.14}$$

where $k^1 = k/S(\omega)$

Output *SNR* said to be maximum under this condition [*Turin*]. Thus, in designing a matched filter for the given equalised pulse shape i.e. $P(\omega)$, one needs to find the impulse response of a network, which is given by the time reversed equalised pulse shape. Once the filter response is decided upon, numerical network realisation techniques can be used to realise the filter parameters [*Su*]. Alternatively, filter pole locations may be arbitrary chosen and response can be optimised as required [*O'Reilly*]. Pre-detection filter realisation strategy for DPIM receiver is presented in Appendix B. 2nd and 3rd order network responses are approximated as shown in Fig. 5.8.

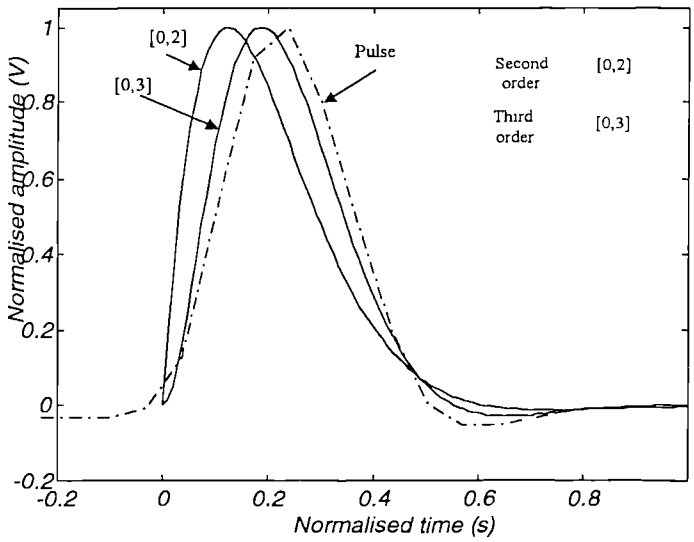

Fig. 5.8 Proposed network responses.

The dotted line shows the digitised DPIM pulse shape, whereas solid lines shows the approximated network responses for filters of order 2 and 3, see Appendix B for normalised filter parameters. It was noticed that the network response becomes closer to the pulse shape as the filter order is increased. In this work a third order passive network is used as the pre-detection filter.

5.5.3 Threshold detector

At the receiver, the incoming signal is a train of pulses whose form is distorted by the channel response. Photo detector output is amplified at the receiver front-end, noise introduced is filtered and the pulses are reshaped. There are many ways one could identify whether a time slot contains a pulse. *Mecherle, Boerner* and *Gagliadi* investigated maximum likelihood detector for PPM pulse detection [*Mecherle*86], [*Boerner*] and [*Gagliadi*76]. This type of detector takes a DPPM word at a time and decide the presence or absence of a pulse by detecting and comparing the maximum number of photons within a time slot. Since DPIM frames are anisochronous, implementing such detectors involves complex circuitry and thus it is not considered. An alternate scheme based on threshold detection which allows decision at the time slot level rather than word level is adopted. A threshold detector compares the processed signal with a preset DC value and restores the original pulse stream with errors. The level of errors introduced depends on the noise introduced into the pulse stream during pre-processing. Threshold level is selected so that minimum error performance is achieved. For binary signal transmission systems, threshold level is best set half of the pulse amplitude [*Menendez-Valdes*]. In section 6.5 optimum threshold level setting for DPIM receiver is discussed. Two types of practical threshold detector strategies can be considered; (1) sampling point detector and (2) threshold crossing detector.

5.5.3.1 Sampling point threshold detection

A filtered signal is compared with a preset signal level within a time window associated with each received DPIM time slot. A pulse is detected whenever the signal crosses the preset threshold level within the time window. The extracted clock at the receiver is

used to device the sampling points. Sampling should be performed ideally at the highest energy point. Assuming the pulse width used is half a time slot, sampling is done at the middle of each slot.

5.5.3.2 Threshold crossing detection

A noise corrupted signal is transparent across the detector above the preset threshold level. The slot in which a received signal first exceeds the threshold is interpreted as the signal slot. For pulses with high rise time the possibility of noise corrupting the rising edge is higher compared to that with one with sharpened rise time. Thus for this type of detector, pulses with improved rise time are preferred. *Garrett* has shown that proportional-derivative and delay (PDD) network followed by pre detection filter can be used to shape DPPM pulses before detection [*Garrette*83/2]. However, this type of filter is very complex to realise [*Hausien*], and for low bit rates it is not practical.

5.5.4 Synchronisation issues

Recovery of data transmitted require only slot timing synchronisation at the receiver for demodulator operation, making synchronisation simpler as compared to PCM\DPPM. In DPIM receiver timing is accomplished in the sync subsystem that is followed by the photo detector operating in parallel with the information channel. In some receivers the decoded data may in fact be used to further improve the timing operation [*Gagliadi*76]. Many techniques have been used in different applications for phase locking, such as resonant circuits, early late gate detection and phase locked loop detection [*Gagliadi*76], [*Duttweiler*]. Phase lock techniques have widely been used and can be implemented using off-the-shelf monolithic integrated circuits (IC) [*Gardner*79] while the other techniques are said to be less than optimum [*Davidson*89]. In DPIM the presence of distinct slot frequency component will aid phase locking.

A block diagram of the phase locked loop (PLL) being used is given in Fig. 5.9. Voltage controlled oscillator (VCO) is set around the slot frequency. Phase detector (PD) compares the phase of the VCO output frequency with the distinct slot frequency of the incoming pulse stream. Output of PD is a measure of the phase difference between the two inputs. The PD output is then filtered by the loop filter (LF) and applied to the VCO.

PLL is in fact a feedback control system where the control strategy is to track the slot frequency phase in order to minimise the phase error between VCO centre frequency and the slot frequency. The VCO will need very little information to be able to track the correct phase provided that the slot frequency component is stable. Frequency adjustment occurs until zero phase difference is achieved and the receiver clock is locked to the correct phase of the slot frequency.

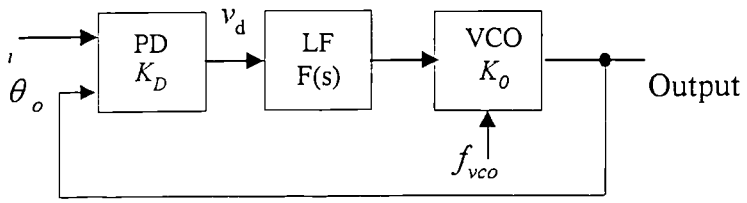

Fig. 5.9 PLL block diagram.

Input signal to the PLL has phase of $\theta_i(t)$ and the VCO output has a phase of $\theta_0(t)$.

For small phase error the detector output can be given by,

$$v_d = K_D \sin\theta_i - \theta_0 \approx K_D(\theta_i - \theta_0) \tag{5.15}$$

where K_d, V rad^{-1} is the phase detector gain factor.

When the VCO gain factor is K_0, rad s^{-1} V^{-1} and the loop filter transfer function is $F(s)$, the loop transfer function can be given by,

$$\frac{\theta_0(s)}{\theta_i(s)} = H(s) = \frac{K_0 K_d F(s)}{s + K_0 K_d F(s)} \tag{5.16}$$

and the phase error becomes,

$$\frac{\theta_e}{\theta_i} = \frac{s}{s + K_0 K_D F(s)} \tag{5.17}$$

Stability of the loop depends on the loop filter from Eqns. 5.16 and 5.17. The VCO frequency drift from the centre frequency (slot frequency) can be made minimum by carefully designing the loop filter. This can be implemented as first or higher order. Higher order filters said to be overly sensitive to changes in gain and circuit components and difficult to stabilise. But second order filter is said to be unconditionally stable and has been widely used in a range of applications [*Gardner*79], [*Gruber*]. Most of the off the shelf PLLs offer limited choice in the designing of the loop filter [*Best*]. In this work second order passive loop filter is considered as a suitable loop filter for the PLL, as shown in Fig. 5.10 .

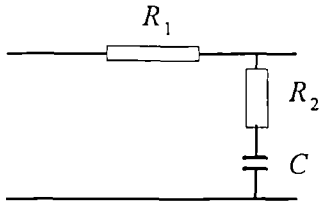

$F(s)$

Fig. 5.10 2nd order loop filter.

Loop filter transfer function is given by,

$$F(s) = \frac{1 + s\tau_2}{1 + s\tau_1} \tag{5.18}$$

where $\tau_1 = (R_1 + R_2)C$, $\tau_2 = R_2 C$

Substituting for $F(s)$ loop transfer function is given by [*Gardner*79],

$$H(s) = \frac{K_0 K_d (s\tau_2 + 1)/\tau_1}{s^2 + s(1 + K_0 K_d \tau_2)/\tau_1 + K_0 K_d/\tau_1} \tag{5.19}$$

where the natural angular frequency of the loop $\omega_n = \left(\frac{K_0 K_d}{\tau_1}\right)^{1/2}$

and the damping factor $\xi = \frac{1}{2}\left(\frac{K_0 K_d}{\tau_1}\right)^{1/2}\left(\tau_2 + \frac{1}{K_0 K_d}\right)$

Thus the filter response given in Eqn. 5.19 can be simplified as,

$$H(s) = \frac{(s\tau_2 + 1)\omega_n^2}{s^2 + 2\omega_n \xi s + \omega_n^2} \tag{5.20}$$

Initially the VCO centre frequency should be set closer to the slot frequency such that the frequency offset is within the capture range of the PLL [*Rich*], which is the maximum frequency offset within which the PLL falls into lock. The system moves into lock if the frequency offset comes into the lock range of the PLL. Lock range is given by [*Best*],

$$\Delta\omega_L \approx 2\xi\omega_N \tag{5.21}$$

and the-lock-in time by,

$$T_L \approx \frac{2\pi}{\omega_N} \tag{5.22}$$

The noise bandwidth of the loop under phase locking in a noisy environment is approximated by [*Meade*],

$$B_L = \frac{\omega_n}{2}\left[\xi + \frac{1}{4\xi}\right] \tag{5.23}$$

Thus the functional blocks of the PLL circuitry should be carefully selected for proper clock synchronisation. Side locking is the resultant otherwise. Side locking is when the PLL locks with the adjacent frequency components of the slot frequency, i.e. $\omega_i \pm \omega_x$, where ω_x is high power frequency components adjacent to the slot component.

The PLL used in this work is the widely available first order Phillips NE564, with maximum operating frequency of 50 MHz, see Fig. 5.11. The resistor R_l , determines the lock range by means of controlling the current flow into pin 2. PLL response time should be fast enough to track a small drift in the slot frequency provided that the VCO centre frequency is held stable.

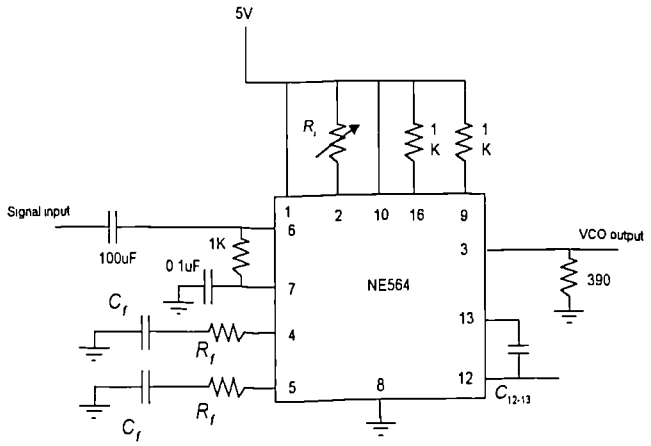

Fig. 5.11 NE564 phase lock loop.

For low value loop filter capacitance PLL time constants are small. For example with the phase detector and VCO coefficients of K_0 = 6.3e+06 rad s^{-1} V^{-1} and K_D = 0.573 V rad^{-1}, respectively [*Philips*] the time required for phase tracking for different capacitance values are presented in Fig. 5.12.

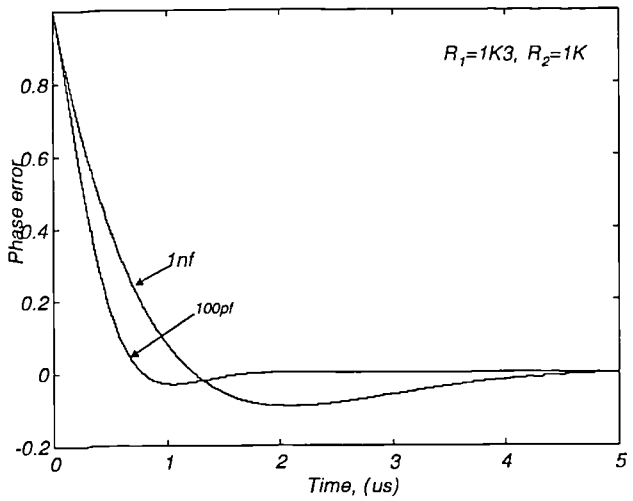

Fig. 5.12 PLL phase error versus lock in time for different loop filter capacitance.

From Fig. 5.12, for 100 pF capacitance the phase error approaches zero at lock in time of 1μs. Whereas, for high value capacitance the phase error approaches zero when the lock in time is greater than 4 μs. Therefore, it is evident that low capacitance or the low time constants give rise to efficient tracking. However, the PLL bandwidth also dependant on the capacitance values. It decreases with the increased capacitance as shown in Fig. 5.13.

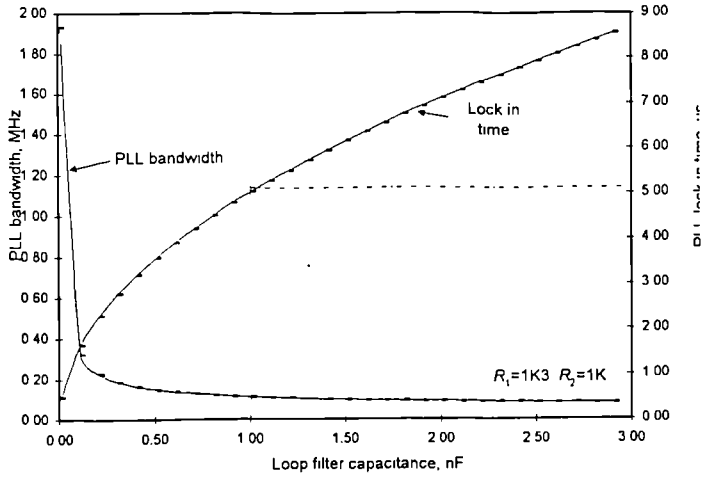

Fig. 5.13 PLL bandwidth and the lock in time vs. loop filter capacitance.

For low noise and high stability, PLL is best operated at low bandwidth and low lock in time. To achieve this a compromise between them may be required. In this design a capacitance of 1 nF was used due to the fact that there was a stable slot component in the DPIM spectrum.

5.6 Receiver Bandwidth

When a low bandwidth receiver detects a short duration pulse, the rising edge of the pulse is preserved, but the falling edge of the output pulse can have a considerable fall time [*Sibley*93/2]. In PCM systems this leads to ISI. Whereas in DPIM system the equivalent is inter-frame-interference(IFI). IFI becomes significant when the fall time exceeds shortest frame (L_s), where $L_s = (1+n_g)Ts$, n_g guard time slots, see chapter 4. Thus, lower limit for receiver bandwidth has to be considered. For simplicity assume that received pulses are rectangular in shape with pulse width equivalent to half-height-width (t_{FWHM}) of Gaussian shape pulses. Minimum bandwidth is derived taking shortest DPIM frame pattern into account. *Sibley* has used fall time as five times the receiver time constant for minimum digital PPM system bandwidth [*Sibley*93/2]. Similar criterion can be used for DPIM. The trailing edge or the first order decay of the receiver to reach zero (fall time) is taken to be five times the time constant. The resultant time constant is the combined equaliser and amplifier time constants. The time should be less than or equal to the DPIM shortest frame L_s to avoid inter frame interference. Thus, we can write (see Fig. 5.14),

$$t_{\max} = L_s + T_s - t_{FWHM} \tag{5.24}$$

It is assumed that $T_s \neq t_{FWHM}$. $t_{\max}$ represents maximum time limit, e.g. five time constants.

Thus minimum allowable receiver bandwidth can be given in terms as t_{max} as,

$$B_{\min} = \frac{1}{t_{\max}} = \frac{1}{L_s + T_s - t_{FWHM}} \tag{5.25}$$

B_{min} gives minimum allowable receiver bandwidth. For higher bandwidth above the minimum, the output pulse will not be attenuated but the receiver noise will increase. Maximum operating frequency can be decided upon taking the minimum bandwidth into account.

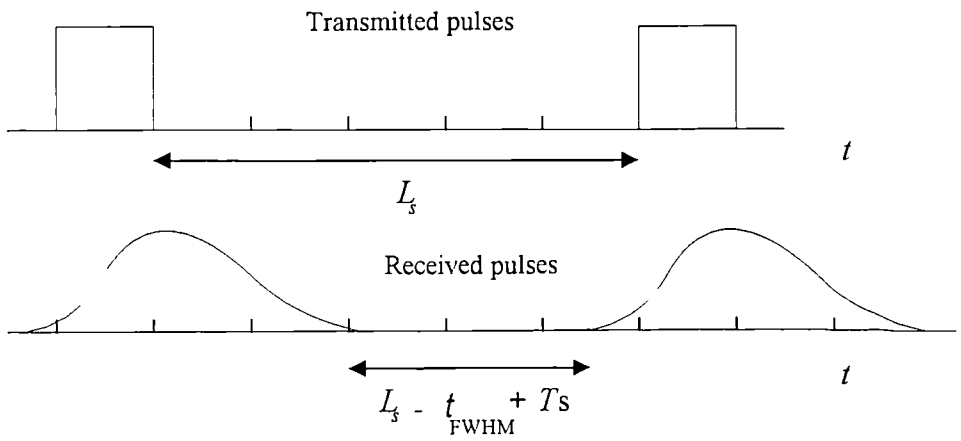

Fig. 5.14 Received pulses at the detector output.

5.7 Summary

In this chapter design implementation of DPIM transmission link was investigated. For analogue signal transmission, modulator was designed around successive approximation analogue-to-digital converter, thus making the circuitry simpler. It was shown that an increase in bit resolution results in an exponential increase of the slot frequency. Nature of the frames suggested that the transmitted average power of the DPIM is higher than DPPM. however, power can be reduced by adopting coding techniques. Pre-detection filter design for the received pulse shapes is described and issues concerning synchronisation and minimum receiver bandwidth were also discussed.

Chapter Six

Receiver Analysis

In the previous chapter issues concerning designing of a point-to-point DPIM link is discussed. This chapter is devoted to DPIM receiver analysis in which an optical DPIM signal is converted into an electrical signal by using either PIN photo diode or an APD. Further signal processing is carried out before decoding the recovered DPIM pulse train and extracting the information. Detailed analysis for filter design, carrier-to-noise ratio, probability of error and *SNR* are given.

6.1 Introduction

The receiver model used in this work is based on the one used by [*Personick*73/1] and is given in Fig. 6.1. The photo detector, either a PIN diode or an APD, converts the optical signal into an electrical signal which is boosted using the pre-amplifier. In this process, noise is added onto the signal and is the principal limiting factor of the receiver sensitivity. The post-amplifier receives a strong signal, so its noise contribution is often negligible. The task of the equaliser is to account for non-linearity caused during the amplification process. The equalised output is input to the pre-detection filter and the

clock extraction circuitry, whose task is two fold, i.e. to limit the noise entering into the threshold detector and to shape the signal to minimise inter-symbol-interference (ISI). At the threshold detector, the filtered signal is sampled at the clock rate, and a decision is made whether the sample lies above or below the threshold level at a given slot duration. An optimum filter will minimise the noise effect, thus keeping the slot error to a minimum.

The system error performance depends on how precisely the pulse positions are resolved. The band limiting nature of the transmission channel introduces pulse spreading which is prone to further detection in the presence of noise. DPIM is being considered for optical communication systems either fibre or free space and these are not always wide band in nature. The nature of the channel band limitation is dependant on the transmission speed or the slot rate in use. In the following, the receiver analysis is performed for narrow-band as well as wide band systems.

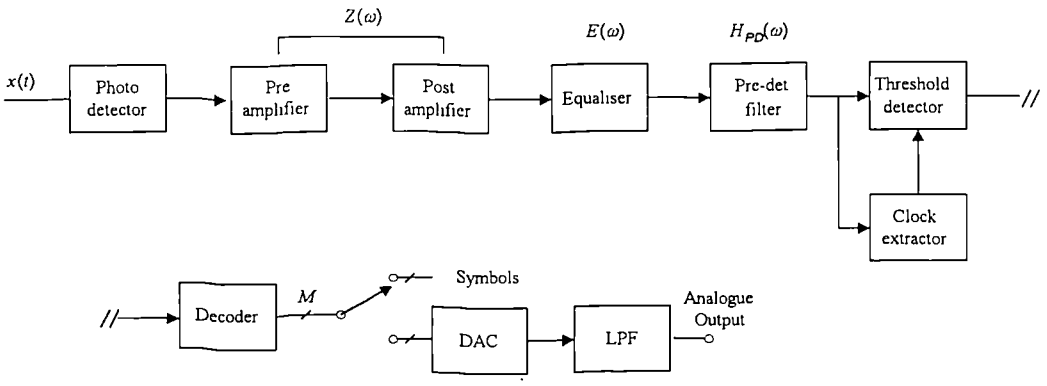

Fig. 6.1 Functional block diagram of the DPIM receiver.

6.2 Narrow-band Analysis

Short pulses such as DPIM have significant spectral widths. Constraints in channel bandwidth results in short DPIM pulses being spread, or stretched, in shape relative to

the transmitted pulses. This stretching causes pulse spreading into adjacent slots (inter slot interference) and in the worst case can overlap into adjacent frames (inter symbol interference). In optical fibre transmission link the received pulse shape is assumed to be Gaussian [*Refi*]. This assumption is also valid for narrow band systems.

A received pulse is assumed to have RMS full width of t_i and a peak optical power of E_i. Pulse shape at the detector is given by $h(t)$ such that,

$$\int_{-\infty}^{\infty} h(t)dt = 1 \tag{6.1}$$

Referring to Eqn. 4.6, the DPIM optical pulses falling on the detector can be express as,

$$x(t) = \sum_{k=-\infty}^{\infty} E_i.h\left(t - T_s\left(2k + \sum_{m=-\infty}^{k-1} S_m\right)\right) \tag{6.2}$$

which represents an infinite pulse stream.

At the receiver front end a detector with responsivity R (A/W) is followed by amplifiers and equaliser with transfer characteristics of $Z(\omega)$ and $E(\omega)$, respectively, the pre-detection filter and subsequently the threshold detector. The signal at the pre-detection filter input becomes,

$$v_{in}(t) = \frac{1}{2\pi}\int_{-\infty}^{\infty} E_i.R\frac{A.R_L}{1+j\omega R_L C_T}\frac{R_2(1+j\omega R_1 C_1)}{(R_1+R_2+j\omega R_1 R_2 C_1)}H(\omega)e^{j\omega t}dt \tag{6.3}$$

where

$$H(\omega) = \Im\{h(t)\},\ Z(\omega) = \frac{A.R_L}{1+j\omega R_L C_T},\ E(\omega) = \frac{R_2(1+j\omega R_1 C_1)}{(R_1+R_2+j\omega R_1 R_2 C_1)}$$

and A is the amplifier gain.

This signal is contaminated by various noise sources in the optical detection and amplification process. The noise corrupted input signal can be represented as,

$$v_{in}(t) = \frac{1}{2\pi}\int_{-\infty}^{\infty} E_t R \frac{AR_L}{1+j\omega R_L C_T} \frac{R_2(1+j\omega R_1 C_1)}{(R_1+R_2+j\omega R_1 R_2 C_1)} H(\omega) e^{j\omega t} dt + n(t) \quad (6.4)$$

where $n(t)$ is the noise introduced by the receiver. For optical receivers $n(t)$ can be taken as zero mean white Gaussian noise with double sided spectral density $S_n(f) = \frac{N_0}{2}$ V^2/Hz.

Figure 6.2 shows parameters corresponding to the Gaussian pulse shape, $h(t)$ [*Senior*].

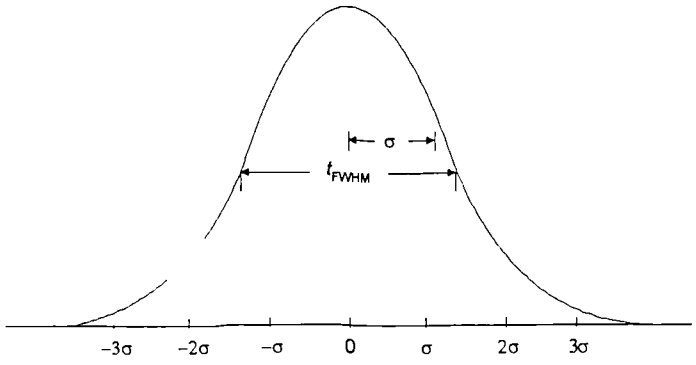

Fig. 6.2 Gaussian pulse shape.

The pulse shape can be given in terms of pulse amplitude of $P_0 = 1/\sqrt{2\pi}\sigma$, and full width half maximum pulse width (t_{FWHM}), approximated to σ as,

$$p(t) = \frac{1}{\sqrt{2\pi}\sigma} e^{-\frac{t^2}{2\sigma^2}} \quad (6.5)$$

The Fourier transform of the Gaussian pulse shape is given by,

$$P(\omega) = e^{-\frac{\omega^2\sigma^2}{2}} \quad (6.6)$$

Taking the above Gaussian pulse shape representation into account, the received DPIM pulse shape with RMS full width of t_t ($\sigma = t_t/2$) is expressed as,

$$h(t) = e^{-\frac{2t^2}{t_i^2}} \tag{6.7}$$

Comparing Eqns. 6.5 and 6.6, the pulse shape transform of Eqn. 6.7 becomes,

$$H(\omega) = t_i \sqrt{\frac{\pi}{2}} e^{-\frac{\omega^2 t_i^2}{8}} \tag{6.8}$$

The level of pulse spreading into adjacent slots varies depending on the received pulse width. This effect is shown in Fig. 6.3 for varying received pulse widths. Time axis is normalised to a time slot and the amplitude axis is normalised to the peak received pulse amplitudes. Received RMS pulse t_i is given by the relation $t_i = \beta T_s$ and pulse spreading is shown for varying β.

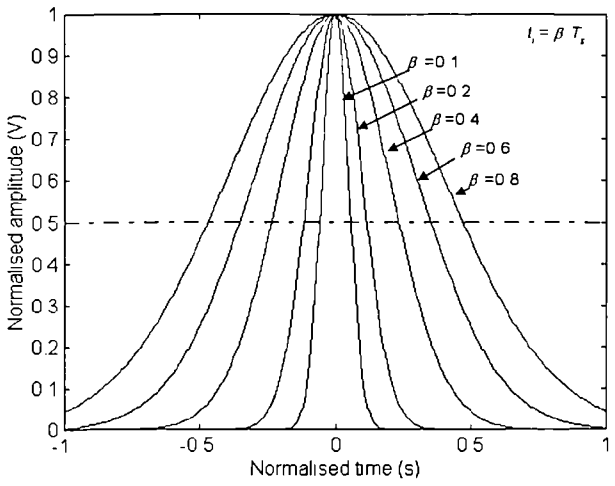

Fig. 6.3 Received DPIM pulse shapes at varying dispersion levels.

Pulse spreading is dependant on the channel bandwidth. A transmission channel can be regarded as a low pass filter, so the higher the cut-off frequency the more high frequency energy it will pass and vice versa. Thus, band limited channels limit the high frequency components passing through them inevitably resulting in pulse spreading. The

effect of dispersed pulses on the system performance is analysed in the later part of this chapter.

Substituting for $h(t)$ from Eqn. 6.7 in 6.4, signal at the input of the pre-detection filter yields,

$$v_{in}(t) = \frac{1}{2\pi}\int_{-\infty}^{\infty} E_i R \frac{AR_L}{1+j\omega R_L C_T} \frac{R_2(1+j\omega R_1 C_1)}{(R_1+R_2+j\omega R_1 R_2 C_1)} t_i \sqrt{\frac{\pi}{2}} e^{-\frac{\omega^2 t_i^2}{8}} . e^{j\omega t} dt \; + \; n(t) \tag{6.9}$$

Frequency matching is performed at the equaliser so that phase distortions are not passed through to the pre-detection filter, Eqn. 6.9 simplified to,

$$v_{in}(t) = A_i . e^{-\frac{2t^2}{t_i^2}} \; + \; n(t) \tag{6.10}$$

where $A_i = \sqrt{\frac{\pi}{2}} t_i E_i RAZZ_q$ Volts

and $Z = \left|\frac{R_L}{1+j\omega R_L C_T}\right| \Omega$, $Z_q = \left|\frac{R_2(1+j\omega R_1 C_1)}{(R_1+R_2+j\omega R_1 R_2 C_1)}\right| \Omega$, are the amplifier and equaliser impedance contributions, respectively.

Pulse transform of Eqn. 6.10 becomes,

$$V_{in}(\omega) = A_i t_i \sqrt{\frac{\pi}{2}} e^{-\frac{\omega^2 t_i^2}{8}} + N(\omega) \tag{6.11}$$

Equation 6.10 shows the noise corrupted signal at the pre-detection filter input. The filter is designed such that noise is band limited and the pulse shape is restored for subsequent detection process.

6.2.1 Pre-detection filter response

Section 5.5.2 gives a brief account of a pre-detection filter for a DPIM receiver. For non-rectangular pulse shapes, the pre-detection filter can either be a sub-optimum filter or matched filter. Both cases are considered in the following sections. In the analysis the receiver bandwidth is assumed to be W Hz, approximated as the transmission bandwidth. The effect of filter bandwidth on the pulse propagation as well as the dispersion due to bit resolution in a fixed link are addressed.

6.2.1.1 Sub-optimum filter

The pre-detection filter frequency characteristics ($H_{PD}(\omega)$) can be approximated as having one sided bandwidth of W Hz. *Matin* and *Gagliardi* showed that filter impulse response can be taken as having Gaussian shape [*Matin*]and [*Gagliardi*76]. On that account sub-optimum filter frequency response is formulated as,

$$H_{PD}(\omega) = e^{-\frac{f^2}{2W^2}} \tag{6.12}$$

Filter time response is obtained by taking the inverse Fourier transform of Eqn. 6.12, which becomes,

$$h_{PD}(t) = \sqrt{2\pi}We^{-(\sqrt{2\pi}Wt)^2} \tag{6.13}$$

The filter output $V_{out}(t)$ is the convolution sum of the input pulse and the filter impulse response. Thus,

$$V_{out}(t) = \frac{1}{2\pi}\int_{-\infty}^{\infty} V_{in}(\omega).H_{PD}(\omega)e^{j\omega t}dt \; + \; n_0(t) \tag{6.14}$$

where $n_0(t)$ is the band limited filter output noise, which can be represented as.

$$n_0(t) = \sigma_n^2 = \frac{1}{2\pi}\int_{-\infty}^{\infty} S_n(\omega)\left|H_{PD}(\omega)\right|^2 d\omega \tag{6.15}$$

Taking the noise equivalent bandwidth into account, band limited noise $n_0(t)$ in Eqn. 6.15 becomes,

$$n_0(t) = \frac{\sqrt{\pi}}{2} N_0 W, \qquad \mathrm{V}^2 \tag{6.16}$$

The pre-detection filter output in the frequency domain is given by,

$$V_{out}(\omega) = V_{in}(\omega).H_{PD}(\omega) \tag{6.17}$$

Substituting Eqns. 6.11 and 6.12 and simplifying it results in,

$$V_{out}(\omega) = A_t t_t \sqrt{\frac{\pi}{2}} e^{-\frac{\omega^2}{2}\left(\frac{\pi^2 t_t^2 W^2 + 1}{4\pi^2 t_t^2 W^2}\right)} \tag{6.18}$$

The time domain signal at the filter output is obtained by taking the inverse Fourier transform of Eqn. 6.18,

$$V_{out}(t) = A_t \frac{t_t \pi W}{\sqrt{1+\pi^2 t_t^2 W}} e^{-\left(\frac{2\pi^2 W^2}{1+\pi^2 t_t^2 W^2}\right)t^2} \tag{6.19}$$

Eqn. 6.19 is best described as a Gaussian shaped pulse, with the RMS full width given as,

$$t_o = \sqrt{\frac{1+\pi^2 t_t^2 W^2}{\pi^2 W^2}} \tag{6.20}$$

For a particular received pulse width t_t and bandwidth W, Eqn. 6.20 gives the RMS pulse width of the pre-detection filter output. The filter output for varying receiver pulse width and filter bandwidth can be observed by analysing the output pulse shape

for different values of W and t_l, see Fig. 6.4. The received pulse width is defined in terms of time slots $t_l = \alpha_l T_s$ and the filter bandwidth is given as $W = 1.5/T_s$. Amplitude and time axis are normalised to received peak pulse amplitude and to a time slot, respectively.

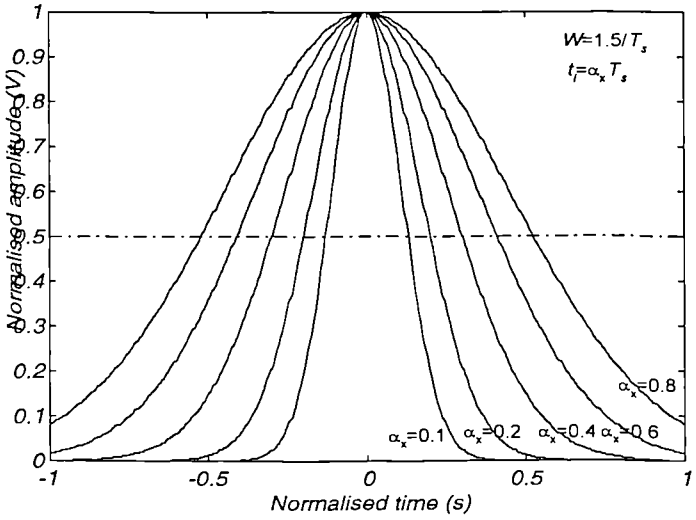

Fig. 6.4 Filter response at bandwidth of $W = 1.5/T_s$ and for varying t_l.

Comparing Figs. 6.3 with 6.4 reveals that for a chosen filter bandwidth the output pulse width further increases spreading into the adjacent time slots. On the other hand, pulse spreading into the adjacent slots may be reduced by means of increasing the filter bandwidth. This effect is best shown in Fig. 6.5 where filter bandwidth is chosen to be $3/T_s$, twice the value employed in the previous case. By comparing Figs. 6.4 and 6.5 for a given received pulse shape, one may increase the filter bandwidth to reduce pulse spreading.

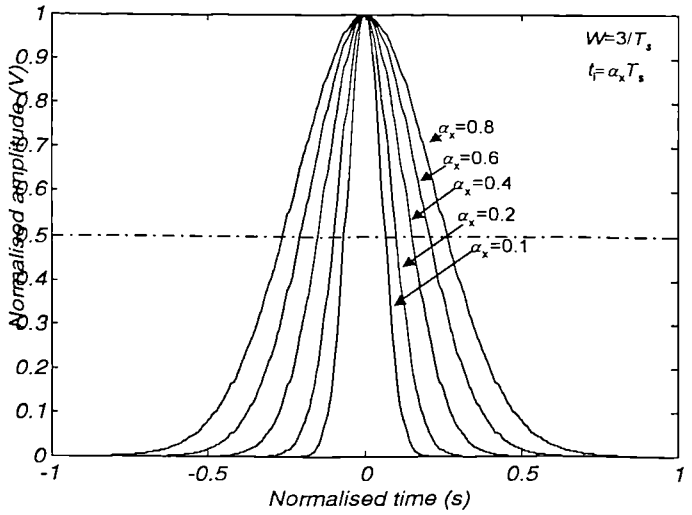

Fig. 6.5 Filter response at bandwidth of $W = 3/ T_s$ and for varying t_l.

This is further investigated by obtaining output pulse shapes for increasing filter bandwidth for fixed received pulse width e.g. $t_l = 0.2\ T_s$. The bandwidth variation is such that $W = x/ T_s$, $x \in 0.2, 0.7, 1.2,...$, see Fig. 6.6.

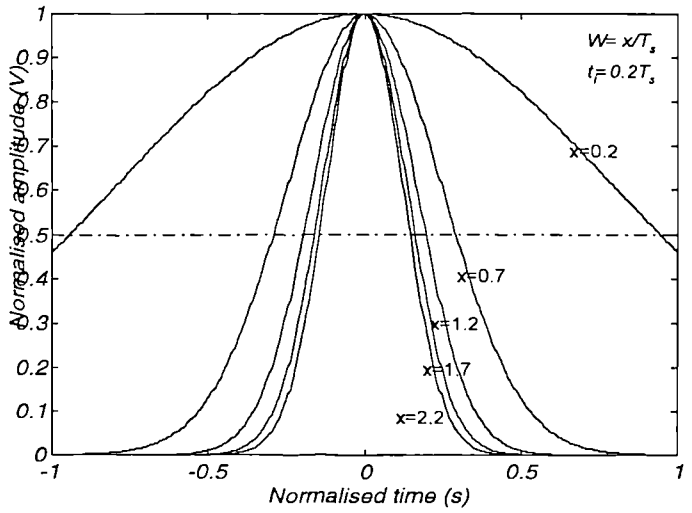

Fig. 6.6 Filter response for varying bandwidth.

From Fig. 6.6, for lower receiver bandwidth, pulse spreading into adjacent time slots is severe. As the bandwidth is increased pulses become narrower, therefore resulting in far less interference to the adjacent slots.

The task of the pre-detection filter is to optimise the detection process by means of reducing the noise whilst avoiding pulse spreading into adjacent slots. As the bandwidth increases pulse spreading decreases, reaching an optimum at around twice the slot rate. This is best explained by looking at the correlation between the output and the input of the filter for varying filter bandwidth. This is shown in Fig. 6.7, where the x-axis shows the filter bandwidth normalised to the slot rate and the y-axis shows the correlation between the output and input pulse shape for received pulse width of $t_i = 0.2\ T_s$.

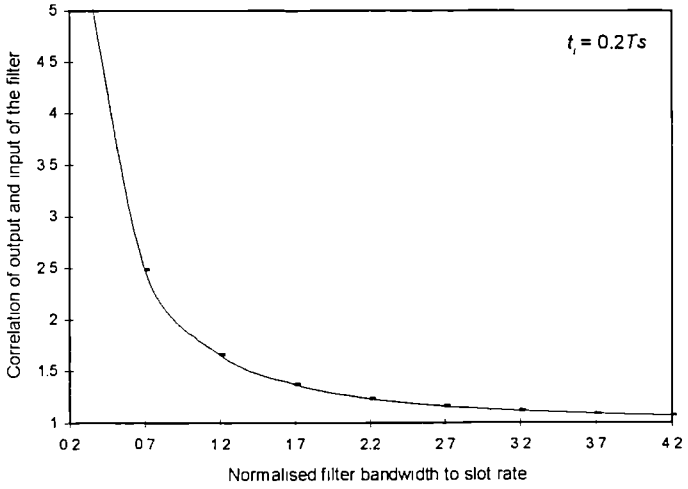

Fig. 6.7 Correlation between filter output and the input at varying filter bandwidth.

As shown in Fig. 6.7, there exists a better correlation between filter input and output as the receiver bandwidth increases. However, the penalty paid is increased noise level as outlined in Eqn. 6.16.

6.2.1.2 Matched filter

By definition, the impulse response of the filter is matched to the incoming pulse shape, see section 5.5.2.2. Thus the received pulse shape given in Eqn. 6.10 and the filter response given in Eqn. 6.12 are identical when the filter bandwidth is related to the received RMS pulse width by,

$$W = \frac{1}{\pi t_i} \tag{6.21}$$

Once the above criterion is met, the RMS output pulse width from Eqn. 6.20 becomes,

$$t_o = \sqrt{2} t_i \tag{6.22}$$

The filter output RMS pulse width is high compared to the received pulse width, showing pulse spreading by the filter.

Substituting Eqn. 6.22 in 6.19, the matched filter output signal can be given by,

$$V_{out}(t) = \frac{A_i}{\sqrt{2}} e^{-\frac{t^2}{t_i^2}} + \frac{1}{2\sqrt{\pi}} \frac{N_0}{t_i} \tag{6.23}$$

In Eqn. 6.21, t_i is not independent of T_s. The dispersion over the channel for a given transmission bandwidth W and bit rate B can be represented by the ratio of slot duration T_s to the RMS pulse full width t_i as,

$$\frac{T_s}{t_i} = \left(\frac{W}{B}\right) \frac{\pi M}{2^M + 1} \tag{6.24}$$

The ratio W/B can be defined as the relative bandwidth of the system, expressed as receiver/transmission bandwidth to the source bit rate. The ratio of slot width to the received pulse width with respect to different relative bandwidths is shown in Fig. 6.8. In Fig. 6.8, the y-axis and x-axis shows the ratio of slot width to received pulse width and bit resolution, respectively. As shown, for a given relative bandwidth, pulse spreading increases as the bit resolution increases, showing the influence of the bit resolution in a fixed DPIM link. On the other hand, pulse spreading is reduced at a particular bit resolution for increased relative bandwidth. Thus the receiver bandwidth should be chosen so as to accommodate specific bit resolution while minimising pulse spreading and hence reduced ISI.

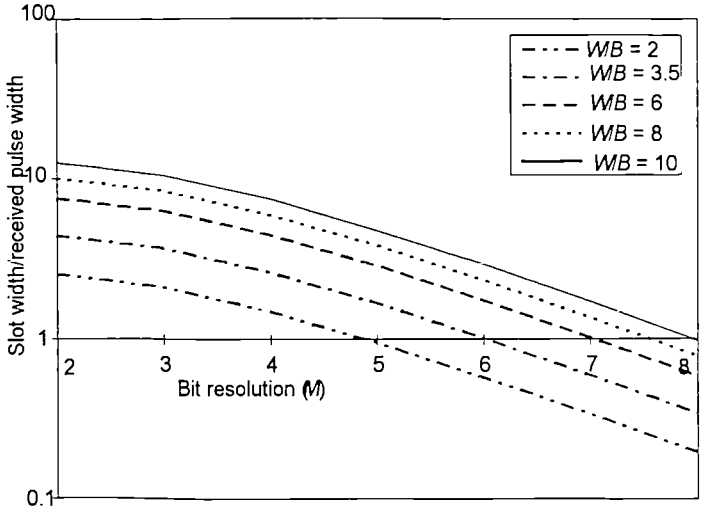

Fig. 6.8 Level of pulse spreading into the adjacent slots.

6.2.2 Carrier-to-noise ratio (*CNR*)

The pre-detection filter output consist of signal as well as noise. *CNR* is defined as the ratio between the carrier power and the noise power at the filter output. This ratio determines the probability of error in the detection process. Low received power with a low noise amplifier gives a similar *CNR* as high received power with a high noise amplifier. In other words *CNR* does not correspond to a particular received power but is solely dependent on the receiver design and varies from one receiver to another. Therefore, performance evaluation and comparison should be made based on *CNR* rather than received optical power. Thus in this analysis system performance is evaluated based on *CNR*.

6.2.2.1 Sub-optimum filter

From Eqn. 6.17 *CNR* at the output of the sub-optimum filter case can be expressed as,

$$CNR_{RC} = 2\pi^{3/2} \frac{t_i^2 W}{\left(1+\pi^2 t_i^2 W^2\right)} \left\{ 1 - e^{-\left(\frac{2\pi^2 W^2}{1+\pi^2 t_i^2 W^2}\right) T_s^2} \right\}^2 \left(\frac{A_i^2}{N_0}\right) \tag{6.25}$$

The first term is that for an ideal matched-filter detection of a single received pulse, while the second term shows the degradation due to the bias introduced by the slot over-spill at the adjacent time slots at the sampling time. From Eqn. 6.25, CNR_{RC} is seen to depend on the received RMS pulse width as well as the receiver bandwidth for a given A_i/N_o ratio. For a fixed A_i/N_o ratio, CNR_{RC} is evaluated for different received pulse width t_i and bandwidth W combinations as shown in Fig. 6.9, where the time axis is normalised to a time slot and the amplitude axis is normalised to the highest filter output level.

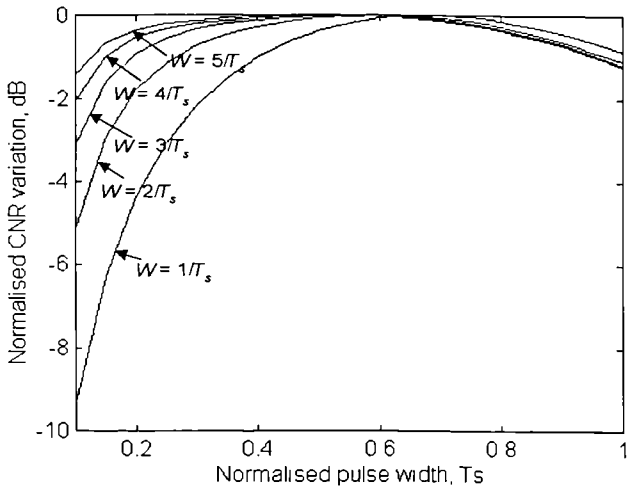

Fig. 6.9 Variation of CNR at the sub-optimum filter output with the received pulse width.

For higher bandwidth W, then CNR_{RC} is less dependant on the received pulse width whereas for low bandwidth it changes from -10 dB to -1 dB over full pulse width T_s. At a pulse width of approximately 0.6 T_s the CNR is at its maximum regardless of W, decreasing slightly by 1 dB for pulse widths greater than 0.6 T_s due to an increase in the slot over-spill. This figure, therefore, can be used to find the optimum bandwidth and pulse width.

6.2.2.2 Matched filter

From Eqn. 6.23, the *CNR* for a matched filter has been obtained using the Schwartz inequality [*Turin*] and taking the adjacent slot over-spill into account [*Martin*92] as,

$$CNR_M = \sqrt{\frac{\pi}{2}} t_i \left\{ 1 - e^{-\frac{T_s}{t_i^2}} \right\}^2 \left(\frac{A_i^2}{N_0} \right) \tag{6.26}$$

where the first term shows the ideal matched filter output and the second term shows the slot over-spill at the adjacent time slots.

6.3 Wide-band Analysis

For wide band transmission media, or only slightly band limited, the received DPIM pulses are essentially rectangular in shape. Pulses are integrated by the receiver front end time constant, $R_L C_T$. Peak voltage occurs at the falling edge of pulses, and the amplifier output is directly presented at the threshold detector.

Eqn. 6.10 can be modified to,

$$V_{wo}(t) = A_i \left(1 - e^{-\frac{t}{R_L C_T}} \right) + n(t) \tag{6.27}$$

The peak amplitude, for received pulses with width of γT_s, can be given as,

$$V_{wo}\Big|_{t=\gamma T_s} = A_i \left(1 - e^{-\frac{\gamma T_s}{R_L C_T}} \right) + n(t) \tag{6.28}$$

Figure 6.10 shows the normalised pulse shape evaluated from Eqn. 6.28 at the threshold detector, for a received rectangular pulse of half a time slot with varying receiver time constants, $\tau_L = R_L C_T$, where R_L and C_T are the total front-end resistance and capacitance,

respectively. The time axis is normalised to the DPIM time slot and the amplitude axis is normalised to the peak amplitude of pulse when $\tau_L = 0.1\ T_s$.

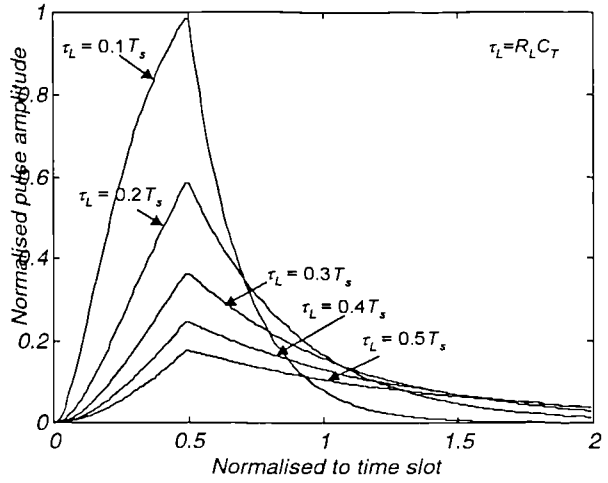

Fig. 6.10 Receiver response for varying front-end time constants.

With reference to Fig. 6.10, the signal strength is the highest at the falling edge of the transmitted rectangular pulse as stated before. The centre of a time slot in this case corresponds to $\gamma = 0.5$.

Thus the carrier-to-noise ratio at the highest signal amplitude can be given as,

$$CNR_W = \frac{2A_i^2}{N_0}\left|1 - e^{-\frac{\gamma T_s}{R_L C_T}}\right|^2 \qquad (6.29)$$

Threshold detection is performed at this point where the energy is highest. Furthermore, as the front end time constant increases the pulse rise and fall times increase giving a slopes that are prone to noise contamination which will severely degrade performance.

6.4 DPIM Error Sources

The pre-detection filter output is the input to the threshold detector. Sampling of DPIM slots are performed at the highest energy point. The decision, whether a pulse is

present or not, is made depending on whether the signal crosses the threshold level at the sampling points or not.

Each pulse is a reference to proceeding and succeeding frames. Noise contamination of the signal at sampling points give rise to transmitted symbols being wrongly detected. This can be divided into three error sources namely: erasure, wrong slot and false alarm errors [*Kaluarachchi*96/1]. The probability of a symbol error is the probability that a transmitted symbol 'k' being an error.

6.4.1 Erasure error (P_e)

Erasure error is when a pulse in the k^{th} time slot is not detected due to noise contamination see Fig. 6.11. This is due to noise in the received pulse forcing the pulse amplitude below the threshold level at the decision time, not necessarily erasing a pulse completely.

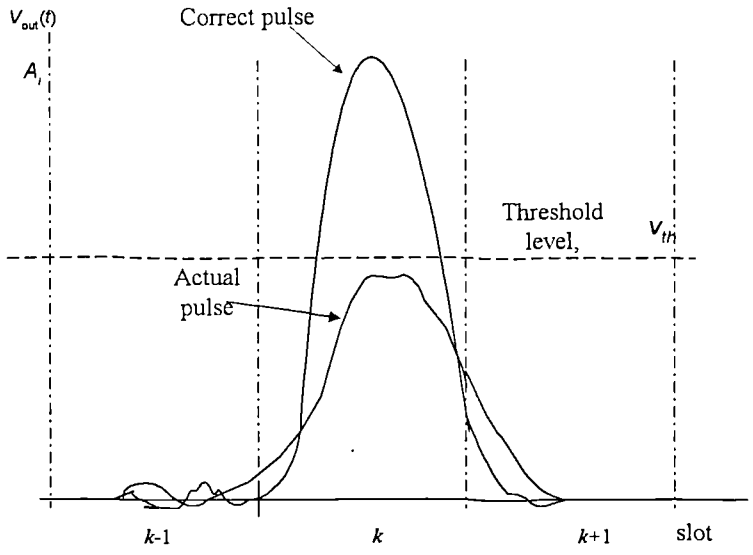

Fig. 6.11 Erasure error concept.

In Fig. 6.11, the correct pulse is the received pulse without noise contamination whilst the actual pulse is the received pulse with noise added. Erasure causes an error in two

consecutive frames in DPIM, unlike in isochronous frame structures e.g. in DPPM where only one frame is effected.

The probability of erasure error (P_e) can be defined as the probability of a transmitted pulse of amplitude A_t falling below the threshold level V_{th}. Where $A_t > V_{th}$ and the threshold level $V_{th} = \alpha A_t$. The parameter α is defined as the threshold factor as shown in Fig. 6.12,

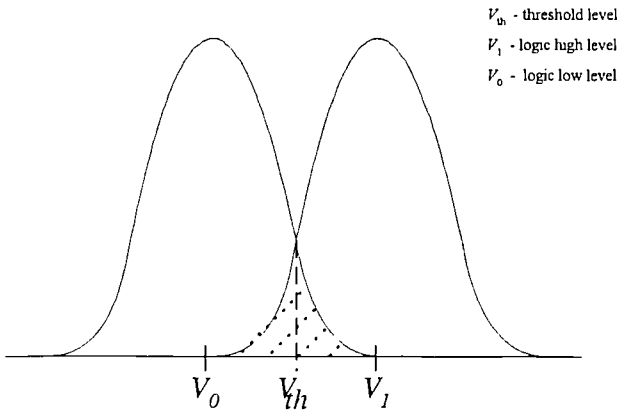

Fig. 6.12 Error concept.

Erasure error is defined as,

$$P_e(V < V_{th} : V_1) = \frac{1}{\sqrt{2\pi}\sigma} \int_{-\infty}^{v_{th}} e^{-\frac{(V-A_t)^2}{2\sigma^2}} dv \tag{6.30}$$

From Eqn. 6.30,

$$P_e(V < V_{th} : V_1) = 0.5 erfc\left((1-\alpha)\frac{A_t}{\sqrt{2}\sigma}\right) \tag{6.31}$$

where σ is the noise deviation or the RMS noise at the threshold detector and $0<\alpha<1$. Thus the probability of erasure error can be given from Eqn. 6.31,

$$P_e(V < V_{th} : V_1) = 0.5 erfc\left((1-\alpha)\sqrt{\frac{CNR}{2}}\right)$$

(6.32)

From Eqn. 6.32, the erasure error depends on the *CNR* and the threshold level. This is numerically evaluated and is shown on Fig. 6.13.

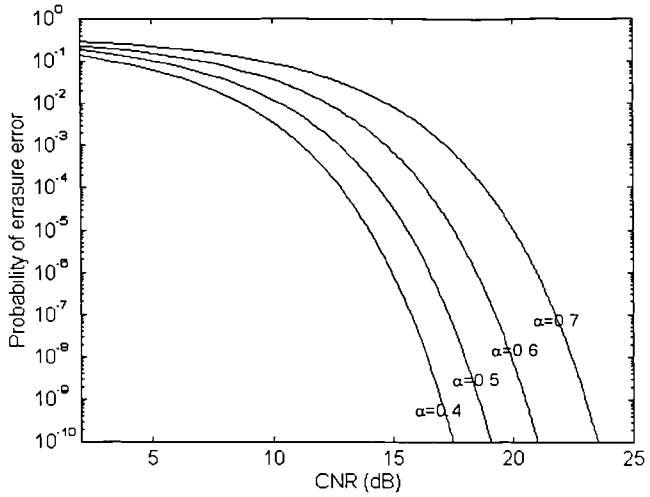

Fig. 6.13 Probability of erasure error for varying threshold level.

For a given *CNR*, the probability of a pulse being undetected is low when the threshold level is held at a low amplitude level. As the threshold level is raised the possibility of noise forcing the pulse below the threshold level becomes higher, see Fig. 6.13. Thus erasure error is the dominant error source at higher threshold levels.

6.4.2 False alarm error (P_f)

This is the opposite of erasure error. False alarm error or threshold violation error is caused by the receiver noise alone exceeding the threshold level (V_{th}) when there is no pulse present at the detection time. This is shown in Fig. 6.14, where a false alarm has occurred in the k-n^{th} time slot. Noise crosses the threshold level in the k-n^{th} time slot, where $k>n>0$. This error source divides a frame into two, giving two symbol errors for each threshold violation.

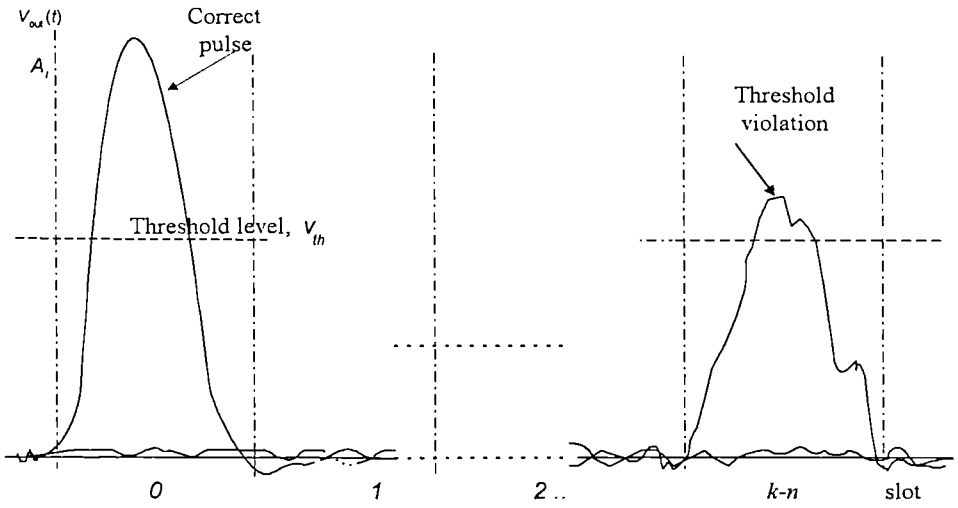

Fig. 6.14 Threshold violation or false alarm error concept.

Referring to Fig. 6.12, threshold violation can be defined for $V_0 = 0$ as,

$$P_f\left(V > V_{th} : V_0\right) = \frac{1}{\sqrt{2\pi}\sigma}\int_{V_{th}}^{\infty} e^{-\frac{v^2}{2\sigma^2}} dv \tag{6.33}$$

The rate of rise of a signal with either a matched filter or a sub-optimum filter is determined by the time constant. Long time constants mean it takes longer time for a pulse to reach its peak while a short time constant means it reaches its peak in a relatively short time. Thus the false alarm error in a time slot can be approximated by,

$$P_f\left(V > V_{th} : V_0\right) = \frac{0.5T_S}{\tau} erfc\left(\frac{\alpha A_i}{\sqrt{2}\sigma}\right) \tag{6.34}$$

where τ is the time during which the output stays above the threshold level and is related to the filter time constant. If a matched filter is considered as a correlator detector, τ is the time when the correlator output becomes zero.

Expressing Eqn. 6.34 in terms of carrier-to-noise ratio,

$$P_f\left(V > V_{th} : V_0\right) = \frac{0.5T_S}{\tau} erfc\left(\alpha\sqrt{\frac{CNR}{2}}\right) \tag{6.35}$$

where T_s is the slot duration and 1>α>0.

Figure 6.15 shows the probability of false alarm error against *CNR* for $\tau = T_s$ and varying threshold levels.

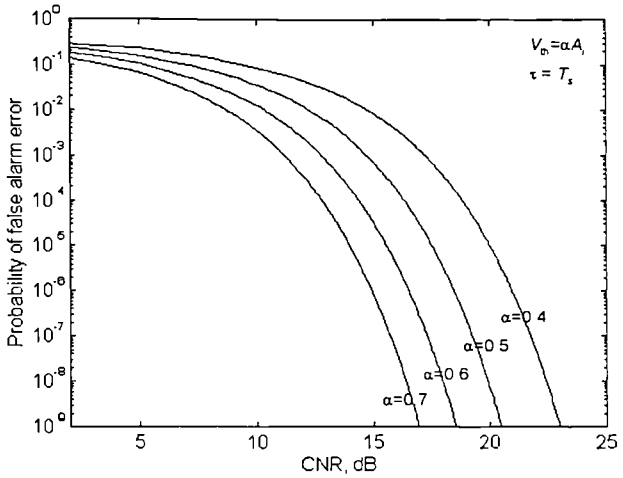

Fig. 6.15 Probability of false alarm error at varying threshold level.

For a given *CNR* threshold violation is high for low α and low for high α. False alarm error also varies indirectly with the time constant of the filter as given in Eqn. 6.35, where τ is dependent on the time constant. This variation is shown in Fig. 6.16, for threshold level of $V_{th} = 0.5A_1$.

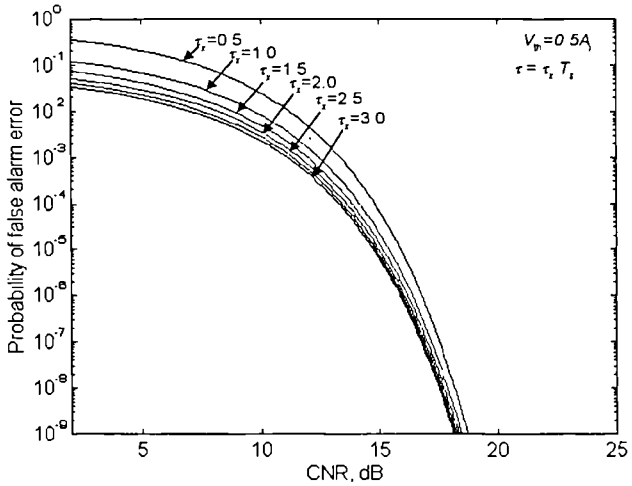

Fig. 6.16 Probability of false alarm error varying with the filter time constant, τ.

From Fig. 6.16, the probability of false alarm error is more sensitive to the filter time constant at low *CNR* levels than at high *CNR* level. It is the highest at $\tau_x = 0.5$ dropping on order of magnitude when $\tau_x = 0.3$. This is due to the fact that the filter with short time constant is more sensitive to noise.

6.4.3 Wrong slot error (P_w)

Wrong slot error is signal dependent and occurs when noise added to the finite slope of the leading/trailing edge of a dispersed pulse crosses the threshold in the proceeding or succeeding time slot, see Fig. 6.17. In this figure noise has corrupted the rising edge of the pulse causing it to cross the threshold level in the k-1th time slot, thus giving rise to a wrong slot error.

With V_2 being the voltage level without noise at the sampling instant in the adjacent time slots, the wrong slot error can be defined as,

$$P_w\left(V > V_{th} : V_2 < V_{th}\right) = \frac{1}{\sqrt{2\pi}\sigma} \int_{-\infty}^{v_{th}} e^{-\frac{(V-V_2)^2}{2\sigma^2}} dv \tag{6.36}$$

where

$$V_2\left(T_s\right) = Ae^{-\frac{T_s^2}{t_i^2}} \tag{6.37}$$

Sampling points are at $t = nT_s$, where $n \in 0,1,2,3,...N$.

From Eqns. 6.36 and 6.37, wrong slot error can be given by,

$$P_W\left(V > V_{th} : V_2 < V_{th}\right) = 0.5erfc\left(\frac{V_{th} - V_2}{\sqrt{2}\sigma}\right) \tag{6.38}$$

In terms of *CNR* Eqn. 6.38 can be modified to:

$$P_W(V > V_{th} : V_2 < V_{th}) = 0.5erfc\left(\left(\alpha - e^{-\frac{T_s^2}{t_i^2}}\right)\sqrt{\frac{CNR}{2}}\right) \tag{6.39}$$

where $1>\alpha>0$.

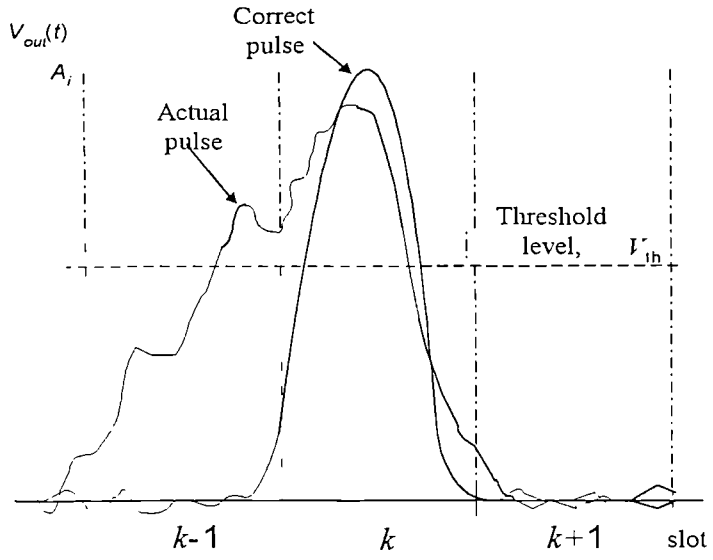

Fig. 6.17 Wrong slot error concept.

Wrong slot error is the most crucial error source in narrow-band channels. How, the bit resolution, relative bandwidth and the received pulse width effect this error source is investigated in this section.

Equation 6.39 is numerically evaluated for different received pulse widths at a threshold level of $0.5A_i$, see Fig. 6.18,

For a given threshold level, the probability of a wrong slot error increases, as the received RMS pulse width is increased, see Fig. 6.18. Corresponding pre-detection filter output pulse shapes are shown in Fig. 6.4. Thus wrong slot error is dominant when received pulses have long rise/fall times.

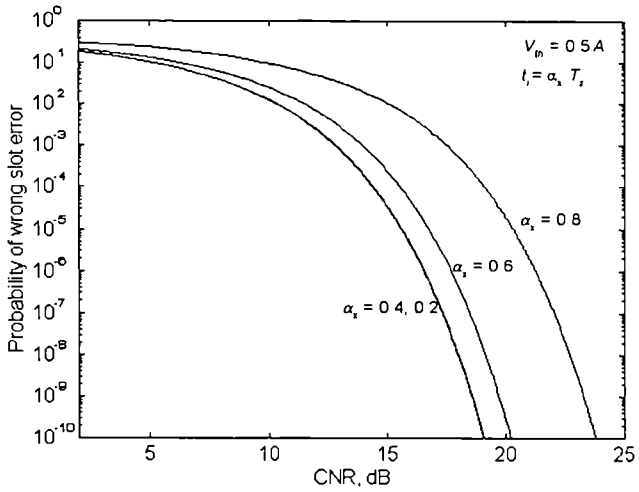

Fig. 6.18 Wrong slot error variation with received pulse width.

Using Eqns. 6.24 and 6.39 the probability of wrong slot error is investigated for a fixed relative bandwidth W/B = 4 and varying bit resolution, with the results shown in Fig. 6.19.

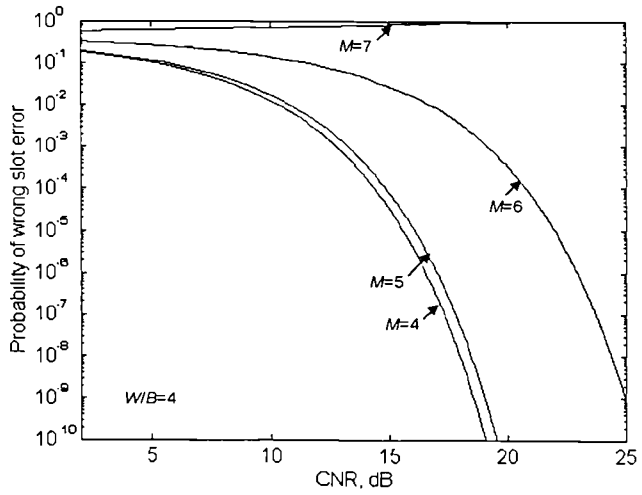

Fig. 6.19 Wrong slot error at different bit resolutions.

For low bit resolution e.g. 4 and 5, the probability of error characteristics is very similar to the previous error source. However, at high bit resolution the characteristics change considerably indicating a big increase in the probability of error. This variation is further investigated for a fixed *CNR* of 20 dB, W/B = 4 and different bit resolution, see Fig. 6.20.

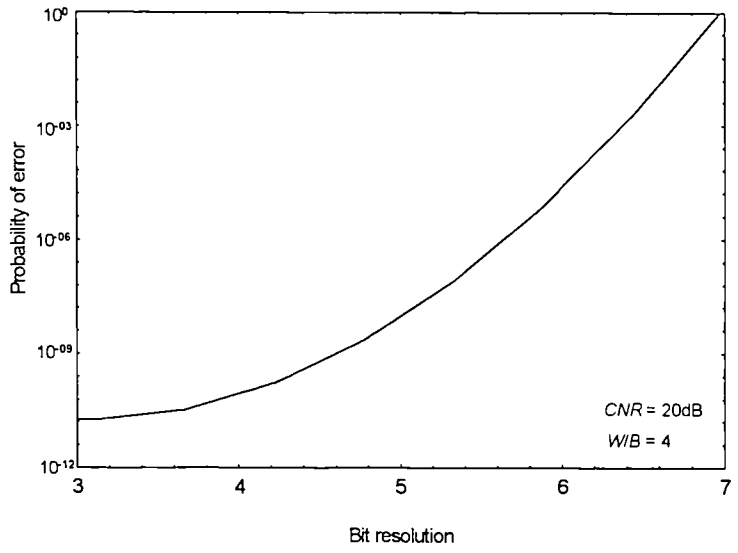

Fig. 6.20 Variation of wrong slot error with bit resolution.

The change in probability of error shows an exponential behaviour. At bit resolution of 3, $P_e = 10^{-1}$ increasing to 10^{-3} at bit resolution of 6. Therefore, in a fixed link one cannot increase the bit resolution beyond a threshold level without effecting the bit error rate.

In section 6.2.1.1, it was shown that pulse spreading can be reduced by increasing the receiver filter bandwidth. The effect of relative bandwidth on the wrong slot error is illustrated in Fig. 6.21.

As the relative bandwidth increases, the probability of wrong slot error drops and this bandwidth is optimum around 6, for the bit resolution in use. This is due to the fact that pulse spreading increases for low relative bandwidth, correspond to a particular bit resolution.

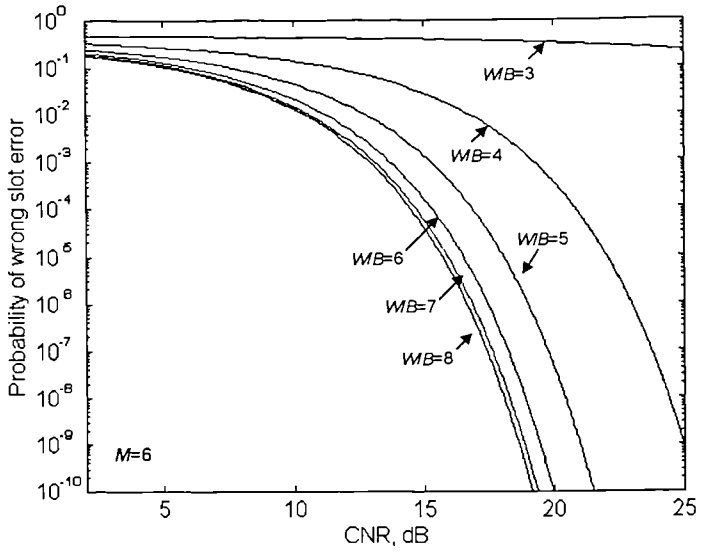

Fig. 6.21 Wrong slot error variation with varying relative bandwidth.

For different bit resolutions and relative bandwidths, the probability of wrong slot error was obtained and it was found that by rule of thumb, for bit resolution of M, a relative bandwidth of at least M is required for near optimum probability of wrong slot error performance.

6.5 Probability of Symbol/Bit Error

The three error sources described in section 6.4 cause symbol errors in DPIM systems. If the symbol corresponding to the present frame is represented by S_0, and if S_j is the symbol in the j^{th} previous frame ($-j$ denotes a future frame) then the transmitted DPIM signalling sequence will be denoted by the vector $S = \{...S_{-2}, S_{-1}, S_0, S_1, S_2 ....\}$. The DPIM symbol error probability is obtained by determining the symbol error probability of the current frame and averaging over all possible symbols. Provided that the start of the current frame is correctly detected, it is assumed that the next correct pulse occurs at the k^{th} time slot (corresponding to symbol k-1) and the probability of a false alarm error has not been compensated by an erasure error.

An erasure error occurs when the pulse in the time slot k is not detected. This can be given by,

$$P(0|k) = P_e \tag{6.40}$$

Due to false alarm errors, a pulse in time slot k can be detected in 1,2,...,k-2 time slots, hence the probability is,

$$P(1,2,3,\ldots k-2|k) = P_f \tag{6.41}$$

A pulse in time slot k can be detected in k-1 due to a false alarm or wrong slot error, hence the probability will be,

$$P(k-1|k) = P_f + \frac{P_W}{2} \tag{6.42}$$

A Wrong slot error is only possible in the succeeding time slot of a DPIM pulse. This is due to the fact that there is an idle time slot after each pulse to act as a guard against frame overspill. Thus at the receiver the decoder is switched off until the second time slot following a pulse.

The probability of a symbol error can be defined as due to the combined effect given by Eqns. 6.40-42. Therefore, the probability of transmitted symbol k being in error can be given by,

$$P_k = P_e + \left(P_f + \frac{P_w}{2}\right) + (k-2)P_f \tag{6.43}$$

For M bit DPIM, the symbol variation is 0..2^M-1, and k varies in the range 1..2^M. Thus the average symbol error rate can be given by [*Atkin*],

$$P_{symbol} = \frac{1}{2^M}\sum_{k=1}^{2^M} P_k \tag{6.44}$$

Equation 6.43 simplifies to,

$$P_{symbol} = P_e + \frac{P_W}{2} + \frac{\left(2^M - 1\right)}{2} P_f \tag{6.45}$$

Correct detection is defined as a pulse at k^{th} time slot is detected correctly, i.e. $P(k|k)$.

Therefore, the probability of correct detection can be given as,

$$P(k|k) = 1 - P_{symbol} \tag{6.46}$$

Substituting for P_{symbol} Eqn. 6.46 simplifies to,

$$P(k|k) = 1 - P_e - \frac{P_W}{2} - \frac{\left(2^M - 1\right)}{2} P_f \tag{6.47}$$

The loss of information for each DPIM pulse error is not the same with PCM, so for comparison purposes, the DPIM symbol error probability should be related to the equivalent source (PCM) probability of bit errors. By considering an average frame length, one may approximate the DPIM probability of symbol error with the PCM bit error rate as considered for DPPM systems [*Sibley*93/2], [*Cryan*92/1]. One may argue that whether this is valid, as DPIM is an anisochronous scheme. By analysing the theoretical results along with the measurements, the validity of the assumption may be proved. Therefore, in deriving equivalent bit error rate, the average DPIM frame is considered and the relation is given by [*Atkin*],

$$P_b = \frac{L_{avg}}{2\left(L_{avg} - 1\right)} P_{symbol} \tag{6.48}$$

where L_{avg} is the average DPIM frame length in time slots.

Substituting for P_e, P_f and P_w in Eqn. 6.45 allows bit error rate performance to be evaluated.

6.5.1 Effect of threshold level on the probability of bit error

The dependency of comparator threshold level on the probability of bit error was evaluated for 4 bit DPIM system, for received pulse width $t_l = 0.3T_s$ and $\tau = T_s$.

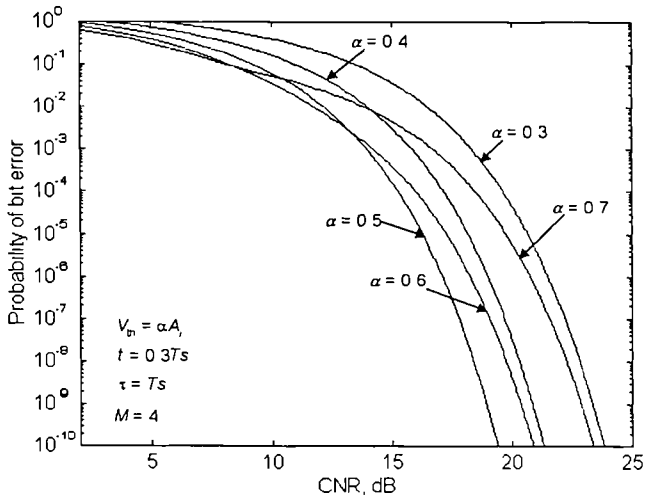

Fig. 6.22 Probability of bit error for varying threshold levels.

As shown in Fig. 6.22, when the threshold factor α increases from 0.3 the probability of a bit error drops until the threshold factor is 0.5. The dominant error source in this region is false alarm error as the threshold level is low. As the threshold is further increased from 0.5, the probability of error starts to increase as erasure error becomes dominant for higher threshold levels. This characteristic is further investigated by evaluating the probability of bit error at a given *CNR* (20 dB) and for a range of threshold level, see Fig. 6.23. The optimum threshold level is confirmed to be ≈ 0.5.

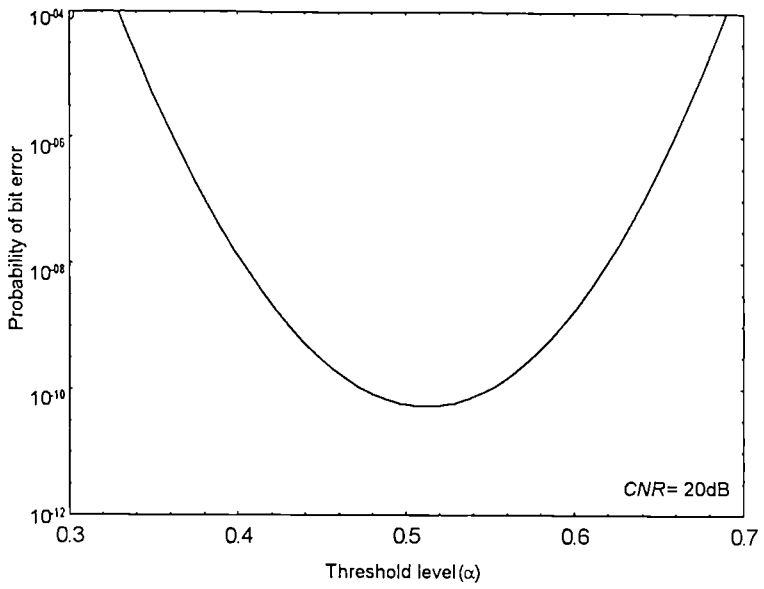

Fig. 6.23 Threshold level effect on the probability of bit error.

6.5.2 Effect of filter time constant on the probability of bit error

The effect of time constant of the pre-detection filter on the probability of bit error is investigated and the results are shown in Fig. 6.24. In the low *CNR* region, the dominant error source is the false alarm as was described in section 6.4.2.

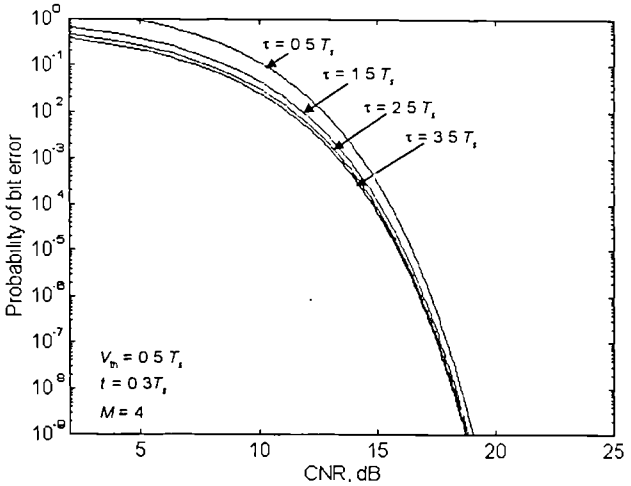

Fig. 6.24 Effect of filter time constant on the probability of error.

6.5.3 Effect of received pulse width on the probability of bit error

The band limited nature of the channel introduces pulse spreading, which in turn result in an increased ISI and consequently the probability of bit errors. This is shown in Fig. 6.25, for a threshold factor of $\alpha = 0.5$, $\tau = T_s$, and $M = 4$.

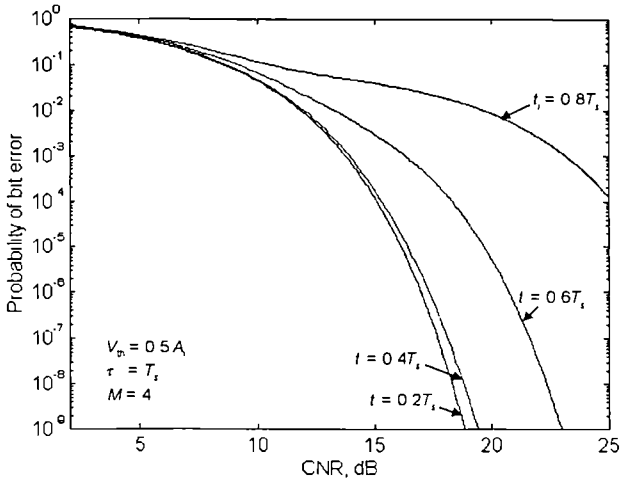

Fig. 6.25 Effect of band limiting on the probability of bit error.

At the low end of the *CNR* range, all three error sources are similarly affected by noise. As *CNR* increases, erasure and false alarm errors drop, but wrong slot error does not due to pulse spreading, i.e. ISI.

6.5.4 Effect of bit resolution on the probability of bit error

For a fixed relative bandwidth, a threshold factor of 0. 5, $t_i = 0.3T_s$ and $\tau = T_s$, the effect of bit resolution on the probability of bit error is illustrated in Fig. 6.26. The bit error rate performance for M = 2 to 5 are very similar, degrading rapidly at higher bit resolution, $M = 6$ and 7.

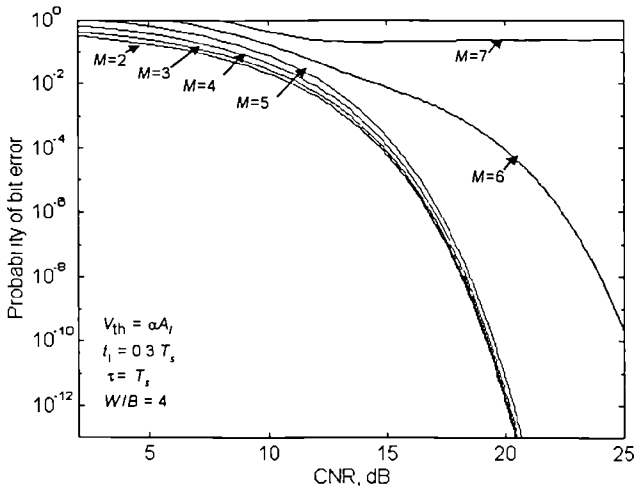

Fig. 6.26 Effect of bit resolution on the probability of bit error.

6.5.5 Effect of relative bandwidth on the probability of bit error

As described in the previous section, relative bandwidth needs to be chosen for higher bit resolution in order to reduce the chance of a wrong slot error. Figure 6.27 shows probability of error versus *CNR* for different values of relative bandwidth.

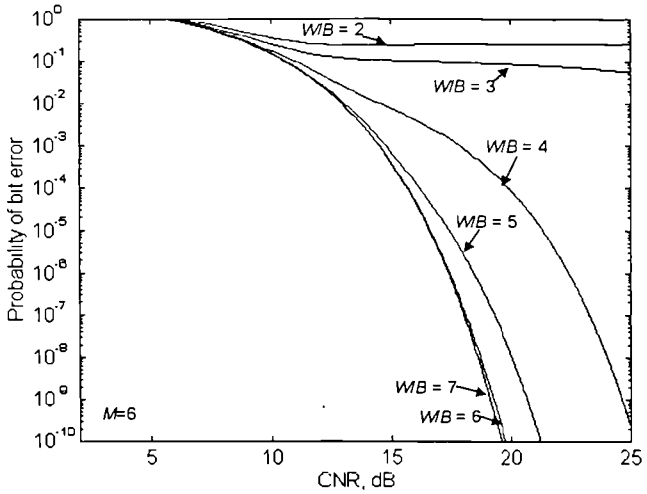

Fig. 6.27 Effect of relative bandwidth on the probability of bit error.

For low relative bandwidth, probability of a bit error is severely degraded by the contribution from the wrong slot error source due to ISI. As the bandwidth increases, the bit error probability reduces. To achieve $P_e = 10^{-9}$ at *CNR* = 19 dB the optimum relative bandwidth is 6.

6.6 Jitter Effect

In receiver analysis it was assumed that jitter effect is negligible or the system is perfectly synchronised. However in practical systems, there are two sources of jitter: threshold induced jitter and clock jitter. The former jitter due to the additive channel noise has little effect because of the sampling nature of the detection process, whereas the latter due to the randomness of the received bit pattern, will have implications on accurate clock recovery using PLL [*Elmirghani*94/4]. The slot clock timing variance and the probability of error due to clock jitter are given by Eqns. 4.35 and 4.36, respectively. Equation 4.36 is evaluated for different PLL bandwidth and the results are shown in Fig. 6.28. It illustrates that the timing variance is lower at low bit resolutions. This can be explained as due to high number of transitions. With high bit resolution there will be a fewer number of pulses at the PLL input within a particular time period.

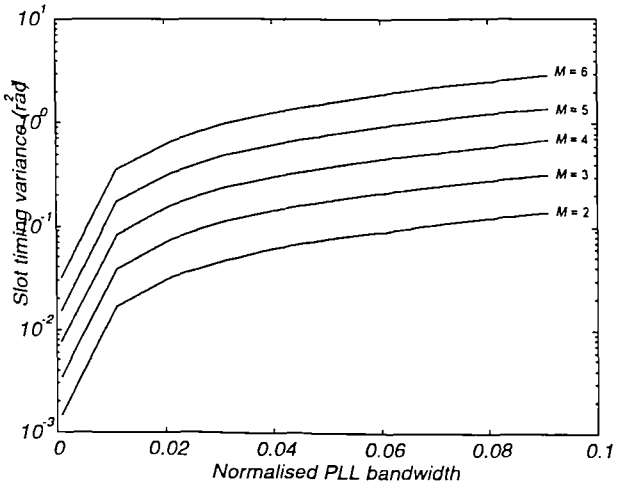

Fig. 6.28 Receiver slot clock timing variance Vs. normalised PLL bandwidth at different bit resolutions.

The more frequent transitions at the PLL input gives an enhanced slot component at the PLL input. Furthermore, it is also shown that the timing variance can be reduced by means of reducing the PLL bandwidth. The PLL bandwidth is also constrained by the

dynamic parameters such as lock range, capture range etc. These parameters are discussed in the chapter 5. A higher level of timing variance due to imperfect slot synchronisation can result in additional error sources being introduced at the DPIM demodulation process. Probability of error introduced due to imperfect slot synchronisation is evaluated from Eqn. 4.37 and the result is shown in Fig. 6.29.

To achieve a probability of error of 10^{-9} at bit resolution of 4, a PLL bandwidth and slot duration product of 3.10^{-2} is required. PLL bandwidth may be increased but the penalty paid is reduced bit resolution for the same probability of error. Therefore, at a chosen bit resolution PLL with low bandwidth is essential in order to minimise the jitter probability of error.

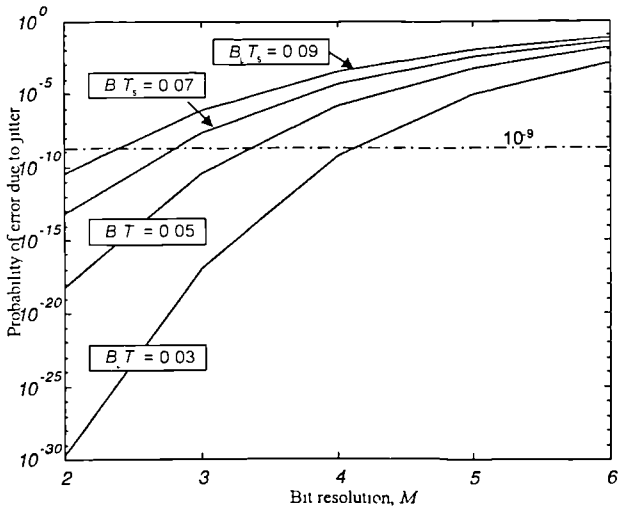

Fig. 6.29. Probability of bit error due to jitter effect Vs. bit resolution for different PLL bandwidth.

6.7 Probability of Error in Comparison with PCM and DPPM

As DPIM is a digital modulation scheme, it is quite appropriate to compare its performance with PCM, which has widely been used by many authors. Assuming that the source of information is a binary bit stream, a comparison can be made based on the

probability of error performance, whereas if the source information is analogue information the comparison should be based on *SNR* performance at the receiver output. PCM demands lower transmission bandwidth compared to DPIM, as PCM slots are wider. However, for comparison, it is assumed that both the systems use the same bandwidth criteria. A common parameter for comparison is the *CNR* at the threshold detector.

Two error sources affect the probability of error in PCM, namely, erasure and false alarm. Wrong slot errors appear as false alarms. The definition of these two error sources are similar to that given for DPIM.

It is assumed that a binary 1 corresponds to 'pulse present' and 0 to 'absent'. False alarm error is when transmitted zero is detected as 1 and is designated by $P_{\varepsilon 0}$ whereas erasure is when transmitted 1 is detected as 0 designated by $P_{\varepsilon 1}$. Assuming the signal amplitude is given by A_c and the threshold level $V_{th} = \alpha_c A_c$, from Eqn. 6.33, the probability of false alarm is of the form,

$$P_{\varepsilon 0} = \frac{1}{\sqrt{2\pi}\sigma_c} \int_{V_{th}}^{\infty} e^{-\frac{v^2}{2\sigma_c^2}} dv \tag{6.49}$$

where σ_c is the RMS noise at the threshold detector input. As the bit period is wider compared to DPIM the effect of the filter time constant is not taken into account. From Eqn. 6.49,

$$P_{\varepsilon 0} = 0.5 erfc\left(\frac{\alpha_c A_c}{\sqrt{2}\sigma_c}\right) \tag{6.50}$$

This is simplified to,

$$P_{\varepsilon 0} = 0.5erfc\left(\alpha_c\sqrt{\frac{CNR}{2}}\right) \tag{6.51}$$

Erasure error can be given by Eqn. 6.32,

$$P_{\varepsilon 1} = 0.5erfc\left((1-\alpha_c)\sqrt{\frac{CNR}{2}}\right) \tag{6.52}$$

Assuming the transmitted bit probabilities for 0 and 1 are P_0 and P_1 respectively, the PCM probability of bit error P_ε can be given by [*Stremler*],

$$P_\varepsilon = P_0 P_{\varepsilon 0} + P_1 P_{\varepsilon 1} \tag{6.53}$$

For binary levels, it is fair to assume that binary levels are equiprobable. Thus $P_0 = P_1 = 0.5$. From Eqns. 6.51, 6.52 and 6.53, the PCM probability of error is thus given by,

$$P_\varepsilon = \frac{1}{4}\left(erfc\left(\alpha_c\sqrt{\frac{CNR}{2}}\right) + erfc\left((1-\alpha_c)\sqrt{\frac{CNR}{2}}\right)\right) \tag{6.54}$$

For DPIM the probability of error is comparable to DPPM as both are of pulsed nature and both are affected by the same three error sources. For M bit resolution DPPM, the probability of symbol error (P_{es}) is given by [*Cryan*93/1],

$$P_{es} = P_e + P_w + \frac{2^M - 1}{2}P_f \tag{6.55}$$

Comparing Eqn. 6.55 with 6.45, it can be said that DPIM probability of symbol error is less affected by wrong slot error compared to that with DPPM This is due to the fact that in DPIM a wrong slot error only occurs on the slot proceeding a pulse, whereas in DPPM both the adjacent pulses are prone to wrong slot error. In obtaining the PCM equivalent probability of bit error, Eqn. 6.49 can be used by substituting P_{es} for P_{symbol} and 2^M for L_{avg}. In terms of receiver bandwidth, DPPM with a compression index of 1

and DPIM with no guard band show similar performance (Fig. 4.3) whereas PCM requires less bandwidth. A simple way of comparing DPIM performance with PCM and DPPM is by setting the decision threshold at 0.5, making erasure and false alarm errors approximately equal. In the wide band case, infinite channel bandwidth is assumed and the matched filter detection of both DPIM and PCM is considered. For PCM system let the received peak optical power and the electrical signal amplitude at the matched filter input be E_c and A_c, respectively. *CNR* at the threshold detector input is dependant on the energy content at the matched filter output.

Since DPIM/DPPM slot widths are very small compared to PCM then for the same peak power the energy delivered by PCM is higher compared to DPIM\DPPM. Therefore, to deliver the same energy at threshold detector, they should be pulsed at higher peak powers compared to that of PCM. The *CNR* between DPIM and PCM, designated by CNR_I and CNR_c, respectively can be given for the wide band case as,

$$\frac{CNR_I}{CNR_c} = \left(\frac{E_I}{E_c}\right)^2 \frac{\gamma M}{2^M + 1} \tag{6.56}$$

Thus for wide band DPIM and PCM to give similar bandwidth with varying bit resolution, their peak power demands should be met as given by,

$$\frac{E_I}{E_c} = \sqrt{\frac{\gamma M}{2^M + 1}} \tag{6.57}$$

where γ is the DPIM pulse duty cycle within a time slot, with an optimum value of 0.5, see Fig. 6.9. Equation 6.57 is plotted over a range of bit resolution and the result is shown in Fig. 6.30.

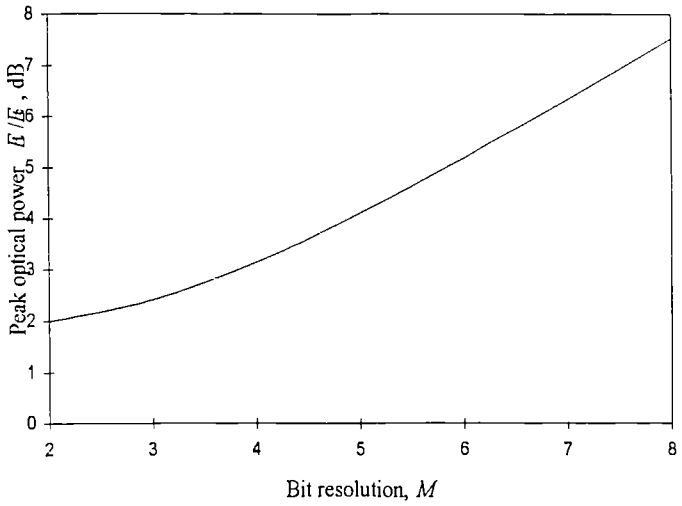

Fig. 6.30 DPIM/PCM peak power variation with varying bit resolution.

Figure 6.30 shows that DPIM peak optical power increases steadily with increasing bit resolution and this must be provided if DPIM is to achieve superiority over PCM. Since DPIM pulses are short in duration compared to PCM and have much smaller duty cycle, then delivering higher peak power is not a major problem. It has been found that the upper limit on the available peak power is set by the catastrophic degradation of the optical emitter being used [*Katz*]. However, theoretical studies have shown that extremely large pulse powers can be obtained before catastrophic facet damage occurs in optical emitters. Allowable peak power seems to vary inversely as the square-root of the pulse width [*Kappeler*]. For example, 4 bit DPIM will require further 2.7 dB peak optical power to achieve the same *CNR* as with PCM. The probability of error performance of DPIM with respect to *CNR* of PCM, is shown in Fig. 6.31 for the case when the peak power is just above the threshold level.

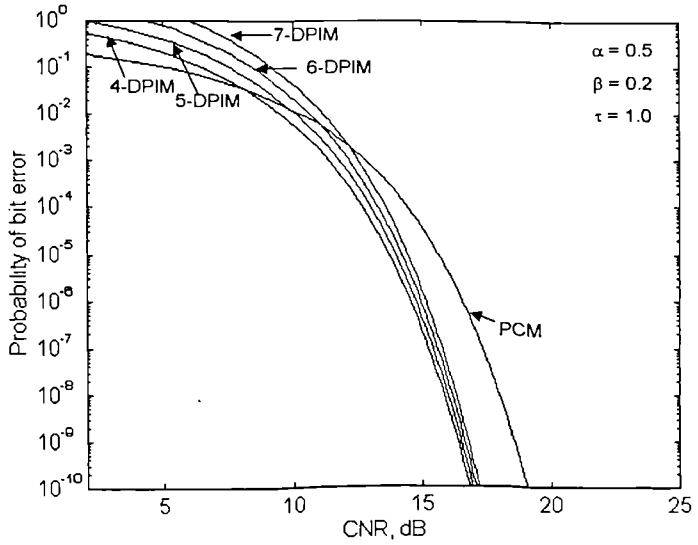

Fig. 6.31 DPIM and PCM probability of error.

At higher *CNR* (i.e. > 12 dB) DPIM shows better probability of bit error performance. To achieve a bit error rate of 10^{-9}, *CNR* requirement for DPIM is ≈ 2 dB less than that of PCM system. However, DPIM performance deteriorates at low *CNR* due to false alarm error being the dominant source. The effect of channel bandwidth on *CNR* is given in Fig. 6.27. Taking into account that PCM bit rate is low compared to DPIM, variation of *CNR* can then be approximated as,

$$\frac{CNR_1}{CNR_c} \approx \frac{1}{\sqrt{2\pi}} \left(\frac{E_1^2}{E_c^2}\right)\left(\frac{B}{W}\right)\left\{1 - e^{-\frac{T_s^2}{t_1^2}}\right\}^2 \tag{6.58}$$

where *W/B* is the relative bandwidth.

To achieve the same *CNR*, from Eqn. 6.58, the DPIM/PCM peak optical power ratio can be given by,

$$\frac{E_1}{E_c} \approx \sqrt{\left(\frac{W}{B}\right)} \frac{(2\pi)^{1/4}}{1 - e^{-\frac{T_s^2}{t_1^2}}} \tag{6.59}$$

The result of Eqn. 6.59 is illustrated in Fig. 6.32 for different values of relative bandwidths, showing high peak power requirement at high bit resolution and relative

bandwidth. This is due to slot spill-over as bit resolution increases. On the other hand, power requirement drops by 23 dB as W/B is increased from 1 to 10 at 6 bit resolution.

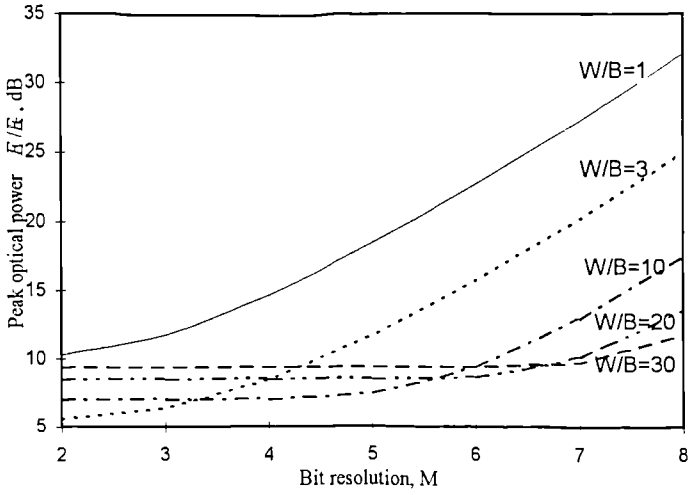

Fig. 6.32 DPIM peak power demand with varying bit resolution.

Having established the necessary power requirement using Eqn. 6.59, the probability of bit error performance can then be evaluated using Fig. 6.31 for narrow band channels.

6.8 *SNR* Performance

For an analogue signal $V(t)$, band limited to f_m Hz and with amplitude range of $\pm V_m$, the sampling criterion is given by Eqn. 4.48. Sampled amplitudes are quantised into L levels, where $L = 2^M$. Each quantised sample is encoded into a DPIM frame, which is in effect a binary stream of pulses, before transmitting it through the channel. At the receiver quantised samples are reconstructed from the decoded symbols. The reconstructed samples are then passed through a low pass filter to obtain the desired signal $V(t)$.

For analogue signal transmission there are two sources of errors, which degrade the DPIM signal to noise ratio (*SNR*):- detection and quantisation rounding off errors. The former is introduced at the threshold detection process, which has been analysed in

detail in the previous section, and the latter are mainly dependent on the bit resolution. The higher the bit resolution, the lower the quantisation error, but this cannot be avoided in discrete modulation schemes. In the following section, how these two errors affect the *SNR* at the receiver output is investigated.

Consider the transmitted k^{th} frame as V_k, which is quantised, or rounded off, to a value $\hat{V}_k$, and is encoded and transmitted as a DPIM frame. Because of the channel noise some of the frames may be detected erroneous at the receiver and reconstructed sample will be $\tilde{V}_k$ instead of $\hat{V}_k$. Assuming that the detection and quantisation errors in the k^{th} sample are designated by ε_k and q_k, respectively, the regenerated pulse stream can be given by,

$$x(t) = \sum_{k=-\infty}^{\infty} bg\left(t - T_s\left(2k + \sum_{m=-\infty}^{k-1} S_m\right) - \varepsilon_{tk}\right) \tag{6.60}$$

where b is the DPIM pulse amplitude after the threshold detector and ε_k is the time displacement due to a detection error in the k^{th} sample. ε_k and q_k are related as,

$$\begin{aligned} q_k &= V_k - \hat{V}_k \\ \varepsilon_k &= \hat{V}_k - \tilde{V}_k \\ \text{and} \quad V_k - \tilde{V}_k &= q_k + \varepsilon_k \end{aligned} \tag{6.61}$$

where the total error during the transmission is $q_k + \varepsilon_k$. The filter used to construction the signal $\tilde{V}(t)$ from $\tilde{V}_k$ has the following response [*Carlson*].

$$\tilde{V}(t) = \sum_{k=-\infty}^{\infty} \tilde{V}_k \operatorname{sinc}\left(2f_m t - t_k\right) \tag{6.62}$$

where t_k is the sampling points or the DPIM pulse stream itself which can be written as,

$$t_k = T_s\left(2k + \sum_{m=-\infty}^{k-1} S_m\right) - \varepsilon_k \tag{6.63}$$

From Eqns. 6.61, 62 and 63,

$$\tilde{V}(t) = \sum_{k=-\infty}^{\infty} (V_k - q_k - \varepsilon_k) \sin c \left(2f_m t - T_s \left(2k + \sum_{m=-\infty}^{k-1} S_m \right) - \varepsilon_k \right) \tag{6.64}$$

Equation 6.64 can be simplified as,

$$\tilde{V}(t) = \sum_{k=-\infty}^{\infty} V_k \text{sinc} \left(2f_m t - T_s \left(2k + \sum_{m=-\infty}^{k-1} S_m \right) - \varepsilon_k \right) - (q_k + \varepsilon_k) \text{sinc} \left(2f_m t - T_s \left(2k + \sum_{m=-\infty}^{k-1} S_m \right) - \varepsilon_k \right) \tag{6.65}$$

$$\tilde{V}(t) = V(t) - e(t)$$

$e(t)$ is the noise introduced during the transmission, given as,

$$e(t) = (q_k + \varepsilon_k) \text{sinc} \left(2f_m t - T_s \left(2k + \sum_{m=-\infty}^{k-1} S_m \right) - \varepsilon_k \right) \tag{6.66}$$

The error signal $e(t)$ is a random process with k^{th} sample $q_k+\varepsilon_k$. This can be taken as wide sense stationary where the mean square value of the process is the same at any instant. Mean square value of noise $e(t)$ can be given by,

$$\overline{e^2(t)} = \overline{(q_k + \varepsilon_k)^2} \tag{6.67}$$

Since q_k and ε_k are independent random variables with zero mean, Eqn. 6.67 may be approximated to,

$$\overline{e^2(t)} = \overline{q_k^2} + \overline{\varepsilon_k^2} \tag{6.68}$$

Equation 6.68 represents the noise associated with the receiver output. As from Eqn. 6.65, the signal and noise power at the reconstruction filter is given by,

$$S_{out} = \overline{V^2}, \quad N_{out} = \overline{e^2(t)}$$

$$SNR_{out} = \frac{S_{out}}{N_{out}} = \frac{\overline{V^2}}{\overline{e^2(t)}} = \frac{V^2}{\overline{q_k^2} + \overline{\varepsilon_k^2}} \tag{6.69}$$

Two error sources are given in the above equation, i.e. decoding noise and the quantisation noise, which affect the *SNR* of the regenerated waveform. Mean square decoding noise is dependant on the probability of symbol error at the threshold detector. Mean square quantisation error can be given by [*Carlson*],

$$\overline{\varepsilon_q^2} = \frac{1}{3}\left(\frac{V_m}{2^M}\right)^2 \tag{6.70}$$

As a consequence of additive noise at the threshold detection process, the detector will occasionally decide incorrectly on the position of DPIM pulses causing symbol errors. A frame in which such an error is committed is incorrectly decoded, and an equivalent analogue error arises with respect to the message sample amplitude concerned. The relative magnitude of this equivalent analogue error or decoding error, due to symbol errors, can be determined in terms of the DPIM probability of symbol error.

For a bit resolution of M, the full scale message sample corresponds to symbol 2^M. Output variation for symbol variation of $1..2^M$ can be given by w where $V_m \geq w \geq V_m / 2^M + 1$. It is reasonable to assume, for probability of symbol error P_{symbol}, any transmitted symbol is equally likely to be incorrect. This probability is governed by the *CNR* at the threshold detector. Then the mean square error (error variance) averaged over all the possible symbols can be given by [*Downing*],

$$\overline{\varepsilon_d^2} = \frac{P_{symbol}}{2^M}\sum_{n=1}^{2^M}\left(\frac{V_m}{2^M}n\right)^2 \tag{6.71}$$

Equation 6.71 simplifies to,

$$\overline{\varepsilon_d^2} = \frac{(L+1)(2L+1)}{6.(L^2)}V_m^2 P_{symbol} \tag{6.72}$$

where $L = 2^M$

From Eqns. 6.69, 6.70 and 6.72 the output SNR_{out} can be given by,

$$SNR_{out} = \frac{6.L^2}{(2L+1)(L+1)P_{symbol} + 2}\left(\frac{\overline{V^2}}{V_m^2}\right) \tag{6.73}$$

The *SNR* is dependent on the probability of symbol error and the quantisation effect. The *SNR* performance of DPIM and PCM (Eqn. 2.15) are plotted against *CNR* (at the threshold detector) for different resolution, see Fig. 6.33.

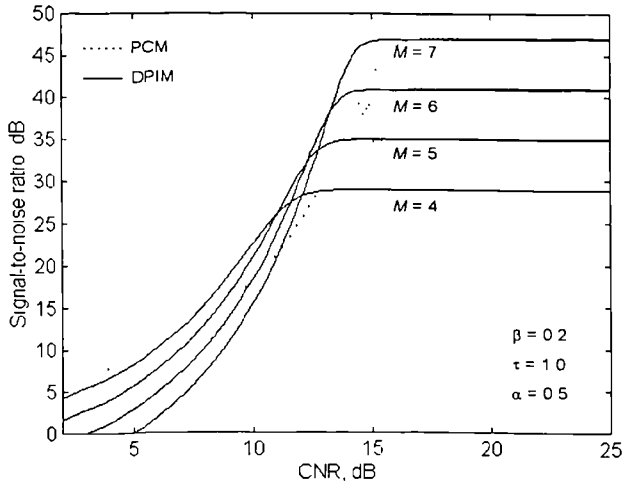

Fig. 6.33 DPIM, PCM *SNR* performance.

In Fig. 6.33 there are two main regions:- threshold and saturation. In the threshold region both PCM and DPIM give high levels of bit errors, resulting sample values at the decoder output that have no relation to the actual samples transmitted (the received signal does not corresponds to the ones transmitted, in other words the received signal is meaningless). At higher *CNR*s, the probability of bit errors become smaller and the majority of the received samples correspond to the ones transmitted. The probability of bit error approaching zero correspond to high *CNR*s, the output noise in Eqns. 6.75 and 2.15 depends entirely on the quantisation error, which in turn depends only on the bit resolution. Further increase in the *CNR* does not improve the output SNR, resulting in a saturated response. Comparing *SNR* of DPIM and PCM, it can be seen that both give similar performance in the saturated region above threshold. DPIM gives low

output *SNR* at low *CNR* region as compared to PCM, but it reaches the saturation region before PCM does. The *SNR* performance of DPIM with reference to PCM is further investigated for the same parameters and is given in Fig. 6.34.

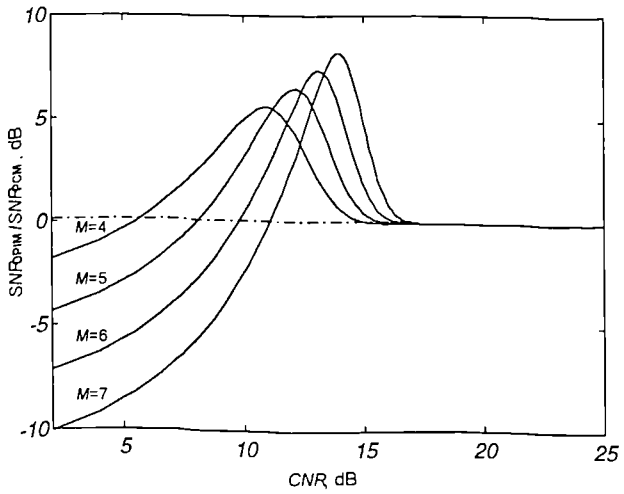

Fig. 6.34 DPIM *SNR* normalised to PCM.

In Fig. 6.34, there exists three regions which can be of importance where DPIM shows, inferior, superior and equivalent performance compared to PCM. At low *CNR* e.g. below 6, 7.5, 9 and 11 dB for bit resolutions of 4, 5, 6 and 7, respectively, DPIM performance is inferior. This is due to DPIM frame pattern being distorted due to propagation of errors into the adjacent frames. As *CNR* increases DPIM shows superior *SNR* performance for a certain range of *CNR*, e.g. 5-15, 7.5-16, 9-17, and 11-17.4 dB for bit resolutions of 4, 5, 6 and 7, respectively. As *CNR* is further increased at a *CNR* value (around 16 dB) both starts to show identical *SNR* performance. This is the noise threshold of both the schemes. Any increase of *CNR* above this threshold does not improve the system performance any further.

Next, DPIM *SNR* is compared with the analogue PIM that described in chapter 3. From Fig. 6.31 it is evident that the DPIM threshold region occur at *CNR* of about 15 dB. Above this level the *SNR* is set by the bit resolution and vary by about 6 dB. By

comparing DPIM *SNR* with PIM that given in Fig. 3.7, it can be seen that DPIM shows *CNR* gain of about 8 dB for 5 bit, 16 dB for 6 bit, 24 dB for 7 bit system, 31 dB for 8 bit system and similar performance with 4 bit system. At higher *CNR* ratios *SNR* of the analogue PIM increases linearly, but the output is subject to non-linear distortions as described in chapter 4.

6.9 Summary

Receiver performance has been analysed in terms of bit error rate for data and *SNR* for analogue signals. There are three error sources which determine, the system probability of bit error performance, namely; erasure, false alarm and wrong slot errors.

False alarm and erasure errors are dominant at low *CNR* levels and are sensitive to threshold level setting at the detector. False alarm error and erasure error sources are dominant at low and high threshold levels, respectively.

Wrong slot error, on the other hand, is affected by the noise corrupting the pulse edges. Receiver analysis has been carried out for both narrow and wide band signals. In the narrow-band case received signal was taken as Gaussian shape, with a pulse width being dependant on the relative bandwidth and bit resolution. For a given relative bandwidth, an increase in bit resolution results in pulse spreading, which in turn introduce more wrong slot errors. Pulse spreading may be reduced by increasing the relative bandwidth. The pre-detection filter employed may also result in pulse spreading, if the filter bandwidth is not chosen at the optimum point. Higher bandwidths reduces pulse spreading, but increases the band limited noise.

Finally, DPIM can deliver higher peak optical power compared to PCM, resulting in higher *CNR* and lower probability of error. In terms of *SNR*, DPIM gives higher performance compared to PCM, around the threshold region, whereas above this region both schemes show identical *SNR* performance. Furthermore DPIM gives substantial *CNR* improvements over analogue PIM.

Chapter Seven

System Implementation

In the previous chapter, the system performance was analysed in detail. A detailed account of the hardware implementation of the point-to-point DPIM system is presented in this chapter.

7.1 Introduction

Performance of the DPIM system has been presented in chapters four and six. A low frequency prototype for the transmission of a continuous signal over an optical fibre cable was designed and constructed in order to verify the performance predictions.

The prototype was implemented on colander ground plane prototype boards and off the shelf components were used. For low frequency input signal (≈15 kHz) the slot frequencies are 510, 990 and 1995 kbps for 4, 5 and 6 bit resolutions, respectively. For such low slot frequencies a guard band is not required, therefore it was not included in the design process. A LED and a PIN diode, both operating at 820 nm wavelength were chosen as the optical source and the detector, respectively. The fibre used is a multimode graded index fibre (62.5/125μm).

7.2 Transmitter

The overall transmitter block diagram is shown in Fig. 5.1. The input signal to the transmitter is an analogue signal of 15 kHz bandwidth, which is level shifted before being modulated.

7.2.1 Modulator

For analogue signal transmission systems, DPIM encoder is built around building blocks of successive approximation DAC, see chapter 5 for details. In order to vary the system bit resolution (2-8), an eight bit DAC with conversion rate up to 30 MHz (Phillips, DAC8702T) was used along with two cascaded four bit binary counters (74F161) and a high speed comparator with propagation delay of 6 ns (DAC9696). The output of the comparator is fed into a flip-flop whose clock frequency determines the guard band, see Fig. 7.1. The flip-flop is clocked with the inverted slot clock, for zero guard band. For comparison at Nyquist rate, the DPIM slot frequency (f_s) and PCM bit rate (B) over a range of bit resolutions (M) are presented in table 7.1.

M (bits)	2	3	4	5	6	7
f_s kbps	150	270	510	990	1950	3780
B kbps	60	90	120	150	180	210

Table 7.1 DPIM slot rate for different bit resolutions.

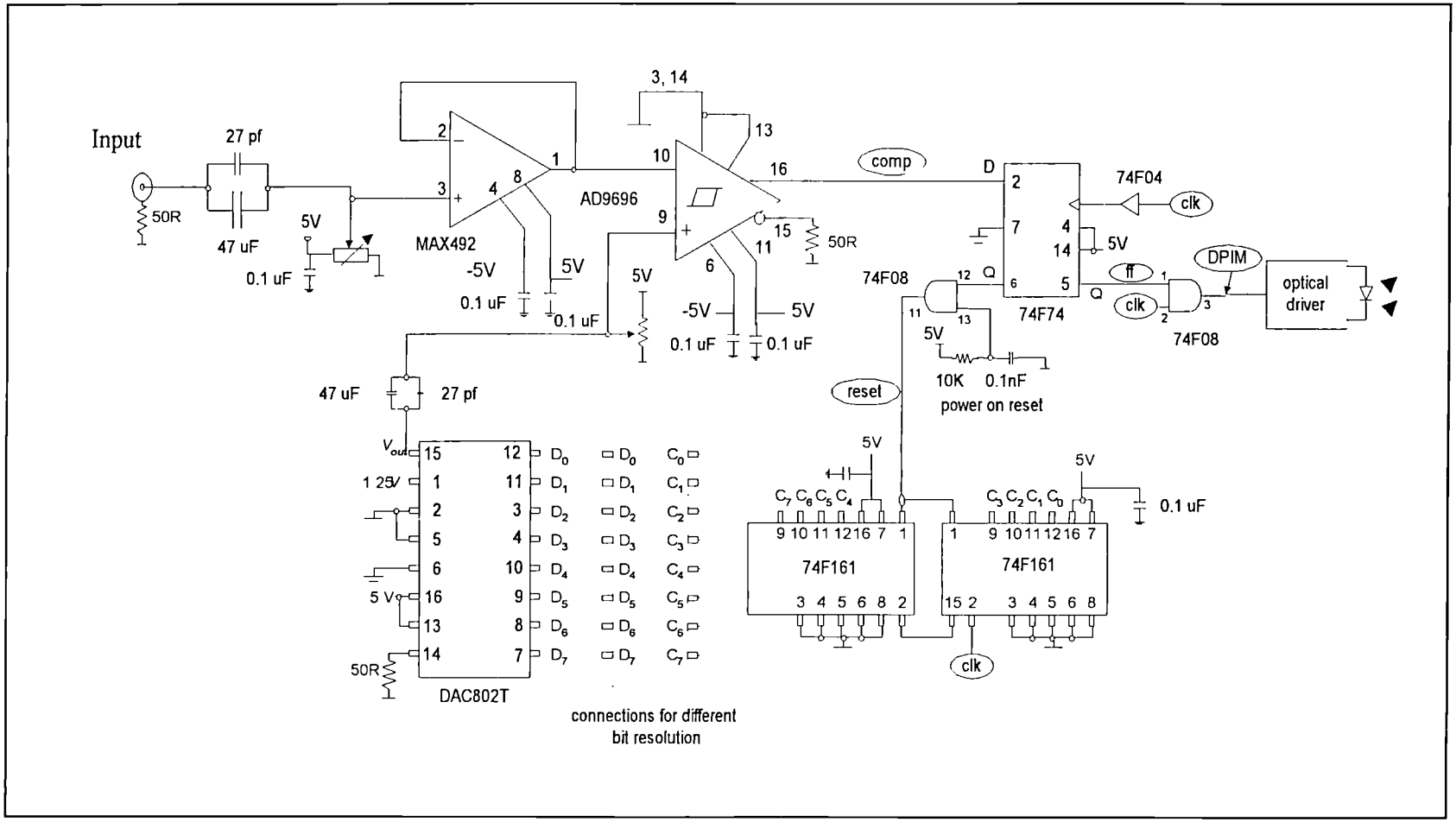

Fig. 7.1 DPIM modulator circuitry.

The DAC input and cascaded counter output ports are represented by D_0, D_1 ....D_7 and C_0, C_1, .. .C_7, respectively. The system bit resolution is determined by how these ports are connected together. For M bit resolution connections can be made as given by,

$$C_i \rightarrow D_{(8-M+i)}, \qquad i \in 0,1,2,.....7 \tag{7.1}$$

e.g. for $M = 4$, the connections should be as: C_0-D_4, C_1-D_5, C_2-D_6, C_3-D_7.

7.2.1.1 Circuit operation

The counters count up at the slot rate and are enabled 1 μs after the modulator is turned on. This time delay is determined by the power on reset timing network. The DAC converts the combined counter output to a voltage level that is determined by its transfer characteristics. The output of the DAC which is a discrete ramp, see Fig. 7.2, is then compared with the level shifted modulating signal at the comparator.

When the DAC output is just above the level shifted modulating signal the comparator output becomes high and its leading edge is used as a timing reference, see Fig. 7.3(a). The comparator output (comp) is fed into the flip-flop which is clocked by the inverted system clock (clck).

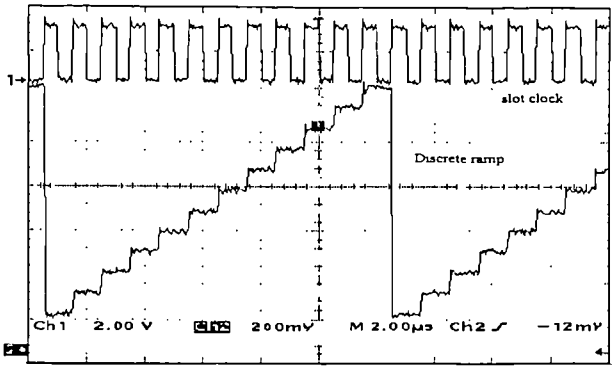

Fig. 7.2 DAC output variation with counter increments.

The inverted output of the flip-flop is used to reset the counters for 1 time slot duration during which the DAC and comparator outputs are set to zero, see Fig. 7.3(c), the non-inverted output of the flip-flop (Q) is then multiplied with the system clock to generate the desired DPIM pulse train. The demodulator operation is highlighted by the time events 1-5 in Fig. 7.3(a) and a-d in Fig. 7.3(c).

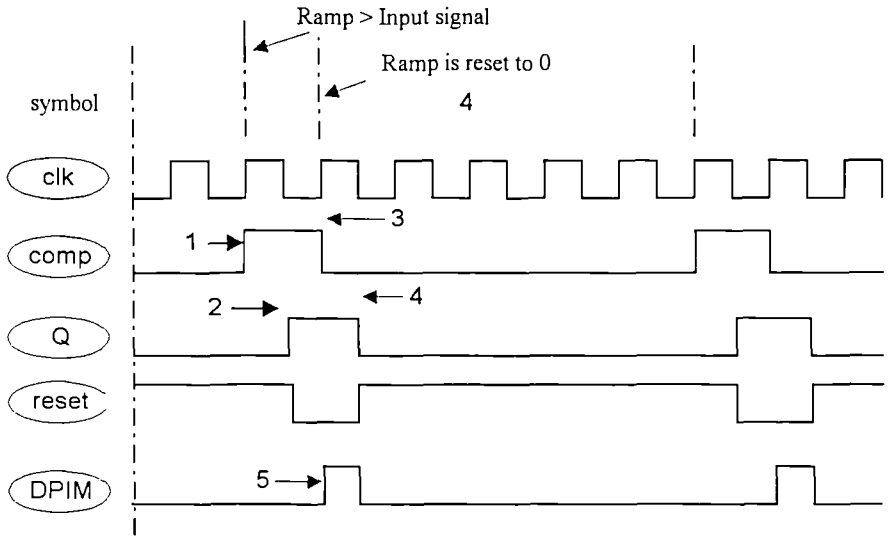

(a)

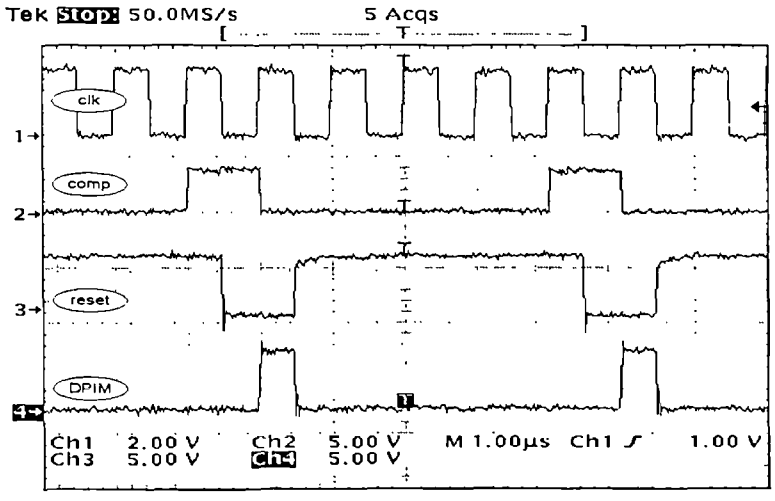

(b)

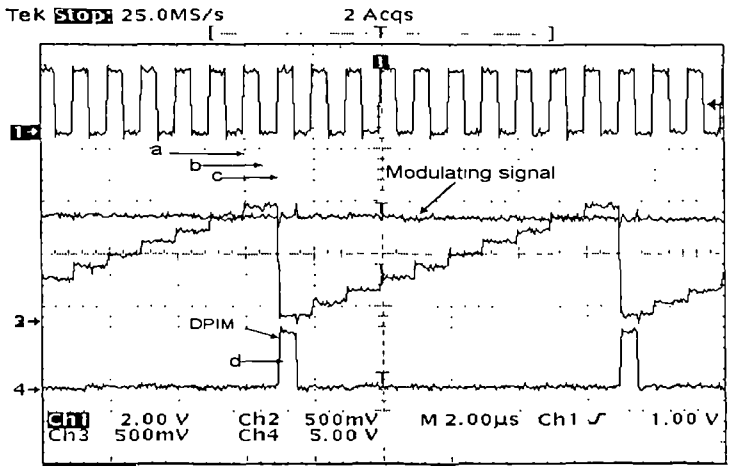

(c)

Fig. 7.3 Transmitter timing diagrams (a) expected, (b) & (c) observed.

Figure 7.3(a) shows that the comparator output status is fed into the flip-flop at the negative clock transition. By this time the DAC output is stable, thus the noise effect at the comparator decision time is minimum. DPIM pulse widths are half of system clock and always inphase with the positive clock edge.

7.3 Optical Link

Since the data rate is reasonably low, off the shelf components were used for the optical link. The light source and the photo diode used were LED (at λ = 820 nm) and PIN photo diode, respectively. However, there is no reason why one should not use laser diode or APD (Avalanche photo diode).

7.3.1 Optical transmitter

One of the major advantage of pulse modulation techniques such as DPIM is that optical source is switched on for a very short duration of time and off for a relatively long period. This results in high peak power and low average power, thus increasing the life time of the optical source. One further advantage is that the number of transitions is reduced considerably compared to PCM, thus resulting in reduced jitter effect. Out of

many driver circuits proposed in literature, a series switching circuit based on common emitter transistor along with speed up capacitor was chosen as the optical source driver, see Fig. 7.4.

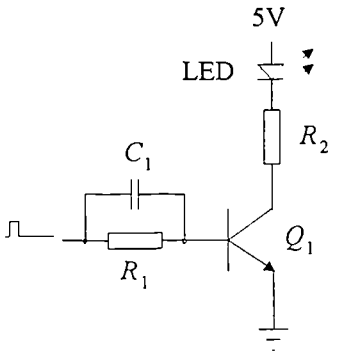

R_1 = 3k3, R_2 = 47 R, C_1 = 12 pF, Q1 = ZTX313

Fig. 7.4 Optical source driver.

Switching speed of this driver circuit is related to the slow charging and discharging of the transistor (Q1, NPN) junction capacitance, as well as the diode capacitance, which is effectively in parallel with high output impedance of the transistor.

7.3.2 Optical receiver

The optical receiver consists of three main subsystems, i.e. receiver front-end, decoder and clock extraction subsystems, see Fig. 5.1. The receiver front-end operation can further be divided into two: pre-processing and post-processing. The pre-processing sub-section consists of a PIN detector followed by a pre-amplifier and a post-amplifier. Since operating frequencies are well within the bandwidth of the components being used an equaliser is not included in the receiver. Post-processing sub-section is combination of pre-detection filter and the threshold detector.

In this work a transimpedance amplifier based around Darlington structure is used as the pre-amplifier, see Fig. 7.5. This type of receiver has low noise and wide

transmission bandwidth due to high current gain and high input impedance. *Aiki* showed that this configuration is superior in terms of stability, noise and bandwidth over well known common emitter-collector configuration [*Aiki*]. The pre-amplifier is followed by the post-amplifier which is a low noise, wide band and high gain amplifier (NE592), see Fig. 7.5.

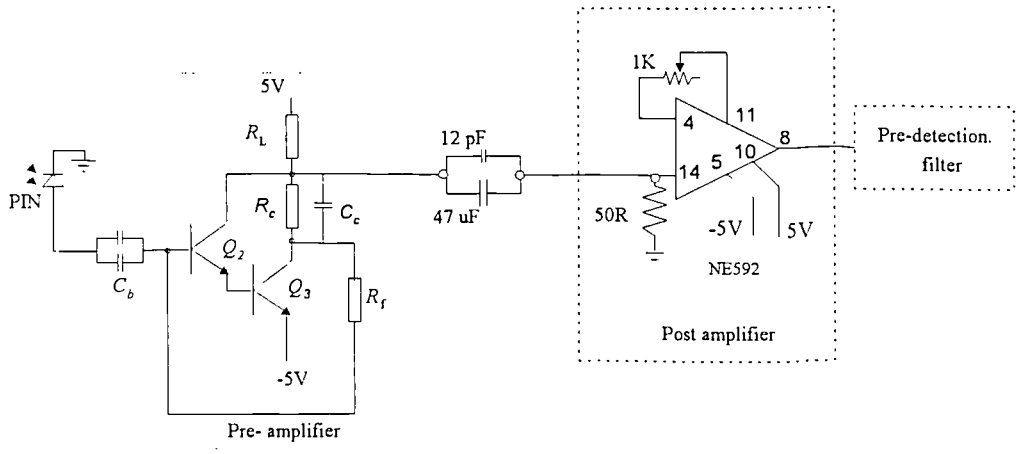

R_L = 330R, R_f = 3k3, R_c = 33 R, C_c = 12 pF, Q_2, Q_3 = ZTX313, C_b = 47 uF//12pF

Fig. 7.5 Optical receiver front-end.

The post-processing sub-section consists of a pre-detection filter and a threshold detector. There are many parameters involved in the DPIM system. Performance evaluation is carried out by keeping certain parameters constant while varying others. One of the parameters that required to be varied with the bit resolution is the system bandwidth. One way of achieving this is by restricting the pre-detection filter bandwidth. Pre-detection filter design is accomplished as given in appendix B. From this work the filter elements to support the bit resolutions of 4,5 and 6 are given in table 7.2.

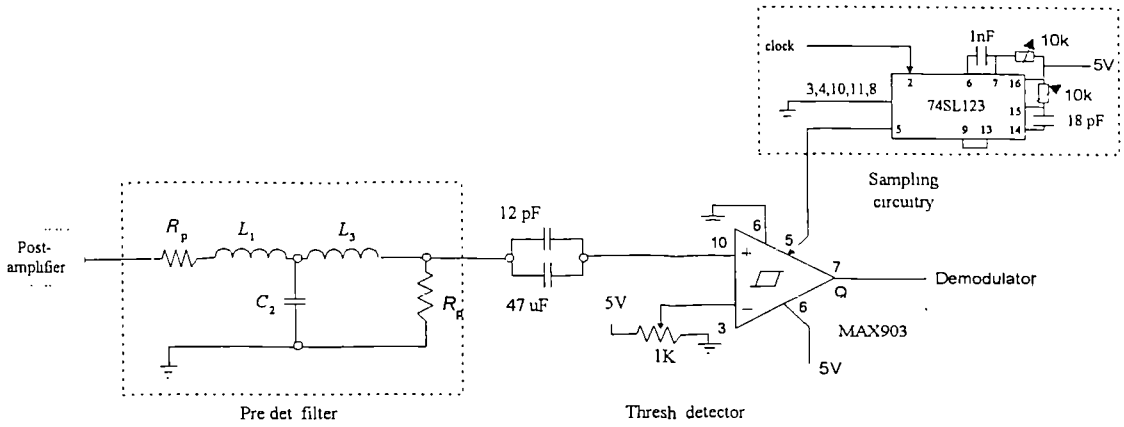

Fig. 7.6 Post processing circuitry.

M	R_p kΩ	L_1 μH	C_2 pF	L_3 μH
4	1	24.2	61.6	665.6
5	1	10	24.7	267
6	1	4.7	12	133

Table 7.2 Pre-detection filter elements for different bit resolutions.

Figure 7.7 shows the pre-detection filter response to an incoming pulse.

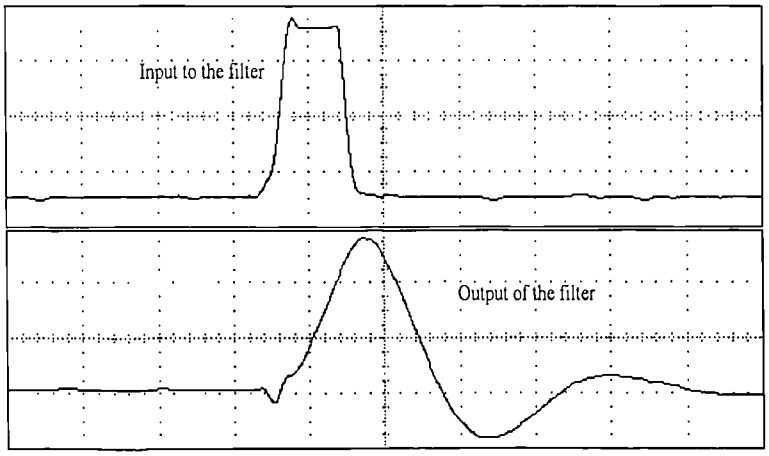

Fig. 7.7 Pre-detection filter response to a pulse.

The pre-detection filter integrates the input pulse energy thus resulting in a maximum peak amplitude at the falling edge. The noise is suppressed by the filter as illustrated in Fig. 7.8.

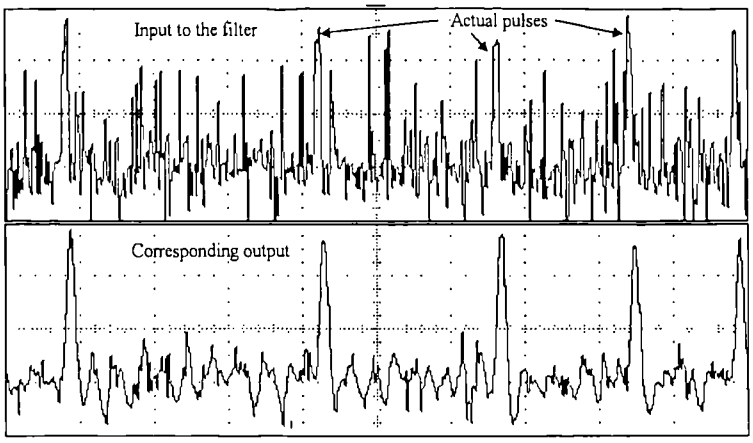

Fig. 7.8 Pre-detection filter response in the presence of noise.

The threshold detector recovers the transmitted pulse stream from the noise contaminated received signal and provides an interface between the analogue part of the receiver and the demodulator. At the threshold detector input, the anisochronous nature of the pulse stream can result in baseline wonder. To minimise this effect, the pre-detection filter output is AC coupled and the threshold level is allowed to vary accordingly, see Fig. 7.6. As shown in this figure the optimal sampling points are achieved by adjusting the positions of the sampling pulses using the IC 74LS123. Sampling point detection can be omitted if the receiver is operated well above the *SNR* threshold which is about 15 dB, see chapter 6.

7.4 Demodulator

One of the advantages of DPIM scheme over DPPM is the simplified decoder structure. Each received pulse acts as the frame initiating pulse, and decoding is simply accomplished by counting the number of time slots within two consecutive pulses. The

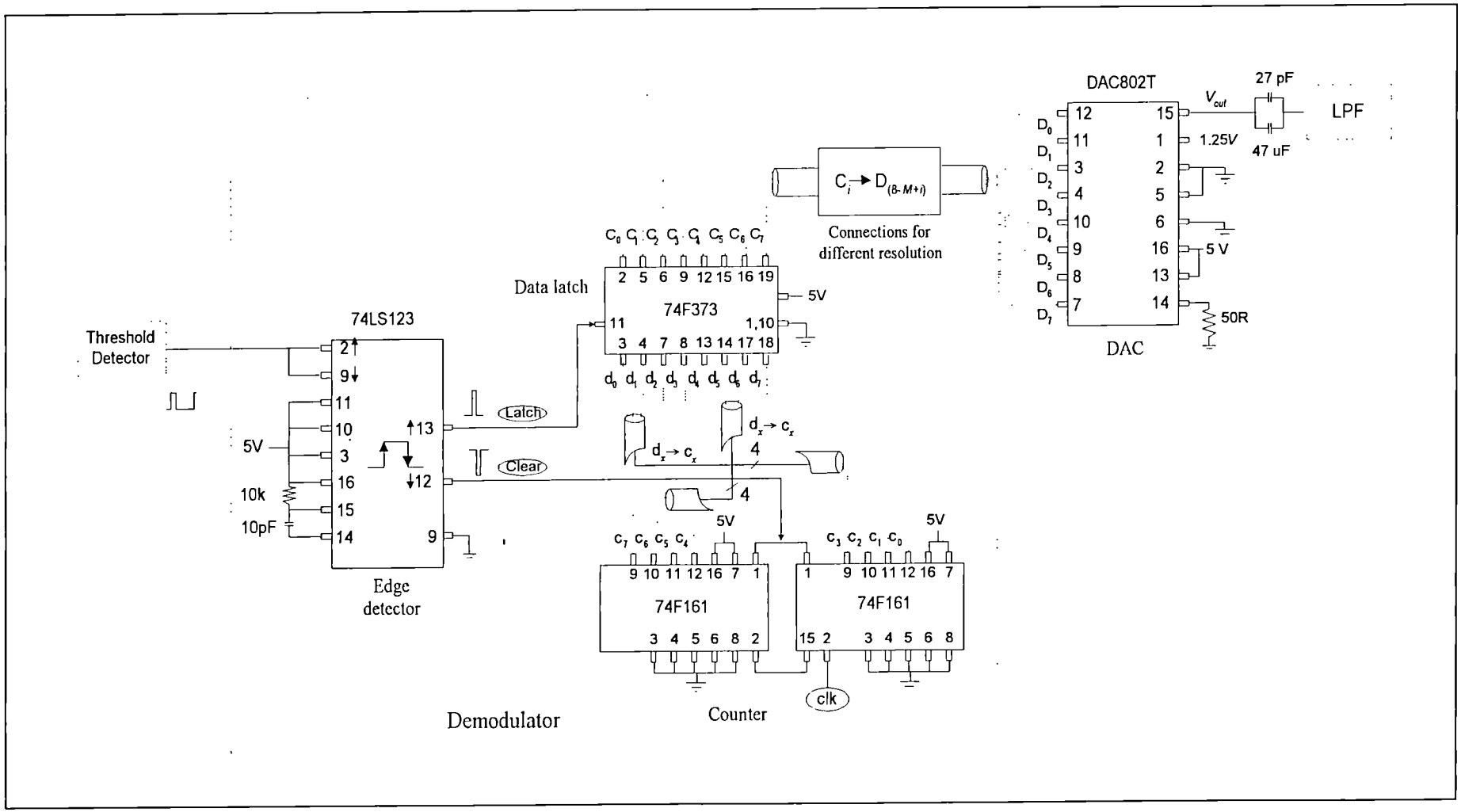

Fig. 7.9 Demodulator circuitry.

demodulator consists of an edge detector (74LS123) , a re-configurable 8 bit binary counter (2 cascaded 74F161) and an 8 bit latch (74F373), see Fig. 7.9.

Two 4 bit counters are cascaded such that they can be reconfigured to operate at bit resolutions 2-8 corresponding to the transmitter. Clock input to the counters are from the synchronisation sub-system (see section 7.5). Data in the counters is latched into the 8 bit data-latch at the leading edge of each DPIM pulse and the counters are initialised to zero at the trailing edge. Decoder operation is shown in Fig. 7.10(a) where time event 1 shows the symbols being latched while event 2 shows the counters being reset. Decoding operation is performed with minimal component count. Figure 7.10(b) shows the measured waveforms corresponding to Fig. 7.10(a).

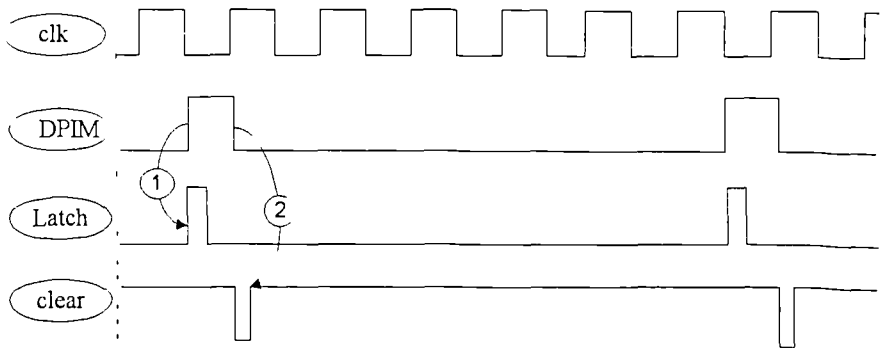

(a)

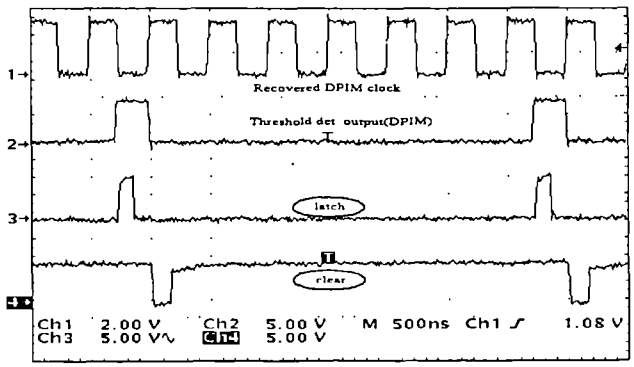

(b)

Fig. 7.10 DPIM demodulator timing (a) expected and (b) measured.

The demodulator output is the input to the DAC. The DAC resolution is set by connecting the combined counter outputs with the DAC inputs, as given by Eqn. 7.1. The DAC conversion range is set at 1.2 V as at the transmitter. Figure 7.11 shows the receiver DAC output when transmitting a ramp waveform, together with the latch and clear signals. Finally, the transmitted signal is regenerated by passing it through a low pass filter. See appendix D for the complete receiver circuit diagram.

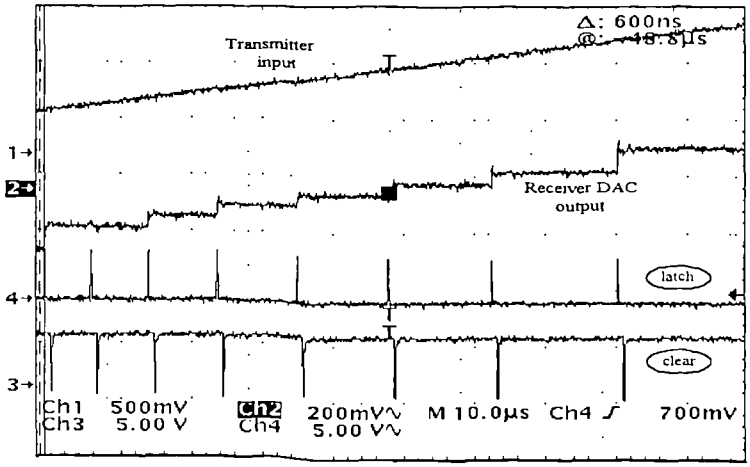

Fig. 7.11 DAC output with decoded symbols.

7.5 Synchroniser Sub-system

A monolithic PLL NE564 [*Philips*] with TTL compatible inputs capable of operating up to frequencies of 50 MHz is used for clock extraction, see Fig. 7.12. The VCO frequency is set by the capacitor network placed between pin 12 and 13. External VCO frequency setting capacitor values ($c_{12\text{-}13}$) are calculated by [*Philips*],

$$c_{12-13} \cong \frac{1}{22 f_s R_c} - c_s \tag{7.2}$$

where f_s is the slot frequency, R_c is the internal resistor, and c_s is the stray capacitance.

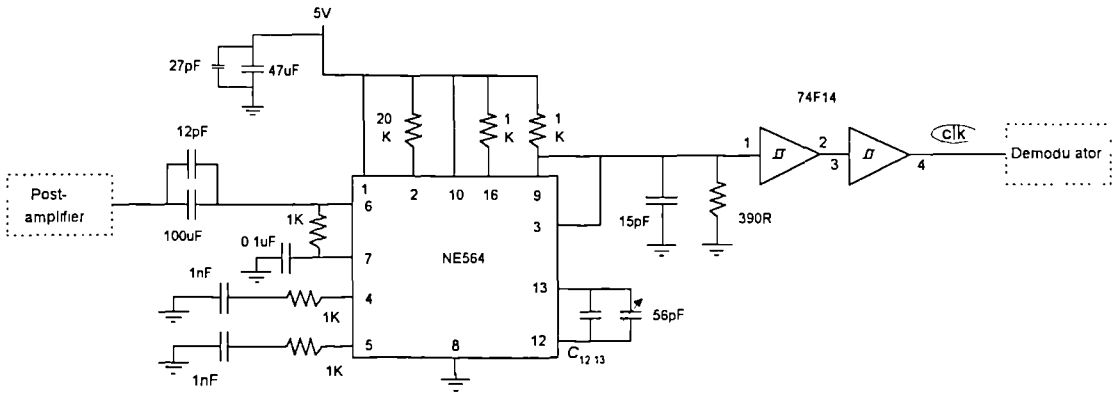

Fig. 7.12 PLL clock extraction circuitry.

The value of the capacitor $c_{12\text{-}13}$ for different slot frequencies are given in table 7.3.

f_s kbps	150	270	510	990	1950	3780
$c_{12\text{-}13}$ pF	3000	1680	891	459	233	120

Table 7.3 PLL timing capacitor for various slot rates.

Stray capacitance was taken to be negligible in the calculations. A variable capacitor of 56 pF was used in parallel with $c_{12\text{-}13}$ for fine tuning. The PLL was tested with a rectangular pulse stream for slot rates corresponding to bit resolutions 4, 5 and 6. At these resolutions the PLL was found to be extremely stable for input signal amplitude as low as 100 mV. The complete link was operated at the above bit resolutions and corresponding slot rates. At slot rates of 510, 990, 1950 kbps, the measured PLL lock ranges were 14, 18 and 45 kHz, respectively. At all three bit resolutions and wide modulating ranges, the PLL was found to be highly stable. Furthermore, it was observed that by reducing the resistance connected at pin 2, lock ranges can be reduced down to few hertz (<10 Hz). Figure 7.13 shows the waveforms corresponding to the synchronised PLL for the 6 bit configuration. In this figure the top trace shows the

received pulse stream, the middle trace the transmitter system clock and the bottom trace the PLL output or the recovered clock.

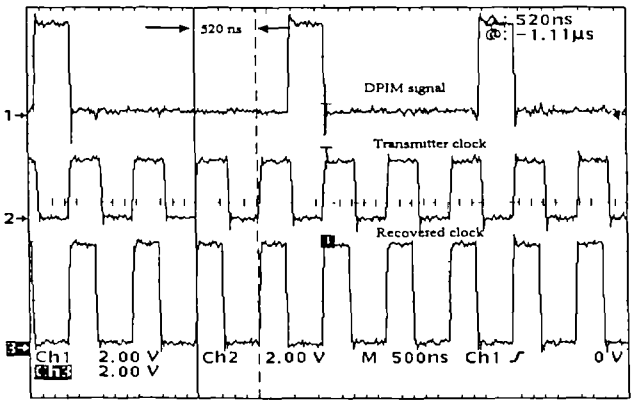

Fig. 7.13 Transmitted and recovered clock waveforms for $M = 6$ at 1.92 MHz.

7.6 Receiver Final Stage - Low Pass Filter

It is essential that the filter should have a flat amplitude response and a linear phase response within the pass band for minimum distortion. The filter used is a 7^{th} order Butterworth low pass filter which has ripple free response in both pass-band and the stop band. The actual values of the filter components were calculated using standard tabulated tables [*Williams*] scaled to the cut off frequency of 15 kHz. Figure 7.14 shows the proposed filter for recovering the information embedded in the signal at the DAC output.

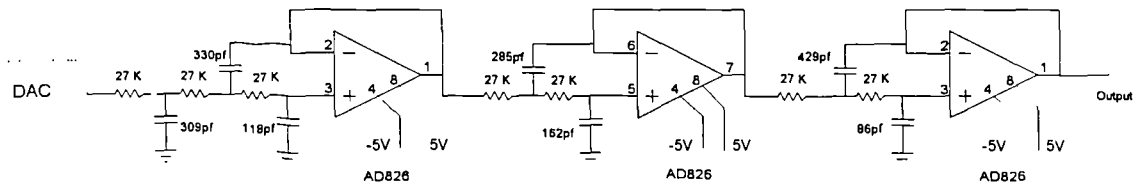

Fig. 7.14 Low pass filter.

The frequency response of the filter is shown in Fig. 7.15, showing the cut-off frequency at 15 kHz.

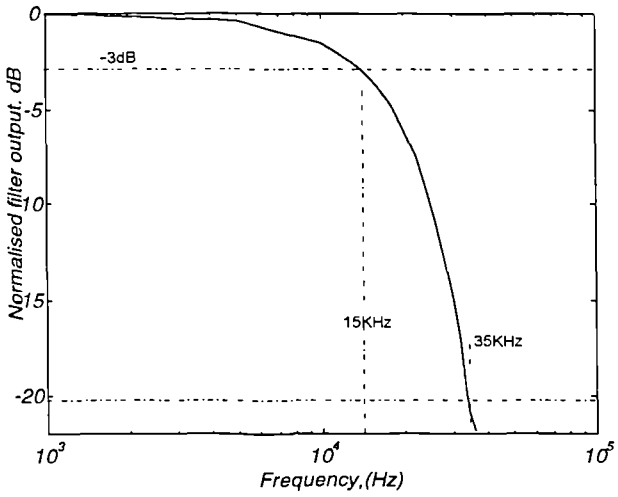

Fig. 7.15 Receiver final stage low pass filter response.

Figure 7.16 shows the filter response for a 4 kHz single tone sinusoid input signal. The upper and lower traces show the input and output spectrums, respectively. This shows that filter does not introduce harmonic distortions.

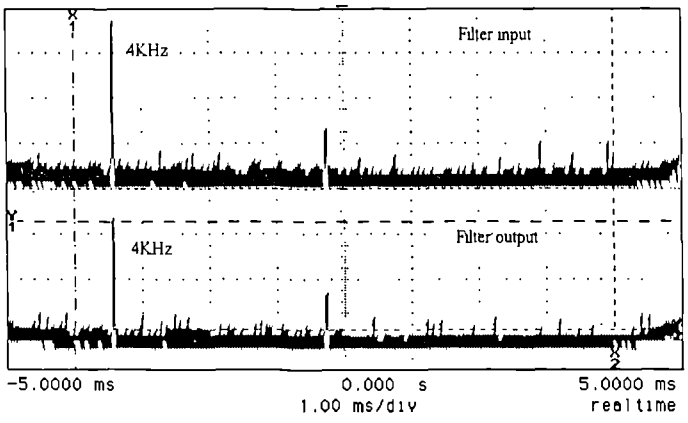

Fig. 7.16 Filter response within the past band.

7.7 Summary

In this chapter, hardware implementation of DPIM transmission link is presented. The operation of each module together with their corresponding measured waveforms are also given.

Chapter Eight

Results

8.1 Introduction

A detailed system overview was given in chapter 5, the spectral profile was modelled and the results were verified experimentally in chapter 4, the receiver performance was analysed and expressions for probability of error and *SNR* were given in chapter 6. In this chapter the complete system performance is verified by testing the system prototype described in chapter 7. The system is used for transmission of analogue signals. Results for spectral profile, *SNR* and harmonic distortion are presented. The BER measurements are also given for digital information transmission.

8.2 Variation of the Slot Component with the Modulation Index

In chapter 4 DPIM spectra were successfully modelled and shown to agree with the measured results. In this analysis the main emphasis was placed on the variation of the spectral profile with the pulse shapes. However, Eqn. 4.17, revealed that spectral profile depends on the symbol sequence or in other words the frame structure. DPIM pulse density variation for momentarily varying analogue signals such as a single tone sinusoidal signal is illustrated in Fig. 2.3, showing high and low densities for low and

high amplitudes, respectively. It was also shown in chapter 4 (Fig. 4.14) that there exists harmonic components of the modulation signal around the slot frequency. Hence, the slot synchronisation is affected by the stability of the slot component and its relative amplitudes with the adjacent sidebands. This relative amplitude variation can be observed by obtaining the spectra with respect to the modulation index. A single tone sinusoidal signal of frequency 10 kHz and amplitude of 1.2 $V_{p\text{-}p}$ corresponds to modulation index of 1 was used as the input signal. For bit resolutions of 4, 5 and 6 the position of the slot component and the power difference were obtained. The position of the slot component is stable for all the modulation indices, but its relative amplitude difference with the adjacent sideband component vary as shown on Fig. 8.1

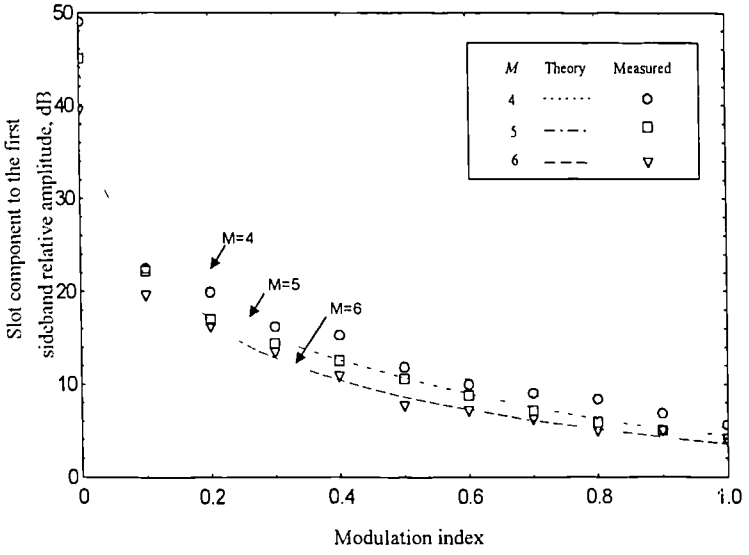

Fig. 8.1 Variation of the relative slot component with the modulation index.

In Fig. 8.1 both theoretical and practical results are just shown for the first sideband. At low modulation indices (< 20 %) the slot component is more prominent than the first sideband. As the modulation index increases, this prominence is lost as the relative amplitude between the slot component and sideband component is reduced. At modulation index of 1 this difference is only 5 dB, which is still adequate enough for a properly tuned PLL to lock onto. This difference is further sensitive to the bit

resolution, increasing by 1 dB/bit. In the absence of the input signal the slot component is distinct and the margin is at its highest, and the receiver can still be synchronised with the transmitter.

8.3 *SNR* Performance

Output *SNR* and system linearity are the crucial parameters that indicate the performance potential of the modulation scheme for analogue systems. For electrical system, *SNR* is dependant on the *CNR* at the threshold detector whereas for optical systems, *SNR* performance is measured against received optical power. Figure 8.2 shows the experiment arrangement for the *SNR* and system linearity measurements.

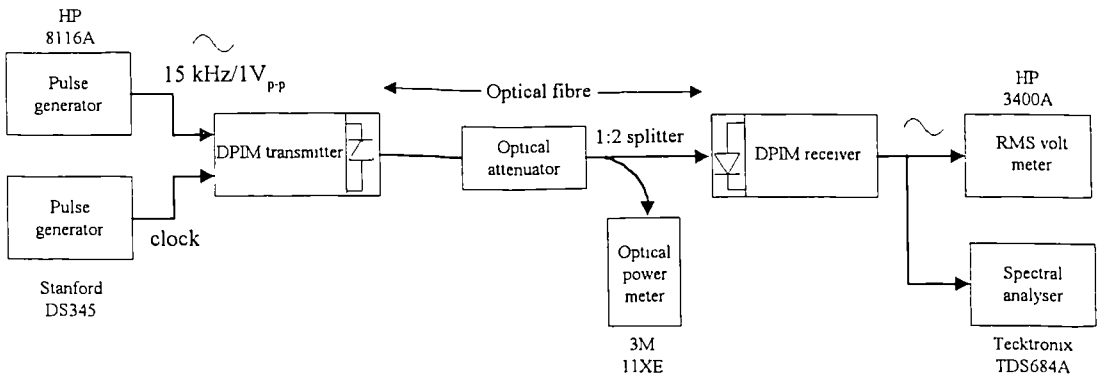

Fig. 8.2 Experiment arrangement for *SNR* measurements.

Transmitter LED couples -28.8 dB into the multimode graded index fibre (62.5/125 μm) of 1m length. An optical attenuator is used to control the optical power level falling at the receiver. The signal is passed through a 1-to-2 optical fibre splitter and the received optical power is monitored by the optical power meter. Various parameters of the optical receiver relevant for sensitivity measurements, are shown in table 8.1.

Receiver parameters		Value
Photo diode resposivity	R	0.6 A/W
Mean avalanche gain	G	1
Receiver equivalent noise current		2.5 pA/√Hz
Photo diode dark current @5V	I_d	1 nA
Load resistance	R_L	680Ω
Operating temperature	T	300 kΩ

Table 8.1 Optical receiver parameters.

In theoretical analysis receiver equivalent noise current is taken to be 2.5 pA/√Hz. Ideally this figure needs to be worked out from Eqn. 5.7. But this requires extensive analysis of the transistor small signal model, which is a tedious task on its own right. Hence, the approximated figure based on analysis given in *Aiki*'s [*Aiki*] work is used. Furthermore, in receiver implementation low noise transistors were used and therefore the noise would be lower than that given in table 8.1. Comparing theoretical with measured results, (as in Fig. 8.3) indicate that this approximation is not too far out of the actual noise figure, as the difference is about 1 dB. The optical receiver tends to saturate above a received optical power level of -35 dBm, but this is not a problem as pulse stream is not intensity modulated.

SNR performance of the output signal was measured using the true RMS volt meter in two steps: (1) measuring signal plus noise, (2) switching the signal off and measuring the noise alone, and making the appropriate subtraction and division. In section 6.7 it was shown that above the DPIM noise threshold level *SNR* is effected only by the quantisation noise, or the bit resolution.

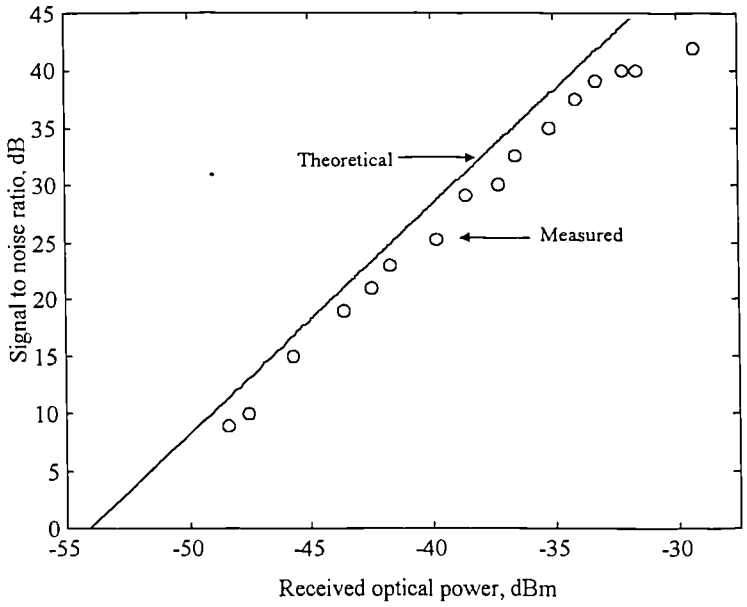

Fig. 8.3 Receiver performance.

Figure 8.4 shows the predicted and measured results for *SNR* versus received optical power for different bit resolutions. The input signal amplitude of 1 $V_{p\text{-}p}$ and frequency of 15 kHz were used.

Above the noise threshold level (≈ -47 dBm) the results agree very closely. However, below the threshold level the measured results show a sharp fall off within 1 dB. This drop is shown by the dotted line in Fig. 8.4.

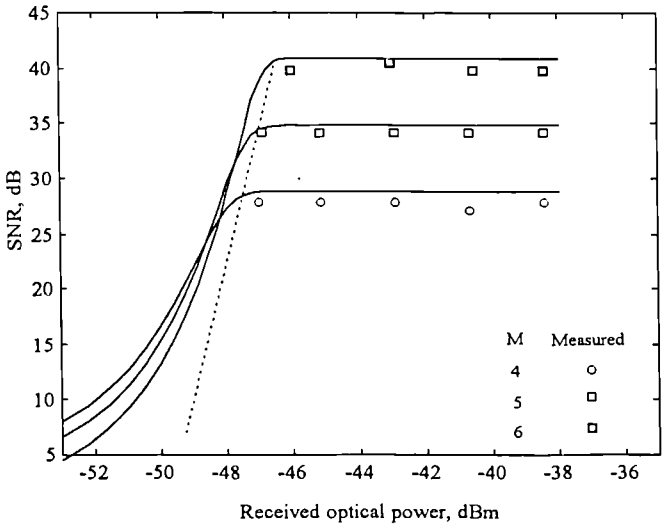

Fig. 8.4 *SNR* Vs. received optical power for different bit resolutions.

For high power the results are within 1 dB of the predicted while for lower power (below the threshold) the difference is about 3 dB. The sharp roll off is due to the presence of error signals in the bit stream thus severely distorting the frame structure. For every 1 bit error, the anisochronous frame nature of DPIM results in two frames being erroneous. Therefore, DPIM system is best operated above the noise threshold level. The *SNR* performance improves by about 6 dB as the bit resolution is increased by one. These results are in agreement with the predicted values given in chapter 6.

8.4 System Linearity

Harmonic distortion associated with the output signal can be taken as a measure of the overall system linearity. In analogue PTM schemes linearity of the ramp waveforms play a major role in this regard, whereas in digital schemes harmonic distortion is mainly caused by the modulation effect. In order to evaluate the overall system linearity, harmonic distortion measurements were carried out at the system output. In analogue signals harmonic distortion is measured in terms of the second and third harmonic terms with respect to the fundamental. As an example, assume that for a sinusoidal modulating signal of $e_i(t)$ the system output is given by $e_0(t)$. The system input and output characteristics can be approximated by,

$$e_0(t) = a_1 e_i(t) + a_2 e_i^2(t) + a_3 e_i^3(t) \tag{8.1}$$

where a_1, a_2 and a_3 are distortion coefficients, that is related to the system.

Taking modulating signal $e_i(t) = V_m \cos \omega_m t$, V_m amplitude and ω_m angular frequency Eqn. 8.1 can be written as,

$$e_0(t) = \frac{a_2}{2} V_m^2 + \left(a_1 V_m + \frac{3a_3}{4} V_m^3 \right) \cos \omega t + \frac{a_2}{2} V_m^2 \cos 2\omega t + \frac{a_3}{4} V_m^3 \cos 3\omega t \tag{8.2}$$

The first term in Eqn. 8.2 shows the DC term, second term the fundamental frequency component, third and fourth terms are second and third harmonic components, respectively. Ideally the latter two components should not exist in the output. However, in a real system the output signal does contain certain level of distortion. In most cases the level of distortion is given in terms of second and third harmonic distortions represented by HD_2 and HD_3, respectively.

$$HD_2 = 20\log_{10}\left(\frac{2a_2V_m}{4a_1 + 3a_3V_m^2}\right), \qquad HD_3 = 20\log_{10}\left(\frac{a_3V_m^2}{4a_1 + 3a_3V_m^2}\right) \quad \text{dB} \tag{8.3}$$

In Eqn. 8.3 harmonic distortions are function of parameters which corresponds to the system operation. Therefore a numerical figure may not be feasible because of parameters being dependant on modulation, transmission and demodulation. Distortions can only be graphically represented and a relationship between the coefficients a_1, a_2 and a_3 can be approximated by graphical means. Second and third harmonic components are measured within the passband of the output and are normalised to the fundamental level. The results are shown for the system with bit resolutions of 4, 5 and 6, in Figs 8.5(a), 8.5(b) and 8.5(c), respectively. Slot frequency was selected at different bit resolutions for varying frequencies as from Eqn. 5.1

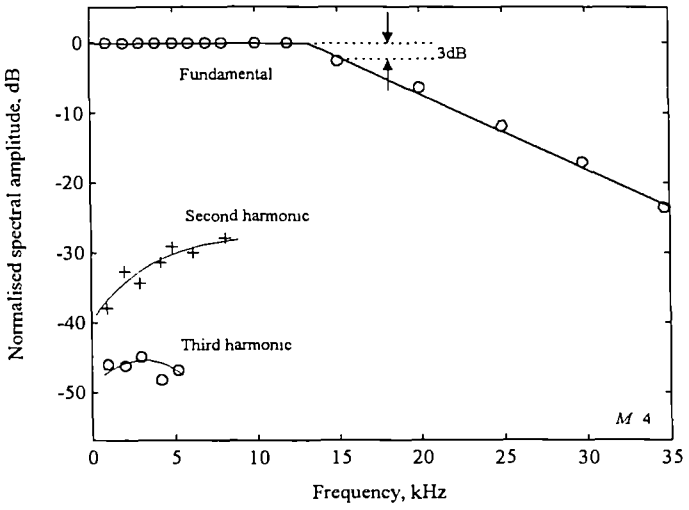

(a)

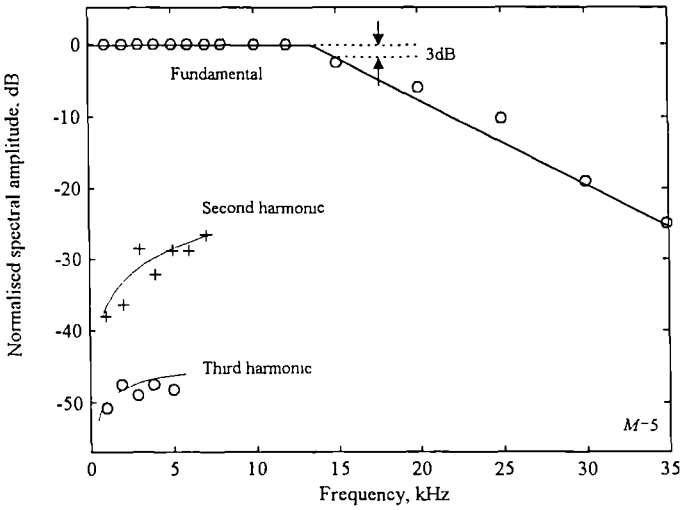

(b)

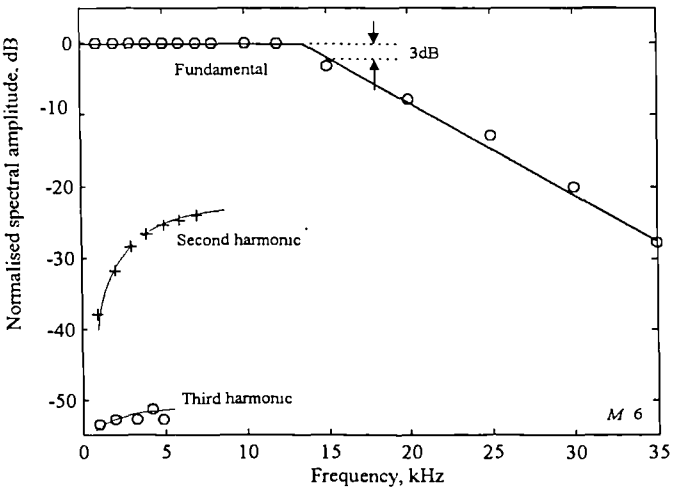

(c)

Fig. 8.5 Measured harmonic distortion profile for different bit resolution: (a) 4 bits, (b) 5 bit and (c) 6 bits.

From Figs. 8.5(a), (b) and (c), it can be seen that at low frequencies, the second harmonic distortion is about -40 dB in all three cases. However, as the modulation frequency increases the distortion level increases as a slowly varying exponential. For 4, 5 and 6 bit resolutions it reaches maximum level of -29 dB, -26 dB and -23 dB, respectively within the passband.

Third harmonic distortion within the pass band, for all systems, nearly have the same profile but different levels. Distortion of -53 dB is the lowest for the 6 bit system compared to -49 dB and -46 dB for 5 and 4 bit resolutions, respectively. In terms of second harmonic distortion, 6 bit system outperforms the other two. Under the same conditions system linearity is also observed qualitatively by observing the regenerated output waveforms for a ramp and a rectangular signals as shown in Figs. 8.6 and 8.7.

From Figs. 8.6(a)-(c), it can be observed that the 4 bit system generates a more linear ramp signal than the other two as was predicted from harmonic distortion measurements. Performance of the 5 and 6 bit systems are indistinguishable.

Similar performance were also observed with rectangular signal as an input, see Fig. 8.7(a)-(c).

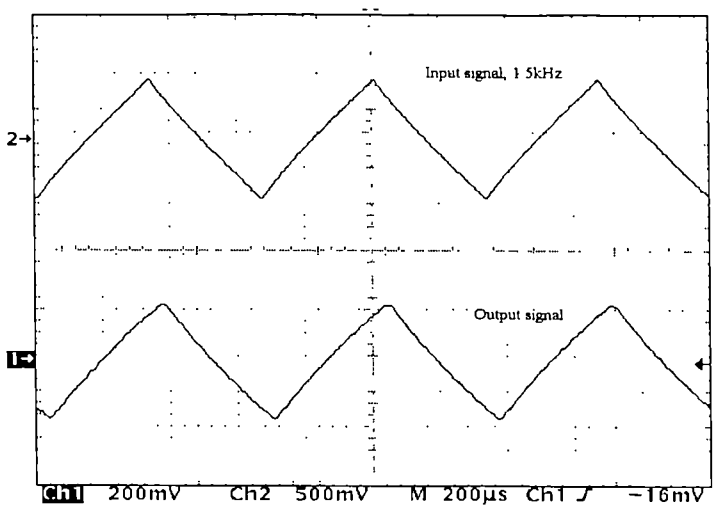

(a)

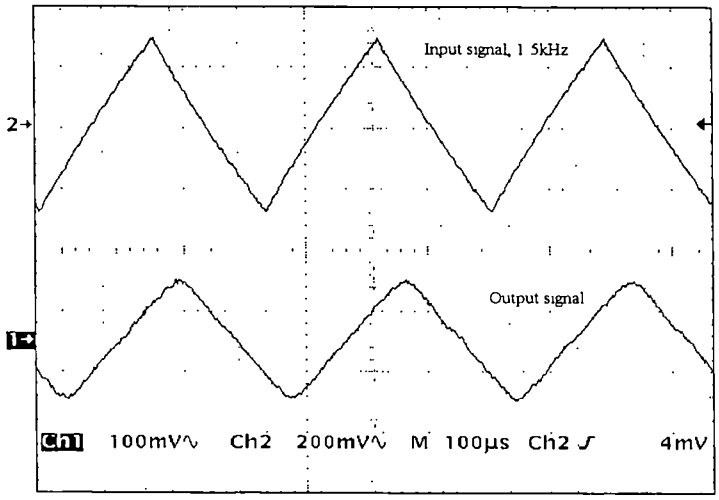

(b)

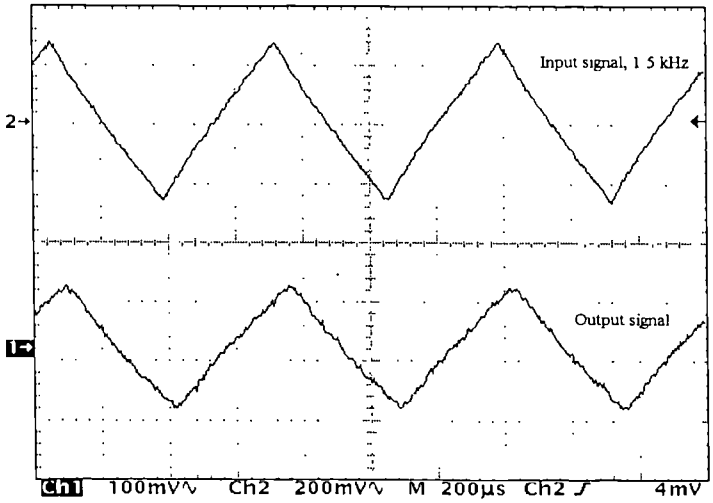

(c)

Fig. 8.6 System linearity response to a ramp signal of frequency 1.5 kHz for : (a) M=4, (b) M=5 and (c) M=6.

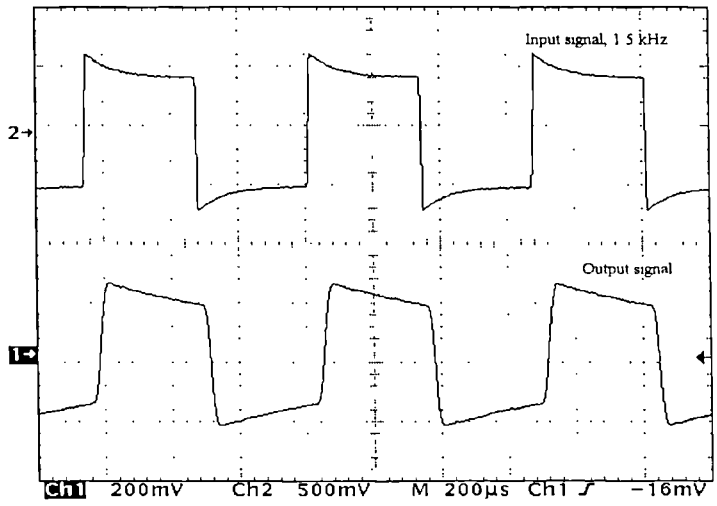

(a)

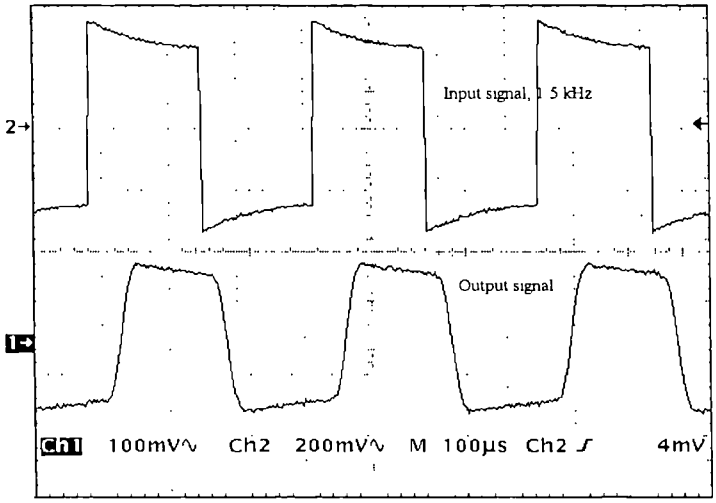

(b)

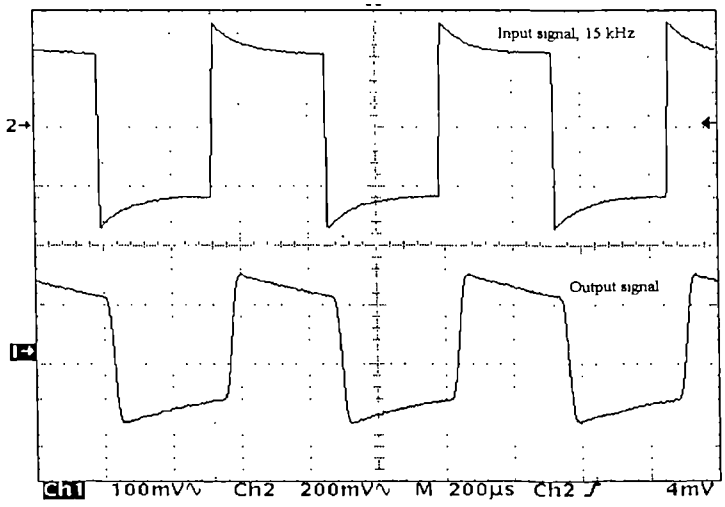

(c)

Fig. 8.7 System linearity response to a rectangular signal of frequency 1.5 kHz for: (a) $M = 4$, (b) $M = 5$ and (c) $M = 6$.

The variation of the harmonic distortion with the modulation index is also an important parameter for analogue signal transmission. Second and third harmonic distortion were investigated for modulating signal of 5 kHz over a full range of modulation indices, see Fig. 8.8.

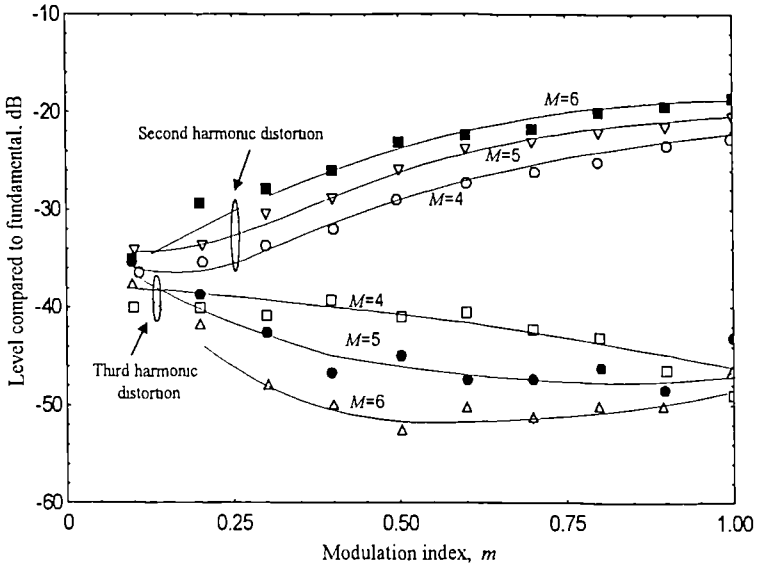

Fig. 8.8 Harmonic distortion Vs. modulation index for different bit resolutions.

Second harmonic distortion shows similar variation in all three systems. At low modulation index (10 %) the second harmonic distortion is about -35 dB for all bit resolutions. The distortion increases as a slowly increasing exponential by about 10 dB for the full range of the modulation indices. Throughout this full range, the second harmonic distortion increases by about 2 dB per 1 bit increase in the bit resolution. Third harmonic distortion is not as uniform as the second harmonic distortion. It is about -37 dB at low modulation index reducing to around -48 dB at 100 % modulation index. The profile also depends on the bit resolution, dropping to its lowest level of -50 dB at m = 50 % for 6 bit resolution. Figure 3.3 in chapter 3 illustrates the 2^{nd} and 3^{rd} harmonic distortion profile of analogue PIM. Comparing the Fig. 8.8 with 3.3 it can be seen that DPIM shows about 10 dB improvement in the 2^{nd} harmonic distortion in the

full range of modulation indices. Third harmonic distortion profile is different to analogue PIM. In DPIM third harmonic distortion reduces with the increase of the modulation index whereas in analogue PIM it increases. At modulation indices of 10 % and 95 %, analogue PIM showed 3 rd harmonic distortion of about -50 dB, and -8 dB, respectively, compared to -35 dB and -48 dB, respectively, in DPIM.

In chapter 4, it was shown that DPIM information capacity is twice as compared to PCM. Therefore, DPIM slot rate can be reduced by a factor of 0.5 and still can achieve the PCM information capacity. From Eqn. 5.1, DPIM slot frequency for modulation signal of 15 kHz at bit resolutions of 4,5 and 6 are 510, 990 and 1950 kHz, respectively, which can be dropped to 255, 495 and 975 kHz, respectively. Thus improving the bandwidth efficiency by a factor of 2, however, the drawback is the signal quality. At this bit resolutions and slot rates harmonic distortion levels are measured and are given in Fig. 8.9, for comparison.

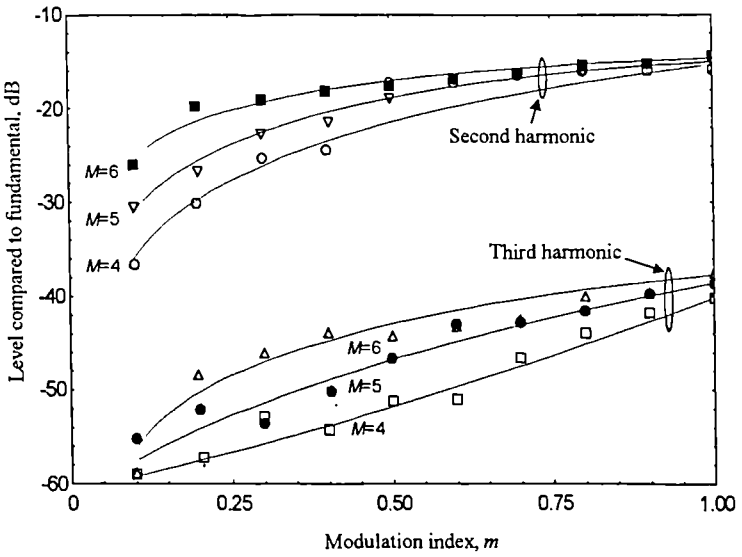

Fig. 8.9 Harmonic distortions Vs. modulation index at half the specified bit rates.

With the current slot rates the second harmonic levels increased and the third harmonic profile has completely changed compared to Fig. 8.8 with proper slot rates. At the top

end of the modulation index, all three systems show similar second harmonic distortion performance, i.e. about 16 dB below the fundamental. Whereas, the third harmonic distortion increases with the increase of the modulation index. The effect of harmonic distortion is best studied by observing the system response to a sinusoidal signal, see Figs. 8.10, for bit resolutions of 4,5 and 6. The input signal frequency and modulation index are 15 kHz and 80 %, respectively. In Figs. 8.10 and 8-11, special features provided by the Tektronix scope have been used to shift the output signal directly underneath the input signal for comparison purposes. Thus, the phase delay introduced by the final low pass filter is not shown.

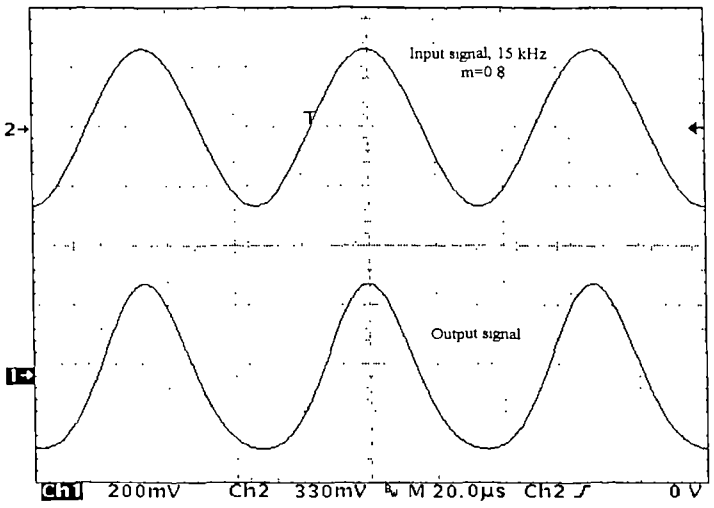

(a)

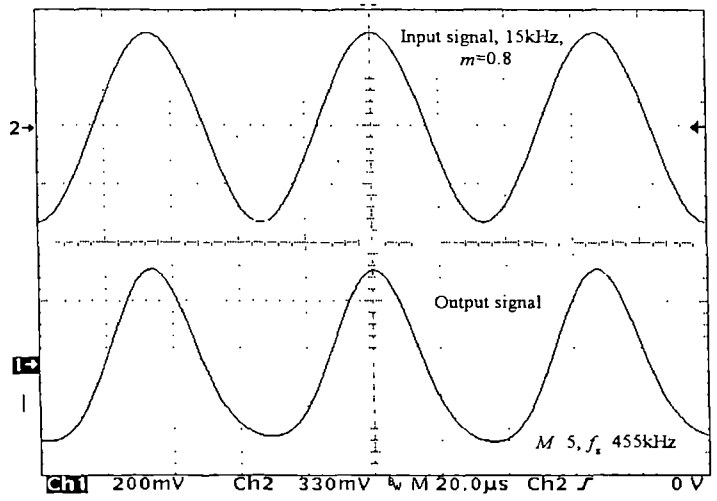

(b)

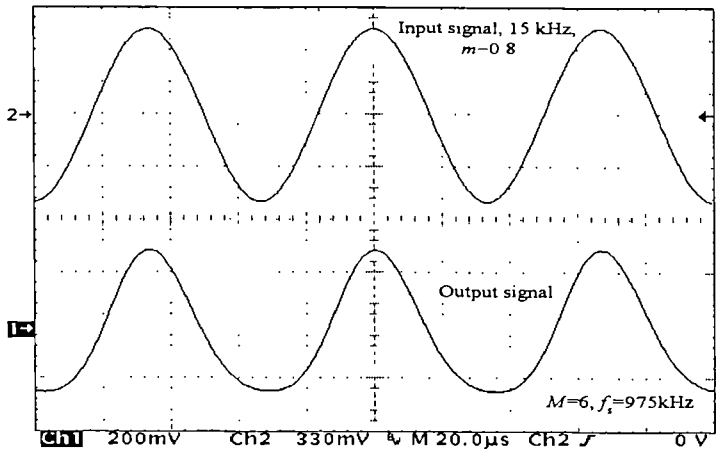

(c)

Fig. 8.10 System response at half the required slot rate for : (a) $M = 4, f_s = 255$ kHz, (b) $M = 5, f_s = 455$ kHz and (c) $M = 6, f_s = 975$ kHz.

Figure 8.10 reveals that reducing slot rate by half have had very little effect on the 4 bit system. Whereas the distinction is quite noticeable in the 5 and 6 bit systems.

For comparison the system slot frequencies were restored as given in Eqn. 5.1, and the responses were measured for the same conditions as above, see Fig. 8.11. It is evident that the quality of the signal has improved considerably compared to Fig. 8.10. But the main advantage in reducing the slot rate is that the same information capacity as that of PCM can be achieved with reduction in bandwidth.

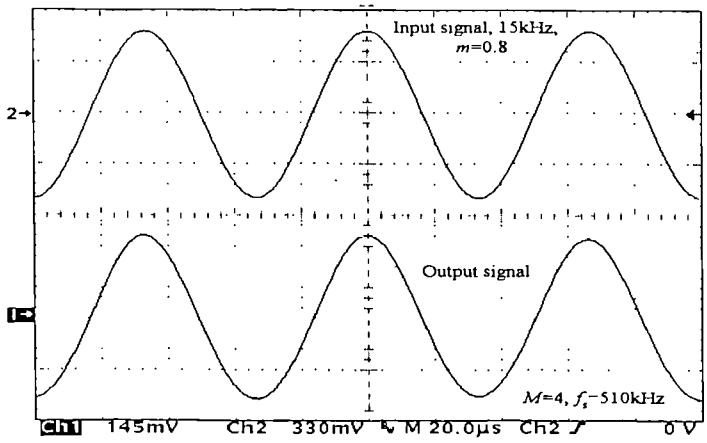

(a)

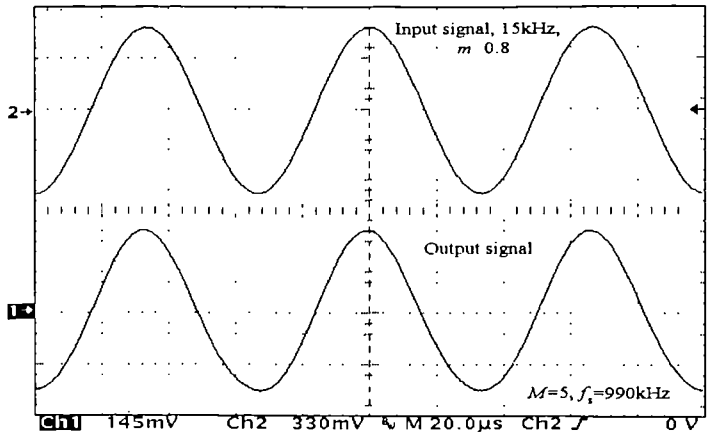

(b)

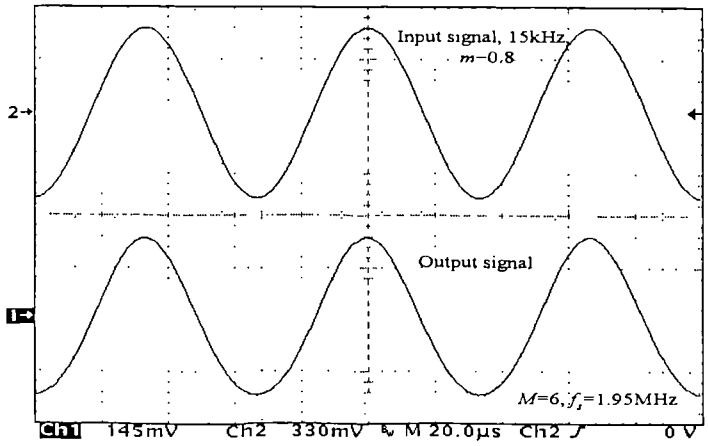

(c)

Fig. 8.11 System response for full slot rate for: (a) $M = 4, f_s = 510$ kHz, (b) $M = 5, f_s = 990$ kHz and (c) $M = 6, f_s = 1.95$ MHz.

8.5 Bit Error Rate (BER) Performance

In a digital communication systems, bit error rate performance is important. In chapter 6, the probability of bit error rate was presented by initially obtaining the probability of symbol error and then normalising it for the bit errors. However, in the practical system this is not possible due to the anisochronous nature of DPIM frames. Therefore, error measurements is carried out at bit level. This process involved comparing each transmitted time slot with the corresponding received slot. Consider a bit sequence at the transmitter of a transmission system being,

$\ldots\ldots a_{i-2}, a_{i-1}, a_i, a_{i+1}, a_{i+2}, \ldots\ldots\ldots$ with $a_i \in \{0,1\}$

and the corresponding sequence at the receiver as:

$\ldots\ldots b_{i-2}, b_{i-1}, b_i, b_{i+1}, b_{i+2}, \ldots\ldots\ldots$ with $b_i \in \{0,1\}$

Therefore bit error probability in the measurements is given as,

$$P_e = P(a_i \neq b_i) \approx \frac{\sum_i a_i \oplus b_i}{\sum_i 1}$$

where

$$a_i \oplus b_i = \begin{cases} 0; \text{ if } a_i = b_i : \text{no error} \\ 1; \text{ otherwise : error} \end{cases}$$

Figure 8.12(a) shows the block diagram representation of the circuit configuration that is adopted in BER measurements.

In Fig. 8.12, the received optical signal is passed through an optical attenuator before being processed by the receiver. An optical 1:2 splitter is used for power monitoring. The delayed electrical DPIM signal is compared with the output of the threshold detector and the resultant error pulses are sampled at point, where the *CNR* is at its highest value, see Fig. 8.12(b). The slot error signal represents the occurrences of the slot errors during the transmission. In Fig. 8.12(b), the threshold detector output signal shows three slot errors. The slot error signal correctly indicates these error slots. Initially the original DPIM signal is delayed by the correct time phase. This is done by running the link with no power attenuation and adjusting the transmitted signal and error free threshold detector outputs to be in line with each other.

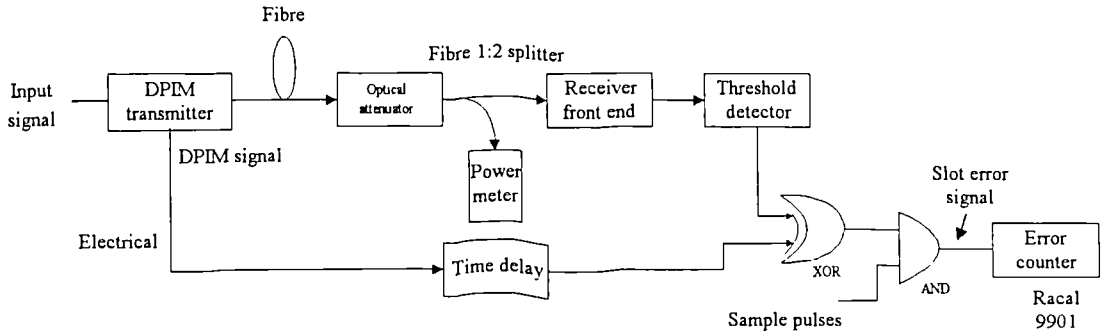

(a)

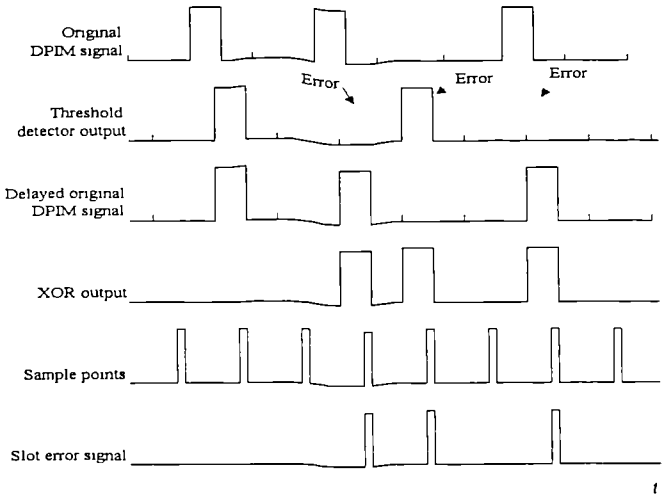

(b)

Fig. 8.12 BER (a) measurement set-up and (b) waveforms.

Chapter 6 gives a full detailed description of the probability of DPIM error which is affected by many parameters. In this section, the effect of threshold level and the bit resolution is investigated. A single tone sinusoidal signal at frequency of 15 kHz was used as an input signal and the slot frequencies were chosen according to Eqn. 5.1. Threshold levels were set at 0.3, 0.5 and 0.7 of the received pulse peak amplitude. By varying the attenuation level errors were read on the error counter. This measurements were carried out over three different threshold levels for bit resolutions of 4, 5 and 6, the results are shown in Figs. 8.13(a), (b) and (c), respectively.

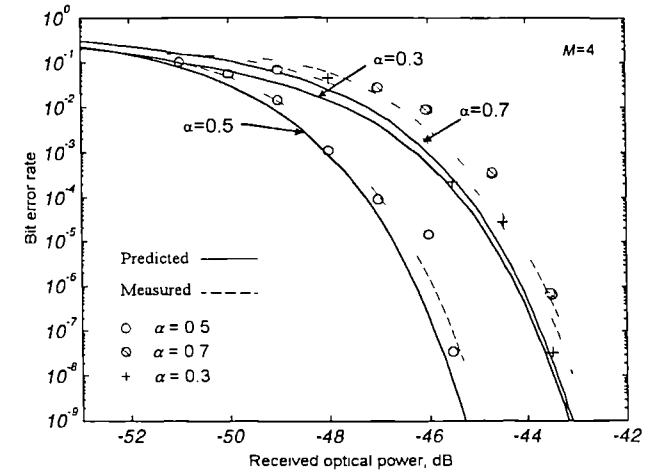

(a)

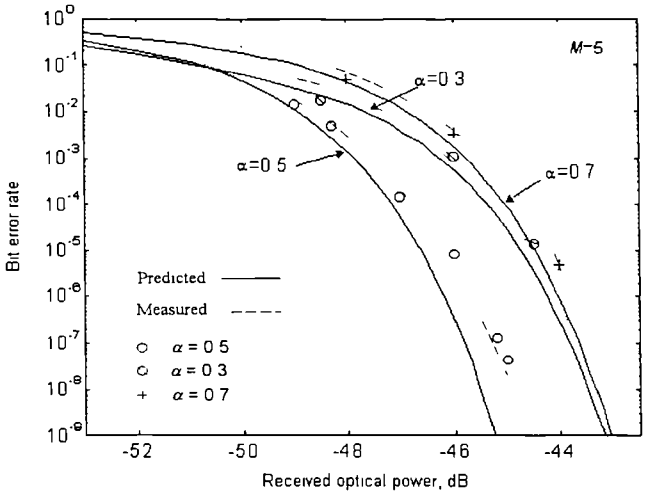

(b)

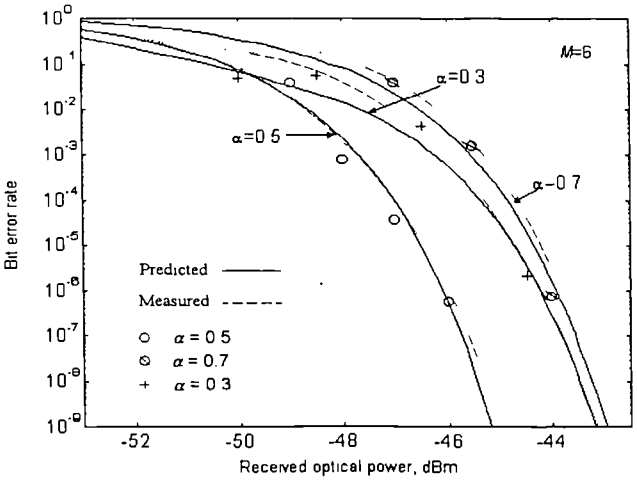

(c)

Fig. 8.13 Bit error rate versus received optical power for: (a) $M = 4$, (b) $M = 5$ and (c) $M = 6$.

In all the above three cases, the bit error rate is threshold level dependant as described in section 6.5.1. Furthermore, at the low received optical power levels (< -52 dBm) the error rate is sensitive to the bit resolution, i.e. error probability increases with the bit resolution. This is due to dominance of false alarm error with increased bit resolution.

A threshold level was found to be about -47 dBm, which corresponds to the *SNR* threshold given in section 8.2. A small change in the received power around this region gave a very high deviation in the number of slot errors. Thus, the measurements were repeated many times and the average value was taken. Error measurements in all three systems showed close agreement with the theoretical predictions, deviation was within 2 dBm at each bit resolution and corresponding threshold levels. From Figs 8.13, it can be seen that for a bit error rate of 10^{-9} at threshold level of 0.5 the required optical power is about -45.5 dBm, or in other words, a receiver sensitivity of -45.5 dBm. This is the optimum threshold level. For lower and higher levels the receiver sensitivity degrades further.

Chapter Nine

Conclusions

A comprehensive investigation of digital pulse interval modulation (PTM) scheme for optical fibre communication systems has been carried out. A comprehensive review of PTM techniques were given and in particular attention was drawn at digital PTM schemes. The DPIM scheme is presented as an alternate pulse time modulation technique for analogue and digital signal transmission. DPIM frame structure is proposed, code properties such as slot frequency variation with bit resolution, information capacity, average frame power, and spectral properties are presented. System performance is analysed in terms of *SNR* for analogue systems and probability of bit error for digital systems.

DPIM is an anisochronous digital PTM scheme. A frame in this scheme is sample dependant and is defined as the discrete time between two successive pulses. Each frame starts with a short duration pulse which performs the dual role of frame initiating and being the reference to the previous frame. To avoid inter-frame-interference in dispersive channels a small number of time slots can be included in each frame, but this

is at the expense of bandwidth. The frame lengths are information dependant and the sampling instant is determined by the frame initiating pulses. A variable length frame structure gives rise to an information capacity of twice that of the isochronous digital PTM schemes, such as PCM\DPPM. This suggests a reduction in the slot rate by a half while still achieving the same information capacity. For digital systems this may be possible but in the case of analogue systems this may result in aliasing particularly at higher modulation indices (i.e. > 50 %). DPIM is not able to support on-line data transmission due to the anisochronous frame nature but off line applications such as transmission data from buffer to another is feasible. Furthermore, information content in a frame can be increased by increasing the bit resolution, but the drawback is an exponential increase in the system bandwidth.

The sampling nature of the scheme give rise to a high pulse density corresponds to a low symbol levels or in analogue systems at low signal amplitudes. This has advantages in certain applications such as speech, where most of the intelligence is encoded in the low signal amplitudes. This means that increased pulse density corresponds to low signal amplitudes due to shortening of frames which will inevitably give rise to an increased average power in the pulse stream. This variation can result in base line wander at the receiver front-end, which will cause degradation of probability of error performance unless threshold detection is carefully performed. The average power fluctuation corresponding to a momentarily varying modulating signal can be minimised by reorganising the DPIM frame pattern by means of incorporating a lookup table in the modulating process for optimum performance. The lookup table vary depending on the application. However, this is only possible when the input to the modulator is a set of symbols. It is not feasible with the modulator and demodulator structures based around DACs, as in this work. This concept is briefly described in section 5.4.

DPIM spectral profile is dependant on the received pulse shape. For rectangular pulses, spectra consist of distinct slot component for pulse widths other than full slot. For full slot pulses, slot component and harmonics coincide with the zeros of the rectangular pulse transform and cancel out the distinct slot component which aids slot synchronisation. However, by non-linear processing such as differentiating received full slot pulses it is possible to regain the distinct slot component, but this is at the expense of additional circuitry.

A carefully tuned PLL circuit can successfully lock onto the slot frequency and its correct phase thus extracting the slot frequency for demodulation, which is made simpler as the DPIM has self synchronised frame structure. Therefore, the demodulation circuitry is simpler than PCM and DPPM. The slot component is dependant on various parameters such as bit resolution, slot width, random nature of the source symbols and the modulation index. An increase in bit resolution reduces the slot component by -2.5 dB per 1 bit increase. Thus, while high bit resolution increases the information content in a frame, it also increases the constraint placed on the PLL circuitry. The slot component is at its highest for a pulse width of duty cycle of 50 %. For lower values, the slot component is lower and varies symmetrically above 0.5. Thus, half width rectangular pulses are the ideal pulse shape for the wide band case.

Periodicity in the information signal results in a set of side tones based around the slot frequency component. The amplitude of these components increases with the modulation index. At the modulation index of 100 %, the relative difference between these components and the slot frequency component is still about 5 dB thus, giving enough head room for a carefully designed PLL to lock onto. However, for an input signal of random nature, the relative slot component is highly distinct by about 15 dB.

Narrow-band channels inherently disperse transmitted rectangular pulses. Under these conditions received pulses can be assumed to have a Gaussian shape. For DPIM with Gaussian pulse the spectra do not show singularities at the slot frequency or its harmonics. Therefore, the PLL can be used in both narrow-band as well as wide-band channels for slot synchronisation, and its performance is not effected by the level of pulse dispersion.

Pulse processing before threshold detection at the receiver is important as DPIM pulses become extremely small at high slot rates. Pre-processing is performed in order to improve the rise time of the pulses and to restrict them within a time slot. This is done by means of sending the pulse stream through a pre-detection filter which is either a matched filter or a sub-optimum filter. A matched filter is designed so that the filter impulse response is matched to the incoming pulse shape. Suitable filter design strategy is described in appendix B. Filter bandwidth determines the amount of noise power passed through to the threshold detector as well as energy spill over to the adjacent slots. A higher filter bandwidth results in a low level of pulse spreading but at increased noise power.

DPIM system suffers from three main error sources namely: erasure, false alarm and wrong slot. All three error sources are sensitive to the threshold level, while the false alarm error is also sensitive to the filter time constant, and the wrong slot error to the relative bandwidth, bit resolution, slot duration and received pulse width. By decreasing the threshold level erasure error can be reduced, but the drawback is that the false alarm error increases as noise can cross the low level threshold. There is thus a trade off between erasure and false alarm. Wrong slot error is due to pulse spreading into the adjacent time slots. This can be reduced by providing more bandwidth and optimising

the receiver filter bandwidth. At low bit resolution, the probability of error performance is similar to PCM. Main error sources are erasure and false alarm. As the bit resolution increases, the slot becomes smaller and the possibility of wrong slot error increases. Furthermore, there are more time slots for false alarm errors to take place. Under these conditions the pre-detection filter should be carefully designed to improve the pulse edges.

In chapter 4 it was shown that the DPIM pulse width is shorter than that compared to PCM. Therefore, to deliver the same carrier-to-noise ratio at the receiver, the DPIM peak power level need to be higher by 2.7 dB compared to PCM, at bit resolution of 4. Provided this is achieved, the probability of error of DPIM shows about 2 dB improvement over PCM.

When the receiver noise is negligibly small, the output *SNR* depends on the quantisation noise similar to that in PCM. DPIM displays a threshold effect around the *CNR* of 15 dB. Above this level the *SNR* is saturated. For 4, 5, 6, 7 and 8 bit DPIM systems this was shown to be 29 dB, 35 dB, 41 dB, 47 dB and 53 dB respectively. This performance is very similar to that of PCM.

The anisochronous frame nature of DPIM results in two frames being in error for every slot error. Thus at low *CNR* ratios a higher level of probability of error can be expected. This was observed during the *SNR* ratio measurements. At the threshold region a slight drop of average received optical power results in a sharp drop of the *SNR*. By comparing *SNR* of DPIM with PCM, there are three regions of interest that correspond to a particular bit resolution, where DPIM shows inferior, superior, and identical performance with PCM. These threshold levels are sensitive to the bit resolution. At a *CNR* of less than 6, 7, 9 and 11 dB corresponding to bit resolutions of 4, 5, 6 and 7,

respectively, DPIM performance is inferior. This can be explained by frame patterns being distorted heavily due to propagation of frame errors into the adjacent frame. Then, up to *CNR*s of 15, 16, 17 and 17.4 dB, DPIM shows better *SNR* performance. This is due to S*NR* threshold of DPIM being lower than PCM. Any further increase of the *CNR* results in identical performance when both schemes suffer only from quantisation noise.

In section 3.5 it was shown that for analogue PIM *SNR* is at 28 dB at *CNR* of 15 dB and rises by 1 dB for every 1 dB increase in the *CNR*. For DPIM at the same *CNR*, the *SNR* is improved by 13 dB at bit resolution of 6. Similar *SNR* performance can also be achieved by analogue PIM provided that *CNR* is at about 29 dB (see section 3.5).

System linearity is bit resolution dependant. As the resolution increases the 2^{nd} harmonic distortion reduces slightly. On average this component is about 29 dB, 26 dB and 23 dB below the fundamental for bit resolution of 4, 5 and 6, respectively. This is again sensitive to modulation index. As the modulation index is increased from 2 % to 100 %, the 2^{nd} harmonic level increases momentarily from 32 dB, 33 dB and 34 dB below the fundamental to 19 dB, 20 dB and 21 dB corresponding to bit resolutions of 6, 5 and 4, respectively. The third harmonic component is 45 dB below the fundamental for all three cases. Which case the harmonic component drops as the bit resolution increases unlike with the 2^{nd} harmonic. However, harmonic distortion performance can be improved by means of increasing the slot rate further (2-3 times the required rate at the expense of increased bandwidth). In comparison with analogue PIM, DPIM shows about 10 dB improvement in the 2^{nd} harmonic distortion. The third harmonic distortion is higher at low modulation index (-35 dB on average compared to -50 dB in PIM), but

this improves with an increase in the modulation index giving -48 dB, on average, compared to -8 dB in PIM at modulation index of 95 %.

Slot synchronisation was successfully achieved for all three bit resolutions under both periodic and random signals. For transmitted optical power of -28.8 dB, receiver sensitivity was -45.5 dBm for bit error rate of 10^{-9}, thus giving high optical power budget.

9.1 Original Contributions

During the cause of this work the author has,

1. Introduced, digital counterpart of pulse interval modulation for optical communication systems.

   Analogue pulse interval modulation can only support analogue signals, whereas DPIM can support both analogue as well as digital information. Frame concept with inclusion of guard band for dispersive channels and the concept involved in selection of slot frequency to support particular information signal were proposed. It was shown that for analogue signal transmission, the DPIM transmitter and the receiver can be implemented based around simple DAC structures.

2. Successfully modelled the DPIM spectra to predict spectral variation for various system parameters, such as data randomness, bit resolution, modulation index, pulse width etc. It was shown that spectra consist of distinct slot components that can be used for slot synchronisation purposes. Further, the spectra was evaluated for Gaussian shaped received pulses and shown to contain distinct slot component without any singularities at the slot harmonics unlike that seen with rectangular pulses.

3. Analysed the DPIM receiver performance in detail. The effect of received pulse width, receiver bandwidth, channel bandwidth and bit resolution on the receiver performance were investigated.

4. Identified the DPIM error sources. It was shown that DPIM consists of three error sources similar to that of DPPM, namely erasure, false alarm and wrong slot error. Variations of the probabilities of these errors were investigated in detail. Resultant probability of error was compared with PCM and DPPM.

5. Modelled the *SNR* expression for DPIM. Predictions based on the model showed identical performance compared to PCM at different bit resolution above a certain *CNR* level. It was also shown that there are three regions of significant importance, where DPIM shows inferior, superior and identical performance compared to PCM.

9.2 List of Publications

1. Kaluarachchi, E.D., Ghassemlooy, Z. : Chapter 8, Digital signal processing for communication systems, Kluwer Academic Publishers, Boston/ Dordrecht/ London 1997, ISBN 0-7923-9932-3, pp 65-72

2. Kaluarachchi E.D., Ghassemlooy Z., Wilson B.: 'Digital pulse interval modulation for optical fibre with direct detection' Proceedings of SPIE Photonics'96 East, 18-22 November 1996, Boston, USA, [2919-11]

3. Kaluarachchi E.D., Ghassemlooy Z.: 'Digital Pulse Interval Modulation: Spectral behaviour', Proceedings of IEEE 4th UK/Australia international symposium on DSP for communication systems, Perth-Joondalup, Australia, 23-26 September 1996, pp 218-223

4. Ghassemlooy Z., Reyher R.U., Kaluarachchi E.D., Simmonds A.J.: 'Digital Pulse Interval and Width Modulation (DPIWM)': Microwave and optical technology letters, 11, (4), March 1996, pp 231-236
5. Kaluarachchi E.D., Ghassemlooy Z., Wilson B.: 'Digital Pulse Interval Modulation (DPIM) for free space optical links', IEE Proceedings on Colloquium on 'optical free space communication links', 19 February 1996, Savoy place, London, pp 3/1-3/5

6. Reyher R.U., Ghassemlooy Z., Simmonds A.J., Kaluarachchi E.D.: 'Digital Pulse Interval and Width Modulation (DPIWM) for optical fibre communication', Proceedings of SPIE Photonics'95 East, 1st International symposium on photonic technology and systems for voice, data communication, 23-26 October 1995, Philadelphia, Pennsylvania, U.S.A., SPIE 2614-08

7. Ghassemlooy Z., Kaluarachchi E.D., Wilson B.: 'Digital Pulse Interval Modulation(DPIM) for fibre transmission': Proceedings of SPIE Photonics'95 East, 1st International symposium on photonic technology and systems for voice, data communication, 23-26 October 1995, Philadelphia, Pennsylvania, U.S.A., SPIE 2614-05

8. Ghassemlooy Z., Kaluarachchi E.D., Reyher R.U. and Simmonds A.J.: 'A new modulation technique based on Digital Pulse Interval modulation(DPIM) for optical-fibre communication', Microwave and optical technology letters, 10, (1), September 1995, pp 1-4

9. Ghassemlooy Z., Reyher R.U., Kaluarachchi E.D., Simmonds A.J., Saatchi R.: 'A novel digital communication system using pulse interval code modulation(PICM) and pulse interval width code modulation(PIWCM)', Proceedings of 3rd IEE international symposium on communication theory and applications, 10-14 July 1995, Charlotte Mason College, Lake District, UK

Submitted for publication

1. Kaluarachchi, E.D., Ghassemlooy Z. :'Digital pulse interval modulation for optical communication systems', Accepted for publication in IEEE transactions on telecommunications

2. Kaluarachchi E.D., Ghassemlooy Z., Wilson B.: 'Digital pulse interval modulation for low to moderate speed communication systems', Accepted for publication in the IEEE 1st International symposium in 'Communication systems and digital signal processing', to be held at Sheffield Hallam University, Sheffield, 6-8 April 1998

Chapter Ten

Future Work

The work presented in this thesis have been tried to complement theoretical predictions with the practical measurements where ever it has been possible. DPIM scheme has been proposed for transmission of analogue as well as digital signal transmission, though the prototype was only presented for analogue signal transmission. Thus it is required to investigate the scheme for transmission of digital information. Author has pointed out that transmission of digital information require temporary buffer at the transmitter and the receiver end. The capacity of the buffer is one of the important factor in such a system. This has to be investigated.

It was briefly shown that the variation of the average power in DPIM frames can be minimised by reorganising the frame structure in the encoding process, by means of incorporating a lookup table. Such frame structure may lead to an improved receiver performance as base line wonder is minimised. Therefore, investigation of applying coding in DPIM is a next logical move forward.

DPIM scheme has been reported to be used in optical wireless applications [*Kaluarachchi*96/1], [*Hadinnapola*], but this is at low bit rate e.g. 1 Mbps. DPPM, showing similar spectral profile to DPIM, has been talked about for such applications over the past few years. Thus both the schemes can assume to suffer from the IR channel in a similar manner. Self synchronised frame structure and slot synchronisation capability by means of PLL, indicates that DPIM is also a good candidate for wireless IR applications. One of the obstacle one would suggest is that whether the IR channel will corrupt a stream of short duration pulses corresponding to low symbol levels. This can be minimised by the lookup table mentioned in the previous paragraph. Thus advantages of DPIM over wireless links also worth investigating.

References

[*Aiki*] Aiki, M.:'Low noise optical receiver for high-speed optical transmission', Journal of lightwave trechnology', **LT-3**, (6), 1985, pp 1301-1306

[*Atkin*] Atkin G.E., Fung K.S.:'Performance analysis of coded optical PPM system using direct and coherent detection', IEE proceedings-I, **137**, (4) 1990, pp 226-232

[*Baister*] Baister, G., Gatenby, P., Laurent, B., Lewis, J.,:'Applications for optical free space links in inter-satellite and intra-satellite communications', IEE colloquium proceedings, 'IEE colloquium on optical free space communication links', Savoy place, London, February, 1996, pp 9/1-9/6

[*Best*] Best, R.E.,:'Phase-Locked loops, theory, design and applications', 2 nd edition, McGraw-Hill Inc, 1993, ISBN 0-07-911486-9

[*Berry*] Berry M.C., Arnold J.M.:'Pulse width modulation for optical fibre transmission of video', IEE conference proceeings on 'The impact of high speed and VLSI technology on communication systems', pp 14-18

[*Biase*] Biase, Valerio Di, Passeri, Paolo, Pietroiusti, R.:'Pulse Analogue transmission of TV signals on optical fibre', Alta Frequenza, **56**, (4), 1987, pp 195-203

[*Blachman*] Blachman N.M.:'The SNR threshold in PPM reception', IEEE transaction on communication, **COM-22**, (8), 1974, pp1094-1098

[*Black*] Black H.S.:'Modulation theory', Van Nostrand Company, London, chapter 17.

[*Boerner*] Boerner, S., Heichler, J.,:'4 PPM Modulator/Demodulator with fully digital signal regeneration', SPIE Proceedings on optical communication(1989), **1131**, pp 195-202

[*Brain*] Brain, M, Lee, T.,:'Optical receivers for lightwave communication systems', Journal of Lightwave technology, **LT-3**, (6), 1985, pp 1281-1300

[*Budinger*] Budinger J.M. et al :'Combinatorial pulse position modulation for power-efficient free-space laser communications', Proceedings SPIE, **1866**, 1993, pp 214-225

[*Calvert*] Calvert, N.M. et al: 'Experimental optical fibre digital PPM system', Electronic letters, **24**, (2), 1988, pp 129-131

[*Carlock*] Carlock, W. G.,:'The two-stage RC low-pass matched filter', *IEEE transac. on communications*, **COM-20**, 1, 1972, pp 73-74

[*Carlson*] Carlson, A.B.,:'Communication systems, An introduction to signals and noise in electrical communication', Second edition, McGraw-Hill, ISBN 0-07-009957-X, Chapter 10

[*Chan*] Chan, H.H., Hussain, A., Elmirghani, R.A., Cryan, R.A.,:' Channel equalisation for optical wireless multi-user systems utilising othogonal codes', IEE colloquium on Optical free space communication links', Savoy place, London, 1996/032, pp1/1- 1/7

[*Cochrane*] Cochrane, P., Heatley, D.J.T., Smyth, P.P., Pearson., I.D.,:'Optical telecommunication future prospects', Electronics & Communication Engineering Journal, August 1993, pp 221-232.

[*Collins*] Collins,O.:'The Design of low jitter hard limiers',IEEE transaction on communications, **44**, (5), 1996, pp 601-608

[*Couch*] Couch II, L.W.:'Digital and analog communication systes', Macmillan publishing, 1993, Fourth edition, ISBN 0-02-325281-2

[*Cryan*92/1] Cryan R.A., Unwin, R.T., Massarella, A.J., Sibley, M.J.N.:'A comparison of coherent digital PPM with PCM', European Transac. on Telecom, **3**, (4), July, 1992, pp 331-340

[*Cryan*93/1] Cryan, R.A., Unwin, R.T.,:'Optical and suboptimal detection of optical fibre digital PPM', *IEE Proceedings-J*, **140**, (6), 1993, pp 367-375

[*Davidson*89] Davidson, F.M., Sun, X.,:'Slot clock recovery in optical PPM communication systems with avalanche photodiode pgotodetectors', *IEEE Trans. on communications*, **37**, (11), 1989, pp 1164-1172

[*Davidson*91] Davidson, F.M., Sun, X.,:'Bandwidth requirements for direct detection optical communication receivers with PPM signaling', **1417**, SPIE Free-space laser communication technologies 3, 1991, pp 75-88

[*Denninston*] Denniston, F.J., Runge, P.K.: 'The glass necklace', IEEE Spectrum, October 1995, pp. 24-27

[*Downing*] Downing, J.J.:'Modulation systems and noise',Prentice-Hall, INC, Englewood Cliffs, N.J. 1964, Chap 7

[*Duttweiler*] Duttweiler, D.L.:' The jitter performance of phase locked loops extracting timing from baseband data waveforms', The Bell system technical journal, January 1976, pp 37-58

[*Elmirghani*93] Elmirghani J.M.H, Cryan R.A., Clayton M :'Investigation of the synchronisation requirements for optical fibre PPM', Proceedings SPIE, 0-8194-1220-1, **1974**, 1993, pp 126-137

[*Elmirghani*94/1] Elmirghani, J.M.H., Cryan, R.A.,: 'Analytic and numeric modelling of optical fibre PPM slot and frame spectral properties with application to timing extraction', IEE Proc-.Commun, December 1994, **141**, (6), pp 379-389

[*Elmirghani*95/1] Elmirghani, J.M.H., Cryan, R.A., Clayton, F.M.: 'On the estimation and synchronization of the cyclostattionary optical fibre PPM process', IEEE Transactions on communications, February/March/April 1995, **43**, (2/3/4), pp 1001-1012

[*Elmirghani*94/2] Elmirghani, J.M.H., Cryan, R.A.:'Optimally filtered self-synchronised PPM PIN-BJT receivers', Microwave and optical technology letters, **7**, (5), April 1994, pp 250-253

[*Elmirghani*94/3] Elmirghani, J.M.H., Cryan R.A. :'Implementation and performance consideration for a PPM correlator-synchroniser', Proceedings on IEEE international symposium on circuits and systems', **3**, (3), 1994, pp 157-160

[*Elmirghani*94/4] Elmirghani et al :'On the design of jitter tolerent synchronisation subsystem for opical fibre PPM', Proceedings on IEEE international symposium on circuits and systems', **3**, (3), 1994, pp 37-40

[*Fyath*] Fyath R.S., Abdullah S.A., Glass A.M. :'Spectral investigation of pulse-interval modulation', Int. Journal of Electronics, **59**, (5), 1985, pp 597-601

[*Gagliardi*76] Gagliardi, R.M., Karp, S., :'Optical communications', John Wiley & Sons Inc, 1976, ISBN 0-471-28915-9, Chapter 9,10

[*Gagliardi*83] Gagliardi, R.M.:'Time synchronization in optical PPM systems',IEEE Globecom83, Sandiego 1983, pp 779-783

[*Gagliadi*87] Gagliadi R., Robbins J., Taylor H. :'Acqusition sequences in PPM communications', IEEE transaction on information theory, **IT-33**, (5), 1987, pp 738-744

[*Gangopadhyay*] Gangopadhyay R., Datta D. :'Timing recovery in optical receivers for NRZ signalling', Electronics letters, **22**, (1), 1986, pp 38-39

[*Garrett*83/1] Garrett, I.:'Digital pulse-position modulation over dispersive optical fibre channels', Proceedings of IEEE Globecom, 1983, pp 733-737

[*Garrett*83/2] Garrett, I.:'Pulse position modulation for transmission over optical fibre with direct or heterodyne detection', IEEE Transaction on communication, **COM-31**, (4), 1983, pp 518-527

[*Garrett*89] Garrett I. et al:'Optical fibre digital pulse position modulation', British telecom technology journal, 7, (3), 1989, pp 5-11

[*Gardner79*] Gardner, Floyd M.:'Phaselock Techniques', 2nd edition, John Wiley & SonsInc 1979, ISBN 0-471-04294-3

[*Georghiades*] Georghiades,Costas. N., Davidson, F.M.,Guest Editorial, Journal on Selected areas in communications; 1995, **13**, (3), pp. 477-478.

[*Gfeller*] Gfeller, F.R., Bapst, URS:'Wireless in-house data communication via diffuse infrared radiation', Proceed. of the IEEE, **67**, (11), 1979, pp 1474-1786

[*Ghassemlooy*91/1] Ghassemlooy Z., Wilson B.:'Principals of optical fibre communications 2', First edition 1991, Published by Sheffield Hallam University

[*Ghassemlooy*92] Ghassemlooy Z., Wilson, B., Betteridge, B.: Pulse Position Modulation Based Spectral Investigation, 4 th Bangor Symposium on Communications, May 1992, pp. 221-225

[*Ghassemlooy*93/1] Ghassemlooy Z., Wilson B., Darwazeh I.:'Optical fibre transmission of video and audio signals using square wave frequency modulation', IEEE Transactions on Consumer Electronics, **39**, (1), 93, pp 33-39

[*Ghassemlooy*93/2] Ghassemlooy Z., Wilson B.:'Optical PWM data link for high quality video and audio signals', IEEE transactions on Consumer Electronics, **40**, (1), 1994, pp 55-62

[*Ghassemlooy*93/3] Ghassemlooy Z., Wilson B., Chao L.:'Digitally generated pulse width modulation transmitted over optical fibre', Inter. J. Electronics, **75**, (3), 1993, pp 433-436

[*Ghassemlooy*93/4] Ghassemlooy Z.:'Pulse position modulation spectral investigation', Int. J. Electronics', **74**, (1), pp 153-158

[*Ghassemlooy*94] Ghassemlooy Z., Wilson B. :'Optical PWM data link for high quality video and audio signals', IEEE Trans. on Consumer Electronics, **40**, (1), 1994, pp 55-62

[*Ghassemlooy*95/1] Ghassemlooy, Z.,Kaluarachchi,E.D., Reyher, R.U., Simmonds, A.J.,:'A new modulation technique based on Digital pulse interval modulation (DPIM) for optical-fibre communication', Microwave and optical technology letters, **10**, (1), September 1995, pp 1-4

[*Ghassemlooy*95/2] Ghassemlooy, Z., Reyher, R.U., Kaluarachchi, E.D., Simmonds, A.J.:'Digital pulse interval and width modulation for optical fibre communication', Proceedings SPIE, **2614**, 1995, pp 60-68

[*Ghassemlooy*95/3] Ghassemlooy, Z., Reyher, R.U., Kaluarachchi, E.D., Simmonds, Saatchi R. :'Pulse interval and width code modulation', Proceedings IEEE 3rd international symposium on communication theory and applications, 10-14 July, Charlotte Mason College, Lake District, UK, 1995

[*Ghassemlooy*96] Ghassemlooy Z., Reyher R.U., Kaluarachchi E.D., Simmonds A.J.: 'Digital Pulse Interval and Width Modulation (DPIWM)': Microwave and optical technology letters, 11, (4), March 1996, pp 231-236

[*Ghassemlooy*97] Ghassemlooy Z. :'PIM distortion measurements', Unpublished work, Sheffield Hallam University, 1997.

[*Grieg*] Grieg, D.D., Levine, A.M.:'Pulse-Time-Modulated multiplex radio relay system-terminal equipment', Proceedings of the I.R.E. March 1946

[*Hadinnapola*] Hadinnapola, R.: 'Robotic control using bidirectional wireless link', Undergraduate project, City University, 1996/97

[*Harison*] Harrison, B.:'Fiber Flag waves on three continents', Lightwave, PennWell publications, October 1996, pp 1-26

[*Hausien*] Hausien,H.H.:'Pulse Position Modulation for optical fibre local area networks', PhD Thesis, University of Bath, 1991

[*Heatley*83] Heatley, D.J.T.:'Video transmission in optical fibre local networks using pulse time modulation', Proceedings of ECOC 83, 9th European conference on optical communication', 1983, pp 343-346

[*Heatley*91] Heatley, D.J.T., Cochrrane, P.:' Future directions in long haul optical fibre transmission systems', Proceedings on IEE conference on telecom, Edingurgh, 1991, pp 157-164

[*Holden*] Holden W.S.:'An optical-frequency pulse position modulation experiment', The Bell system technical journal, **54**, (2), 1975, pp 285-296

[*Hubbard*] Hubbard, W.M. :'Utilization of optical-frequency carriers for low- and moderate-bandwidth channels', The Bell system technical journal, **52**, (5), 1973, pp 731-765

[*Hullett*75/1] Hullett, J.L., Doan, H.B., Rosman, G., 'A modified receiver for optical transmission systems', IEEE trans. on commun, 1975, pp 1514-1518

[*Hullett*75/2] Hullett, J.L., Muoi, T.V.,'A modified receiver for digital optical fibre transmission systems', IEEE trans. commun., 1975, pp 1518-1521

[*Hullett*76] Hullett, J.L., Muoi, T.V.:'A feedback receiver amplifier for optical transmission systems', IEEE Trans on commun, **COM-24**, 1976, pp 1180-1185

[*Issa*] Issa,A.A.:'Noise performance of the pulse slope modulation system', Electronic letters, **29**, (25), 1993, pp 2171-2173

[*Jelonek*] Jelonek, Z.:'Noise problems in pulse communications', Journal IEE Pt. 3-A, **94**, 1947, pp 533-545

[*Kahn*] Kahn.Joseph M, Barry, J.R.:'Wireless infrared communications', Proceedings of IEEE, **85**, (2), 1997, pp 265-297

[*Kaluarachchi*96/1] Kaluarachchi,E.D.,Ghassemlooy,Z., Wilson,B.: 'Digital pulse interval modulation for wireless systems', SPIE's Photonics east 18-22 November 1996, Boston, USA, [2919-11]

[*Kaluarachchi*96/2] Kaluarachchi E.D, Ghassemlooy Z., Wilson B. : 'Digital Pulse Interval Modulation(DPIM) for free space optical links', IEE Proceedings on Colloquium on optical free space communication links, 19 February 1996, Savoy place, London, pp 3/1-3/5

[*Kappeler*] Kappeler, F.:'Pulse power performance and stability of 880nm GaAlAs/Gaas oxide-stripe-lasers', IEE Proceed Pt I, 129, pp 256-261

[*Karp*] Karp Sherman, Gagliardi R.M.:'The design of pulse position modulated optical communication system', IEEE Transactions on communication technology, **COM-17**, 6, 1969, pp 670-676

[*Kashima*] Kashima, N.,:'Optical transmission for the subscriber loop', Artech House Inc, 1993, ISBN 0-89006-679-5

[*Katz*] Katz, Joseph:'Average power constraints in AlGaAs semiconductor lasers under pulse-position-modulation conditions', *Optical communications*, **56**, (5), 1986, pp 330-333

[*Lee*] Lee, T.:'Effect of junction capacitance on the rise time of LEDs and the turn-on delay of injection lasers', Bell system technical journal, **54**, (1), 1975, pp 55-68

[*Marougi*] Marougi S.D., Sayhood K.H. :'Signal-to-noise performance of the pulse-interval and width modulation system', Electronic Letters, **19**, (14), 1983, pp 528-530

[*Martin*89] Martin J.:'PPM for local area networks', SPIE proceedings on 'Fibre optics 89', **1120**, 1989, pp 14-24

[*Martin*92] Martin, J.D., Hausien, H.H.:'PPM versus PCM for optical local-area networks', IEE Proceedings-I, **139**, (3), 1992, pp241-250

[*Meade*] Meade, M.L.:'Lock-in amplifiers: principles and applications',Peter Peregrinus Ltd., London, UK, 1983, ISBN 0906048 94 X

[*Mecherle*86] Mecherle, G. Stephen,:'Detection alternatives for pulse position modulation (PPM) optical communication', *Proceedings SPIE on Optical technologies for communication satellite applications*, **616**, 1986, pp 105-117

[*Mecherle*85] Mecherle, G. Stephen,:'Impact of laser diode performance on data rate capability of PPM optical communication', IEEE MILCOM-85, Boston, MA, 1985, pp 115-121

[*Menendz-Valdes*] Menendz-Valdes, Pedro:'Performance of optical direct receivers using noise corroupted decision thesold', *IEEE Journal of lightwave technology*, **13**, (11), 1995, pp 2202-2214

[*Mogensen*] Mogensen,G.,:'Review: Wide-band optical fibre local distribution systems', Optical quantum electronics, **12**, 1980, pp 353-381

[*Moreira*96] Moreira, A.J., Valadas, R.T, De Olivera Duarte, A.M.,:'Reducing the effects of light interference in wireless infrared transmission systems', IEE colloquium proceedings, 'IEE colloquium on optical free space communication links', Savoy place, London, February, 1996, pp 5/1-5/10

[*Moreira*95] Moreira, A.J., Valadas, R.T, De Olivera Duarte, A.M.,:'Modulation methods for wireless infrared transmission systems- performance under ambient light noise and interference', SPIE's Photonics East'95 Symposium, Philadelphia, October 23-26, 1995

[*Muoi*78] Muoi, T.V., Hullett, J.L.,:'Receiver Design for optical PPM systems', *IEEE Transac. on communications*, **COM-26**, (2), 1978, pp 295-300

[*Muoi*83] Muoi, T.V.,' Receiver design for digital fibre optic transmission systems using Manchester(Biphase) coding', IEEE trans. on commun., **COM-31**, 1983, pp 608-619

[*Nakagami*] Nakagami, T; Sakurai T; 'Optical and Optoelectronic devices for optical fibre Transmission Systems', IEEE Communication magazine, **26**, (1), 1988, pp. 14-16.

[*Nishida*] Nishida et al, :'Field experiment of PIM-IM optical fibre communication system and its stability against environment conditions', OSA/IEEE meeting on optical fibre transmission field experiment of PIM-IM optical fibre transmission', February 1977, pp 1-4

[*Nicholls*] Nicholls,P., Greaves, S.D., Unwin, R.T.,:'Optical wireless telepoint', IEE colloquium proceedings, 'IEE colloquium on optical free space communication links', Savoy place, London, February, 1996, pp 4/1-4/6

[*Okazaki*78] Okazaki A.:'Pulse-Interval Modulation applicable to narrowband transmission', IEEE transaction on cable television, **CATV-3**, (4), pp 155-164

[*Okazaki*79] Okazaki A.:Still picture transmission by Pulse Interval Modulation', IEEE transaction on cable television, **CATV-4**, (1), 1979, pp 17-22

[*O'Reilly*] O'Reilly, J.J., Watkins, L.R., Schumacher, K.,:'New strategy for the design and realisation of optimised receiver filters for optical telecommunication', *IEE Proceedings*, **137**, (3), 1990, pp 181-185

[*Personick*73/11] Personick, S.D.:'Receiver design for digital fibre optic communication systems, I', The Bell system technical journal, **52**, (6), 1973, pp 843-874

[*Personick*73/2] Personick, S.D.:'Receiver design for digital fibre optic communication systems, II', The Bell system technical journal, **52**, (6), 1973, pp 875-886

[*Philips*] Philips Semiconductor, Data handbook, 1992 Signetic company, pp265

[*Pires*] J.J.O., Da Rocha J.R.F.:'Digital pulse position modulation over optical fibre with avalanche photodiode receivers', IEE Proceedings pt J, **133**, (5), 1986, pp 309-313

[*Prati*] Prati, Giancarlo, Gagliardi, R.M.:'Decoding with stretched pulses in laser PPM communications', *IEEE trans. on communications*, **COM-31**, (9), 1983, pp1037-1045

[*Prokis*] Prokis,J.G, Salehi, M..;'Communication Systems Engineering', Prentice Hall International Editions 1994, pp 179

[*Refi*] Refi, James, J.,:'Fibre bandwidth and its relation to system design', Journal of optical sensors, **2**, (2), 1987, pp 89-105

[*Reyher*] Reyher, R.U. :Digital anisochronous pulse time techniques', Mphil Thesis 1995, Sheffield Hallam University

[*Rich*] Rich,M.A.:'Designing phase-locked oscillators for synchronization', *IEEE Trans. on communications*, **COM-22**, (7), 1974, pp 890-896

[*Roza*] Roza, E.:'Analysis of phase-locked timing extraction circuits for pulse code transmission', IEEE transaction on communications, **COM-22**, (9), 1974, pp 1236-1249

[*Runge*] Runge, P. K.,:'Undersea lightwave systems', AT&T technical journal, February 1992, pp 5-13

[*Sato*78] Sato, M., Murata, M., Namekawa T. :'Pulse interval and width modulation for video transmission', IEEE Transac. on cable television', **CATV-3**, (4), 1978, pp 165-173

[*Sato*79] Sato, M., Murata, M., Namekawa, T.:"A New Optical Communication System Using the Pulse Interval and Width Modulation Code". *IEEE Transactions on Cable Television,* **CATV-4**, (1), *1979,* pp 1-9

[*Sato*94] Sato K., et al :'Performance analysis of Multi-Pulse PPM with imperfect slot synchronisation in optical direct-detection channel', IEICE Trans. Communication, **E77-B**, (8), 1994, pp 1032-1039

[*Senior*] Senior, J.:'Optical fibre communications, principles and practice', 1985 Prentice-hall international Inc, London, ISBN-0-13-638248 7

[*Sibley*93/1] Sibley, M.J.N., Massarella, A.J.,:'Detection of Digital pulse position modulation over highly/slightly dispersive optical channels', SPIE vol **1974**, 0-8194-1220-1/1993, pp 99-110

[*Sibley*93/2] Sibley, M.J.N.:'Design implecation of high speed digital PPM', SPIE vol **2024**, 1993, pp 342-352

[*Sibley*93/3] Sibley M.J.N.:'Design implication of high speed digital PPM', SPIE proceedings on 'Multigigabit fibre communocation systems', **2024**, pp 342-352

[*Shalab*95/2] Shalaby, H.M.H. :'Capacity and cutoff rate for optical overlapping pulse-position modulation', IEEE Transac. on Communication, **43**, (2/3/4), 1995, pp1284-1288

[*Shalaby*95/1] Shalaby H.M.H. :'Maximum achievable throughputs for uncoded OPPM and MPPM in optical direct-detection channels', Journal of lightwave technology, **13**, (11), 1995, pp 2121-2128

[*Sklar*] Sklar, B.:'Digital communications, fundamentals and applications',Prentice Hall, 1988, ISBN 0-13-212713-X 025, Chapter 1

[*Smith*] Smith, R.G., Personick, S.D.:'Receiver design for optical fibre communication systems', ED H Kresselel, Springer-verlag, New York, 1980, chapter 4

[*Stremler*] Stremler, F.G.:' Communication Systems' 3rd Edition (ADDISON WESLEY, 1992), pp 168-176, pp 130-145, pp 43

[*Su*] Su, L., Kendall:'Time domain synthesis of linear networks', 2 nd Edition, 1971, Prentice-Hall, INC

[*Sugiyama*89] Sugiyama H, Nosu K. :'MPPM: A method for improving the band utilization efficiency in optical PPM', Journal of lightwave technology', **7**, (3), 1989, pp 465-472

[*Sugiyama*93] Sugiyama H. :'Method for block synchronisation in optical PPM', IEE Proceedings-J, **140**, (6), 1993, pp 377-384

[*Suh*] Suh, S.Y.,:'Pulse width modulation for analogue fibre-optic communication', Journal of lightwave technology, **LT-5**, (1), 1987, pp102-112

[*Sun*90] Sun X., Davidson F.M. :'Word timing recovery in direct setection optical PPM communication systems with avalanche photodiodes using a phase lock loop', IEEE transactions on communications, **38**, (5), 1990, pp 666-673

[Sun90/2] Sun X., Davidson F.M., Field, C.: '50 Mbps free space direct detectection laser diode optical communication system Q = 4 PPM signalling', SPIE 1218 Free space laser communication technology 2', 1990, pp 385-395

[*Tripathi*80] Tripathi J.N. :'Spectrum measurement of pulse-interval modulation', Int. Journal of Electronics, **49**, (5), 1980, pp 415-419

[*Tripathi*83] Tripathi J.N. :'Measurement of signal-tonoise ratio in pulse-interval modulation', Int. J. of Electronics, **55**, (2), 1983, pp 247-252

[*Turin*] Turin, George, L.,'An introduction to matched filters', *IEEE Transactions on Information theory'*, **IT-7**, pp 311-329

[*Ueno*75] Ueno Y., Yasugi T.:'An optical fibre cable communication system using pulse-interval modulation', IEE 1st European conf. on optical fibre cable communication', 1975, pp 156-158

[*Ueno*78] Ueno Y., Yasugi T.:'Optical fibre communication systems using Pulse-Interval Modulation', NEC research & development, (48), 1978 January, pp 45-51

[*Van den Broeke*93] Van den Broeke, L.A.Dick et al:'An analogue multi-channel integrated optical transmission system for video signals', SPIE, 1974, 1993, pp 83-89

[*Van den Broeke*95] Van den Broeke, L.A.Dick et al:'A low cost multichannel optical transmission system for video signals', IEEE transactions on communications, 43, (9), 1995, pp 2493-2501

[*Williams*] Williams, Arthur,B.:'Electronic filter design handbook', ISBN 0-07-070430-9, McGraw-Hill book company, 1981

[*Wilson*88] Wilson B., Ghassemlooy, Z.,:'Multiple sidetone structure in pulse width modulation', Electronic letters, **24**, (9), 1988, pp 5196-518

[*Wilson*91] Wilson B., Ghassemlooy, Z., Lok, A.:'Spectral structure of multi tone PWM', Electronic letters, **27**, (9), 1991, pp 702-704

[*Wilson*96] Wilson, G. S.:'Digital modulation and coding', Prestice-Hall Inc 1996, ISBN 0-13-210071-1, Chapter 2

[*Wilson*91] Wilson,B., Ghassemlooy, Z., Heatley, D.J.T.:'Properties and applications of pulse time modulation techniques for fibre broadband communication networks', International conference on information engineering 91 (ICIE'91), pp 693-702

[*Wilson*91/2] Wilson,B., Ghassemlooy, Z., Cheung J.C.S. :'Spectral prediction for pulse interval and width modulation', Elect. Letters, **27**, (7), 1991, pp 580-581

[*Wilson*92] Wilson,B., Ghassemlooy, Z., Chao, L.:'High speed pulse time modulation techniques', SPIE proceedings, Boston 92

[*Wilson*92/2] Wilson B., Ghassemlooy Z., Cheung J.C.S. :'Optical pulse interval and width modulator for analogue fibre communications', IEE Proceedings-J, **139**, (6), 1992, pp 376-382

[*Wilson*93] Wilson,B., Ghassemlooy, Z.:'Pulse time modulation techniques for optical communication: a review', IEE proceedings-J, **140**, (6), 1993, pp 346-357

[*Wilson*95] Wilson, B., Ghassemlooy, Z., Chao, L.:'Squarewave frequency modulation techniques', **43**, (2/3/4), 1995, pp1505-1512

[*Wilson*95/2] Wilson B, Ghassemlooy Z. :'Analogue optical fibre communications', IEE Telecommunications series 32, ISBN 0 85296 832 9

[*Wisely*] Wisely, D.R.,:'A 1 Gbits/s optical wireless tracked architecture for ATM delivery', IEE colloquium proceedings, 'IEE colloquium on optical free space communication links', Savoy place, London, February, 1996, pp 14/1-14/7

[*Wu*] Wu Y. et al :'Addressed audio and video signal transmission through optical fibres, IEEE Transactions on Consumer Electronics, **40**, (1), 1994, pp 35-41

[*Yichao*] Yichao W., O'Reilly J.J. :'Repeated optical fibre communication based on line-coded digital PPM transmission', Proceedings of Globecom'85, New Orleans, 1985, pp 698-702

Appendix A

DPIM Receiver Noise Analysis

Receiver noise for PCM receiver has been studied in detail by [*Smith*], [*Personick*73/1,2]. In his general receiver model comprises high impedance receiver and FET or bipolar transistor pre-amplifiers. In this work receiver model presented by the above authors were used and expressions were modified for DPIM process.

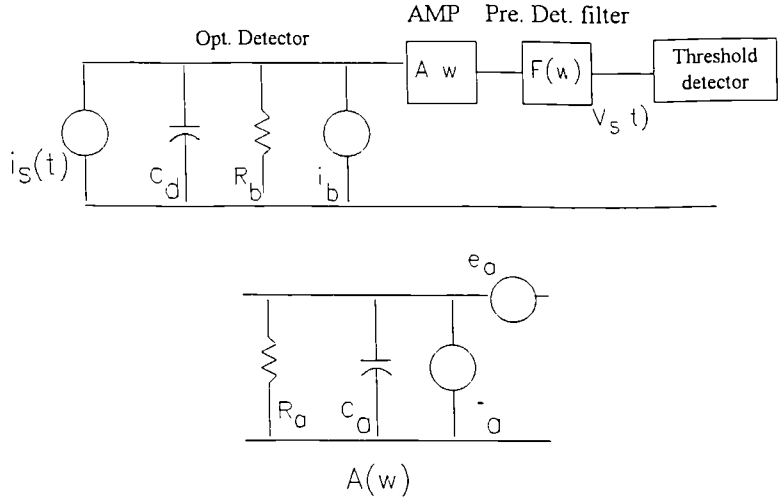

Fig. A.1 Equivalent receiver circuit front end.

Basic receiver given in Fig. A.1 consist of a photo detector, a low noise amplifier (pre-amplifiers $A_1(\omega)$ and a post-amplifier $A_2(\omega)$ combined) and a pre-detection filter (combination of equaliser $E(\omega)$ and the pulse shaping filter $F_s(\omega)$).

Optical detector in Fig. A.1 shows the depletion capacitor (C_d), bias resistance R_b and the noise sources associated with the bias resistor i_b. Generated current on incident of photon energy is represented by $i_s(t)$. The amplifier circuit consist of stray capacitance

C_a associated with the interconnections of the detector to the input of the amplifier, the amplifier input transistor R_a and the noise sources associated with the amplifier i_a and e_a. For a photo-diode current generated by the incident light of power, $P(t)$, is given by

$$i(t) = \frac{\eta q}{h\Omega} GP(t) \tag{A.1}$$

where $h\Omega/\eta q$ is the photon energy in electron volts, η is the quantum efficiency of the diode and G is the average detector internal gain, for a PIN photo-diodes this value can be taken as 1. Responsivity of the detector is given by $R_0 = \eta q/h\Omega$ A.W^{-1}.

Total input admittance at the receiver front-end is given by,

$$Y_{in}(\omega) = \frac{1}{R_b} + \frac{1}{R_A} + j\omega(C_b + C_A) = \frac{1}{R_T} + j\omega C_T \tag{A.2}$$

The transfer function of the receiver front-end becomes,

$$H_T(\omega) = \frac{A_1(\omega)A_2(\omega)E(\omega)F_s(\omega)}{Y_{in}(\omega)} \tag{A.3}$$

From Eqn. A.3 the signal output at the threshold detector input can be given by,

$$V_{sout}(\omega) = H_T(\omega)I_s(\omega) \tag{A.4}$$

$I_s(\omega)$ is the Fourier transform of the signal current $i_s(t)$.

Noise associated with the detector are two fold, i.e. signal dependant noise and signal independent noise. Former is due to randomness associated with the rate of arrival of photons at the detector whereas the latter is due to the contribution of the amplifier and the biasing circuit as well as signal independent currents flowing in the detector [*Smith*].

When the slot frequency is f_s ($T_s=1/f_s$) an infinite optical pulse stream falling on the detector can be given in the form,

$$P(t) = \sum_{k=-\infty}^{\infty} b_k h_p\left[t - T_s\left(2k + \sum_{m=-\infty}^{k-1} S_m\right)\right] \tag{A.5}$$

where k index to a DPIM frame pulse in the pulse stream. b_k is DPIM pulse energy in a time slot. Pulse shape, $h_p(t)$ is normalised such that,

$$\frac{1}{T_s}\int_{-\infty}^{\infty} h_p(t)dt = 1 \tag{A.6}$$

Output pulse shape is selected such that it's maximum value occur at $t = 0$ and is unity. Thus with minimum or no ISI, the pre-detection filter output can be given by,

$$v_{out}(T_x) = s_x + n(T_x) \tag{A.7}$$

T_x is the DPIM sampling time.

For a pulse stream given in the form of A.5 the output voltage is of the form,

$$v_{out}(t) = \sum_{k=-\infty}^{\infty} s_k h_{out}\left[t - T_s\left(2k + \sum_{m=-\infty}^{k\ 1} S_m\right)\right] + n(t) \tag{A.8}$$

where $h_{out}(t)$ is the pulse shape at the output, $n(t)$ shows the noise associated which are introduced at the receiver and s_k is the output pulse amplitude.

$$v_{out}(t) = \int_{-\infty}^{\infty}\left(\frac{\eta q}{h\Omega}\right) GP(t^1)h_T(t - t^1)dt^1 + I_0\int_{-\infty}^{\infty} h_T(t^1)dt^1 \tag{A.9}$$

Where I_0 consist of current not directly related to photon energy falling on the detector corresponding to DPIM pulses, i.e. dark current, current due to background radiation and is assume to be constant.

Output variance is given by,

$$\sigma_n^2 = \int_{-\infty}^{\infty}\left(\frac{\eta q^2}{h\Omega}\right)G^2P(t^1)h_T^2(t-t^1)dt^1 + I_0\int_{-\infty}^{\infty}h_T^2(t^1)dt^1 \tag{A.10}$$

In terms of inverse Fourier transform on A.9 and A.10 and assuming that amplifier noise spectral density is independent of the frequencies concerned in the design (white noise),

$$v_{out}(t) = \frac{1}{2\pi}\int_{-\infty}^{\infty}\left(\frac{\eta q}{h\Omega}\right)GP(\omega)H_T(\omega)e^{j\omega t}d\omega + I_0H_T(0) \tag{A.11}$$

$$\sigma_n^2 = \frac{1}{2\pi}\int_{-\infty}^{\infty}\left(\frac{\eta q^2}{h\Omega}\right)G^2P(\omega)\left[H_T(\omega)*H_T(\omega)\right]e^{j\omega t}d\omega + I_0(\omega) \tag{A.12}$$

where

$$H_T(\omega)*H_T(\omega) = \int_{-\infty}^{\infty}H_T(\omega^1)H_T(\omega-\omega^1)d\omega^1, \qquad H_T(-\omega) = H_T^*(\omega)$$

This can be written in terms of signal dependant and signal independent noise as follows,

$$v_{out}(t) = \frac{1}{2\pi}\int_{-\infty}^{\infty}\left(\left(\frac{\eta q^2}{h\Omega}\right)G\sum_{k=-\infty}^{\infty}H_P(\omega)e^{-j\omega T_s\left(2k+\sum_{m=-\infty}^{k-1}S_m\right)}\right)H_T(\omega)e^{j\omega t}d\omega + I_0H_T(0) \tag{A.13}$$

There are a few noise generating mechanisms that can be optimised by the receiver designer, such as thermal noise contributed by passive and active receiver elements. These noise sources can be controlled to a limited extend by the circuit topologies.

$n_s(t)$ Explains the current due to shot noise process on the detector due to random multiplied Poisson nature of the current $i_s(t)$.

$n_R(t)$ Johnson noise current source of the bias resistor R_b, and the two-sided spectral density, is given by $2k\theta/R_b$ where k is Boltsman's constant and θ is absolute temperature.

$n_I(t)$ Output noise due to the amplifier input current noise source $i_a(t)$, two sided spectral density is given by S_I.

$n_E(t)$ Noise due to amplifier input voltage noise source $e_a(t)$, two sided spectral density is given by S_E.

Total noise variance can be given by,

$$N = n_s^2(t) + n_R^2(t) + n_I^2(t) + n_E^2(t) \tag{A.14}$$

Noise sources are generally frequency dependant. The mean square output noise current due to a particular noise source is given by the integral over the mean square input noise current density and the squared magnitude of the transfer function, $H_T(\omega)$.

Random noise due to Poisson process ($n_s(t)$)

The variance $n_s^2(t)$ is given by,

$$n_s^2(t) = \frac{1}{2\pi}\int_{-\infty}^{\infty} q^2 \lambda_0 G^2 \left|H_T(\omega)\right|^2 d\omega \tag{A.15}$$

where λ_0 is the dark current electrons per second. Shot noise is generated by the photo current. This noise source is a function of the system configuration and components and cannot be modified by the receiver designer.

Amplifier noise sources

Amplifier noise is twofold. Noise due to series voltage generator $e_a(t)$ and shunt current generator $i_a(t)$. Amplifier and circuit noise of the receiver is given by [*Smith*].

Noise due to series noise source can be given by,

$$n_E^2(t) = \frac{S_E}{2\pi}\int_0^\infty |Y(\omega)|^2 |H_T(\omega)|^2 d\omega \tag{A.16}$$

Due to shunt current source i_a can be given by,

$$n_I^2(t) = \frac{S_I}{2\pi}\int_0^\infty |H_T(\omega)|^2 d\omega \tag{A.17}$$

Due to bias resistor R_b,

$$n_R^2(t) = \frac{2k\theta}{2\pi R_b}\int_0^\infty |H_T(\omega)|^2 d\omega \tag{A.18}$$

Substituting for $Y(\omega)$ in A.16,

$$n_E^2(t) = \frac{S_E}{2\pi}\left(\frac{1}{R_T^2}\int_0^\infty |H_T(\omega)|^2 d\omega + C_T^2\int_0^\infty \omega^2 |H_T(\omega)|^2 d\omega\right) \tag{A.19}$$

thus

$$I_0(\omega) = \frac{1}{2\pi}\left(\left(\lambda_0 q^2 G^2 + \frac{2k\theta}{R_b} + S_I\right)\int_{-\infty}^\infty |H_T(\omega)|^2 d\omega \; + \right. \tag{A20}$$
$$\left. \mathrm{S_E}\left(\frac{1}{R_T^2}\int_0^\infty |H_T(\omega)|^2 d\omega + C_T^2\int_0^\infty \omega^2 |H_T(\omega)|^2 d\omega\right)\right)$$

From Eqn. A.12,

$$\sigma_n^2 = \frac{1}{2\pi}\int_{-\infty}^\infty \left(\frac{\eta q^2}{h\Omega}\right) G^2 \sum_{k=-\infty}^\infty \left(H_P(\omega) e^{-j\omega T_s\left(2k+\sum_{m=-\infty}^{k-1} S_m\right)}\right)\left[H_T(\omega) * H_T(\omega)\right] e^{j\omega t} d\omega \; + \tag{A.21}$$

$$\frac{1}{2\pi}\left(\left(\lambda_0 q^2 G^2 + \frac{2k\theta}{R_b} + S_I\right)\int_{-\infty}^\infty |H_T(\omega)|^2 d\omega + \mathrm{S_E}\left(\frac{1}{R_T^2}\int_0^\infty |H_T(\omega)|^2 d\omega + C_T^2\int_0^\infty \omega^2 |H_T(\omega)|^2 d\omega\right)\right)$$

Anisochronous nature of the pulse stream requires all the history of frames to be summed up. We define the pulse positions if the DPIM pulse stream by L_k, where

$$L_k = \sum_{k-\ \infty, k\neq 0}^{\infty} \left(2k + \sum_{m=-\infty}^{k-1} S_m \right) \tag{A.22}$$

where S_m represents data coded into DPIM.

Noise on the DPIM pulse at $t = 0$ due to the other pulses can be given by evaluating Eqn. A.21 for $t = 0$ and averaging over all the frames given by S_k for pulses at L_k. On the other hand, S_k depends on the information source. Thus noise contribution from the other DPIM pulses on the pulse at $t = 0$ varies depending on the data being transmitted. In order to obtain an average variance we could assume that pulse stream has an average length frame and the pulse positions deviate from this average.

Thus, L_k may be approximated as,

$$L_k = kL_{avg} \pm l_m \tag{A.23}$$

where $l_m = 1, 2, \ldots, L_{avg} - 1$, k=1, 2, 3, ... N.

From Eqns. A.1, A.3, A.4 and A.8 system transfer function is the ratio between the pulse shape at the threshold detector and the photo-detector output which can be given by,

$$H_T(\omega) = \frac{H_{out}(\omega)}{H_p(\omega)} \tag{A.24}$$

Substituting $H_T(\omega)$ in Eqn. A.21 becomes,

$$\sigma_n^2 = \frac{1}{2\pi}\left(\frac{\eta q^2}{h\Omega}\right) \mathrm{G}^2 \int_{-\infty}^{\infty} \sum_{k=-\infty}^{\infty} \left(H_P(\omega) e^{-j\omega T_s\left(kL_{avg}+l_m\right)} \right) \left[\frac{H_{out}(\omega)}{H_p(\omega)} * \frac{H_{out}(\omega)}{H_p(\omega)} \right] e^{j\omega t} d\omega +$$
$$\frac{1}{2\pi}\left(\left(\lambda_0 q^2 G^2 + \frac{2k\theta}{R_b} + S_I + \frac{S_E}{R_T^2} \right) \int_{-\infty}^{\infty} \left| \frac{H_{out}(\omega)}{H_p(\omega)} \right|^2 d\omega + S_E C_T^2 \int_0^{\infty} \omega^2 \left| \frac{H_{out}(\omega)}{H_p(\omega)} \right|^2 d\omega \right) \tag{A.25}$$

Equation A.25 gives the variance at the receiver front end owing to the signal dependant and signal independent noise. The variance of the output signal can be examined by averaging for all possible frames in the pulse stream. Effect of shot noise on the received pulse stream can be evaluated by examining the noise effect on the pulses at the pulse at $t = 0$ and the effect of the rest of the pulses as well as from the idle time slots.

Shot noise effect can be evaluated by separating the first term into two parts for $k = 0$ and for the rest of the values in the summation,

$$\sigma_n^2 = \frac{1}{2\pi}\left(\frac{\eta q^2}{h\Omega}\right)\mathrm{G}^2 \int_{-\infty}^{\infty} H_P(\omega)\left[\frac{H_{out}(\omega)}{H_p(\omega)} * \frac{H_{out}(\omega)}{H_p(\omega)}\right]d\omega +$$

$$\frac{1}{2\pi}\left(\frac{\eta q^2}{h\Omega}\right)\mathrm{G}^2 \int_{-\infty}^{\infty} \sum_{k=-\infty, k\neq 0}^{\infty} \left(H_P(\omega)e^{-j\omega T_s\left(kL_{avg}+l_m\right)}\right)\left[\frac{H_{out}(\omega)}{H_p(\omega)} * \frac{H_{out}(\omega)}{H_p(\omega)}\right]e^{j\omega t}d\omega +$$

$$\frac{1}{2\pi}\left(\left(\lambda_0 q^2 G^2 + \frac{2k\theta}{R_b} + S_I + \frac{S_E}{R_T^2}\right)\int_{-\infty}^{\infty}\left|\frac{H_{out}(\omega)}{H_p(\omega)}\right|^2 d\omega + S_E C_T^2 \int_0^{\infty} \omega^2 \left|\frac{H_{out}(\omega)}{H_p(\omega)}\right|^2 d\omega\right)$$

(A.26)

The summation in Eqn. A.26 can be written as[*Davidson*91],

$$\sum_{k=-\infty, k\neq 0}^{\infty} e^{-j\omega k L_{avg}} = \left[\sum_{k=-\infty}^{\infty} e^{-j\omega k L_{avg} T_s}\right] - 1 = \frac{2\pi}{L_{avg}T_s}\left[\sum_{k=-\infty}^{\infty}\delta\left(\omega - \frac{2\pi k}{L_{avg}T_s}\right)\right] - 1 \qquad \text{(A.27)}$$

And the exponential term that gives the pulse location variance from the average frame position with probability of $1/(L_{avg}\text{-}1)$ can be given by when $t = T_s$ and $k \neq 0$,

$$e^{-j\omega(l_m-1)T_s} = \left|e^{-j\omega(l_m-1)T_s}\right| = \frac{1}{L_{avg}-1}\sum_{l_m=1}^{L_{avg}-1} e^{-j\omega(l_m-1)T_s} = \frac{\sin^2\left(L_{avg}\right)\omega T_s/2}{\sin^2 \omega T_s/2}$$

(A.28)

Thus substituting A.27 and A.28 in A.26. This can be further simplified by taking $y = \omega T/2\pi$,

$$\sigma_n^2 \frac{T_s^2}{q^2} = \left\{ \frac{\eta}{h\Omega} G^2 \int_{-\infty}^{\infty} H_P(2\pi y/T_s) \left[\frac{H_{out}(2\pi y\ T_s)}{H_p(2\pi y\ T_s)} * \frac{H_{out}(2\pi y/T_s)}{H_p(2\pi y/T_s)} \right] dy + \right.$$

$$\frac{\eta}{h\Omega} \frac{G^2}{L_{avg}} \sum_{k=-\infty}^{\infty} H_P(2\pi k/L_{avg}T_s) \frac{H_{out}(2\pi k/L_{avg}T_s)}{H_p(2\pi k/L_{avg}T_s)} * \frac{H_{out}(2\pi k\ L_{avg}T_s)}{H_p(2\pi k\ L_{avg}T_s)} -$$

$$\frac{\eta}{h\Omega} \frac{G^2}{L_{avg} - 1} \int_{-\infty}^{\infty} \frac{\sin^2(L_{avg})\pi y}{\sin^2 \pi y} H_P(2\pi y/T_s) \left[\frac{H_{out}(2\pi y/T_s)}{H_p(2\pi y/T_s)} * \frac{H_{out}(2\pi y\ T_s)}{H_p(2\pi y\ T_s)} \right] \mathrm{dy} +$$

$$\frac{T_s}{q^2} \left(\left(\lambda_0 q^2 G^2 + \frac{2k\theta}{R_b} + S_J + \frac{S_E}{R_T^2} \right) \int_{-\infty}^{\infty} \left| \frac{H_{out}(2\pi y\ T_s)}{H_p(2\pi y/T_s)} \right|^2 dy + \right.$$

$$\left. \left. \frac{S_E}{T_s} (2\pi C_T)^2 \int_0^{\infty} y^2 \left| \frac{H_{out}(2\pi y\ T_s)}{H_p(2\pi y\ T_s)} \right|^2 dy \right) \right\}$$

(A.29)

Taking,

$$I_1 = \int_{-\infty}^{\infty} H_P(2\pi y/T_s) \left[\frac{H_{out}(2\pi y\ T_s)}{H_p(2\pi y\ T_s)} * \frac{H_{out}(2\pi y\ T_s)}{H_p(2\pi y/T_s)} \right] dy$$

$$\Sigma_1 = \frac{1}{L_{avg}} \sum_{k=-\infty}^{\infty} H_P(2\pi k/T_s) \left[\frac{H_{out}(2\pi k\ T_s)}{H_p(2\pi k/T_s)} * \frac{H_{out}(2\pi k\ T_s)}{H_p(2\pi k\ T_s)} \right]$$

$$I_x = \frac{1}{L_{avg} - 1} \int_{-\infty}^{\infty} \frac{\sin^2(L_{avg})\pi y}{\sin^2 \pi y} H_P(2\pi y/T_s) \left[\frac{H_{out}(2\pi y/T_s)}{H_p(2\pi y/T_s)} * \frac{H_{out}(2\pi y\ T_s)}{H_p(2\pi y/T_s)} \right] \mathrm{dy}$$

$$I_2 = \int_{-\infty}^{\infty} \left| \frac{H_{out}(2\pi y/T_s)}{H_p(2\pi y/T_s)} \right|^2 dy$$

$$I_3 = \int_0^{\infty} y^2 \left| \frac{H_{out}(2\pi y/T_s)}{H_p(2\pi y/T_s)} \right|^2 dy$$

Averaging noise over a time slot $\sigma_d^2 = \sigma_n^2 \frac{T_s^2}{q^2}$

$$\sigma_d^2 = \left(\frac{h\Omega}{\eta}\right)^2 \left\{ \frac{\eta}{h\Omega} G^2 \left(\mathrm{I}_1 + \Sigma_1 - I_x\right) + \frac{T_s}{q^2} \left(\left(\lambda_0 q^2 G^2 + \frac{2k\theta}{R_b} + S_I + \frac{S_E}{R_T^2} \right) \mathrm{I}_2 + \frac{S_E}{T_s} \left(2\pi C_T\right)^2 I_3 \right) \right\} \quad \text{(A.30)}$$

In the above analysis we considered the preamplifier with high impedance front end. Thus the transfer function of the amplifier can be given by $A_1(\omega)$,

$$A_1(\omega) = \frac{AR_a}{1 + j\omega R_a C_a} \quad \text{(A.31)}$$

where A is the frequency independent open loop gain of the amplifier.

For transimpedance preamplifier (Fig A.2) the transfer characteristics $A_F(\omega)$can be given as,

$$A_F(\omega) = \frac{Z_F}{1 + \frac{1}{A} \frac{Z_F(\omega) + Z_i(\omega)}{Z_i(\omega)}} \quad \text{(A.32)}$$

where $Z_F(\omega)$ is the impedance of the feedback path for the combination of the feedback resistor R_F and the parasitic capacitance associated with it C_F, and $Z_i(\omega)$ are the amplifier input impedance. For infinite open loop gain the feedback amplifier transfer function simplifies to,

$$A_F(\omega) \approx Z_F = \frac{R_F}{1 + j\omega R_F C_F} \quad \text{(A.33)}$$

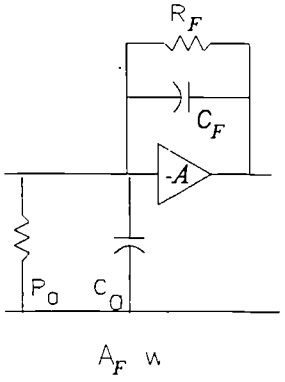

Fig. A.2 Transimpedance amplifier

For a optical receiver with transimpedance preamplifier Eqn. A.30 can be modified as follows [*Hullett*76],

$$\sigma_{Fd}^2 = \left(\frac{h\Omega}{\eta}\right)^2 \left\{ \frac{\eta}{h\Omega} G^2 \left(I_1 + \Sigma_1 - I_x\right) + \frac{T_s}{q^2}\left(\left(\lambda_0 q^2 G^2 + \frac{2k\theta}{R_b^1} + S_I + \frac{S_E}{R_x^2}\right) I_2 + \frac{S_E}{T_s}\left(2\pi C_T\right)^2 I_3\right)\right\} \qquad \text{(A.34)}$$

where $R_b^1 = \dfrac{R_b R_F}{R_b + R_F}$ and $R_x = \dfrac{R_F R_T}{R_F + R_T}$

I_1, Σ_1, I_2 and I_3 are dimensionless quantities which are functions of only the shapes of the input and output pulses where the length of time slots has been scaled out.

Abbreviations of the symbols being used

$\eta/h\Omega$	-	detector quantum efficiency/energy in a photon
T	-	DPIM bit period
G	-	Average detector internal gain
Q	-	Number of noise standard deviations between signal and threshold at receiver output Q=6 for an error of 10^{-9}.
e	-	Electron charge
$k\theta$	-	Bolstman's constant times the absolute temperature
R_T	-	Total parallel resistance including at the detector and the amplifier
R_b	-	Detector biasing resistor
C_T	-	Total detector and amplifier shunt capacitance
S_I	-	Amplifier shunt noise source spectral height (two sided), ampere^2/Hz
S_E	-	Amplifier series noise source spectral height (two sided), volt^2/Hz

Appendix B

DPIM Pre-detection Filter Realisation

B.1 Optimum filter

Given the equalised pulse shape $g_e(t)$ the time reversed and delayed impulse response of the filter or the network can be given by,

$$y(t) = g_e(t_d - t) \tag{B.1}$$

where $t_d = t_m$, t_m being the point where the energy is highest at the filter output. $g_e(t)$ can be experimentally obtained by digitising the equalised pulse at the receiver. Filter response is approximated as a train of singularity functions of the same type and τ seconds apart, can be given by,

$$y(t) = \sum_{i\ 0}^{N} u_{-2}(t - \tau_i) \tag{B.2}$$

Here we assume received pulses are dispersed, therefore ramp form singularity function is used to approximate pulse shape from digitised values. Matched filter in this case is a passive network whose response is matched to the time reversed $y(t)$ given in Eqn. B.2. Design of matched filter involves obtaining a filter network to give impulse response identical to pulse shape as in Eqn. B.2. Thus, the starting point is Eqn. B.2. Network response $H(s)$ can be approximated to $Y(s)$ (pulse shape transform) by means of using Pade approximation method [*Chan*], [*Su*]. In this scheme an impulse response of a given order

passive network is equated to the pulse shape transform and the network parameters are obtained. See the following steps.

Laplace transform on Eqn. B.2 is given by,

$$Y_1(s) = \sum_{i=0}^{N} Y_i \frac{e^{-s\tau_i}}{s^2} \tag{B.3}$$

where Y_i represents the coefficients of the delayed samples, t_i represents time delays and

$$L\{u_{-2}(t)\} = \frac{1}{s^2}$$

Taylor series expansion on $Y_1(s)$ yields,

$$Y(s) = \sum_{i=0}^{N} \frac{Y_i}{s^2} \sum_{j=0}^{\infty} \frac{(-st_i)^j}{j!} \tag{B.4}$$

By equating Eqn. B.4 to $[m,n]$ Pade approximation,

$$Y(s) \cong H(s) = \frac{P_{mn}(s)}{Q_{mn}(s)} = \frac{a_0 + a_1 s + a_2 s^2 + \ldots + a_m s^m}{b_0 + b_1 s + b_2 s^2 + \ldots + b_n s^n} \tag{B.5}$$

For simplicity all pole filter networks are considered, thus $m = 0$. From network transfer function $H(s)$ standard filter design methodology is used to obtain the filter parameters for a specific filter order. Figure B.1 gives the normalised digitised DPIM pulse. This pulse can be given by the singularity functions as,

$$\begin{aligned} y(t) = {} & -0.0320u_{-2}(t) - 0.0320u_{-2}(t-.07) - 0.0301u_{-2}(t-.13) - 0.0056u_{-2}(t-.2) + \\ & 0.12431u_{-2}(t-.27) + 0.5179u_{-2}(t-.33) + 0.9115u_{-2}(t-.4) + 0.9944u_{-2}(t-.47) + \\ & 0.7853u_{-2}(t-.53) + 0.4783u_{-2}(t-.6) + 0.1902u_{-2}(t-.67) + 0.0056u_{-2}(t-.73) + \\ & -0.0527u_{-2}(t-.8) - 0.0546u_{-2}(t-.87) - 0339u_{-2}(t-.93) - 0.0113u_{-2}(t-1) \end{aligned} \tag{B.6}$$

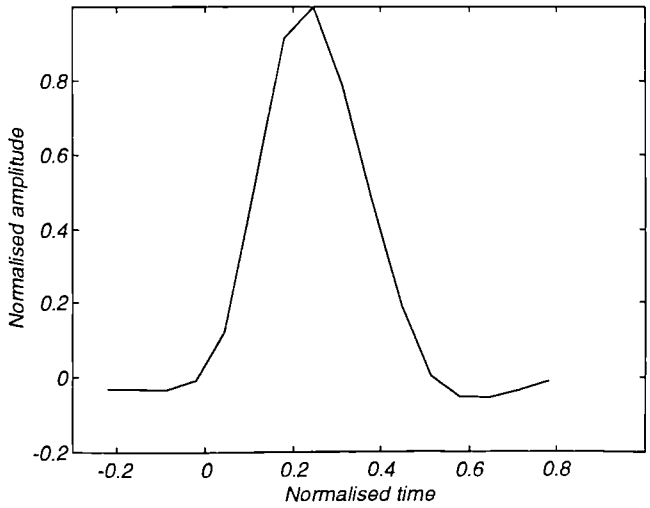

Fig. B.1 Digitised DPIM pulse.

Laplace transformation of Eqn. B.6 following steps given in Eqn. B.3-4 is given by,

$$Y(s) = 3.755 - 5.1943s + 3.579s^2 - 1.622s^3 + 0.515s^4 - 0.105s^5 - 0.0158s^6 + \quad \text{(B.7)}$$
$$0.002s^7 + 0.009s^8 - 0.0054s^9 - 0.0020s^{10} + 0.0006s^{11} + 0.0001s^{12} + \ldots\ldots$$

From Eqn. B.7 was equated to Pade approximation for networks of order [0,2] and [0,3] as given in Eqn. B.5. Obtained network responses are given in Eqns. B.8, B.9.

[0,2,] Response

$$H_{[0,2]}(s) = \frac{k}{s^2 + 2.85s + 3.09} \quad \text{(B.8)}$$

[0,3] Response

$$H_{[0,3]}(s) = \frac{k}{s^3 + 6.45s^2 + 17.45s + 20.15} \quad \text{(B.9)}$$

k is a constant, 1 in this case.

Target network response is given by Fig. B.2.

Figure B.2 shows the approximated matched filter response in comparison with the incoming DPIM pulse shape. Higher order filter closely approximates pulse shape, i.e. [0,3], [0,4] in contrast to [0,2] but at the expense of the circuit complexity.

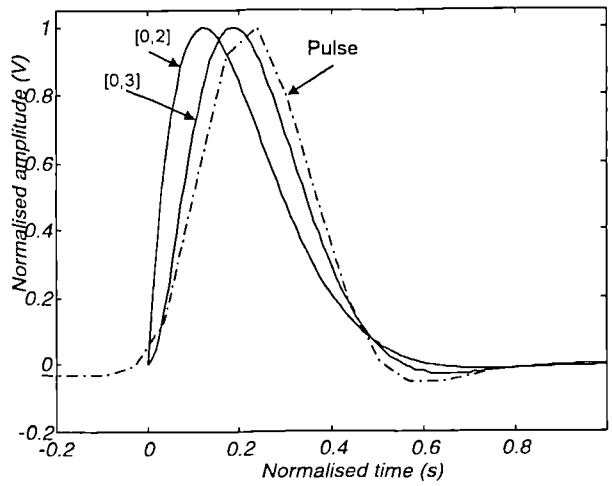

Fig. B.2 DPIM pulse and the network responses.

Normalised network components were obtained by partial fraction decomposition of transfer functions and are given in table B.1. Fig. B.3 shows the network structures.

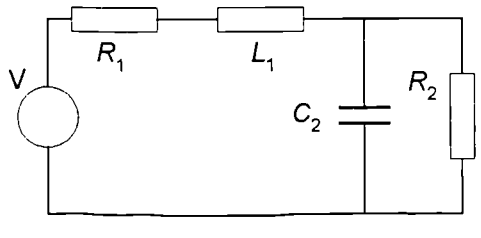

(a)

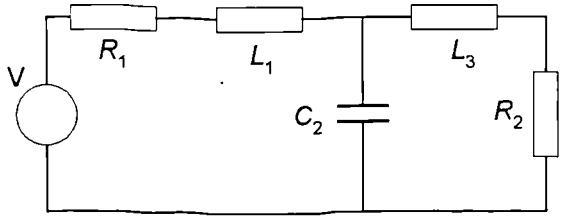

(b)

Fig. B.3 Filter networks: (a) 2nd order and (b) 3rd order approximation.

For the frequency of interest network components are calculated from the normalised values, see table B.1.

	[0 2]	[0 3]
$R_1(\Omega)$	1	1
$R_2(\Omega)$	1	1
L_1(H)	0.7015	0.30986
C_2(F)	2.8509	0.77099
L_3(H)	-	8.37155

Table B.1 Normalised component values for the filter networks

B.2 Sub-optimum Filter

Another attractive strategy for design of realisable filter is to use the idealised optimum filter impulse response as the design target and to approximate it using a practical network structure. Compared to the optimum filter this type of filters are inferior but simple to design, and their output performance can be made as close as 0.5 dB compared to optimum case [*Gibson*]. High order complex filter structures may be required in order to match the target filter response [*O'Reilly*]. He argues that it is not possible to achieve exact target filter response but the nature of the error space is such that response may be apparently very far from ideal and yet yield almost optimum performance.

For reduce complexity a low order all-pole filters readily realisable as doubly terminated ladder network is chosen as the starting point. Initially, filter order is selected and poles are

placed in the left hand side of the *s*-plane. Filter impulse response is optimised by varying the pole locations and comparing it with the target response.

For an N^{th} order all-pole filter $N = N_r + 2N_c$ where N_r is the number of real poles and N_c is the number of complex poles which are in conjugates. Network transfer function is given by $H(s)$,

$$H(s) = \frac{k}{\prod_{i=p}^{N_r}(s+\sigma_p)\prod_{q=1}^{N_c}(s+\delta_q+j\omega_q)(s+\delta_q-j\omega_q)} \tag{B.10}$$

where $-\sigma_p$ are real poles and $\delta_q \pm j\omega_q$ are complex poles and k is a constant.

Inverse Laplace transform of Eqn. B.10 gives the impulse response of the filter. Error between impulse response of the approximated network and the target response $m(t)$ is given by [*Chan*],

$$E_K = \sum_{i=1}^{n}\left[m(t_i) - h(t_i : X^K)\right]^2 \tag{B.11}$$

E_K gives a square performance index which represents the level of correlation between the target response and the approximated, in the k^{th} iteration with corresponding pole locations. $m(t_i)$ and $h(t_i)$ represents the i^{th} discrete time. Lower the value of E_K better the approximation and vice versa. Pole locations are chosen arbitrarily. Optimisation routine generally cannot guarantee that any highest correlation found (lowest E_K) is actually the global minimum or the global optimum point. Only the pole locations corresponding to the best response, from the iterations is taken and are used in filter realisation. Thus the whole process is based on trial and error. One may use the transfer function obtained by the Pade approximation in section B.2 and use the roots as the starting point in the optimisation

process. Once the optimum pole locations are found filter network is designed by using well known partial fraction decomposition of the network transfer function and transforming the terms of the resulting sum analytically [*Williams*].

In designing sub-optimum filter initial poles were estimated from the pole locations obtained from the Pade approximation process. Network transfer functions for 2nd and 3rd order network structures are given by Eqns. B.12 and B.13, respectively. 2nd order network transfer function,

$$H_2(s) = \frac{k}{s^2 + 2.04s + 2.01} \tag{B.12}$$

3rd order network transfer function

$$H_3(s) = \frac{k}{s^3 + 6.76s^2 + 20.95s + 28.02} \tag{B.13}$$

From Figs. B.2 and B.4 it can be seen that with Pade approximation process network response are closely matched with the pulse shape, on the other hand in the optimisation process better rise time and less pulse spreading were obtained. Normalised network components are given in table B.2.

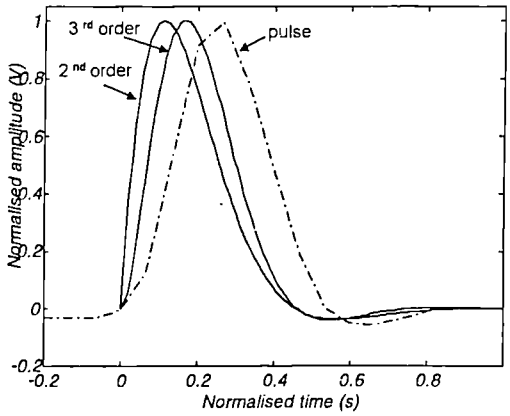

Fig. B.4 Network response and original pulse for sub-optimum filter

	2nd	3rd
$R_1(\Omega)$	1	1
$R_2(\Omega)$	1	1
L_1(H)	0.9761	0.2959
C_2(F)	2.0490	0.6183
L_3(H)	-	10.929

Table B.2 Normalised component values for the filter networks.

Appendix C

DPIM Prototype Schematic

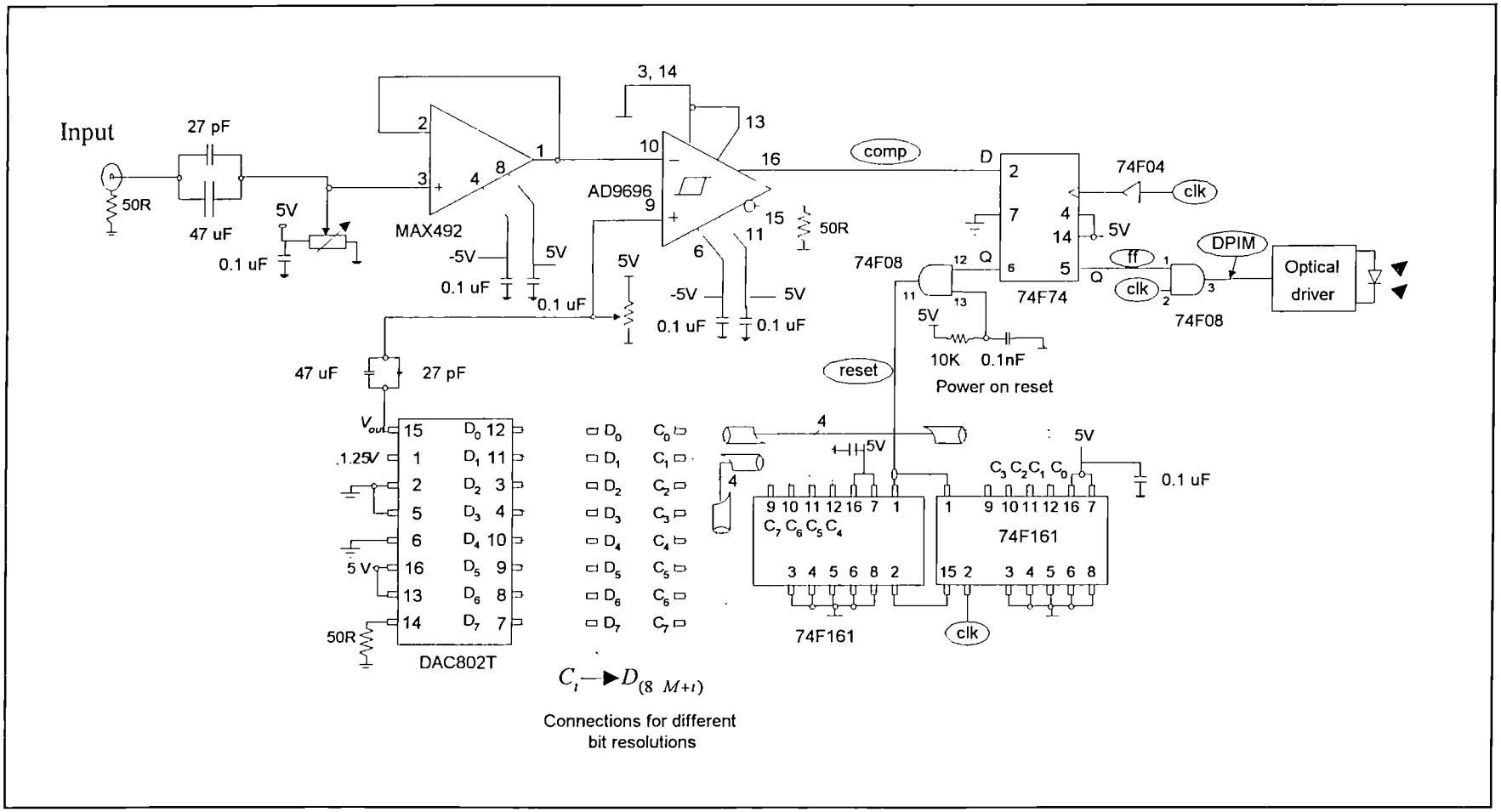

DPIM Transmitter

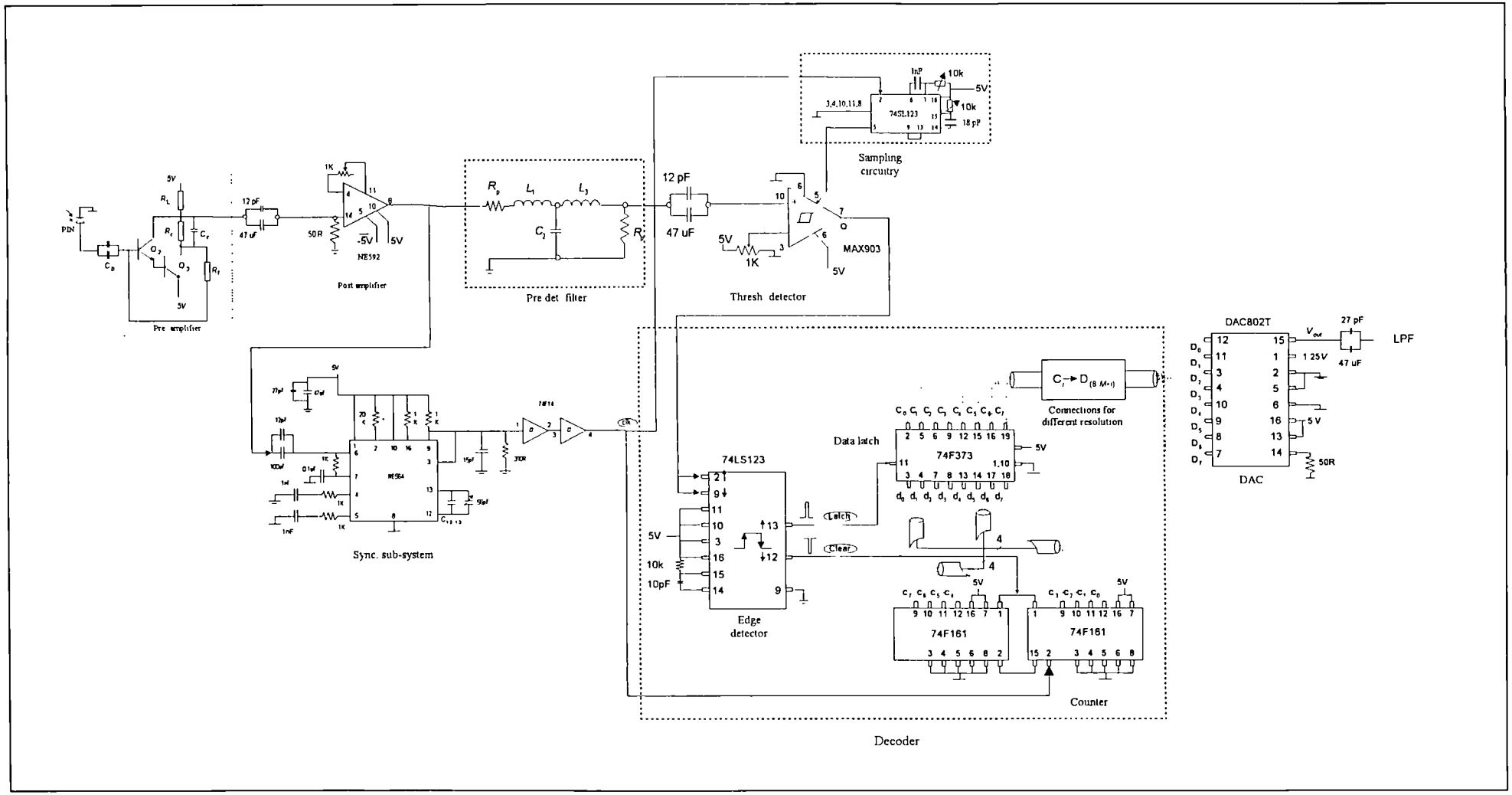

DPIM Receiver